Using Weighted Alpha Complexes in Subsurface Modelling

Reconstructing the shape of observed natural objects

Bart H.M. Gerritsen

Using Weighted Alpha Complexes in Subsurface Modelling

Reconstructing the shape of observed natural objects

Proefschrift

ter verkrijging van de graad van doctor
aan de Technische Universiteit Delft,
op gezag van de Rector Magnificus prof. ir. K.F. Wakker,
voorzitter van het College voor Promoties,
in het openbaar te verdedigen op maandag 26 november 2001 om 16.00 uur
door Bartholomeus Hendrikus Maria GERRITSEN
werktuigkundig ingenieur
geboren te Renkum

Dit proefschrift is goedgekeurd door de promotoren:

Prof.dr.ir. K. van der Werff
Prof.dr.ir. J.T. Fokkema

Samenstelling promotiecommissie:

Rector Magnificus, voorzitter
Prof.dr.ir. K. van der Werff, Technische Universiteit Delft, promotor
Prof.dr.ir. J.T. Fokkema, Technische Universiteit Delft, promotor
Prof.dr. J-L. Mallet, Ecole Nationale Supérieur de Géologie de Nancy, Frankrijk
Prof.dr.ir. I. Horváth, Technische Universiteit Delft
Prof.dr. S.B. Kroonenberg, Technische Universiteit Delft
Dr. R.C. Veltkamp, Universiteit Utrecht
Dr.ir. W. Zijl, Nederlands Instituut voor Toegepaste Geowetenschappen TNO
Prof.ir. C.P.J.W van Kruijsdijk, Technische Universiteit Delft, reservelid

Cover design: Roel Savert

Published and distributed by: DUP Science

DUP Science is an imprint of
Delft University Press
P.O.Box 98
2600 MG Delft
The Netherlands
Telephone: +31 15 27 85 678
Telefax: +31 15 27 85 706
E-mail: DUP@Library.TUDelft.NL

ISBN 90-407-2247-1

Printed in The Netherlands

Acknowledgements

Being with the Netherlands Institute of Applied Geoscience TNO for more than a decade now, I came to appreciate the beauty of natural sciences even more than I already did. Occasionally, as a non-earth scientist, I may have found myself alienated from the knowledge and skills I developed in earlier positions. But I also felt privileged enough, having reached out to a level of understanding of the universe that I personally consider a bare minimum for an intellectual human being to have. Although I realise that full apprehension of the shear coincidences in the evolution that brought life into being is probably beyond men's capacity. Absorbing all that I've seen of it, however, made great pleasure and definitely enriched me as a human being.

Work on which this thesis is based was initially embedded in a wider scope; see the Preface to this thesis. Laying out a road map for a new modelling and simulation approach, we soon realized that a suitable mathematical basis for the description of pre-shaped primitive subsurface objects was lacking. And in fact, that every analytical such description beyond a sampling point set was simply getting out of reach for the time being. At that point, serendipity had it that I came across α-complex software and a Silicon Graphics workstation could be made at my disposal. Exactly what I needed and from then on, things really took off.

As with many non-trivial pursuits, engagement, motivation and finally, the actual advancements came with ups and downs, roughly in equal numbers. This thesis is no exception to that rule. This is where support from family, friends and colleagues comes in for safekeeping. I am heavily indebted to many people in my vicinity. First and foremost to Ipo Ritsema, with whom I shared many of the founding ideas laid down in this work. Unfortunately, our ways split halfway. Nonetheless, we managed to exchange visions, ideas and formulations up to the final drawings of this thesis. Furthermore, to all my present and former colleagues, for the numerous fruitful and enjoyable discussions, more in particular, to Dr. Ewan Campbell, now with Clyde. Led astray by overwhelming geological detail, discussion with Ewan always sort of rolled me back into some framing geological context. To Dr. Wouter Zijl for the many discussions on mathematical details, set forth by fluid flow and other problems in the subsurface, and the many discussions on daily what-have-you affairs we felt were often much more topical than fluid flows. To Dr. Rob Arts, Rogier Westerhoff and Pascal Winthaegen for their assistance in preparing seismic data. To all the colleagues who helped me with the use of the DIANA finite element software. To Dr. Jan-Diederick van Wees for the helpful comments. To the colleagues at the Delft University of Technology; Sevgi Tigrek for her fine interpretation of the L8 section in the North Sea, and advising me on the geology of that region. To Dr. Philip Steeghs, who developed the instantaneous time dip attribute used in the South Marsh Island (Gulf of Mexico) salt dome case study. To Rutger van Spaendonck, for preparing seismic attribute data and discussing details with me. To Stijn Staffhorst, for our joint hands-on efforts, fighting the astonishing practicalities of alpha shape software. To Dr. Remco Veltkamp at the Utrecht University, for assisting me on the hairy details of mathematics boiling down from this thesis and for his many technical advises. To Prof.dr. Imre Horváth, for the appreciated discussions on mathematical and engineering details and for the advises on writing a good thesis. Also for his guidance regarding the publications that sprang off of this research. I also want to say warm thanks to Prof.dr. Jean-Laurent Mallet, for the discussions we had on (implementations of) geometric and topological software details, commonly in association to his celebrated and award-winning Gocad

project. And of course to Prof.dr. Jacob Fokkema, for his decisive support and guidance in the case studies on seismic data. His striking ability to turn more or less mature ideas into something with at least a sense of practical value struck me over and over again. Scientists and students of his group are privileged to have a geophysicist and personality like Jacob in their midst. And of coarse to my mentor throughout the years, Prof.dr. Klaas van der Werff. We know each other for many, many years now, in which we developed a productive and highly appreciated, respectful, long-standing relationship. I'm very much obliged for his many suggestions, ideas, discussions, evaluations, motivations, and above all his never ceasing trust and patience, keeping me on the right track all these years.

I'm also very grateful to Silicon Graphics for granting me access to their latest giant graphics grinding machines. To Ben Geesink and Dr. Jan Thorbecke at SGI, for assisting me (increase the swap space once again). Without their support, there would have been no result on the Gulf of Mexico case. I'm very much beholden with respect to the non-published material on NCSA's founding approach to alpha shapes and its implementation in software, kindly made available by Prof.dr. Herbert Edelsbrunner. Furthermore, I feel the urge to say thanks to all the anonymous and named authors of public domain software used in this work. Most prominently of course Michael Facello's and Ernst Peter Mücke's software, developed at the NCSA and Ken Clarkson's software, developed at Bell Labs. Sharing agreed achievements on the Internet is still the fuel for the scientific engine. My work undoubtedly benefited from their intellectual efforts.

Finally, I would like to emphaticly express my gratefulness to the TNO Netherlands Institute of Applied Geoscience, the Dutch Geological Survey. For providing me with the opportunity to conduct this study, for their financial and immaterial support and for their urge to finally materialise all the knowledge gathered.

To all the family and friends I say, things'll turn for the better from now on!

Contents

Annexes

List of Figures

List of Tables

Preface

The work done within the scope of this thesis, as ever, is just a little step along the path towards longer term objectives. It is believed to fit in the general shift of natural sciences over the passed couple of decades, towards the support of *sustainable development and management* of natural resources, at a global scale and in a broader sense. Owing to this shift, the modelling of *natural objects* has benefitted strongly from growing attention, the fruits of which are showing up in wide-area earth observation systems, "green" engineering, genetic analysis and modification techniques, space programmes, and a wealth of other realms. The advent of boosting computing-power being a critical precursor and a prerequisite alike.

As a first consequence, an ever higher level of modelling detail and accuracy has been pursued. Secondly, consensus has grown among scientists on the suite of developments required to materialise the desired shift: *empirical exploration* of natural resources needs to be swapped with *predictive exploration*. Key incentive is to bring in the *dynamics*, so as to get a handle on the ruling dynamic process behaviour, rather than creating merely a more detailed description based on current observation. Understanding the dynamic behaviour is also the key to turn *descriptive models* into *predictive models*. Figure 1–1 illustrates this. Proper evidence of this capacity is shown for example in the Australian 4D Geodynamical Model (Price,1997, Cox et al.,1997, Hronsky ,1997,Mueller et al.,1998). Process-based dynamic modelling should thereby benefit more from the advancements in simulation techniques, such as genetic and evolutionary simulation approaches and the power of distributed computing power. Furthermore, *concurrent engineering*, *scenario development* and *rapid modelling* techniques have accelerated the modelling cycle.

Modelling has led away from the domain of *geometric* modelling and brought to a higher level of abstraction, thus turning it into true *scenario-driven*, *knowledge-based* modelling. Object feature-based modelling paradigms, analogous to what has become customary in engineering and design, is bound to invade natural sciences too. Editing will migrate from geometric and topological manipulation directly on faces, edges, etc. to *variations* on a restricted number of *characteristic dimensions* and constrained high-level variables. In natural sciences, where modelling usually involves shape reconstruction, editing often seeks to optimise inversion problems of some sort, with observed data bearing knowledge of the physical parameters of the target object. The use of reusable, adaptable pre-shaped objects, autonomous yet interacting, is a possible solution reaching to that extend. In addition to merely the geometry and topology, more and more *features* and *functions* can be predefined within these *primitives*, driving the simulated static and dynamic *behaviour* of the instantiated objects within the framing model. Whatever knowledge may be embedded, a model and its constituent objects can be further *constrained* as more or more precise data becomes available. Of course, new modelling approaches shall remove (at least in part) the apparent model mismatch between many of the current geometric and numerical models.

An *omni-potent* modelling approach, enabling the aforementioned longer term objectives is still lacking. Conventional geometric and topological modelling approaches, usually inherited from design and engineering disciplines, are too immature to cope with the intrinsic shape complexity of natural objects. Simulation is at the very heart of dynamic control. The model mismatch with simulation can be traced back to a mismatch between geometric and topological requirements on the models that statistics, fractals, finite element and (control volume) finite difference

methods need. Conversions into cellular decompositions or spatial enumerations are commonly needed, probably requiring interpolation. Topology, all too often, is restricted to manifold topology . Numerical accuracy and stability further narrow the geometric and topological modelling freedom.

At the Netherlands Institute of Applied Geoscience, much in similar vein, we have launched the idea of working on a new approach to subsurface modelling, considering the earth as a collection of *organisms* or dynamic systems. A complex dynamic earth system consists of interacting subsystems framed in a single structural and stratigraphical system architecture coined *earth architecture*. Earth architectures contain full subsystem relations in space, time and property dimensions at all relevant geological scales. The various *life cycle states* of the subsystems change over time under the influence of geologic events, the behaviour of other earth systems and human acting. *Hyper-spatial data structures* are used to describe and store collected *a priori knowledge* (spatio-temporal and property constraints) in the form of parametrised, pre-shaped objects, *shapes* for short. Shapes, collected in an *earth catalogue*, can be used to instantiate dynamic systems within a model at various scales. A model in this regard, is a geoscientific framework framing all the shapes and their constraints and giving context and meaning to the embedded a priori knowledge.

No suitable geometric *primitive* shape could be found for the complex subsurface objects, until we came across the concept of α-complexes. α-Complexes appear to be able to bridge the gap between point set topology and complex polyhedral objects, offering various handles for parametrisation, subjectivity-through-weighting, constraints, and pre-storage of subdivisions. They offer the necessary implicit control through parameter variation that paves the way for mature and unimpeded knowledge-based subsurface modelling. On top of that, they show descriptive lucidity and completeness. At present, α-complexes are singled out as the principal candidate to define the pre-shaped primitives in the earth catalogue. Training data sets can be used to equip them with multi-purpose sampling data point sets, best-guess initial weight sets and sensible domain constraints on the α-ranges.

The eventual longer-term objective is to implement shapes by creating a collection of distributed objects, together making up a living subsurface model. Every object obeying pre-stored rules, within the regime of the Earth Architecture, but further capable of evolving according to any simulation scenario it is fed with. Further constraining data, typically seismic, can be brought in to drive the inversion of model and observation. Planned acquisition can be used to obtain targeted reliability at minimum cost. The idea of creating a lively collection of interconnected natural objects is steadily growing towards reality. In the forthcoming years, technical developments in the area of distributed computing are foreseen to become mature enough to facilitate the required technical environment. A modelling system like this bears all the characteristics needed for concurrent modelling, which, in turn, is believed to bring about important cost savings inducing economic exploration and exploitation of less trivial natural resource occurrences, and spiralling further.

Chapter 1

Introduction

1.1 Natural objects

The vast majority of all the objects in our living environments are *natural objects*, endowed by nature in an evolutionary development process. They differ from men-crafted *engineering objects* (or: *artifacts*) in a number of ways. "Fitness for purpose", technical limitations and a strive for design and production cost minimisation typically induce a smooth and regular shape for engineering objects, whereas natural objects generally possess a "rougher" shape. Natural objects are studied, among others by means of destructive and non-destructive observation. Occasionally, the shape of natural objects is so complicated, that only a *sampling data set*, such as a CT-scan, a measure robot output or a seismic reflection image can accurately represent them; other descriptions are either overly elaborate, complex or virtually impossible. A sampling data set typically consists of 2D contour data, 2D cross-sections, 2D or 3D sample data points, and the like. The human mind has the perceptual capability of constructing an object out of these points, but in terms of computer representations, it is only through a shape reconstruction recipe that the observed object's solid model can be attained. For instance, through triangulation or spanning of the convex hull. Moreover, evolving (*"living"*) objects may fall apart into multiple parts, e.g. moving clouds. As a result, creating or reconstructing natural objects using computer models is complicated.

Engineering objects are studied and crafted in engineering sciences, architecture and industrial design. In contrast, natural objects are studied primarily in *natural sciences*. Examples are medicine, biology, earth sciences, astrophysics, etc. In engineering sciences, engineers and designers came to understand how to unambiguously describe engineering objects in terms of boundaries and volumes over the past couple of decades. Today, using predefined primitives, sweeps, extrusion and part-whole descriptions, fairly complex objects and assemblies can be created. Chiefly relying on *explicit* descriptions of geometry and topology. Practical implementations exploiting these capabilities, however, are often limited to engineering objects and assemblies, with regular mathematical properties. As soon as natural objects are to be modelled, many such practical approaches fall short. The more so if modelled objects of this type are to be submitted to some numerical analysis tool, e.g. for stress analysis. Also, many of today's modelling approaches are incapable of handling changing topologies. Problems of this kind are encountered regularly in *clinical imaging* and *medical scene analysis*, *subsurface modelling*, *im-*

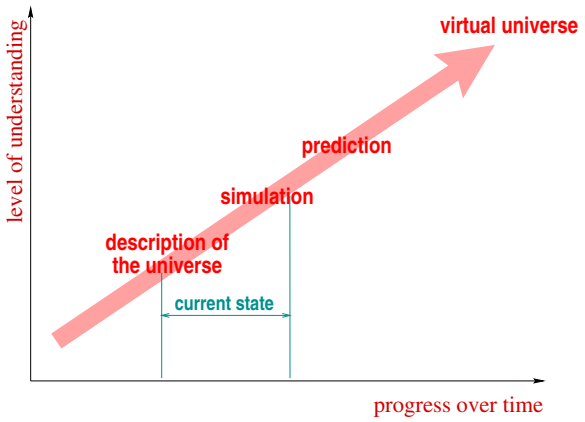

Figure 1–1: *abstraction levels in the creation and use of models and its potential meaning in terms of modelling capabilities. The level of understanding grows over time, with an indication of the present state.*

age analysis and a wealth of other geometry-dominated natural object recognition and modelling problems.

The above contrast between natural and engineering objects does not inasmuch imply a watershed as it suggests; measuring robots probing an engineering object will produce a "noisy" data set, while a raindrop may resemble a perfectly smooth object. But generally, contrary to the "free form" modelling world of engineering, natural sciences deal almost exclusively with *observed* sampling data sets followed by *shape reconstruction* Often,the object of interest cannot be isolated from its hosting environment; it has to be studied *in situ*, i.e., while remaining embedded in its hosting "background". When determining the shape of a carcinoma, for example. Even on a detailed medical image, telling sane tissue apart from damaged tissue is far from trivial. Imperfections in the observation and inhomogeneous hosting material can blur the shape to be reconstructed. This is another distinction between engineering design and natural object modelling: it takes *data processing* and *interpretation skills* and *craftsmanship* to shape natural objects on the basis of imperfect observations. To some extent, lacking data can be replaced by *a-priori knowledge*, qualified guesses or corrections to the sampling data set; the scanned data set of a human heart may show a "hole" near the outlet to the aorta but one may safely assume that the patient would have passed away if it were really there. The handling of hosting *background* material is also complicated. A mere data classification is generally not sufficient. Usually, location, proximity and spatial and temporal *inter-event* information has to be taken into account as well. Chapter 3 will elaborate on this.

For a correct understanding, a more adequate notion is needed of what is meant by the shape and the model of a natural object. The object's shape will be discussed mainly in terms of geometry and topology. The desire to come up with a crisp definition of a natural object is firmly felt here. But this would set us up a mighty endeavour: it is virtually impossible to cover the natural objects subject to study in natural sciences with a single succinct definition. A number of common characteristics can be enumerated, though:

- **Identity**

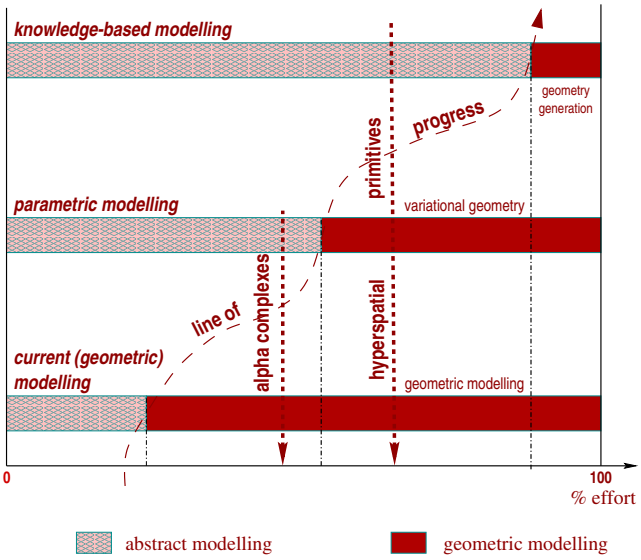

Figure 1–2: *abstraction levels in the creation and use of models and its potential meaning in terms of modelling capabilities for earth science applications. The figure sketches the relative effort of pure geometric modelling versus more abstract modelling approaches, like parametric (variational) subsurface modelling and knowledge-based modelling (after [SM94], with modifications).*

A natural object has an identity admitting it to be pointed to, referenced, etc., as it differs by a (limited) number of properties from other objects.

- **Finite in space**

  A natural object is assumed to be finite in space. It can be sampled by a finite set of sample points.

- **Finite in time**

  Natural objects, in the sense of living organisms ([RG96]), can grow together, assimilate, connect, encapsulate one another, etc. On the other hand, natural objects may crack, wear, be torn apart, split, erode, dissolve, change phases, be expelled from hosting material and indeed vanish completely. Ideally, a dynamic model of a natural object has the capacity to reflect all these state changes in a genuine birth-life-death cycle. Natural objects are therefore not necessarily connected and may have holes of any topological nature. Neither are all (parts of an object) necessarily convex (too be explained further down).

- **Compound objects**

  A natural object may in fact be a compound of multiple objects or object parts. One such natural object compound may consist of a target object embedded in some hosting material. Another example is a multi-phase system of immiscible fluids and gasses (e.g., [BB91, ABBM94, Tak98]). It was already noted that in practice the separation between the various compounds may be intangible indeed.

- **Roughness**

  Natural objects are rough. Owing to their shape, surface textures and the impact of ongoing natural processes, surface curvatures may spread across a wide range. This is in fact the feature that makes the modelling of natural objects a *scale-dependent* process and limits the meaning of fractal descriptions (e.g., [HB94]).

- **Dimension**

  In this thesis, a natural object basically possesses a finite volume and mass, so as to endorse a physical interpretation. Still, this doesn't obstruct the dimension from being raised to dimensions beyond three if modelling operations desire so. More on this, shortly.

Of coarse, there's much more to say to common characteristics, but these are the prevailing ones in this context. Although objects can be recognised by interpreters within sampling data point sets, turning them into solid object representations with a correct geometry and topology is far from trivial. To turn a geometric model into a numerical model or even a process model often requires that the geometric model is further simplified, to allow proven numerical schemes to be applied. Abridging the gap between the world of observations in points and the world of solid geometric and numerical modelling therefore takes a revision and extension of classical tools mostly inherited from the domain of CAD. One new development capable of providing an answer to just those questions is formed by the α-complex.

1.2 New developments based on α-complexes

The modelling of natural objects is a realm where α-complexes came up-front as a new and intuitive way of modelling. Awaiting a more concise definition and roughly speaking, an α-complex may be understood as a triangulation governed by a single geometric parameter α, giving rise to the term α-complex. See the elementary and real data example in figure 1–3 and 1–5, respectively. A triangulation of a finite point set in d-dimensional model space E^d is a tessellation of the underlying convex space spanned by that point set with a collection of connected non-overlapping simplices (points, edges, triangles, tetrahedra, ..., depending on d). The points become vertices of the simplices in the triangulation. Unlike a triangulation, an α-complex may be an "incomplete" tessellation, in the sense that part of the underlying space may not be covered by simplices. It thus resembles something in between the point set itself and the triangulation of that point set. What exactly, depends on α that determines how close the α-complex is to the triangulation. A low value of α yields an α-complex close to just the point set, a higher value of α results in a complex which matches or nearly matches the triangulation. The effect of a variation of α is that a certain degree of coarseness can be obtained. Figure 1–3 shows this, with α increasing from left to right. In the leftmost picture of figure 1–3 the α-complex is separated, with two exteriors and three interiors. The bounded exterior in the centre is an internal hole, called a *void*. In the centre left picture, the void has become filled, with one unbounded exterior remaining. The separation has been lifted by a *singular* edge (observe the solid edge), connecting both parts. Interiors remain separated. In-filling of the boundary cavities starts. In the centre right picture the separation is completely lifted and only one interior is left. In the rightmost picture of figure 1–3, the α-complex grows towards the triangulation and its α-shape (the α-complex without internal edges) towards the convex hull. The sliver-like triangles near the boundary of the convex hull enter the α-complex last. In contrast with triangulations,

a single α-complex may consist of multiple (separated) parts. It doesn't need to be connected, nor convex. All pictures in figure 1–3 show a single α-complex.

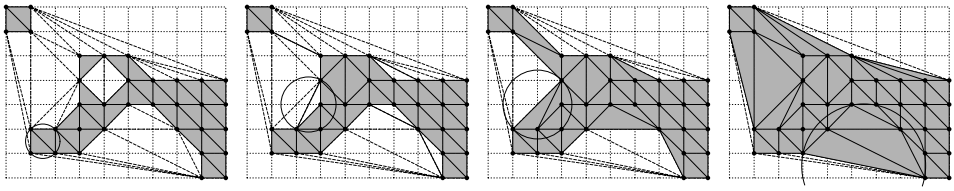

Figure 1–3: *example of a simple α-complex. The data points are located on a regular grid, but are themselves irregularly spaced. The α-value (proportional to the squared diameter of the sphere) grows left-to-right from low to high and so do the edges that enter the α-complex. Gray-filled triangles and solid edges belong to the α-complex. The dashed lines indicate the underlying triangulation.*

A formal definition of an α-complex will be given in chapter 2. Effectively, the α parameter inflicts an upper bound on the length of the edges in the triangulation. Edges exceeding this upper bound drop from the triangulation. What remains after this *α-filtration* is an α-complex. Repeating this process for varying α yields an entire family of α-complexes, called the *α-family*, *generated* by the same point set. It is somewhat harder to understand the impact of α-filtration on triangles, tetrahedra, etc. This will be explained in chapter 2.

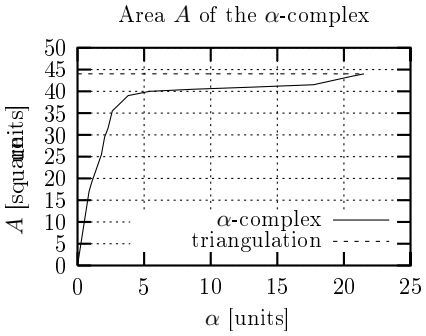

Figure 1–4: *increase of area with growing α. For a monotonically increasing α, the area of the α-complex increases monotonically too. For $\alpha \to \alpha_{max}$, the area of the α-complex approaches that of the triangulation.*

The underlying space occupied by an α-complex is called an *α-shape*. It is an α-complex without internal edges. For example, the most complete α-complex is the triangulation, for which α is high enough to prevent any edge from being dropped. No edge is filtered off. The underlying space occupied by the triangulation is the convex hull and for this α, the corresponding α-shape is identical to the convex hull. If the partitioning of the underlying space is irrelevant, α-shape can also be read where α-complex is written. In the absence of crisp criteria to prefer one α-complex over the others, selecting an α-value is somewhat subjective. Typically modellers will attempt to reflect their *a priori conception* in the eventually preferred α-complex.

In the context previously described, α-complexes offer various advantages over for example triangulations, tessellations and hulls, at little extra cost. Like triangulations, tessellations and

Figure 1–5: *example of an evolving α-complex with α increasing left-to-right: left: $\alpha = 3.096634e+01$, yielding a complex that is little more than just the point set with a few singular edges, gradually developing into right: an overly fat ($\alpha = 1.805128e+03$) complex obscuring all the fine details of the face and the neck, almost grown into the convex hull. The most appropriate α for the details of the face is approx. $\alpha = 1.444991e+02$, the value of the central picture (data set by Silicon Graphics, number of points $N = 2780$).*

convex hulls, they are defined (or: *generated*) by an input data point set. But unlike triangulations, tessellations and hulls, they offer the additional flexibility to capture holes and separations. The use of α-complexes can significantly simplify the modelling of natural objects and improve the eventual modelling results. This is intuitively seen from the examples and will be made explicit in the forthcoming chapters. The α-complex may also be merged with other triangulated geometries, or may be transcribed into an "ordinary" solid.

The sample data points can be attributed a *weight*; a real-valued magnitude expressing the dominance of that point over other points. Weight acts as a bias in addition to α. With weights, the evolvement of an α-complex is not only determined by *proximity* (as reflected by the α-value), but also by *dominance*. In a neighbourhood of points with higher weights, the α-complex tends to develop at lower α-values, whereas negative weights discourage the α-complex to develop. Sometimes, a distinction is made between non-weighted and weighted α-complexes. Here, that distinction will not be made and α-complexes herein shall always be *weighted*. Of course, all weights can be chosen equal, possibly zero. Weighting, on top of variation of α, makes "special modelling effects" possible, and is in fact the key to practical applications. Chapter 4 is devoted to weighting.

1.3 Previous work

The concept of α-complexes is mainly due to Edelsbrunner ([EKS83, Ede87, Ede92, EM94]) and builds on the results of regular triangulations of weighted point sets (e.g., [Lee91, ES96]). Weighted points are commonly interpreted as spheres and balls. The study of the sphere and ball intensified in the early twentieth century, in the research of the geometry of complex numbers. Classical such studies can be found in [Coo16, Bra47, Max52]), with more recent work in [Sch79, Hah94, BP94, Bix94, Bix98]. The study of α-complexes finds its roots in, among others, the study of simplicial complexes. Good starting points are [Cox73, Mun75, Mun84]. Paoluzzi et al., in [PBCF93], pointed out the suitability of multi-dimensional simplicial complexes for geometric modelling. They did not encompass, however, non-regular complexes, like α-complexes. Applications of simplicial complexes to geological modelling were also reported in [ABB+97].

Literature on weighting strategies is sparse; the theory of weighting is fairly well understood, particularly in conjunction to sphere-geometry (e.g., [Aur87b, AI87, Ede87, Ede92]), but the use from the modellers' perspective is faintly addressed ([AAL+99, Ger98]). The mathemat-

ical foundation of representation schemes is mainly due to Requicha and Voelcker ([Req80]). In more recent work, Kalay, in [Kal89] further works out a number of details of various representation schemes. Further, refer to [Req83, Zei91].

Taking a somewhat wider scope, several key solutions, contributing to the concept of α-complex-modelling, can be identified. Firstly, foundations of computational geometry were laid down by Preparata and Shamos in [PS85], Edelsbrunner in [Ede87], Aurenhammer in [Aur87b, Aur87c, AI87], De Berg et al. in [dBvKOS97], and many others. Mehlhorm et al. in [MMN+97] discuss many general dimension implementation details. Lee in [Lee91] described regular triangulations, fundamental to the derivation of weighted α-complexes. A profound overview of the history and the current state of Voronoidiagrams is presented in [OBSC00]. Recently, Aichholzer et al. in [AAL+99] explored *skew Voronoi diagrams*, an approach in which the basically scalar weight is replaced by a weight *vector*. A valuable source for geometric graphs in general is Gross and Tucker [GT87] and O'Rourke [O'R94]. Brisson in [Bri90] discussed implementation details of the "cell tuple"; general dimension geometric and topological data structures.

Regarding the application of α-complexes, not so much can be found in literature. Edelsbrunner et al., in [EFL98], described an application of α-shape-modelling to macro-molecular docking and Gerritsen, in [Ger98] described applications in earth sciences. Tentative applications to hyper-spatial modelling have been described in [GR97, Ger98, GVdWV00a]. The latter also gavemore detailed descriptions with respect to weighting strategies and the effects of weighting in general. Gerritsen et al. also presented a method to carry out finite element computations over α-complexes, using a commercial finite element analysis package in [GZT01]. Parameterisedobjects were used as template objects in shape reconstruction for an application in the reconstruction of coronary vascular trees in [SdGN+90].

Shape theory from a topological point of view can be found for example in [MS82]. Stochastic geometry is discussed among others by Diggle in [Dig83], Stoyan and Stoyan in [SS94], Tijms in [Tij94], Stoyanet al. in [SKM95], Barndorff-Nielson et al. in [BNKVL99] and Okabe et al. in [OBSC00]. Marked point processes (to be discussed in chapter 4) is discussed, among others by Stoyan et al. in [SKM95] and Sigman in [Sig95]. Statistical shape analysis is discussed by Dryden and Mardia in [DM98]. Scale-space analysis (chapter 3) is discussed by Ritter and Wilson in [RW96] and Lindeberg in [Lin94]. A recent survey paper on shape matching was presented by Veltkamp and Hagedoorn in [VH01].

*Fractals*have been applied for simulation purposes, but mainly in cases where constraining data was absent or sparse (e.g., [HB94]). Fractals generally provided (too) little control over the shape reconstruction. Another development is Medial Axis Transform (e.g., [Ogn94], [OBSC00]): a shape description that defines internal region and boundary information, at various scales. MAT is well-suited for rough boundaries but not for internal holes and separations.

A pioneering attempt to reconstruct an ordered sequence of natural subsurface objects within a constraining framework using knowledge-based modelling was presented by Simmons in [Sim92]. Simmons' problem solver is based on a "generate-test-debug" cycle, bearing similarity with the approach presented in chapter 3. One of the prime contributions from his work is probably the ability to generate *geological scenarios* (in this context: a possible history to the given present geology in terms of geological events) and evaluate them against a dynamic set of constraints. In the case of failure, the fault typart of the scenario is repaired after which the next cycle is entered. In parallel, but independent from Simmons, Flewelling, Frank and Egenhofer [FFE92] developed a 3D-GIS environment in which scenarios can be examined that

might explain how the current state came into being. For low-complexity geological problems, see also Meseguer [Mes89] and Kumar [Kum92]. Variational geometry and its relation to knowledge-based modelling is discussed for example by Woodbury in [Woo90], Taylor in [Tay92], Tong and Sriram in [TS92b] and Syan and Menon in [SM94].

1.4 Objectives

The primary objective of this thesis is to explore the merits and the value of a modelling approach with α-complexes and to verify and validate its model description correctness for the modelling of subsurface objects and natural objects in general within the light of longer-term objectives of high-abstraction, knowledge-based modelling. Assumptions are that observed data points are available, along with property value sets for the objects to be modelled and that a solid model description is the target. The description must be geometricly and topologically adequate to cope with the abundant level of detail of natural objects. Also, numerical modelling must be possible using the same model. Moreover, the object model description shall support static behaviour, dynamic behaviour and process modelling. The modelling of subsurface objects shall be put in the context of inversion-based, possibly iterative, constrained forward modelling. A formal evaluation of the α-complex as an object description and as a representation is considered critical for a successful embedding of such a modelling approach with existing and legacy modelling environments.

These objectives demand an *evaluation study* more than anything else, with emphasis on practical value. Therefore, the focus will be on modelling aspects, *not* on geoscience details, *not* on mathematics and *not* on implementation details. The use of mathematics will be instrumental, in support of formalisation of relevant aspects of the evaluation.

1.5 Scope

1.5.1 Planned acquisition

Planned acquisition is an acquisition strategy for sampling data points by which a coarse model is step wise refined by determining, sampling and adding only those points that further contribute to some optimised model. The process is stopped when the desired optimisation level is reached or further improvement ceases to occur. The optimisation level is usually a trade off between acquisition cost and increase of quality. Planned acquisition, for instance driven by a step wise refined reliability model is foreseen in the gathering of sampling data points. Planned acquisition is mostly based on *stochastic geometry*. This topic has gained much attention, lately. See for example [Dig83, SS94, Tij94, SKM95, RW96, DM98, BNKVL99, OBSC00]. The subject by itself is beyond the scope of this thesis. The main issue here is that sampling data points may be added batch-by-batch, as local demands require. The collection of training data for instance, may assist in deriving typical scenario's, parametrised object templates (*primitives*) and typical values. A few remarks regarding planned acquisition will be made in chapters 3 and 4. The modelling approach to be designed shall not obstruct its introduction.

Level	Geometry	Topology	Properties	Applications
6	dynamic	dynamic	dynamic	virtual universe, paleo-reconstruction modelling, complex, geomechanics driven basin analysis, dynamic virtual reality models
5	dynamic	dynamic	static	simulation and prediction models, like geomechanical studies, basin analysis, simple paleo-reconstruction modelling, simple virtual reality models
4	static	dynamic	static	simulation and simple prediction models, fault systems studies, simple (hydraulic) fracturing studies, crack propagation studies and 3D GIS applications
3	dynamic	static	dynamic	simple prediction models, long geological timespan simulation models, e.g, compaction studies or migration studies, hydrocarbon generation and diagenesis studies, accurate reservoir depletion studies, or advanced groundwater and polution studies and 3D GIS applications
2	static	static	dynamic	state-of-the-art simulations, usually resulting in time series of properties developments. For example, production monitoring and "ordinary" GIS applications
1	static	static	static	description of the universe, current status

T able1–1: *classification of geometry and topology in levels of complexity with application examples taken from earth sciences. Up to level 3 is common ground in today's geoscience modelling applications, from level 4 onwards is the target for tomorrows geoscience needs. After Ritsema and Floris, [RF94], modified.*

1.5.2 Dynamic geometry and topology

A natural object model is a living thing and the model shall be dynamic, i.e., allow for a dynamic geometry and topology and time-dependent property values. As stated earlier, natural objects can assimilate, erode, etc. As a consequence, dynamic geometry and topology are required to accommodate simulation of this kind of dynamic behaviour. Table 1–1 peeks into a useful levelling of the various degrees of "dynamics", to recur further down this thesis.

1.5.3 Hyper-spatial modelling

Following pioneering approaches in physics and statistics, there is a steadily growing tendency in natural sciences to endow models with an increasing number of dimensions. Three dimensional models extend to four dimension for time, usually referred to as *spatio-temporal models* (e.g., [FFE92, ABB+97, OBSC00]). Models extended with an arbitrary dimensional *parameter space* are usually referred to as *multi-dimensional* or *hyper-spatial* models. In mathematics, the term *general dimension* is customary to indicate arbitrary dimension.

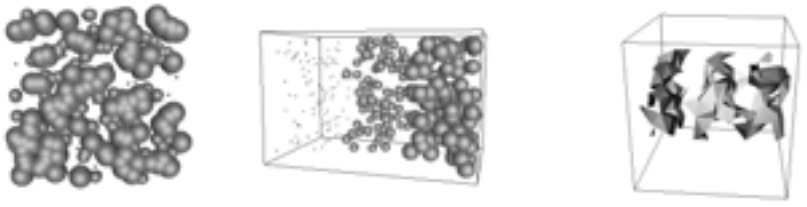

Figure 1–6: *principle of hyper-spatial modelling on stratified data in hyperspace. Left: three classes (reflected by sphere radius) of data randomly distributed in space. Centre: after augmenting model space by the 1-dimensional radius parameter space, the mixed classes of data appear as strata in hyperspace. Right: an α-complex of this data set will naturally find three clusters.*

Why hyper-spatial modelling? The motivation to augment geometry space with parameter space is in fact manifold (also see figure 1–6):

- It allows for a generic geometric and algorithmic approach, regardless the number of parameters. Hyper-spatial modelling leads to a mathematically coherently integrated approach to various sorts of data: geometry, topology, time, properties, guesses, uncertainties, ... It makes data commensurable, in a mathematical sense. In a sense, parameters become *geometrically coupled/un-coupled* in parameter space. Great prudence must be exercised with respect to causality and time.
- It allows for generalisation of *property-ruled geometry*, thereby supporting fundamental operations, such as projections and intersections and level set cut-offs and fundamental objects, such as graphs and triangulations.
- It supports generic d-dimensional "total space" in versionschemes, with d-dimensional data sets, including the same parameter space. The inversion itself is beyond the scope of this thesis and will be further disregarded.

- Having a d-dimensional topology at hand, greatly facilitates the k-dimensional constraints solving frequently required in order to obtain meaningful or (physically) possible solutions.
- It is easier to work with "holes" in the d-dimensional object in a geometric sense than with lacking, out-of-range data in the "select-from-database" approach.
- With the advent of *reliability analyses* (e.g., for Decision Support Systems) and *error analysis* it is no longer sufficient to create *iso-surfaces* by running property-based queries over a database. By creating reliability contours over a iso-surface, it is easily seen that reliability constraints lead to holes in the iso-surface. The required set of data may well be a set of unconnected volumes, rather than a surface. For generalised queries like these, it is much more convenient to rely on an *spatial engine* based on local hyper-spatial topology. Specifically in the event that a slight modification in the query induces a rerun of the database query.
- Non-manifold topologies can be "unrolled" such that they become manifold, by adding more dimensions. The practical meaning of this is that systems of which the topology changes over time, can be unrolled in time, such that their history is preserved. For example, when studying the morpho-dynamics of a "caniballistic", labyrinthine meandering river system.
- Hyper-spatial shapes facilitate the storage of pre-defined grids, triangulations, hulls, α-complexes, and, related to the grid size, proper time steps for iterative processes. A *floating-scale geometry and topology* can be implemented, operating silently within the scope of a single object, optimised for that object at that scale, without user intervention. The same holds for up-scaling of properties and parameter values.

Many aspects mentioned above have not yet been discussed, but will be in the forthcoming chapters, as far as directly linked with α-complexes. Others, such as visualisation of hyper-spatial models are considered beyond the scope. The discussion on the role of time has two sides to it, neither of which will be discussed in detail in this thesis:

1. A mathematical side: Is spatio-temporal space Euclidian?
2. A philosophical side: What is the effect of adding the time-dimension to space with regard to logic, causality, reversibility, etc?

For an answer on the first aspect, see for example [Cox73, Ban90]. For the second, refer to a fairly verbose treatise in [Rei58, Ruc82, Gar88].

General dimension comes down to *low* general dimension in practical implementations, due to the many restrictions imposed by time and space complexity. Hyper-spatial modelling by itself is a huge research topic in its own right that can only be pondered upon in this thesis.

1.5.4 The geometric description

The geometric description in this thesis is always polyhedral by nature (e.g.,[Cox73, PS85, Ede87, Kal89, PBCF93]). Description is either by means of its interior, its boundary or by its constituting parts. Geometry is not necessarily deterministic. Moreover, *stochastic geometry* ([Dig83, SS94, Tij94, SKM95, BNKVL99]) has advanced by leaps and bounds in the past decade.

Stochastic geometry yields a set of more or less likely models, rather than just a single determined one. Deterministic geometries can also be based on or constrained by stochastic observed data. A stochastic approach is also the key to (geometric) reliability analysis. *Shape theory* and *statistical shape analysis* have progressed in a similar manner during the past decades. Mainly under the influence of image pattern recognition, feature extraction, biometric recognition, etc. [DM98]. Also see [RW96, Lin94, VH01].

1.5.5 Topology

Geometry is a much more widely understood term than topology. Some workers ([Mun75, Kal89]) refer to topology as "rubber sheet geometry": move around the vertices, as long as the connectivity doesn't change, the topology remains the same. Shape theory from a topological point of view can be found for example in [MS82]. A good source is also [Edg90], and the classical references for topology are [Mun75, Mun84]. Manifold as well as non-manifold topology are considered with natural object models, and regularisation will be considered to make topology manifold on a part-by-part basis if necessary. This topic will be further discussed in chapter 2.

With α-complexes, topology is sort of implicit. There is no need to explicitly describe the topology. It is uniquely determined by the sample points, the weights and the α-value. α-Complexes inherit their topology from simplicial complexes, to be explained in chapter 2.

1.5.6 Numerical modelling

The approach in this thesis will be to use the triangles, tetrahedra, etc., of the α-complex and use them as grid elements in finite element computations. Somehow, a fix has to be found for the separations and singular faces that α-complexes may contain. A serious problem is also posed by the "slivers"; the sharp, needle-like elements of which the aspect ratio (element shape, say) can be very odd (fig. 1–3). Many numerical computations become suspicious when fed with such triangles. Figure 1–3 already showed that many slivers (but not necessarily all of them) are formed near the border of the convex hull when α approaches its maximum value. In many practical circumstances, these slivers may be dropped from the α-complex without severe penalty. More on this, in chapter 3.

1.6 Contributions from this thesis

No applications of weighted α-complexes were found in literature. The application of α-complexes for the description of subsurface features has been introduced by the author in [GR97] and [Ger98] and in a more general sense for natural objects in [GVdWV00a] and [GVdWV01]. The same holds for hyper-spatial modelling of subsurface features [RG96]. No earlier integrated approach for geometric, topological and property data within a single data structure has been encountered in literature, although generic k-faces were introduced by others. Using primitive instancing is completely new to subsurface modelling. Capturing the geometry and topology of *shape families* by means of an icon α-complex is not previously presented in literature. Instantiation of shape families using transformations on the icon α-complex wasn't found in earlier work either. Also, α-complexes are evaluated in a formal sense, as an object description and as a representation scheme, which has not been done earlier.

Transformations may be applied on the points sampling the object before the α-complex is determined. This has not been studied and described in literature before. In this thesis, the implication for the α-complex and for the Lebesgue measure, a d-volume, say, will be discussed.

Weighting strategies for the purposes as in this thesis are completely absent in literature. Various weighting strategies are developed in this thesis. For the most appealing strategy for natural objects, a quantification has been worked out to determine the relative distribution of the weight over the point set, the up-scaling of the weight to match the nearest neighbour distribution, and the use of *attractor* models, to obtain a hole-free (part of the) object. The author also describes how the empirically observed sample points can be fruitfully supported by the use of a theoretical model, for which the *Poisson marked point process* will be presented in chapters 3 and 4. Using this weighting strategy within this modelling framework, a *semi-automated* object extraction can be obtained, capable of finding solid object descriptions of objects in seismic data on the basis of *determinant properties* but without any prior knowledge.

Also, shown by practical application in this thesis is a strategy to run finite element computations over α-complexes, exploiting the relation between the α-complex and the underlying, embedding triangulation. To the author's knowledge, neither of these matters have been described in literature before. See [Ger98, GZT01] for more details. The authors point out and demonstrate how this can be used in geodynamic deposition/erosion models. Erosion and deposition are described by means of evolutionary maps and homeomorphisms. Evolutionary maps have never been applied to subsurface modelling before. Erosion and dilation are well understood morphological operators, but only on point sets, not on α-complexes.

The longer term perspectives and goal of creating a *virtual universe* (see figure 1–1 and table 1–1 and the Preface to this thesis) has come into closer reach now that the geometry and topology description can be solved in a satisfying manner using α-complexes.

1.7 Organisation of this Thesis

From this point on, this thesis is organised as follows. Chapter 2 introduces the fundamentals underpinning the notion of an α-complex. To that extent, it starts with the definition of a sample point pattern, or *point process*. Two related subdivisions, induced by the same point process appear to encode how the α-complex will develop with changing α and weight: the weighted Voronoi diagram and the corresponding regular triangulation. They will be discussed in chapter 2 too. The virtues of α-complexes will be described in the light of their application in natural object modelling. Next, chapter 3 merits the modelling process with α-complexes and sets forth the modelling framework, to be put to work in the cases to be worked out. Chapter 4 discusses one of the very cornerstones of the use of weighted α-complexes: the design of the weight set. Various weighting strategies will be explored. In chapter 4, the gearing mechanisms of weighting, based on the geometric and topological features of ball and sphere *configurations*, will be discussed. Modelling ingenuity is primarily embedded in the details of chapter 3 and 4. These chapters also illustrate how a theoretical model can be fit to the empirical sampling data point set, like a Gaussian curve to a histogram. Chapter 5 more formally seeks to explore the qualifications of α-complexes as a solid object description and as a formal representation scheme. It also gives an introduction to the treatment of the important subject of spatial occupancy and consistency. Chapter 6 shows α-complexes applied to practical problems in a number of tentative case studies in the earth sciences. It puts the developed modelling framework and weighted α-

complex-based icons to a test. Chapter 7 concludes this thesis. A number of open issues and aspects boiling down will be singled out as suggestions and directives for further research and collected in this chapter, too.

Annexes complete this thesis. Annex A recaptures the underpinning mathematical concepts. Part of the audience may want to read Annex A up front. Should this annex still leave too many aspects untouched or contain too many blind spots, then the reader is referred to the standard references given in there. Annex B contains a guide for the terminology practised in this thesis. A Nomenclature is also contained near the end of this thesis. It outlines the typesetting and the symbols used in the text. Checking out the Nomenclature is recommended. Next, annex C explains why the Laguerre distance, dominantly present in this thesis, is neither a measure nor a metric. Annex D describes guidelines for point set analysis and the verification of the Poisson null-hypothesis of point sets.

Chapter 2

Alpha complexes

2.1 Overview of this chapter

In this chapter, the concept of an α-complex will be introduced, along with its background, as far as instrumental given the scope and objectives of this thesis. The practical approach taken in this thesis rules out many mathematical complications, without loss of practical value. In the majority of the discussions, point set topology and regular triangulations tend to frame the mathematical context. An elementary example of an α-complex was already given in chapter 1, figure 1–3 and a "real data" example was given by figure 1–5.

This chapter starts, in section 2.2, with a description of the various spaces and sets in which and by which an object is represented in the process from sampling to the eventual α-complex model. Next, in section 2.3, the concept of an α-complex will be formalised, along with its "building blocks": the point process and the related subdivisions of space that such a point process introduces. The point process formalises the sampling data point set. Two related subdivisions, induced by the same point process appear to encode how the α-complex will develop with changing α and weight: the weighted Voronoi diagram and the corresponding regular triangulation. Moreover, these two subdivisions appear to be closely related. Once these two subdivisions have been discussed, the process of deriving the α-complex from the information provided by these two subdivisions can be treated.

Next, section 2.4 shows the basic effects of varying α and weight. Section 2.5 discusses how a family of α-complexes can be formed out of a single point set by variation of α. To study this aspect, three more concepts are needed. The simplicial complex, the skeleton and the power set. Every α-complex is also a simplicial complex. Section 2.5 therefore introduces the simplicial complex and skeletons drawn from the simplicial complex first, followed by the power set. These concepts allow proper classification of the faces to expect in an arbitrary α-complex.

After this exposure, section 2.7 will pay attention to some specific geometric features of the α-complex, such as holes, in all their topological variety. In modelling practices, many discussions turn out to be linked somehow to the presence or absence of holes. An α-complex can also be regarded as a (geometric) graph. This view will be presented in section 2.6 and the most important graphs related to the α-complex, the nearest neighbour graph and the local-furthest neighbour graph will also be discussed in this section. Finally, in section 2.8, combinatorial

aspects will be discussed.

2.2 Objects, sets and spaces

In this thesis, E^d shall denote a d-dimensional Euclidian space for some $d \geq 0$. An arbitrary dimensional space like this is also known as a *general dimension* space. Notation $\mathbb{E}^d$ refers to the set that covers space E^d. Sets and spaces are difficult to separate and when subtle differences do not matter, sets and spaces will be used interchangeably. The set of real numbers is commonly denoted as $\mathbb{R}$. Later on, when the issue of weighted points will be discussed, these two spaces will be combined in a space covered by the set of weighted points. Furthermore, space S will denote the *sample space* in which the *sampling data point set* $\mathbb{S}$ is represented. When associated with a point process, in a more morphological context, this set will also be denoted as the *set of landmarks*. Anonymous *topological spaces* will be denoted by X.

2.2.1 Sample space S

The observed sampling data point set $\mathbb{S}$, by which a physical object is sampled, is largely determined by the observation technique. In practice, for the locations, we mostly have that $\mathbb{S} \subset \mathbb{R}^2$ or $\mathbb{S} \subset \mathbb{R}^3$, i.e., members of $\mathbb{S}$ being defined by 2 or 3 spatial coordinates. From a mathematical point of view, we define $\mathbb{S}$ in general dimension, i.e., $\mathbb{S} \subset \mathbb{E}^d$. Single point space E^0 can be defined in the same way and sampling it takes no coordinates. A single point represents the entire space. We will see later that it yields a trivial null-triangulation and α-complex. $\mathbb{S}$ can also be an empty set, yielding another trivial triangulation and α-complex. More on this, in chapter 3. The set $\mathbb{S}$ is not necessarily defined in Cartesian coordinates. The members of $\mathbb{S}$ may for example be specified relative to one another, along spaces curves or in cylinder coordinates. More on this aspect in chapter 3.

The central role of $\mathbb{S}$ is that its members *generate* the triangulations, complexes and hulls of the object model. In a topological sense, sample points become the vertices of the triangulations. Points also act as a container (location) for property values in parameter spaces. The members of $\mathbb{S}$ are assumed to be in general position. When in general position, all positively oriented k-simplexes have a finite positive determinant and hence a positive (Lebesgue) measure for the length, area, volume, ... , d-volume.

An open set is denoted as $\mathring{\mathbb{S}}$, a closed set by $\bar{\mathbb{S}}$, and a set complement by $\mathrm{Compl}\,\bar{\mathbb{S}}$. The following further precisions and restrictions apply to sampling data point set $\mathbb{S}$ in this thesis:

(*i*) Set $\mathbb{S}$ is a finite compact set.

(*ii*) Set $\mathbb{S}$ is in general position.

(*iii*) Since assumptions are that $\mathbb{S}$ is compact and therefore closed, it always samples the complete boundary of the sampled object, which includes the internal boundaries.

If these preconditions are not fulfilled by the end of the sampling process, $\mathbb{S}$ has to be brought to meet these requirements in a data preparation step before the α-complex can be determined.

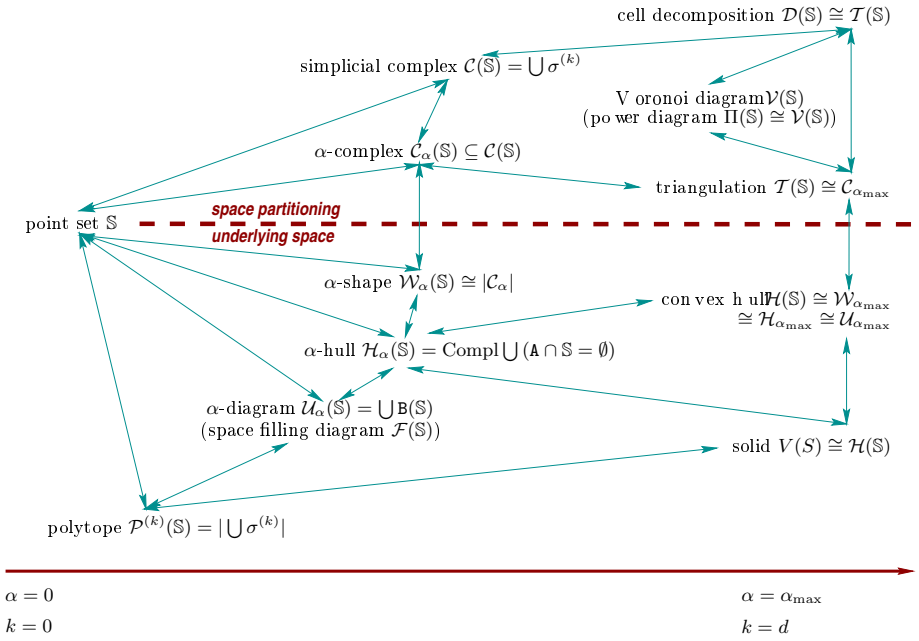

Figure 2–1: *relations between mathematical concepts discussed in this chapter. Upper part reflects space partitioning concepts, lower part the matching underlying space concepts. For clarity, tilde notations to denote weighting have been dropped. The relation of a polytope with α-diagram, α-hull and solid depends on the definition of a polytope. See Annex A.*

2.2.2 Topological space and its subdivision

A *topological space* with its subdivisions is a convenient notion to describe an α-complex, Voronoi diagram, or triangulation from a topological point of view. Topological spaces can be regarded as an abstraction of more concrete spaces like the Euclidean space. As it turns out later, in section 2.5.2, every α-complex is also a simplicial complex. The reverse is not true. Triangulations the way defined in this thesis are also instances of a simplicial complex. That is why the topological space of a simplicial complex is a convenient concept to study for instance how properties of set $\mathbb{S}$ set forth to properties of simplicial complexes *generated* or *spanned* by $\mathbb{S}$. The theory of simplicial complexes is wealthy and maturely developed [Cox73, Mun75, MS82, Mun84, Eng89]. Therefore, the relation with the simplicial complex will be exploited. Many of the α-complex' properties are obviously inherited from the simplicial complex.

A topological space has a (topological) dimension. Various such topological dimensions exist, but in this work, topological dimension will always be the *Čech–Lebesgue covering dimension*, denoted as $\dim X$. According to the *embedding theorem* (e.g., [Mun75, Nag83]), under certain conditions, a topological space can be embedded in Euclidian model space $M \subset E^d$. With what has been stated for sample space S, the following is immediate about the simplicial complex $\mathcal{C}(\mathbb{S})$:

(*i*) With $\mathbb{S}$ being finite and compact, $\mathcal{C}(\mathbb{S})$ will be compact too.

(*ii*) A compact $\mathcal{C}(\mathbb{S})$ can be embedded in a compact model space $M \subset E^d$.

With $\mathbb{S}$ being finite and compact in this thesis, its Voronoi diagram, triangulation, hull etc., will also be finite. Bounded by the convex space spanned by $\mathbb{S}$, Voronoi cells, d-simplices, etc., are all bounded, too. To indicate this and distinguish it from an *unbounded* subdivision, containing unbounded cells, some authors write $\mathcal{D}(\mathbb{S}) \bigcap \mathbb{S}$ rather than just $\mathcal{D}(\mathbb{S})$. In this thesis, some subdivision $\mathcal{D}(\mathbb{S})$ of topological space X, spanned by $\mathbb{S}$ shall be understood as a subdivision bounded by the convex hull of $\mathbb{S}$ and the notation $\bigcap \mathbb{S}$ is further discarded.

2.2.3 Model space M

In practice, 2-space E^2 (the XY-plane, say) and 3-space E^3 are among the most frequently encountered modelling spaces. Dimensions beyond three (*hyper spaces*) are mainly used to span parameter spaces, obtained by augmenting geometry with a parameter (sub-)space:

Definition 2.1 (parameter (or: property) space)
A parameter space is a subspace $R^m \subseteq E^d$ in which m parameters (or: properties) are located according to their values •

With $m = 2$, a parameter space may be seen as the familiar cross plot. Parameter spaces in general are in fact multi-dimensional crossplots. When attached to the geometric information, the whole of the augmented space is commonly denotes by the term *hyperspace*. Classical applications are encountered in *factor analysis*. Figure 1–6 in chapter 1 already illustrated its principle.

Observation 2.1 (property locations)
A precondition for the use of parameter spaces is that parameter values are defined in the sample points •

The hyper-spatial approach works in all dimensions equally well, but is compellingly more complicated to handle and visualise in higher-dimensions. In practice, hyper-spatial is always *low* hyper-spatial. Natural objects as considered in this work are inherently three-dimensional. For modelling and simulation purposes, two-dimensional object representations are sometimes convenient. Spatio-temporal spaces ($XYZt$, say) are used to describe dynamic models, including *time topology*. However spatio-temporal space is not Euclidian perse, due to cause-event-effect relations between temporal events. Further discussion is postponed to chapter 3.

In the previous chapter, the notion of an icon has been introduced. The icon is generally defined in some topological (hyper)space X whereas the instantiation for modelling purposes takes place in model space M, not necessarily hyper-spatial. For Euclidean spaces (refer to [Mun75, Mun84, Nag83, Eng89]), the dimension of a subspace $M \subset E^d$ also has dimension d, iff $\mathrm{Int}\, M \neq \emptyset$. A product space $M \subset E^d \times R$ has dimension: $\dim M \leq \dim E^d + \dim R$ and in practice $\dim M = d + 1$.

CLASS	in $\partial\mathcal{C}_\alpha$	in $\operatorname{Int}\mathcal{C}_\alpha$	$\exists\sigma^{(k+1)} : \sigma^{(k)} \in \sigma^{(k+1)}$
singular	$\surd$		no
regular	$\surd$		yes
interior		$\surd$	$k < d$

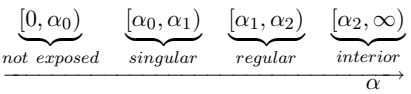

Table 2–1: *classification of the k-faces* $\{\sigma^{(k)}\}$ *of an* α*-complex in terms of singular, regular and internal faces. In general, a k-face goes through the intervals as indicated in the table. Faces need not become singular, faces may become regular or interior straight away upon becoming first* α*-exposed. For* α *sufficiently large, all faces have become either regular or interior.*

2.3 Alpha complexes

2.3.1 The Poisson point process

An α-complex is always based on (or: *generated by*) a point set. Sampling an object yields an empirical point set $\mathbb{S}$. In stochastic geometry, such point sets are usually referred to as *point processes*. Based on a point set $\mathbb{S} \subset \mathbb{E}^d$, say, in some arbitrary dimension $d \geq 0$, the point process $\Phi_{\mathbb{S}}(\mathbf{x})$ defines some spatial relation, empirical or in terms of probabilities, among the members of $\mathbb{S}$, and among arbitrary points $\mathbf{x} \in E^d$ and members of $\mathbb{S}$. For example, $\mathbb{S}$ may be a randomly distributed set of points in E^d, and the point process may formalise the distribution of distances among the members of $\mathbb{S}$ and between an arbitrary $\mathbf{x}$ and the nearest-by member of $\mathbb{S}$. In the context of morphology and point processes, the set of points $\mathbb{S}$ is usually called the set of *landmarks*, the role of which will be further explained in section 3.3.

One branch of stochastic geometry is concerned with the study of point patterns *generating* triangulations and tessellations [Hal88, SKM95, Møl94, BNKVL99, OBSC00]. This thesis addresses this type of problems applied to the input data set for weighted α-complexes. More precisely, the design of a weight set for a weighted α-complex, such that the level of geometric detail (or: resolution) can be controlled locally. A point process is called a *marked* point process (an *mpp* for short) if every point carries some value drawn from some *marker set* $\mathbb{V}$ embedded in *marker space* V. Often, the marker represents some geometric shape (typically, a disc, a rectangle, a sphere, etc.) of which the size is proportional to the marker value. This is the case in this work too: the marker value $w \in \mathbb{W}$, the *weight*, is represented by a (d)-ball of radius $\sqrt{w}$, giving the mpp $\Phi_{\tilde{\mathbb{S}}}(\mathbf{x})$. The set $\tilde{\mathbb{S}}$ is identical to set $\mathbb{S}$, but each of its members has now been assigned a marker: a real-valued weight $w \in \mathbb{W} \subset \mathbb{R}$. Set $\tilde{\mathbb{S}}$ so becomes the ordered Cartesian product $\tilde{\mathbb{S}} = \mathbb{S} \otimes \mathbb{W}$ with $\tilde{\mathbb{S}} \subset \mathbb{E}^d \times \mathbb{R}$. From a geometric point of view, a member $\tilde{s}_j \in \tilde{\mathbb{S}}$ can represented by a d-ball $\mathtt{B}_j$ of radius $\sqrt{w_j}$, centred in $\mathbf{s}_j$. Its *region-of-dominance* is bounded by a $(d-1)$-sphere $\mathtt{S}_j = \partial\mathtt{B}_j$, called the *weight-sphere*. Notice that the weights are generally not

independent. Among other things, we are interested in the *coverage* of space by the union of the interiors of these balls. Weight cannot be un-coupled from the underlying point process. As it turns out later, weighing is basically a *cover ageproblem*. Such an mpp is called a *cover age process*, for obvious reasons. If only the total coverageor non-coverage of space is of interest, then coverage processes are commonly indicated as *Boolean models* or more generally *germ-grain models* [Hal88, SKM95].

A *Poisson point process* (a *ppp* for short) is a point process of which the points are spaced according to a Poisson distribution with *intensity* λ, with λ defined as the number of events per unit of space. In 3D, for example, λ represents the number of points per unit volume. If sampling the process is invariant to shifting the sampling window, then the process is called *stationary* and if also invariant under rotation, the process in called *isotropic*. A point process that is stationary and isotropic is called a *homogeneous* process and *inhomogeneous* otherwise. Inhomogeneous ppp's cannot be characterised by a scalar λ; in that case λ is different everywhere in space: $\lambda = \lambda(\mathbf{x})$. Coverage processes can be studied as topological coverings, more precisely, as partitionings of space in non-overlapping partitions. See [Mun84] for details. Voronoi tessellations and triangulations are such space partitionings. Voronoi diagrams based on a ppp are sometimes called *Poisson Voronoi diagrams* and the corresponding triangulations *Poisson triangulations* (e.g., [OBSC00], Ch. 5).

2.3.2 The weighted Voronoi tessellation

In an "ordinary" first-order, Euclidean nearest-site Voronoi diagram (e.g., [Ede87, Aur87b]), the nearest neighbour distance is based on Euclidean metric. In the presence of weights, Voronoi cells are defined by *weighted distances*. To discriminate weighted from Euclidian distance, the former will be denoted by a tilde over the symbol. For two weighted points $\tilde{\mathbf{s}}_i, \tilde{\mathbf{s}}_j \in \tilde{\mathbb{S}}$, with $\tilde{\mathbf{s}}_i = (\mathbf{s}_i, w_i)$ and $\tilde{\mathbf{s}}_j = (\mathbf{s}_j, w_j)$, $L(\tilde{\mathbf{s}}_i, \tilde{\mathbf{s}}_j)$, $\mathbf{s}_{i,j} \in \mathbb{S}$, $\mathbf{w}_{i,j} \in \mathbb{W}$ (refer to figure 2–2), the Laguerre weighted distance is defined as:

$$L(\tilde{\mathbf{s}}_i, \tilde{\mathbf{s}}_j) = \langle \mathbf{s}_i - \mathbf{s}_j, \mathbf{s}_i - \mathbf{s}_j \rangle - (w_i + w_j) \tag{2–1}$$

where $\langle \cdot, \cdot \rangle$ denotes the standard inner-product. The Laguerre distance can also be written in the form: $L(\tilde{\mathbf{s}}_i, \tilde{\mathbf{s}}_j) = \|\mathbf{s}_i - \mathbf{s}_j\|^2 - (w_i + w_j) = \|\mathbf{s}_i\|^2 + \|\mathbf{s}_j\|^2 - 2\langle \mathbf{s}_i, \mathbf{s}_j \rangle - (w_i + w_j)$. Apparently, the Laguerre distance between two weighted points is equal to the squared Euclidean distance minus the sum of their weights, cf. figure 2–2. Spaces endowed with a Laguerre weighted distance are non-metric. Even if all weights are positive, some weighted distances may become negative. Moreover, if only one weight is chosen large enough, *all* weighted distances are negative. Let $L(\mathbf{x}_1, \mathbf{x}_2)$ denote a weighted distance between two of its points $\mathbf{x}_1$ and $\mathbf{x}_2$. As shown in annex C, L is not a symmetric bilinear positive definite form, because the condition $L(\mathbf{x}_1, \mathbf{x}_2) \geq 0$ does not hold for all points $\mathbf{x}_1$ and $\mathbf{x}_2$. This (rather technical) matter is further elaborated upon in Annex C.

A point that seeds a Voronoi cell is called a *nucleus*, to refrain from confusion with Voronoi vertices. In a Voronoi diagram generated by $\tilde{\mathbb{S}}$, all members of $\tilde{\mathbb{S}}$ become a nucleus, see figure 2–3, left picture. A weighted Voronoi diagramis then defined as follows:

Definition 2.2 (weighted Voronoi diagram)
A weighted Voronoi diagram is a partitioning of space into Voronoi cells: non-overlapping d-cells

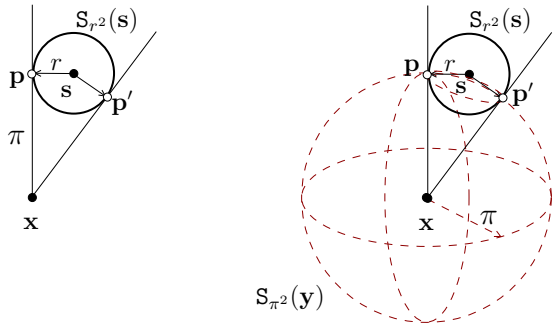

Figure 2–2: *left: Laguerre distance* $L(\tilde{\mathbf{s}}_1, \mathbf{x}) = \pi^2$ *of* $\mathbf{x}$ *with respect to* (1)*-sphere* $\mathtt{S}_{w_1}(\tilde{\mathbf{s}}_1) = \mathtt{S}_{r^2}(\tilde{\mathbf{s}}_1)$ *in* E^2*. Right: similar configuration in* E^3*;* $\mathbf{x}$ *has been assigned an orthogonal weight:* $\tilde{\mathbf{s}}_2 = (\mathbf{x}, w_2) = (\mathbf{x}, \pi^2)$ *intersects* $\tilde{\mathbf{s}}_1 = (\mathbf{s}, w_1)$ *exactly in* $\mathbf{p}$ *and* $\mathbf{p}'$ *and* $L(\tilde{\mathbf{s}}_2, \tilde{\mathbf{s}}_1) = \langle \mathbf{x} - \mathbf{s}, \mathbf{x} - \mathbf{s} \rangle - (\pi^2 + r^2) = 0$.

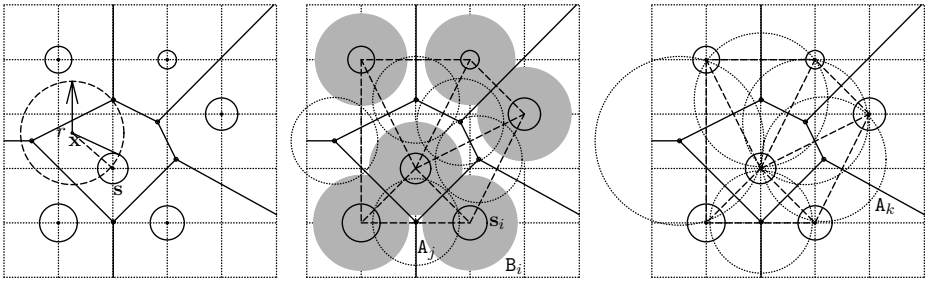

Figure 2–3: *Relations between weighted Voronoi diagram (solid), regular triangulation (dashed) and* α*-exposedness. Left:* $L(\mathbf{x}, \tilde{\mathbf{s}})$ *to the closest nucleus, equal to the squared radius of the dashed sphere. Centre: coverage* $\mathcal{B}$ *by gray weight-plus-alpha balls* $\mathtt{B}_i$ *on the vertices of* $\tilde{\mathbb{S}}$ *and the associated coverage* $\mathcal{A}$ *by dotted* α*-balls* $\mathtt{A}_j$ *in the radical centres. Right: local orthogonal* α*-balls* $\mathtt{A}_j^{\lozenge}$*.*

around the nuclei $\tilde{\mathbf{s}}_j = (\mathbf{s}_j, w_j)$ *composed of all those points* $\mathbf{x}$ *for which* $\tilde{\mathbf{s}}_j$ *is the nearest nucleus, in terms of weighted distance* •

In mathematical terms, a Voronoi diagram is built of k-faces: k-dimensional elements such as vertices, edges, etc. up to d-faces (or: *d-cells*). A k-face is denoted by $\sigma^{(k)}$. The bounding $(d-1)$-face separating one Voronoi cell from an adjacent cell is contained in the *radical plane* of the two nuclei and Voronoi vertices are at the intersection points of radical planes, called the *radical centres*. A radical plane $\mathtt{H}_{ij}^{\lozenge}$ of two weighted points $\tilde{\mathbf{s}}_i$ and $\tilde{\mathbf{s}}_j$ is a hyperplane consisting of points $\mathbf{x}$ at equal weighted distances to both weighted points: $L(\mathbf{x}, \tilde{\mathbf{s}}_i) = L(\mathbf{x}, \tilde{\mathbf{s}}_j)$, for all points $\mathbf{x}$ in $\mathtt{H}_{ij}^{\lozenge}$, see figure 2–4. Radical planes are generally *not* in general position and generally $\binom{d+1}{2}$ such planes intersect in a single 0-flat (point). Refer to table 2–2. If the weights of $\tilde{\mathbf{s}}_i$ and $\tilde{\mathbf{s}}_j$ are equal, $\mathtt{H}_{ij}^{\lozenge}$ perpendicularly bisects the edge $\tilde{\mathbf{s}}_i\tilde{\mathbf{s}}_j$. When unequal, $\mathtt{H}_{ij}^{\lozenge}$ still perpendicularly intersects $\tilde{\mathbf{s}}_i\tilde{\mathbf{s}}_j$, but not in the middle. Assume that nuclei have unequal weights but further grow at equal rate, e.g., proportional to α. Then radical centres are the last points of the Voronoi cell to be swept out by the growing nuclei. The associated growing nuclei reach their radical centre simultaneously.

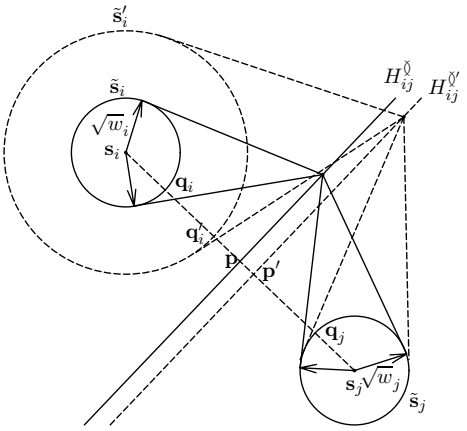

Figure 2–4: *the radical plane $\mathtt{H}_{ij}^{\emptyset}$ of two weighted points $\tilde{\mathbf{s}}_i = (\mathbf{s}_i, w_i)$ and $\tilde{\mathbf{s}}_j = (\mathbf{s}_j, w_i)$ intersects edge $\tilde{\mathbf{s}}_i\tilde{\mathbf{s}}_j$ halfway in $\mathbf{p}$ if $w_i = w_j$ (solid) and moves away from the middle if weights w_i and w_j change by unequal amounts (dashed). With $\mathbf{q} = \mathbf{s}_i + \mu(\mathbf{s}_j - \mathbf{s}_i)$ and $\delta^2 = \langle \mathbf{s}_j - \mathbf{s}_i, \mathbf{s}_j - \mathbf{s}_i \rangle$, $\mu_{\mathbf{q}_i} \leq \mu_{\mathbf{p}} \leq \mu_{\mathbf{q}_j}$. Furthermore, $\mu_{\mathbf{q}_i} = \mu_{\mathbf{p}} = \mu_{\mathbf{q}_j} = 0 \Leftrightarrow w_i = 0, w_j = \delta^2$ and $\mu_{\mathbf{q}_i} = \mu_{\mathbf{p}} = \mu_{\mathbf{q}_j} = 1 \Leftrightarrow w_i = \delta^2, w_j = 0$*

SPACE	E^1	E^2	E^3	E^4	$\cdots$	E^d
$\operatorname{card}\sigma^{(d)}$	2	3	4	5	$\cdots$	$d+1$
planes through $C^{\emptyset}$	1	3	6	10	$\cdots$	$\binom{d+1}{2}$

Table 2–2: *Combinatorial aspects of radical centres. The number of radical planes required to define a radical centre $C_{\emptyset}$ in E^d is given by $\operatorname{card}\sigma^{(d)}$, but generally, more radical planes pass through this centre (bottom row).*

Voronoi tessellations are often studied in combination with ball unions. Also in this thesis. After all, a Voronoi tessellation can be constructed by a growing ball union $\mathcal{B} = \bigcup \mathtt{B}_i$ centred in the nuclei $\mathbf{s}_i$ from which all the overlap has been removed and alternately, by a ball union $\mathcal{A}$ of α-balls $\mathtt{A}_j$ in the radical centres. With balls $\mathtt{B}_i$ growing proportional to α^2, the corresponding balls $\mathtt{A}_j$ shrink at a rate proportional to α^2, until $\mathtt{A}_j$ is just a point (zero-radius ball) when $\mathtt{B}_i$ sweeps out the radical centre at which $\mathtt{A}_j$ is centred. Both of these coverage processes can be seen in figure 2–3, central picture. In this thesis, the focus will be on $\mathcal{B}$. Figure 2–5 demonstrates this sweeping process of coverage $\mathcal{B}$ in greater detail, for increasing α.

What relates a family of growing balls to a corresponding family of α-exposed faces is the notion of a (geometric realisation of a) nerve $\mathcal{N}(\tilde{\mathbb{S}})$. Defining the balls as subsets of $\mathbb{E}^d$, $\mathcal{N}(\tilde{\mathbb{S}})$ contains a k-face connecting $k+1$ weighted points if the $k+1$ subsets have a common intersection.

DEFINITION 2.3 (NERVE)
Let Y be a cover of E^d. Then the nerve $\mathcal{N}_{rv}Y$ is an abstract simplicial complex composed of the collection of non-empty intersections of subsets of cover Y •

See e.g., [Mun84]. In other words, as soon as two balls touch, they become connected by an edge

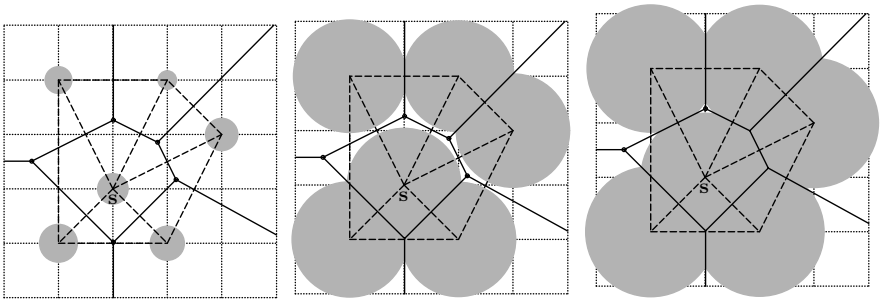

Figure 2–5: *Voronoi cell swept by growing weight-plus-α-balls $\mathtt{B}_j$. The Voronoi is shown by the solid lines. The size and the union of the gray weight-plus-α-balls $\mathtt{B}_j$ increases left to right, with $\alpha = 0$ in the left picture. Observe in the central picture, that only one of the five radical centres (Voronoi vertices) has been swept out.*

and as soon as three balls intersect in a common point they become connected by a triangle, etc. This means that in figure 2–5 no triangles are formed in the left picture, one (dashed) triangle is formed in the central lower part of the central picture (generated by the three lowest $\mathtt{B}_j$) and that in the right picture, all triangles are formed, except the leftmost and the topmost. The leftmost radical centre is in this case the last one to be swept out, which can be verified by noticing that the corresponding radical α-ball $\mathtt{A}_j^{\emptyset}$ takes the highest α-value, as indicated in the right picture of figure 2–3. Observe that *any* pair of intersecting balls also forms a Voronoi edge, as any pair of balls (intersecting or not) has a radical plane. See figure 2–5. As shown by Edelsbrunner in [Ede92, Ede93]:

OBSERVATION 2.2 (GEOMETRIC NERVE OF THE WEIGHTED VORONOI DIAGRAM)
The geometric realisation of the nerve of the ball union $\mathcal{B}$ associated with weighted Voronoi diagram is the regular triangulation •

With variable size balls, the nerve varies as well: with $\mathbb{X}_2 \subseteq \mathbb{X}_1$:

OBSERVATION 2.3 (NERVE CONTAINMENT OF A SUB-COVER)
If a set $\mathbb{X}_1$ is contained in the nerve of a cover Y, then so is its subset $\mathbb{X}_2$ •

and, referring to [Ede92, Ede93] for details:

OBSERVATION 2.4 (NERVE OF THE BALL UNION AND α-COMPLEX)
The geometric realisation of the nerve of the growing ball union sweeping the weighted Voronoi cells is an α-complex, a subcomplex of the regular triangulation •

Here is the very essence of the relation of a coverage by a ball union $\mathcal{B}$ of weight-plus-alpha balls $\mathtt{B}_j(\mathbf{s}_j)$ and the resulting α-complex. The event of two balls touching, so forming an edge in the nerve happens to coincide with the event of that edge becoming α-exposed (dashed spheres in right picture figure 2–3). Edelsbrunner in [Ede93] showed this duality and also showed that a deformation-retraction can be formulated that takes the family of ball unions onto the α-family. This duality relation will be exploited in the weighting strategy described in chapter 4. It reduces introducing or removing vacancies from α-complexes to a coverage-by-weight problem,

also known as the *space filling problem* ([Ede92]). Changing weight *independently* brings about local changes in the ball of the nucleus and in the radical planes of the nucleus with its neighbours and therefore in the Voronoi cells of the nucleus and its neighbours. If the ball radius changes, then consequently the α-exposedness of the corresponding edge in the triangulation changes.

2.3.3 Regular triangulation

Associated to the weighted Voronoi diagram is the *regular triangulation*. What sets off a regular triangulation from a Delaunay triangulation is the notion of weights. A *weighted* sampling data point set induces a *weighted* triangulation ([Aur87b, Lee91, Ede92]). Every finite point set can be triangulated in finitely many ways. Within this family of triangulations, some triangulations are preferred over others. The preferred triangulation discussed inhere is the regular triangulation. Formally a d-triangulation is defined as follows:

DEFINITION 2.4 (d-TRIANGULATION)
A d-triangulation of some topological d-space X is a partitioning of that space into non-overlapping d-simplices •

The term triangulation is not restricted to subdivisions in E^2 and indeed, a d-triangulation in this context can be in any dimension. As such, it is obviously also a *cell(ular) decomposition*, as figure 2–1 reveals. The intersection of two simplices, if non-empty, is also a face of the triangulation, along with all its subfaces.

A regular triangulation is determined by two criteria: firstly, *regularity* of each of its constituting k-faces and secondly, *orthogonality*. Regular triangulations are associated with the notion of *regularity* and regular simplices:

DEFINITION 2.5 (REGULAR SIMPLEX)
A d-simplex in a triangulation is said to be regular if all vertices not *belonging to the simplex have positive weighted distance to each of the $d+1$ vertices in the simplex* •

If a point in $\mathbb{S}$ has negative distance with respect to another member of S, it cannot take part in the regular triangulation; it is ruled out as redundant:

DEFINITION 2.6 (REDUNDANT POINT)
A sample point not fulfilling the regularity criterion is classified as redundant •

This gives rise to the following observations:

OBSERVATION 2.5 (COINCIDING POINTS)
Regarding the sphere around a weighted point as its region of dominance, *and realizing that a point with negative weighted distance must be located in that sphere, a redundant point may be regarded as a generalisation of two zero-weight points that coalesce* •

OBSERVATION 2.6 (ZERO-IMPACT OF REDUNDANT POINTS)
Redundant points cannot take part in a regular triangulation and as a consequence, with $\tilde{\mathbf{s}}_j$ a redundant point, the regular triangulation $\mathcal{T}(\mathbb{S} - \{\tilde{\mathbf{s}}_j\})$ of $\mathbb{S} - \{\tilde{\mathbf{s}}_j\}$ is equal to $\mathcal{T}(\mathbb{S})$.

Orthogonality is defined as follows:

DEFINITION 2.7 (ORTHOGONAL SPHERES)
Two spheres are said to meet orthogonally (or: be orthogonal) if they intersect at a $90°$ *angle* •

Figure 2–6 illustrates this for a pair of spheres in a 2-space, but in fact this holds true for spheres of any dimension, even for 0-dimensional spheres (points). In figure 2–6, left picture, two such intersection points $\mathbf{p}$ and $\mathbf{p}\prime$ exist for spheres $\mathtt{S}_{w_1}(\tilde{\mathbf{s}}_1)$ and $\mathtt{S}_{w_2}(\tilde{\mathbf{s}}_2)$ in E^2. These points coincide if and only if the radius of one of the spheres is zero, i.e., when one of the spheres is a point located exactly on the other sphere.

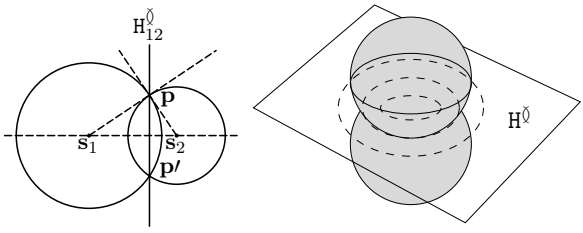

Figure 2–6: *left: two spheres in 2-space* E^2 *that meet orthogonally. The line passing through the two intersection points* $\mathbf{p}$ *and* $\mathbf{p}\prime$ *is called the radical plane. Any third sphere orthogonal to both spheres has its centre on this radical plane* $\mathtt{H}^{\emptyset}_{12}$*. Right: two spheres in* E^3*. The dashed circles that lie in the "glass" radical plane are equi-distant lines with respect to both spheres.*

OBSERVATION 2.7 (DIMENSIONS AND RATIO'S ORTHOGONAL SPHERES)
The intersection points of two orthogonal spheres in E^2 *constitute a pair of triangles, of which the sides are given by the Euclidean distance between the two centres, the radius of one sphere and the radius of the second, orthogonal sphere.*

For two 2-spheres in E^3, infinitely many such intersection points exist, because there are infinitely many pairs of orthogonal tangential support planes. All these intersection points lie on a circle contained in the radical plane (figure 2–6, right picture). In E^d, this generalises straightforwardly.

OBSERVATION 2.8 (ZERO EQUI-DISTANT SPHERE)
Two orthogonal $(d-1)$*-spheres in* E^d *intersect in a* $(d-2)$*-sphere* $\mathtt{S}_0$*, contained in the* $(d-1)$*-radical plane. The* $(d-2)$*-sphere* $\mathtt{S}_0$ *is the set of all points in the radical plane with zero-distance with respect to both orthogonal spheres.*

In fact the regularity and orthogonality criteria come together in the following: for each k-face in a regular triangulation there exists an empty $(d-1)$-sphere, that orthogonally intersects the weight spheres of all vertices of the face, and so that all other vertices not belonging to that face have non-negative weighted distance to each of the vertices of the face (regularity). Notice the conjunction of the orthogonality criterion with the α-exposedness: once α is high enough to erect such a sphere, the face mentioned above becomes α-exposed. For $\alpha \to \infty$, all such spheres can be created, and $\mathcal{N}(\tilde{\mathbb{S}})$ grows into triangulation $\mathcal{T}(\tilde{\mathbb{S}})$ of $\tilde{\mathbb{S}}$. Also notice that by definition, such spheres must be located in the radical centres, to obtain orthogonal intersection. With $\mathbb{S}$ being finite and a bounded α-complex, α will not go to ∞, but reach a maximum value $\alpha_{\max}$ beyond which no new faces will become α-exposed anymore, and the α-complex is identical to the triangulation.

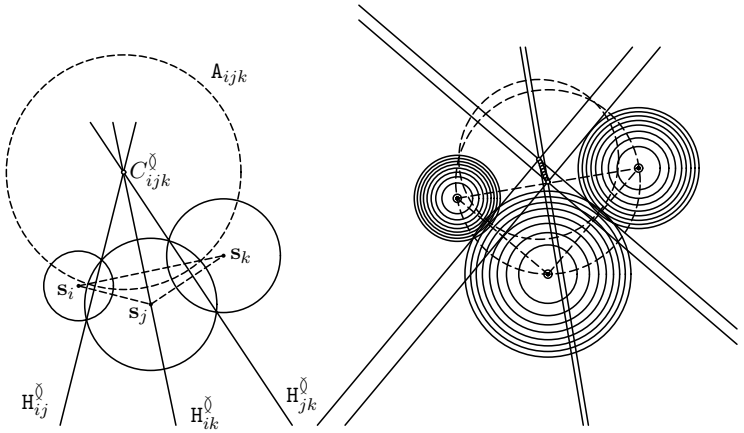

Figure 2–7: *left: radical planes* $\mathtt{H}^{\emptyset}$ *of three weighted points in* $\mathbb{E}^2$ *that meet in a radical centre* $C^{\emptyset}_{ijk}$*. The real ball* $\mathtt{A}^{\emptyset}_{ijk}$ *(dashed) is empty and the dashed triangle will be contained in the triangulation. Right: regular triangulation of three vertices decaying into a zero-weight Delaunay triangulation. The radical plane moves as the weights change and so does the radical centre (open dot). For clarity intermediate radical planes and* α*-balls are not shown.*

Delaunay triangulations can be regarded as zero-weight regular triangulations, which is easily understood if one realizes that if weight decays to zero, the local Delaunay criterion of $d+1$ vertices lying on a common $(d-1)$-sphere with no point lying in its interior, complies precisely to the regularity and orthogonality criterion. Without dwelling on mathematical details, this fact is demonstrated in figure 2–7, right picture. In this figure, three pencils of concentric spheres are visible, depicting three weighted points of which the weight varies from some maximum value down to zero-weight. While the weight decreases down to zero, the radical centre traverses the path indicated by the small open dots until located in the intersection of the perpendicular bisecting radical planes, corresponding to the Delaunay triangulation. Figure 2–7 also shows the movement of the radical plane and the α-ball (start and end situation are displayed). The final α-ball corresponds to the circumscribing Delaunay ball. The triangulation in this case is a trivial

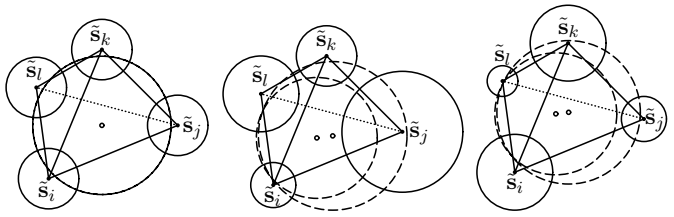

Figure 2–8: *applying local criterion to find the regular triangulation. Left: switching diagonals is irrelevant in this case; the two empty real orthogonal* α*-balls coincide and the weighted distances along solid and dotted diagonals are equal. Centre: flipping diagonals is now required to restore the local criterion. Right: criterion is fulfilled and flipping would breach the local criterion.*

one and is not influenced by the changing weight.

Edelsbrunner and Shah in [ES96] showed that like for the Delaunay triangulation, a local criterion can be applied to obtain a globally preferable triangulation. Figure 2–8 shows an instance. In the left picture, switching does not change the meeting of the criterion, as both diagonals have equal weighted norms. In the central picture the balanced situation of the left picture has been perturbed by increasing the weight of $\tilde{\mathbf{s}}_l$ and $\tilde{\mathbf{s}}_j$. Flipping diagonals is now required to restore the local criterion, because orthogonal α-ball $\mathtt{A}^{\emptyset}_{ikl}$ (dashed) is not empty. The (also smaller) orthogonal α-ball $\mathtt{A}^{\emptyset}_{ijk}$ is empty and so is α-ball $\mathtt{A}^{\emptyset}_{jkl}$. In the right picture, weight is distributed such that the criterion is fulfilled and flipping would only violate the local criterion. Examine the impact of weight changes on the triangulation.

2.3.4 Weighted α-complex

Earlier in the section, the relation between a growing ball union and the α-complex has been discussed, and the role of the nerve therein. The fact that the faces of the α-complex are also found in the triangulation of the same point set, suggests that an α-complex can also be obtained from that triangulation *by filtration*, and indeed, such approaches have been proposed [Ede92, Mue93, EM94]. Triangulations and α-complexes are instances of the much wider class of simplicial complexes to be introduced in section 2.5. An *α-complex* $\mathcal{C}_\alpha(\mathbb{S}) \subseteq \mathcal{C}$ is a subcomplex of the simplicial complex $\mathcal{C} \cong \mathcal{T}(\mathbb{S})$ formed by a triangulation $\mathcal{T}$ of the point set $\mathbb{S} \subset \mathbb{E}^d$. $\mathcal{C}_\alpha$ is not just any subcomplex drawn from $\mathcal{C}$. Rather, $\mathcal{C}_\alpha$ can only result from an *α-filtration* let $\mathbb{F} = \{\mathtt{F}^{(k)}\}$ be the set of k-faces (in this case: k-simplices) of $\mathcal{C} \cong \mathcal{T}$, with $0 \leq k \leq d$. Then the faces $\mathbb{F}_\alpha = \{\mathtt{F}^{(k)} | \mathtt{F}^{(k)} \in \mathcal{C}_\alpha\}$ of $\mathcal{C}_\alpha$ are those faces of $\mathbb{F}$ that are *α-exposed* for a given value $\alpha \geq 0$. All α-exposed faces pass the filtration, those that are not α-exposed do not. Firstly, observe that apparently $\mathbb{F}_\alpha \subseteq \mathbb{F}$, in other words, the α-complex is completely erected by faces also found in the triangulation. Secondly, a more concise definition is needed of α-exposedness. Assume an α that monotonically increases from zero towards infinity. A face $\mathtt{F}$ becomes α-exposed for some α-value if an empty $(d-1)$-sphere exists of radius $\sqrt{\alpha}$, that intersects all weighted points $\tilde{\mathbf{s}}_j$ of $\mathtt{F}$ orthogonally (e.g., [Coo16, Max52, Ede93, Bix94]), in accordance with the regularity criterion. This leads to the following definition of a weighted α-complex that will be further adhered to in this thesis:

DEFINITION 2.8 (WEIGHTED α-COMPLEX)
Given a weighted point set $\tilde{\mathbb{S}}$ and a real value $\alpha \geq 0$. A weighted α-complex $\mathcal{C}_\alpha(\tilde{\mathbb{S}}) \subseteq \mathcal{C}$ *is a subcomplex of the simplicial complex $\mathcal{C} \cong \mathcal{T}(\tilde{\mathbb{S}})$ formed by a regular triangulation $\mathcal{T}$ of $\tilde{\mathbb{S}}$ containing all k-faces of the triangulation that pass the α-filtration for the given value of α* •

Also, refer to [Lee91]. The spatial occupancy by an α-complex is called an *α-shape* and an α-complex is in fact a triangulated α-shape. If the partitioning of the underlying space is irrelevant, α-shape can also be read where α-complex is written. Varying α defines a finite ordered family of α-complexes, called *α-family* $\mathbb{A}$. The point set is the lower extreme member of that family, the triangulation the upper extreme α-complex and the corresponding convex hull the equivalent α-shape.

Back to the process of α-filtration. All topological spaces discussed in this thesis shall be *triangularizable*, a bold term with the simple meaning that it admits one or more triangulations. More details on triangularizability can be taken from [Sha77], for example. More in particular,

every convex polyhedron can be triangulated (e.g.,[Mun84]), and being a polyhedron, every convex polytope can so too. They are triangularizable topological spaces. For example, every convex hull, a convex polytope, is triangularizable with every k-simplex, $0 \leq k \leq d$ again a convex hull and polytope. All that the notion of an α-complex adds to a triangulation is a *parametrisation by* α acting as a *filtration*, no new faces. See figure 2–12. The following observation follows immediately from definition 2.8:

OBSERVATION 2.9 (EMBEDDING $\mathcal{C}_\alpha(\mathbb{S})$ IN $\mathcal{T}(\mathbb{S})$)
Each α-complex "filtered" from $\mathcal{T}$ is again embeddable in the topological space $\mathcal{T}$ •

2.4 Varying alpha and weight

2.4.1 The domain of α and w

There are no compelling mathematical reasons to restrict the domain of either α or w. From a modellers' perspective, there is, however. For convenience, assume that all weight are zero. As soon as α drops into negative values, the underlying triangulation is no longer the nearest site triangulation, but flips to the furthest site triangulation. The same holds for the dual Voronoi diagram. From a modellers' perspective, this is often *counter-intuitive*. Instead of attracting one another, points become repulsive. For this simple practical reason, negative α's are disregarded in this thesis.

The situation with negative weights is quite different. Again from a modellers' perspective, negative weight is an important tool to slow down or *demote* the pace of growth of an α-complex in certain areas, as α increases. A negative weight can shift the entrance of certain k-faces in the α-complex to higher values of α. Negative weight, increasing the weighted distance, has to be compensated for by an equal-magnitude positive value of α first. Negative weights will be discussed in greater detail in chapter 4. The various aspects involved in the definitions of the domain of α and w are displayed in table 2–3.

2.4.2 The relation between weight and distance

The effects of weight and α add up. More precisely, weight acts as a bias to α. Weight and distance come together in a weighted distance. Weighting can be regarded as being equivalent to a geometric transformation ([Ede92]). Looking at the definition of the Laguerre distance, obviously adding positive weight decreases distances. So, in a neighbourhood of high weights, points tend to connect more easily than in neighbourhoods with lower weights. Increasing α means larger distances can be abridged, larger weight means a decrease of weighted distances or, equivalently, a bias to the starting value of α. Figure 2–9 shows the various parameters in play. Experiment 2.1 and figure 2–10 shows how a similar α-complex can be created with a zero-weight and a zero-alpha α-complex. In other words the effect of a certain α can be completely replaced by the equivalent effect of weight, as already pointed out by Edelsbrunner in [Ede92].

EXPERIMENT 2.1 (INTER-CHANGEABLE EFFECT OF DISTANCE AND WEIGHT)
Given an initially regularly spaced zero-weight point set in E^2. The original lattice (or: grid) is depicted in figure 2–10, right picture. For this point set, there exists a $0 \leq \lambda \leq 1$ and an $\alpha \in [\alpha_1..\alpha_2]$, with $0 \leq \alpha_1 \leq \alpha_2 \leq \lambda\alpha_{\max}$, such that the α-complex for that α is similar to a graph

	$\alpha \in [0, \infty]$	$\alpha \in [-\infty, \infty]$
Zero-weigh t	- *null*-spheres - nearest neighbours - irregularly spaced only Mucke (1993), Edelsbrunner and Mucke (1994)	- *null*-spheres - furthest/nearest neighbours - irregularly spaced only Edelsbrunner et al. (1983), Edelsbrunner (1987)
$w \in [0, \infty]$	- r-spheres - no demotion of points - irregularly/regularly spaced - nearest neighbours	- i-spheres - no demotion of points - irregularly/regularly spaced - furthest/nearest neighbours
$w \in [-\infty, \infty]$	- i-spheres - promotion/demotion of points - irregularly/regularly spaced - nearest neighbours Gerritsen (1998), Gerritsen et al. (2000,2001)	- i-spheres - promotion/demotion of points - irregularly/regularly spaced - furthest/nearest neighbours Edelsbrunner (1992,1993)

T able2–3: *aspects related to the domain choices for* α *and* w. *The term* i*-spheres refers to* imaginary *spheres, with imaginary radius, to be discussed in chapter 4.*

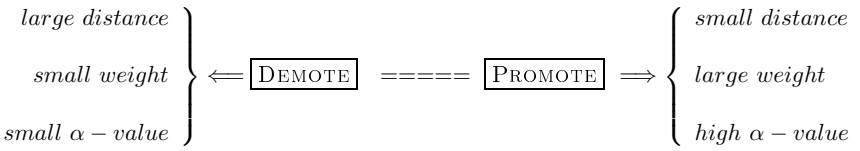

Figure 2–9: *the various parameters acting upon an α-complex. At the left, the "demoters", at the right the "promoters".*

4-connecting all nearest neighbours. In other words: the α-complex looks similar to the lattice itself. Observe that all 2-balls are equally large, fully determined by the magnitude of α. Next, the outer points (remote from the centre) are translated outwards (see left picture), such that for the same value of α, a 1-skeleton α-complex *remains as in the left figure. In this geometric transformation, weights remain zero. Points that moved under the transformation have become unconnected from the remaining 1-skeleton and the skeleton contains exactly those points that were map on their original locations.*

Now, let us revert to the original point set, located on the original lattice in the right figure. Weight of the same magnitude as α above, is now assigned to the point that were not moved and zero to the ones that moved (right picture). As figure 2–10 shows, the same α-complex is formed. The figure shows the similar and inter-changeable effect of α and weight: $\mathcal{C}_{\alpha=w}(\mathbb{S} \otimes \mathbb{W}|_{w_i=0}) = \mathcal{C}_{\alpha=0}(\mathbb{S} \otimes \mathbb{W}|_{w_i=\alpha})$ •

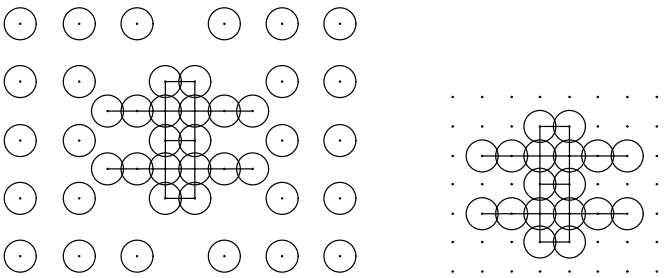

Figure 2–10: *result obtained from experiment 2.1. left: irregularly spaced but equally weighted points, right: regularly spaced, but unequally weighted points. Spheres represent weight; same size means same weight. Points with no spheres (right) have zero weight. The α-complex here is a 1-skeleton ("wire-frame"), the effect however, can be generalised.*

It is precisely this possibility to substitute distance for weight v.v., that sets forth a hyper-spatial approach to shape reconstruction on the basis of observed physical properties in the sample points. Equivalent classes of properties lead to to equivalent classes of weight. In parameter space, equivalent classes of properties tend to cluster naturally based on distance information and distinct clusters in parameter space naturally leads to distinct weights. This aspect will be further elaborated upon in chapter 4. Also, revisit figure 1–6.

The big difference between α and w is that weight is "static", whereas the α-value has a "dynamic" nature. More precisely, weight acts upon the regular triangulation during its creation

and its effect is "staticly" reflected in that triangulation. Its effect is fixed, once this triangulation has been generated. In contrast, the role of α does not cease with the triangulation process, but lies in the α-filtration process, afterwards. It is this varying of the α-value that delivers the α-family.

2.5 Families and faces

2.5.1 Familiar faces

It is of utmost importance to understand which of the faces of a triangulation may be encountered under what conditions in an α-complex. Most and for all to understand the topological features of an α-complex. The exact topology has great consequences for aspects, such as numerical modelling and conversions. To study this aspect, three more concepts are needed. The simplicial complex, skeletons and power set.

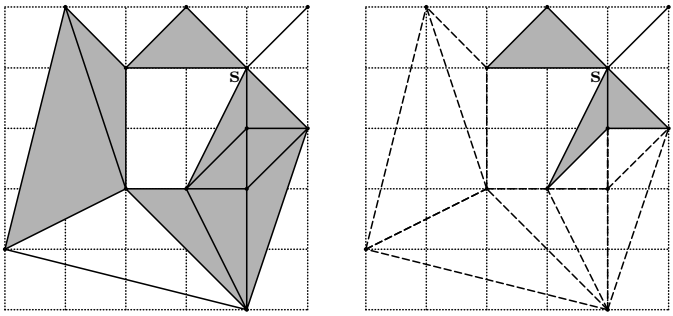

Figure 2–11: *left: a simplicial complex consisting of the grayed triangles plus the solid edges. Right: the (closed) star $\bar{St}$ s subcomplex of the simplicial complex, made up by the gray closed triangles plus the solid edges emanating from* **s**.

2.5.2 Geometric simplicial complexes

Simplicial complexes were already silently introduced in the preceeding part of this chapter. A more structured discussion follows in this section. A simplicial complex is an important and fairly well understood mathematical construction. Inhere, a simplicial complex is basically a *geometric simplicial complex*, as opposed to an *abstract simplicial complex* (e.g., refer to [Mun75, Mun84]). Consider again a triangulation of a finite compact point set. A triangulation in this context, is also a simplicial complex. But the class of simplicial complexes is much wider than the class of triangulations. Moreover:

Definition 2.9 (simplicial complex)
A finite geometric simplicial k-complex $\mathcal{C}(\mathbb{S})$ in E^d is a connected or unconnected collection of simplexes, with $0 \leq k \leq d$, all satisfying two properties:

(*i*) *Every subface of a each simplex needs to be a simplex contained in the complex too.*

(*ii*) *The shared subfaces (in the intersection of any two simplices) needs to be a simplex in the complex too* •

It is basically composed of members of $\mathbb{S}$ plus a collection of closed faces with members of $\mathbb{S}$ as vertices. Faces are *not* necessarily those also found in the regular triangulation. See for instance figure 2–11, containing faces not complying to the local criterion.

OBSERVATION 2.10 (FINITENESS)
A triangulation of a finite compact set $\mathbb{S}$ has finitely many d-simplices all with finitely many subfaces and out of this collection of faces, finitely many simplicial complexes can be created •

DEFINITION 2.10 (SUBCOMPLEX)
A subcomplex is any part of a complex that is itself a complex •

It can be shown (e.g., [Mun84]) that if the simplicial complex is finite (which is always the case in this work), the underlying space is compact and so are its subcomplexes. A simplicial complex may degenerate to a linear graph or point set. One specific subcomplex applied in chapter 4 is the *star of a vertex* $\mathbf{s}_j$:

DEFINITION 2.11 (CLOSED STAR)
The close dstar $\overline{St}\,\mathbf{s}_j$ (or simply: $St\,\mathbf{s}_j$) of vertex $\mathbf{s}_j \in \mathcal{C}(\mathbb{S})$ is the subset of all closed faces of $\mathcal{C}$ incident upon $\mathbf{s}_j$ •

See figure 2–11. The notion of stars generalises to general dimension. For further details, see [Mun84, Eng89]. Further observe:

OBSERVATION 2.11 (SHARED FACES AND STARS)
Faces incident upon two vertices are found in the intersection of their stars •

2.5.3 Skeleton

A k-skeleton is related to a subcomplex of a simplicial complex in the following manner:

DEFINITION 2.12 (k-SKELETON OF A SIMPLICIAL COMPLEX)
A k-skeleton $\mathcal{K}^{(k)}$ of a simplicial complex is a subcomplex composed of all the k-faces and their subfaces •

For instance, the 0-skeleton of a simplicial complex $\mathcal{C}(\mathbb{S}) \cong \mathcal{T}(\mathbb{S})$ is point set $\mathbb{S}$, and the 1-skeleton of the triangulation is a spanning, connected linear graph containing $\mathbb{S}$ and the nearest neighbour graph, to be discussed in section 2.6.

2.5.4 Power set $2^{\mathbb{S}}$

A power set is a suitable notation for a closed collection of proper subsets. For example in the following reasoning. The set of faces $\mathbb{F}$ created during triangulation of $\mathbb{S}$ is finite and well (but not necessarily uniquely) defined. Out of these faces, a finite set $\mathbb{C}$ of simplicial complexes can be created. Assume a simplicial complex $\mathcal{C} \in \mathbb{C}\backslash\{\mathcal{T}\}$, so not identical to the triangulation. Then

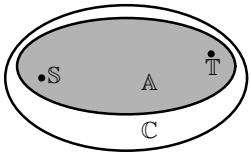

$\mathbb{A} = \{\mathcal{C}_\alpha(\mathbb{S})\}$ set of α-complexes
$\mathbb{C} = \{\mathcal{C}(\mathbb{S})\}$ set of simplicial complexes
$\mathbb{S}$ set of generating points
$\mathbb{T} = \{\mathcal{T}(\mathbb{S})\}$ set of triangulations

Figure 2–12: *set relations between faces of α-complex and triangulation. All members of $\mathbb{A}$ can be obtained by appropriate α-filtration from the set $\mathbb{F}$. For consistence, set $\mathbb{T}$ is the set of triangulations of $\mathbb{S}$ with generally one, but possibly multiple triangulations. Multiple triangulations (e.g., due to degeneracies) lead to multiple families in $\mathbb{A}$.*

the set of k-faces constituting each of these complexes $\mathcal{C}$ is a member of the power set of $\mathbb{F}$ in the following sense:

$$\{\sigma_{\mathcal{C}}^{(k)}\} \subseteq \mathbb{F}^{(k)} \in 2^{\mathbb{F}^{(k)}} \subseteq 2^{\mathbb{F}} \tag{2–2}$$

where notation: $2^{\mathbb{F}}$ denotes a *power set of* $\mathbb{F}$. A power set is defined by the following definition in which it is important to notice the term *proper*:

Definition 2.13 (power set)
A power set $2^{\mathbb{S}}$ of $\mathbb{S}$ is the set of all proper subsets that can be drawn from $\mathbb{S}$ •

Example 2.1 (vertices power set member)
The set of vertices $\{\sigma^{(0)}\} \subseteq \mathbb{F}^{(0)}$, contained in a $\mathcal{C} \in \mathbb{C}\backslash\{\mathcal{T}\}$ is a subset of $\mathbb{S}$. If its cardinality $\operatorname{card}\{\sigma^{(0)}\} < \operatorname{card}\mathbb{S}$, *the subset belongs to the power set of $2^{\mathbb{S}}$ of $\mathbb{S}$, which in turn is a member of the power set $2^{\mathbb{F}}$* •

Among the faces of the triangulation are all faces of any possible α-complex that can be generated by $\mathbb{S}$. Faces not contained in $\mathbb{F}$ are not encountered in the α-complexes. So for the faces of an arbitrary α-complex, including the triangulation itself, one may state:

$$\{\sigma_{\mathcal{C}_\alpha}^{(k)}\} \subseteq \mathbb{F}^{(k)} \in \left(2^{\mathbb{F}^{(k)}} \bigcup \mathbb{F}^{(k)}\right) \subseteq \left(2^{\mathbb{F}} \bigcup \mathbb{F}\right) \tag{2–3}$$

For the power set of faces of a triangulation, this leads to a hierarchy as in figure 2–13.

2.5.5 Singular, regular and interior faces

We are now in a position to give a classification of the faces of an α-complex, already displayed in table 2–1. It is convenient to define the minimum and maximum α-values for which the α-complex is unequal to one of the trivial extremes: the point set and the triangulation :

Definition 2.14 ($\alpha_{\min}$ and $\alpha_{\max}$)
The smallest α of the smallest α-complex other than the point set $\mathbb{S}$ is termed $\alpha_{\min}$, the smallest α for which the α-complex is identical to the triangulation is termed $\alpha_{\max}$ •

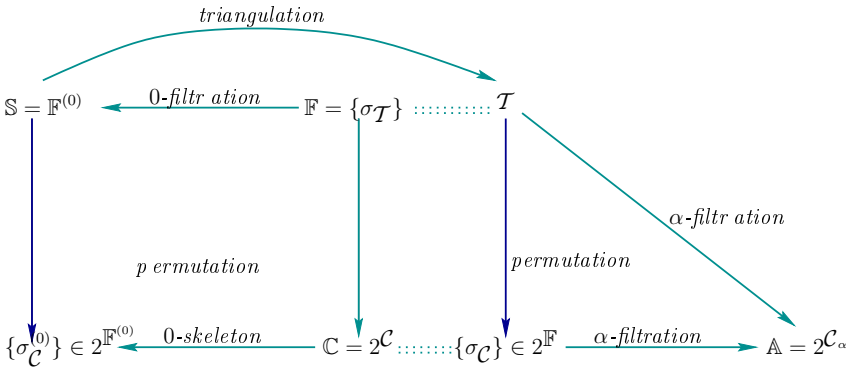

Figure 2–13: *hierarchy diagram of the power sets of k-faces of a triangulation.*

OBSERVATION 2.12 ($\alpha_{\min}$ AND $\alpha_{\max}$)
Generally, $\alpha_{\min} \neq 0$ and $\alpha_{\max}$ is finite. Further observe that $\alpha_{\min}$ is the α-value for which the first one or more edges become α-exposed and $\alpha_{\max}$ is the α-value for which the last d-face becomes α-exposed.

With α growing from $\alpha_{\min}$ to $\alpha_{\max}$, more and more and ultimately all faces become contained in the α-complex. Thereby, in general, faces asynchronously traverse the following stages:

- **Singular face:**

  When a k-face becomes α-exposed but the $(k+1)$-face it is bound to be incident upon does not yet. Or, equivalently: the k-face belongs to the k-skeleton, but does not belong to the $(k+1)$-skeleton. Singular faces are always contained in the boundary and are never interior.

- **Regular face:**

  When a k-face is α-exposed and so is a $(k+1)$-superface it is incident upon: the k-face belong to the $(k+1)$-skeleton. The k-face is contained in the boundary of a $(k+1)$-dimensional complex.

- **Interiorface:**

  When a k-face is contained in the interior of some $(k+1)$-dimensional complex: in this case too, the k-face belong to the $(k+1)$-skeleton. By observation 2.17: if the superface is α-exposed, then the k-face is so, too.

2.5.6 The α-family

For a finite point set, a finite set of triangulations can be generated, and by the same token, a finite set of α-complexes can be filtered off. This finite set of α-complexes may be ordered by α-value. Starting out with the canonical vertices set for $\alpha < \alpha_{\min}$, one finds for increasing values of α a new α-complex for every insertion of one or more faces into the previous α-complex, until arriving, for $\alpha = \alpha_{\max}$ at triangulation $\mathcal{T}$. For $\alpha < \alpha_{\min}$, points may be lead to enter the

α-complex only if their radius is real, i.e., if $w + \alpha > 0$. This detail is further left unconsidered here. The α-family is now defined as follows:

DEFINITION 2.15 (α-FAMILY)
The set $\mathbb{A}$ of order ed pairs $(\mathcal{C}_\alpha(\mathbb{S}), \alpha)$ is called the α-family •

where α is the smallest α yielding that complex. Generally, within this family, w e ha v e the follo wing:

OBSERV A TION 2.13 (NOT NECESSARILY UNEQUAL α-COMPLEXES FOR UNEQUAL α)

$$\alpha_1 \neq \alpha_2 \;\not\Rightarrow\; \mathcal{C}_{\alpha_1} \neq \mathcal{C}_{\alpha_2}$$

OBSERV ATION 2.14 (UNEQUAL INTERVALS OF α)

$$i \neq k \vee j \neq l \;\Rightarrow\; \alpha_i - \alpha_j \;\neq\; \alpha_k - \alpha_l$$

As a consequence, the ordering of the α-family b y α delivers a partially ordered set. A strict partial order relation can only be obtained by the introduction of an α-rank:

DEFINITION 2.16 (α-RANK)
The α-rank ϱ is a unique index into the α-family •

as proposed by Mücke in [Mue93] and Edelsbrunner and Mücke in [EM94]. Definition 2.15 can be modified accordingly. Strict ordering of the α-family is beneficial, as it allows for a more efficient storage schemes and faster queries. A single α-rank covers a range of α-values and increments only when the corresponding α-complex expands. Notice also that this definition allows us to topologically sort the set $\mathbb{A}$, according to the index ϱ.

2.5.7 Alpha exposedness

Alpha exposedness is less trivial than it may seem at first glance. Here, it will be discussed in greater depth to gain proper understanding of α-filtration. A simplex in E^d is said to be α-exposed if there exists an empty real $(d-1)$-sphere, radius $\sqrt{\alpha}$, that is orthogonal to eac h of the v ertices if the simplex. This $(d-1)$-sphere is the boundary of a d-ball, called an α-ball. An α-ball in E^d can be regarded as a weighted point with weight α, giving rise to the following definition of α-exposedness given in [Ede92]:

DEFINITION 2.17 (α-EXPOSEDNESS, EDELSBRUNNER, 1992)
A simplex is α-exposed if ther e exists a weighted p oint, with weight α such that this point is orthogonal to each of the vertices if the simplex and all other vertic es have p ositive weighted distance to this weighted p oint •

OBSERV ATION 2.15 (α-EXPOSEDNESS OF A REGULAR SIMPLEX)
F oreach regular simplex there exists an $\alpha \in [0, \infty)$ for which the simplex is α-exposed •

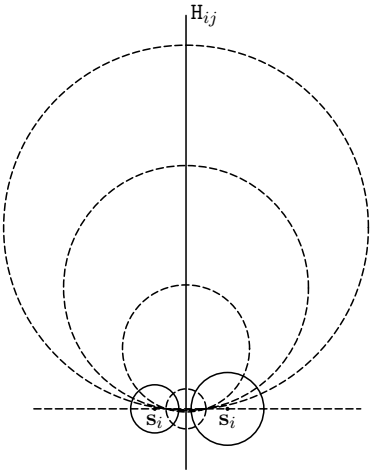

Figure 2–14: *k-simplex, $k < d$, α-exposed by infinitely many α-balls, like here edge $s_i s_j$. The minimum-radius ball is located at the intersection of the carrying line connecting the centres and the radical plane. As the centre of the orthogonal α-ball moves away along the radical plane, its radius becomes greater and greater. When infinitely far remote, the ball becomes a half plane and the edge becomes contained in its border.*

If the orthogonal α-ball is empty all vertices have indeed positive weighted distance to this α-weight weighted point. For a k-simplex, with $k < d$, infinitely many α-balls exist, that cause the k-simplex to be α-exposed. We have the following:

OBSERVATION 2.16 (STRICTLY INCREASING α-BALLS)
If a k-face, $k < d$, has become α-exposed for $\alpha = \alpha_1$, then for any α-value $\alpha > \alpha_1$, again an orthogonal α-ball can be found •

As an example, see the edge in E^2 in the left picture of figure 2–14. The two weighted vertices *generate* a *hyperbolic pencil of spheres* (to be introduced in chapter 4), with all orthogonal spheres passing through two distinct points lying on the edge. The *minimum*-radius and *maximum* radical α-ball are the ones of principal interest. The minimum radical α-ball because this ball determines the α-value for which the face first enters the α-complex. The maximum radical α-ball, with infinite radius corresponding to $\alpha = \infty$, because it guarantees that all vertices in the border of the convex hull can be connected by an edge for some $\alpha \in [0, \infty)$.

For a d-simplex in E^d, there exist exactly one orthogonal α-ball, or none. The generalisation of α-exposedness of an edge to α-exposedness of a k-face in general would take a detailed technical discussion, which will be skipped here. The interested reader may refer to [Ede92, Mue93, EM94]. One more important aspect will be mentioned, however:

OBSERVATION 2.17 (α-EXPOSEDNESS OF SUPERFACES)
If all subfaces (e.g., the edges of a triangle) are α-exposed, then that is not a sufficient condition for the face to be α-exposed too, as figure 2–15 illustrates. On the other hand, if a superface is α-exposed then so are its subfaces •

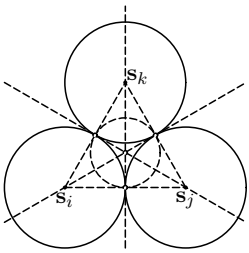

Figure 2–15: *α-exposed edges belonging to a non α-exposed triangle. A real orthogonal sphere located in the radical centre exists. In this case, the orthogonal α-ball coincides with the inscribed ball. Only when the chosen α-value permits the formation of this α-ball, the triangle will become α-exposed, whereas edges are α-exposed for an α close to zero.*

2.6 The α-complex as a graph

2.6.1 Geometric graph

In order to be able to relate a triangulation to nearest neighbour information, to be discussed shortly, the notion of a *geometric graph* is now introduced:

Definition 2.18 (finite geometric graph)
A finite geometric graph is a graph in which a finite set of edges represent distances of some kind between vertic esand a finite set of vertices represent points in spac e•

F or instance, a Delauny triangulation can be considered as a geometric graph. Geometric graphs are assumed undirected. If not explicitely stated, they are also assumed finite and simplicial:

Definition 2.19 (simplicial geometric graph)
A geometric graph is said to be simplicial if it contains no self-loops or multiple edges among any pair of vertiœs •

How is this with weighted vertices and weighted distances? As stated earlier, swapping Euclidean distance by the Laguerre weighted distance causes space to become non-metric. See Annex C. Recall that weighted distances are not necessarily positive. A graph with edges based on a Laguerre distance may cause arcs (edges) to represent negative distances. As a consequence:

Observation 2.18 (not a geometric graph)
The regular triangulation is not a geometric graph •

2.6.2 The nearest and the local-furthest neighbour graph

The nearest neighbour and local-furthest neighbour appear to be the vertices associated with the smallest and greatest α-value, resp. For this reason, nearest and local-furthest neighbour information is of keen interest in local neighbourhood analysis. Let $\mathcal{T}(\mathbb{S})$ be the triangulation of point set $\mathbb{S}$. Then the nearest neighbourgraph is defined as follo ws:

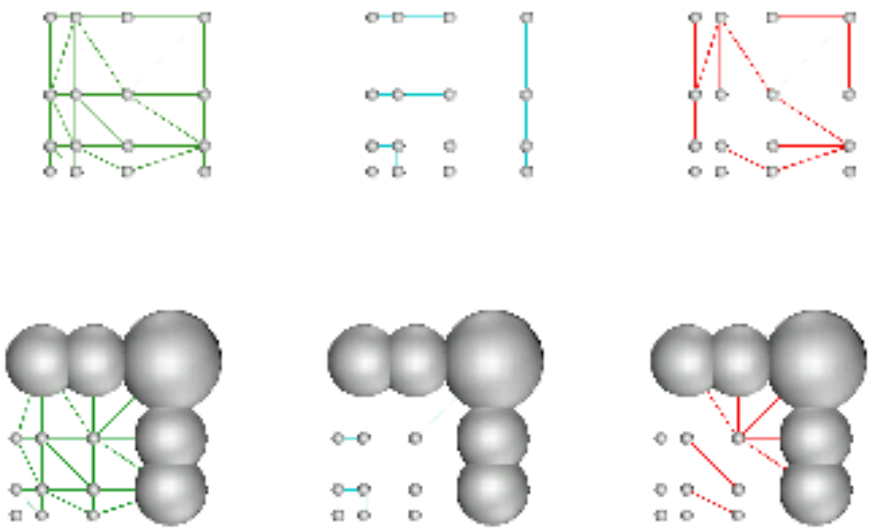

Figure 2–16: *nearest and local-furthest neighbour graph of a weighted point set. Top row: zero-weigh t case, bottom row: w eigh ted caseLeft-to-right: triangulation, $\mathcal{NNG}$ (centre) and $\mathcal{LFNG}$ (right). Weights are indicated as weight balls.*

Definition 2.20 (nearest neighbour graph $\mathcal{NNG}$)
The ne arest neighbour graph $\mathcal{NNG}(\mathbb{S})$ connects each member in $\mathbb{S}$ to another member that is:

(*i*) *connected by an arc in $\mathcal{T}(\mathbb{S})$, and:*

(*ii*) *closest by* •

and, in similar vein:

Definition 2.21 (local-furthest neighbour graph $\mathcal{LFNG}$)
The local-furthest neighbour graph $\mathcal{LFNG}(\mathbb{S})$ connects each member in $\mathbb{S}$ to another member that is:

(*i*) *connected by an arc in $\mathcal{T}(S)$, and:*

(*ii*) *furthest apart* •

Remark that the second condition in definition 2.20 implies the first. The objective here is more to match the definitions 2.20 and 2.21 of $\mathcal{NNG}$ and $\mathcal{LFNG}$ and put them in the context of the triangulation. Also see figure 2–16. Further notice that the $\mathcal{LFNG}$ as defined here, may coincide but has no explicit relation to the furthest-site triangulation (e.g., [Ede87, O'R94]).

As a direct consequence of the definition of $\mathcal{NNG}$ and $\mathcal{LFNG}$:

OBSERVATION 2.19 (TRIANGULATION AND $\mathcal{NNG}$ AND $\mathcal{LFNG}$)
$\mathcal{NNG}(S) \subseteq \mathcal{T}$ and $\mathcal{LFNG}(\mathbb{S}) \subseteq \mathcal{T}$ •

Local-furthest and nearest neighbours are defined in the setting of a *local* neighbourhood, more precisely for a vertex $\mathbf{s}$:

OBSERVATION 2.20 (ARC IN $\mathcal{T}(S)$ AND STAR)
For the arc in $\mathcal{T}(S)$ mentioned in definition 2.20, $\mathbf{s}_i\mathbf{s}_j$ say, one has that $\mathbf{s}_i\mathbf{s}_j \in St\ s_i \bigcap St\ s_j$ •

Neither nearest neighbour nor local-furthest neighbour relations are symmetric. Therefore, their graphs need be directed, as appropriate. Furthermore, neither nearest neighbour nor local-furthest neighbour relations are unique. One vertex may have multiple nearest and/or local-furthest neighbours and a vertex may be the nearest- and/or local-furthest neighbour of multiple other vertices and also, vertices may be another vertex' nearest and local-furthest neighbour at the same time, and vertices may have one and the same vertex as local-furthest and nearest neighbour. A notable instance of "non-uniqueness" is formed by regularly spaced vertices. Neither $\mathcal{NNG}$ nor $\mathcal{LFNG}$ are generally connected or complete, but both are spanning. Figure 2–16 shows an example of a $\mathcal{NNG}$ and a $\mathcal{LFNG}$ of a weighted point set. Both graphs will return in chapter 4 and will be used in the case studies of chapter 6. For a further introduction, see e.g. [O'R94].

2.7 Holes

Holes play an important role in modelling with α-complexes. Indeed, α-complexes can be appreciated inasmuch for their ability to model what is *not* there, i.e., by their holes, as for their capabilities of snapping materialised subspace. The *duality* in object and *void space* is particularly suited for the modelling of dual shapes, such as two-phase systems. This aspect will be further exploited in chapter 5. But the variety in which holes appear leads astray easily. Some further definitions and classifications are therefore needed (also see table 2–4):

DEFINITION 2.22 (VARIOUS HOLES)
A cavity *is a* depression *lying in the boundary of the object, accessible via the (unbounded) exterior of the object.*

A pocket *is a cavity with a small "neck".*

A void *is an entirely internal hole. This is a special hole in that it creates an additional (bounded) exterior of the object.*

A handle or tunnel *is a pathway from boundary to boundary, piercing the object. It can be regarded as a pocket or a void with two distinct connections (necks) to the single unbounded exterior of the object* •

A bit more formal:

DEFINITION 2.23 (GENUS)
The genus is a topological characteristic indicating the number of handles on an object and a genus g object is an object with g handles •

HOLE	(none)	Cavity	Pocket	Void	Tunnel	Separation
Genus	0	0	0	0	> 0	0
Int	1	1	1	1	1	> 1
bounded *Ext*	0	0	0	1	0	0
unbounded *Ext*	1	1	1	1	1	1

Table 2–4: *Topological characteristics of various types of holes.*

Triangulations of a point set in E^d bounded by set $\mathbb{S}$ have no unbounded cells. They always have at least one exterior. When a (triangulated) object contains one or more voids, m say, there will be m additional (bounded) exteriors, completely surrounded by the interior.

OBSERVATION 2.21 (DISJOINT EXTERIORS AND INTERIORS)
Disjoint exteriors imply multiply connected interiors, and vice versa •

OBSERVATION 2.22 (SEPARATION OF $\mathrm{Cl}\,\mathcal{C}_\alpha$ AND $\mathrm{Int}\,\mathcal{C}_\alpha$)
Closure $\mathrm{Cl}\,\mathcal{C}_\alpha$ *may be connected, while* $\mathrm{Int}\,\mathcal{C}_\alpha$ *is separated* •

Figure 2–17 shows this.

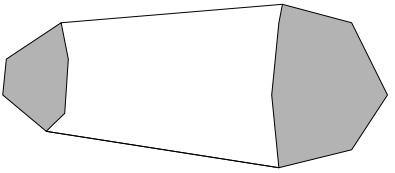

Figure 2–17: *example of an α-shape for which its interior (grayed)* $\mathrm{Int}\,\mathcal{W}_\alpha$ *is separated, but not the closure* $\mathrm{Cl}\,\mathcal{W}_\alpha$ *thereof.*

Starting out with a triangulation (i.e., $\mathcal{C}_\alpha \cong \mathcal{T}$), and assuming a monotonically decreasing value of α, voids may grow into pockets, pockets into cavities and/or handles and handles may grow into separations of the α-complex. During this process, the genus (number of handles) changes according to table 2–4. For specific intervals of α, the genus may be alternating between zero and non-zero. In chapter 4, it will become clear how a negative weight may be used as a seed for an internal hole and how this void may finally grow into a non-zero genus object.

2.8 Time and storage complexity

The exact asymptotic storage complexity of a d-simplex (i.e., the number of its k-faces) is given by:

$$\mathrm{card}\,\mathbb{F} = \Theta(2^{d+1}) \tag{2–4}$$

EXAMPLE 2.2 (FACES OF A 2-SIMPLEX)
A 2-simplex (triangle) is made up of 2^3 (sub)faces: one 2-face plus three 1-faces (edges) plus three 0-faces (vertices) plus the only "improper" -1-face, empty set $\emptyset$, which totals up to 8 •

See [PS85, Ede87]. Notice that edges, vertices and indeed also the empty set are simplexes themselves. Asymptotic time and storage complexities of triangulation, α-complex and α-shape are given in table 2–5. The time complexity to generate the regular triangulation turns out to be the yardstick. A triangulation in E^d can be found in $\mathcal{O}(n^{\lceil \frac{d}{2} \rceil})$ running time. Deriving the α-family from this triangulation by means of α-filtrationα-filtration can be done in time linear in the number of faces, obtaining both α-complex and α-shape (see [Mue93, EM94]).

E^d	$\mathcal{W}_\alpha(S)$	$\mathcal{C}_\alpha(S)$	$\mathcal{T}(S)$
time	$\mathcal{O}(n^{\lceil \frac{d}{2} \rceil})$	$\mathcal{O}(n^{\lceil \frac{d}{2} \rceil})$	$\mathcal{O}(n^{\lceil \frac{d}{2} \rceil})$
storage	$\Theta(n^{\lfloor \frac{d+1}{2} \rfloor})$	$\Theta(n^{\lfloor \frac{d+1}{2} \rfloor})$	$\Theta(n^{\lfloor \frac{d+1}{2} \rfloor})$

TABLE 2–5: *asymptotic time and storage complexities.*

Mücke shows that for a point set $\mathbb{S}$ in E^3, with $\operatorname{card} \mathbb{S} = N$, at most $2N^2 - 5N$ α-shapes can be formed. For further details, see [Mue93]. Complexities for general dimension were not found in literature. For the storage complexity, we may further take the triangulation as an upper bound. For E^d, Seidel ([Sei91]) shows that the storage complexity cannot exceed exact bound $\Theta(n^{\lfloor \frac{d+1}{2} \rfloor})$, as table 2–5 indicates.

The time complexity of α-complex queries, for example for point locations, can be done in $\mathcal{O}(n)$, which follows trivially with what is found for triangulations in [MSZ99]. Point location is not further discussed in this work. Generally, in E^d, k radical planes of $k+1$ points in general position intersect in a single $d-k$-flat. Permutations of ordered pairs out of $d+1$ points generate m radical planes, with:

$$m = \binom{d+1}{2} = \frac{1}{2}\frac{(d+1)!}{(d-1)!} \tag{2–5}$$

For a d-simplex, the m radical planes intersect in a single 0-flat (point), causing the arrangement of radical planes to be not in general position and not simple. More details can be found in [Aur87b, BP94]. Also, refer to table 2–2.

Chapter 3

Modelling steps

3.1 Overview of this chapter

In chapter 1, α-complexes have been proposed for the geometric and topological description of subsurface objects. In the previous chapter, the background of α-complexes has been introduced in greater detail. In this chapter, attention will be focused on the application of α-complexes in the modelling process. A framework or environment to support this modelling process does not yet exist; it has to be developed. A modelling process like this has two sides: firstly, finding an appropriate α-complex that adequately captures the sampled object and secondly, the re-instantiation of templatised primitive objects, stored as an α-complex. This chapter will set forth a modelling framework covering both of these aspects.

First thing in this chapter, is a discussion on the notion of shapes in section 3.2. Goal of the discussion is to identify the important aspects of shapes and families of shapes. Also in this section, a few classes of shapes of special importance for the modelling of natural objects. Modelling with α-complexes is a multi-step process. In section 3.3, an initial *kernel modelling framework* for modelling with α-complexes will be postulated, which will be further expanded and refined in the course of this chapter. Section 3.4 discusses the details of the sampling data point set, among other things, the organisation of the sampling data point set. Next, in section 3.5, attention turns to the analysis of the sampling data point set. Section 3.6 contains a discussion on transformations. More in particular, how they can be applied as a preprocessing step to further precondition $\mathbb{S}$, and the pitfalls that come along with transformations. This section also discusses normalisation as a special instance of transformation. The modelling steps triangulation and α-family derivation, being automated steps without further human interaction, are not discussed in this chapter. Details were given in chapter 2. Section 3.7 sheds some light on further details of the assignment of weights. Weighted is the subject of chapter 4. The final modelling steps, transcribing the α-complex in another representation, will be discussed in section 3.8. Section 3.9 present the point processes as a foundation for the theoretical model. Then, section 3.10 presents a further refined and expanded modelling framework. Section 3.11 treats the aspects involved in the modelling of dynamic problems with α-complexes. Of particular interest to geological models is the treatment of dilation and erosional processes.

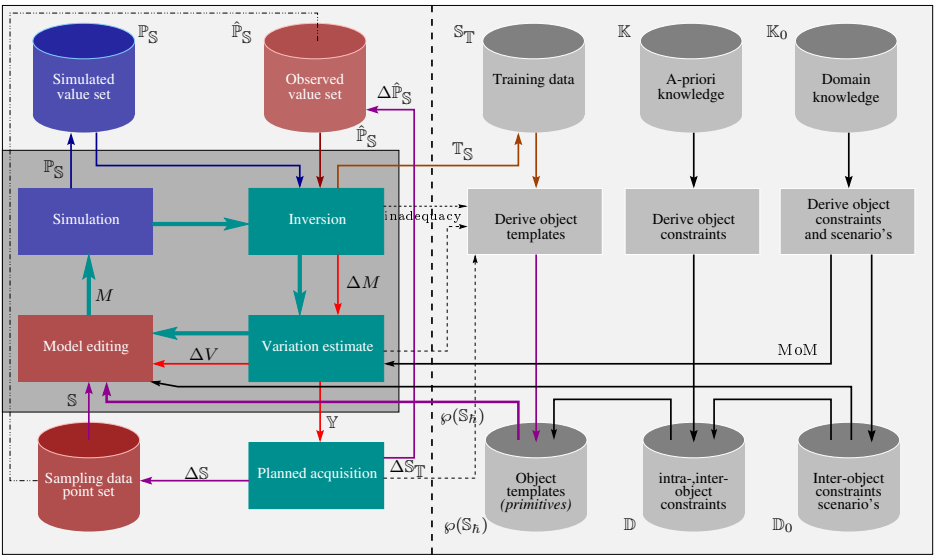

Figure 3–1: *wider scope of a constrained simulation- and inversion-based forward modelling environment, using planned acquisition and α-complex geometry and topology. The figure shows how, eventually, the modelling can be embedded in a knowledge-based approach. The grayed box at the left reflects the part for which a modelling framework will be outlined in this chapter. The modelling iterations stop when the* measure-of-merit *(Taylor in [Tay92]) cannot be improved anymore.*

3.2 Shapes

3.2.1 What is a shape?

In the preceeding chapters, the notion of a shape has been introduced, relying on the reader's intuitive understanding of what a shape involves. A more precise definition of a shape is now due. Following Kendall (1977), the definition of shape reads as follows:

DEFINITION 3.1 (SHAPE, KENDALL, 1977)
Shape is all the geometric information that remains when location, scale and rotational effects are filtered out from an object •

Shape in this work, applies to the shape of natural objects. Natural objects can be classified in so many ways that no attempt will be made here. Neither has there been or will there be made an endeavour to come up with a definition of what a natural object is exactly. Even without a precise definition, the use of this widely applied definition may be debatable for subsurface modelling. Firstly, orientation may be relevant with regard to differences in horizontal and vertical properties and in conjunction to this point, in a sequence of events and environments, processes like gravity, erosion and flooding may typically act differently on differently oriented shapes. Size issues may also be important. These issues will not further be discussed in this thesis but will be posted as open problem, i.e., marked for further research. See chapter 7.

In this thesis, an object's shape can be represented in different manners and in different spaces. Refer to chapter 2. The shape of an observed object in sample space is described by a set of *landmarks*, a definition of which will be given below. In topological space, a shape will usually be discussed in a topological manner, possibly neglecting the geometric details all together. In model space, the space is usually represented by an α-complex.

In this chapter, the sampling of objects will mostly be discussed in terms of landmarks (cf. Bookstein, 1978), a term in customary use in morphology. A landmark, until a more precise definition will be given, is a characteristic point of the object, typically shared by all such shapes. Such landmarks will be exactly the points expected in a sampling data point set.

3.2.2 Shape classification

Shape classification in all its details, though looming at the horizon of this thesis, is beyond the scope of this thesis. A very crude outline will be given here, just to pick up enough context for the remainder of this chapter. For further details, refer to [SS94, DM98]. From now on a shape is assumed to comply with definition 3.1. A suitable definition for the *size* of an object, represented by its set of landmarks S has been proposed by Dryden and Mardia (1998):

DEFINITION 3.2 (SIZE)
Size is the positive real valued factor λ that can be decreased or increased, such that the shape $\mathcal{W}(\mathbb{S})$ is being preserved •

In mathematical terms, with set function $\mathcal{W}(\mathbb{S})$ indicating the shape generated by $\mathbb{S}$:

$$\mathcal{W}(\lambda\mathbb{S}) = \lambda\mathcal{W}(\mathbb{S}), \quad \lambda > 0 \tag{3–1}$$

Shapelassification is usually done against a *family* of shapes, and based on the value(s) of one or more characteristic *shape parameters*. A shape parameter is defined as follows:

DEFINITION 3.3 (SHAPE PARAMETER)
A shape parameter is a real valued parameter that given a set of landmarks S sets off a single characteristic of the individual shape against a typical value or distribution of that characteristic among the family •

Let $\mathsf{G} : E^d \mapsto R$ represent a real-valued shape parameter relation. Then, with $\mathbb{S} \subset \mathbb{E}^d$ and $\mathsf{g} \in \mathbb{R}$, set function $\mathsf{g} = \mathsf{G}(\mathbb{S})$ denotes a shape parameter that depends on the set of landmarks. In the case of shape analysis (refer to figure 3–1), landmarks are usually reworked into *Helmertized landmarks* (denoted: $\mathbb{S}_\hbar$), i.e., landmarks from which location information has been removed and the size (scale) has been normalised. This operation is sometimes referred to or combined with *homologisation*, an operation aiming to send certain reference points, or origins among the landmarks, into fixed locations in sample space, in order to enhance comparison of shapes. For further details, refer for example to to [SS94, DM98].

DEFINITION 3.4 (SHAPE SPACE)
Shape space is the (hyper-)space spanned by the set of all possible shapes belonging to a common family, in which shapes are being represented by the set of landmarks, possibly augmented by weight and value sets and possibly by time •

Definition 3.5 (icon)
An icon is a member of a shape family that is believed to be a typical representative of that family
•

Icons will generally serve as sample models on which the templatised shapes (or: primitives) $\wp(\mathbb{S}_\hbar)$ will be based. See figure 3–1.

3.2.3 Shape matching

Once a family of shapes has been analysed and its shape parameters are known, unknown objects can be matched against these parameters. The term *shape matching* will be used for that process. The problem of shape matching can now be formulated as follows:

Formulation 3.1 (shape matching)
Given a set of landmarks sampling an unclassified object, pose the hypothesis that the object belongs to a shape family and try to achieve acceptance or rejection of the hypothesis. If the hypothesis can be accepted then the shape is an instance of the family and it can therefore be reconstructed from the family icon by choosing appropriate values for the shape parametersfrom their valid domains. If the hypothesis must be rejected, the unknown shape does not belong to this family and instantiation cannot generally take place with this family's shape parameters within valid range.

The idea of the matching procedure is to bring landmarks in normalised form, by successively removing positional (location and orientation) information, along with size and scale. This process is well-studied and extensively discussed in the literature. See e.g., [DM98, BNKVL99]. For a recent survey on shape matching, refer to [VH01].

This subsection is concluded with a quote taken from [SS94]:

Quote 3.1 ([SS94], pp. 54: descriptive power of shape parameters)
"In most cases, one cannot expect that form (shape) parameters uniquely determine figures (objects) in the sense that a (full and unique) reconstruction is possible".

perhaps best understood by looking at the matching process in mathematical terms. Let $\mathbf{X}_{\mathbb{S}_\hbar}$ be an $N \times d$ matrix representing the landmarks in its rows. Furthermore, let $\mathbf{E}$ be an $N \times d$ matrix representing the uncertainty of the landmark locations in its rows. Then for the reconstruction process of shape $\mathcal{W}(\mathbf{X}_{\mathbb{S}})$:

$$\mathcal{W}(\mathbf{X}_{\mathbb{S}}) = \mathcal{W}\left(\lambda(\mathbf{X}_{\mathbb{S}_\hbar} + \mathbf{E})\mathbf{T}_R + \mathbf{I}\mathbf{O}^T\right) = \mathcal{W}(\lambda\mathbf{X}_{\mathbb{S}_\hbar}\mathbf{T}_R + \mathbf{I}\mathbf{O}^T + \mathbf{E}') \tag{3–2}$$

where $\mathbf{T}_R$ is a $d \times d$ rotation transformation matrix and $\mathbf{O}$ is a $d \times 1$ matrix containing the components of the translation vector of some reference point of the shape. The $N \times 1$ matrix $\mathbf{I}$ contains the components of N-unit vector $\mathbf{1}^N$. The term $\mathbf{E}'$ is the important point: some *uncertainty*, or: *fuzziness* remains.

3.2.4 The two fundamental modelling problems

Building natural object shapes from scratc his a formidable task. Therefore, modellers usually turn to a sketch, *cartoon* or an icon of an existing physical object to create a possible *realisation* of such a shape. Object templates, called primitives, serve exactly that purpose. In order to give further structure to the discussion, the following modelling problems are to be formulated, both considered in the context of α-complexes:

	Free form	Shape reconstruction
Nature of the data	synthetic, immaterial subjective volatile	observed from physical model only subject to error and noise to be honored
MoM	generally lacking subjective	optimisation object-/ cost function best fit with physical model
anatomic landmarks	largely absent	dominantly present
mathematical landmarks	computed	computed
pseudo landmarks	taken for anatomic landmarks	additional constraints and detail

Table 3–1: *summary of the principle characteristics of the two classes of modelling problems in the context of the use of α-complexes. MoM is an acronym for: measure-of-merit.*

Formulation 3.2 (free form shaping)
The shape, represented by the α-complex is built from a modeller-generated, (pseudo-)*landmark point set, based on a* simulated *or* assumed *geometry and a-priori knowledge. Generally, the set of possible solutions to the problem is not limited to a single solution and changes to the data point set S and/or the weight set W may be used to alter the shape. Usually, no crisp measure-of-merit exists (MoM) and the selection of the preferred shape is the modellers' choice* •

Formulation 3.3 (shape reconstruction)
The sampling data point set is now based on observed *data. Generally, the observation will be subject to noise and errors. Although basically multiple solutions can be found, a single "best fit" can generally be identified according to optimisation of some objective or cost function. This commonly takes the form of a constrained interpolation problem. The observed* (anatomic) *landmarks, are commonly left untouched (one doesn't change observations) and control must therefore come from changes to weight set $\mathbb{W}$ or from additional acquisition of (pseudo)-landmarks* •

Table 3–1 summarises. Both classes of problems fit in the conceptual modelling environment of figure 3–1. Roughly speaking, the left part of the scheme is the inversion environment, the right part is the knowledge part including the primitives and the scenarios. At the core of this modelling environment is the constrained simulation- and inversion-based forward modelling problem (grayedbox), the origin and motivation of which was introduced in chapter 1. Notice also that generally, both modelling problem classes will be submitted to some form of numerical analysis.

At first glance, the two classes of modelling problems seem to mutually exclude one another. In this thesis, however, the two problems gracefully coexist, although shape reconstruction

remains the dominant problem. Finding the icon is basically shape reconstruction and the same goes for constrained re-instantiation. Free-form modelling occurs within the bounds of fuzziness (as mentioned in the previous subsection) and to bring in a-priori knowledge that is not represented by the existing set of landmarks.

Finally, notice that finding an icon among a family of shapes and re-instantiation of shape instances from this icon have many aspects in common, such as sizing and positioning, and the constraining to observed data.

3.2.5 Shape families

Families in this context are most conveniently subdivided according to the process that they undergo. More precisely:

DEFINITION 3.6 (SHAPE FAMILIES)

- **Raw shape family**

  A raw shape family is a collection of shape-identical objects, of which the hypothesis of their Helmertized landmarks being identical to those of the icon has not yet been accepted or rejected.

- **Formalised shape family**

  A formalised shape family is a family of which all members have been accepted to have the same shape, identical to the shape of its icon.

- **Realisation of a shape family**

  A realisation of a shape family is a set of instantiated shapes, the icon variety, generated by the icon by means of shape parametervariation (variational geometry).

- **Transformed shape family**

  A transformed shape family is a transformation of a realisation of a shape family •

EXAMPLE 3.1 (SHAPE FAMILIES)
A set of balls, resized to have arbitrary finite radii, is a realisation of a shape family of the formalised shape family of balls. After mixing these balls by arbitrarily random moves of their centres in space, a transformed shape family is obtained. However, all the resulting balls can be traced back to the formalised family of balls. Their Helmertized landmarks are identical to that of the ball icon. A set of sheared *shape family members, i.e., a set of shape instantiations, generated by the same icon but transformed using a different shear transformation, forms a realisation of a shape family, but as a raw shape family, can no longer be traced back to a formalised shape family. Due to the shearing, which changes the shape, their Helmertized landmarks even if corrected for orientation, differs* •

EXAMPLE 3.2 (TRANSFORMED SHAPE FAMILIES)
Figure 3–2 shows a family of a linearly (affinely) transformed shape and a sheared shape from a section of a meandering river icon. The leftmost shape is the icon. The central shape was obtained by an anisotropic transformation and has therefore not the same shape as the icon. Also the sheared shape family member at the right has a different shape than the icon. The rightmost shape was obtained by shearing along the X-axis by $60°$*. Refer to figures 6–38 and 6–39, for a further expanded family* •

Figure 3–2: *linearly (affinely) transformed shape family member (central) of a section of a meandering river icon at the left, transformed by an anisotropic scaling transformation (scaling vector* $(2\ 1)^T$*). Right: family member obtained by shearing transformation along X-axis by* $60°$.

3.2.6 Property-ruled geometry and topology

In the observation of physical objects, it is not always feasible to have physical access to the (interior of the) target object. Quite often, an object can only be observed while embedded in its background material. Some observation techniques are based on reflections of some signal (for example echoscopy, reflection seismic, ultra sound) some are based on the principle of *tomography*. Refer for example to [BCM+93]. Different observation techniques may deliver different sets of landmarks and observed value sets of different properties each reveal a different geometry. Moreover, using a different sampling technique often delivers a different value set on the *same* property. The geometry so becomes dependent on the observed property and observation method. We regard to such shapes as *property-ruled shapes*:

Definition 3.7 (property-ruled shape)
A shape is called property-ruled if it is directly depending on the measured property or observation technique •

See figure 3–3. An illustrating example has been presented in [XJG+99]:

Example 3.3 (melonama and non-melonama)
A surgeon locating and removing a skin cancer will somehow rely on tissue properties to determine where to cut. Frequently, there will not be just a single dominant property, but a suite of properties, each with their own local and global significance. Different experts apply different criteria and rules and merit the observed facts differently. The weighting of properties in order to discriminate object material from its background leads to the belief in this thesis that in the current practices, the shape of natural objects is in fact property-ruled •

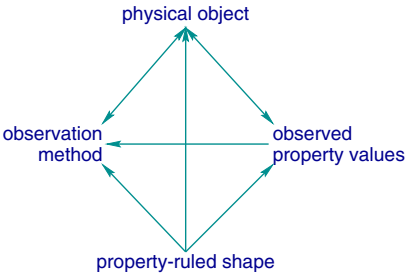

Figure 3–3: *dependency diagram for a property-ruled shape. A source-to-destination arrow denotes a dependency of the source on the destination.*

3.2.7 Stratified shapes

Shapes can be stratified, or more precisely, be sampled such that the sampling data points appear as *strata*:

Definition 3.8 (stratified data)
Sampling data points are said to be stratified if their values cluster in layers. Each layer has its typical value range •

An example of stratified data was shown in chapter 1, figure 1–6. For convenience, if the sampling data points show to be stratified, the corresponding layered shapes are also referred to as stratified shapes.

3.2.8 Geometrically coupled shapes

Shapes can be geometrically coupled in the following sense:

Definition 3.9 (geometrically coupled objects)
Two objects are said to be geometrically coupled if a change in one is necessarily coupled to a complementary spatial occupancy change in the other •

Example 3.4 (multi-phase objects)
Consider a system of immiscible fluid and solid phases. A volume change in one phase induces an equally large volume change in one or more coexisting phases •

It is not uncommon (e.g., [Kal89, RG96]) to also attribute a shape (geometry and topology) to fluid and gaseous bodies, yielding fluid objects and gaseous objects. Or to couple their shape in the frame of a multi-phase system (e.g., [BB91, ABBM94, Tak98]).

3.2.9 Holes

One of the celebrated capacities of α-complexes is their capability of handling the topology of all sorts of holes in an intrinsic manner. Even in a dynamic way: as α changes, or the point set, one type of hole may decay into another type, holes may fade away and new ones may invade

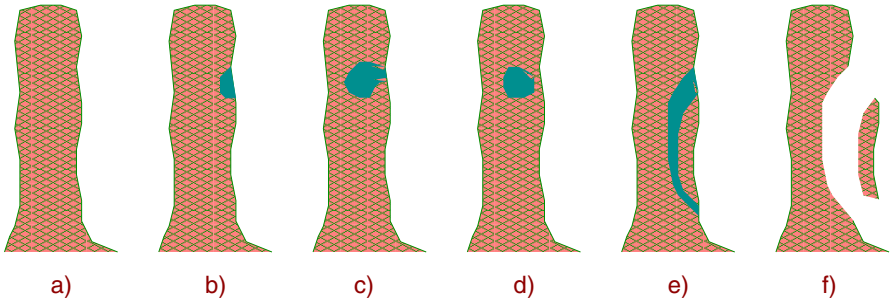

Figure 3–4: *salt diapir with various forms of holes, to illustrate the terminology; left to right: a): diapir without holes (a simple shape), b): diapir with cavity or boundary hole, c): diapir with pocket, d): diapir with internal hole, or void, e): diapir with tunnel or handle, f): separation. A void induces a separation of the exterior, while the others do not. Observe that the interior of a)..e) is connected, the interior of f) is separated.*

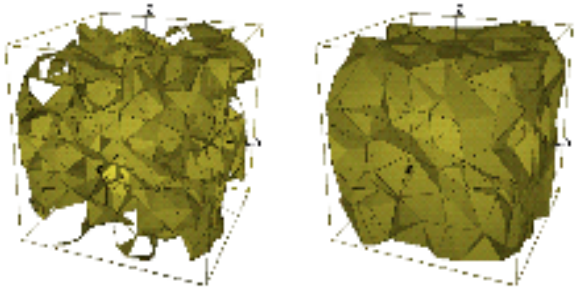

Figure 3–5: *α-complex containing tunnels (left) and nearly similar α-complex, without tunnels (right). The left complex has genus > 0, the right is a genus 0 complex. Generally, the (boundary) surface and the curvature of the right complex will be smaller than that of the left complex.*

the complex. This is of particular interest for the modelling of for instance geometrically coupled objects, like multi-phase immiscible solid-fluid systems. In chapter 2, some of the topological features were already discussed. Here, figure 3–4 shows an example, the terms and the topological characteristics. Figure 3–5 shows an example of nearly equal shapes, with tunnels and tunnel-free.

3.3 Modelling shapes with α-complexes

Now that families of shapes, their classification and the role of properties have been discussed, it is time to look at the modelling approach itself, based on the use of α-complexes. The nuts and bolts of α-complexes ha vebeen discussed in greater detail in chapter 2. The focus in the previous chapter w asmore on mathematical background and technical details. In this chapter, the focus will be on application of α-complexes to practical modelling problems. This section presents a *kernel modelling framework* for modelling with α-complexes. This kernel framework will be refined and expanded in the course of this chapter. Before this can be done, the individual

components need further clarification, which will be done in the sections following this one.

3.3.1 A kernel modelling framework

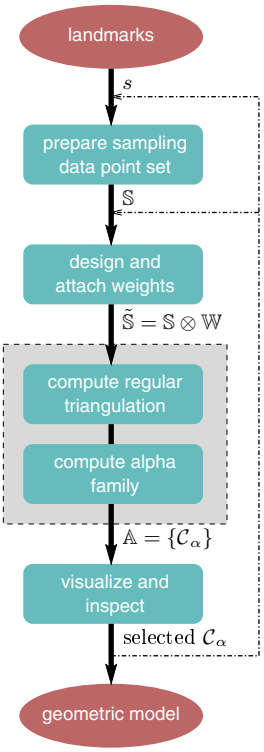

Figure 3–6: *the kernel modelling framework containing the basic steps involved in modelling with α-complexes. Some steps may be void, occasionally. Starting point is always a sampling data point set and the final result is always a geometric model, represented by an α-complex. Triangulation and α-complex computation are steps with no or little human interaction. The modelling ingenuity is chiefly in the first steps.*

The kernel of a modelling framework for α-complex modelling is depicted in figure 3–6. In its essence, it closely resembles the approach presented in [Mue93, EM94]. It will be further expanded in this chapter. The first steps involve the preparation of the *sampling data point set* (landmark set) $\mathbb{S}$, possibly endowed with one or more sets of property values sampled at those locations, and the *weight set* $\mathbb{W}$. The more meaningful points in the data set, the landmarks, are guiding in the determination of the weights. Optionally, transformations may be used beforehand to precondition $\mathbb{S}$. Then, the α-family is determined, which was also described in chapter 2. To draw the preferred complex from this α-family, some *measure-of-merit* ([Tay92]) is needed, indicating the goodness of fit for each α-complex. If no such measure is available, subjective criteria may be used instead. Various modelling cycles (iterations) may be needed

before a satisfactory result is obtained.

Once identified, the appropriate α-complex may be converted into alternate representations. The α-complex may also be merged with other triangulated geometries, or may be transcribed into an "ordinary" solid. For dynamic problems, the modelling cycle may be time-geared: sample points sets, weights and preferred α-values may vary over time. The same holds for cost- and objective functions. These topics will be dealt with near the end of this chapter.

How does this kernel modelling framework relate to the grayedbox in the conceptual modelling environment in figure 3–1? A paleological or geological *scenario* is retrieved from a knowledge base, imposing the "living environment" and evolutionary regime for the objects to instantiate. Scenarios enable certain geodynamic processes and constraints. Then, objects are instantiated from icons stored in the *earth catalogue* data base of templatised icons (primitives). After fitting a theoretical model to the instantiated shape (to be discussed later in this chapter) simulation can take place, yielding expected value sets that can be compared to observed value sets. This *inversion*, together with some measure-of-merit, tells where the shapes so far need adjustments in order to improve the merit-of-measure. Improvement can be brought about by geometric changes on the landmarks, by changing weight and by changes of α. The latter two are less likely than the former. Weights, α and constraints are foreseen to be determined by knowledge-base stored rules.

Until the knowledge-base part of the environment will have been developed, icons are derived directly from the observed landmark set. As long as simulation is absent, and the inversion is still un-installed, evaluation is simply the experts view on the α-complex created so far. Physical fitting criteria, such a estimated volumes, areas and so on may assist in finding the best α-complex. This is exactly what the kernel modelling framework supports; no more, no less.

3.4 The sampling data set

3.4.1 Landmarks and value sets

The sampling data point set $\mathbb{S}$ may consist of various types of landmarks. A further subdivision of the landmarks is therefore convenient:

DEFINITION 3.10 (LANDMARK)
A landmark is a point which identifies a salient feature of a shape. More specifically:

Anatomic landmark *An anatomic landmark identifies a feature shared by every instance of a family of shapes.*

Mathematical landmark *A mathematical landmark is a feature representing an extremity of a mathematical property, such as maximum curvature, local or global maximum or minimum, singularity, etc.*

Pseudo-landmark *A pseudo-landmark is a constructed landmark that has been introduced by the modeller, so as to reflect certain a-priori knowledge, constraint or hypothesis* •

There are many synonyms for landmarks: first of all *sample points*, but also: *sites*, *markers*, *anchor points*, *control points* and a few others. In this work, landmarks are always points in space

and/or time. Anatomic landmarks are always observed or simulated, mathematical landmarks are always computed, pseudo-landmarks are simulated or specified.

Organising sample points on a lattice brings up a discussion as to whether landmarks identified in the grid nodes can be classified as anatomic landmarks. There are many arguments in favour of regarding grid nodes as mathematical landmarks. Further discussion is not in the interest of this thesis and will be abandoned here.

Commonly, in the landmarks, some process is being sampled, in this work typically some physical property. This set of properties is called the *(property)value set* belonging to $\mathbb{S}$, and is denoted $\mathbb{P}_{\mathbb{S}}$:

DEFINITION 3.11 ((PROPERTY)VALUE SET)
A value set $\mathbb{P}_{\mathbb{S}}$ belonging to $\mathbb{S}$ is an observation of some processin the points in $\mathbb{S}$ •

In this work, the value set is input for the design of the weights $\mathbb{W}$. Strictly speaking, this does not belong to the kernel modelling framework and it is therefore not shown in figure 3–6. The sampling of some physical objects in this thesis is mostly sparse sampling:

DEFINITION 3.12 (SPARSE SAMPLING)
A sampling is said to be a sparse sampling if the number of the sample points is only a small portion of the available observation points that can be chosen of •

EXAMPLE 3.5 (SAMPLING SEISMIC CUBE)
A sampling data point set consisting of a seismic cube can generally not be considered as sparse. Interpreted seismic horizon picks will generally be sparse •

No generic definition of what "small" is exactly can be given. In this work, small will be defined as less than one-quarter, unless stated otherwise. The motivation for this choice is that one out of four is in the same order of magnitude as one sample point for each tetrahedron in E^3. Other choice can be taken equally well.

3.4.2 Landmarking

Sometimes, the initial sampling data set is abundant enough to complete the picture in a single modelling process. Brett and Taylor found for example that in their studies, on smooth objects and on biological objects, no more than some ten percent of the observed points can be classified as anatomic landmarks. Observations came from sliced data (contours) that were triangulated, see [BT00]. More often, however, further sampling of anatomic landmarks is necessary.

Once the anatomic landmarks are sufficiently present in the sampling data point set, additional landmarks typically pseudo-landmarks may be added, to reflect topological details, form features, a-priori knowledge, constraints, hypothesis and other desired details. This brings up the matter of data commensurability; how to unify data of various nature. In the current concept of α-complex-modelling, heterogenous data types have to be "transformed" into an appropriately weighted sampling data point sets, anticipating some appropriate value of α.

When faced with a stratified object, sampling is not always as straightforward as it appears. In *stratified domains*, the various *strata* have to be covered in the sampling. In order for the strata to be captured in the resulting α-complex, all the essential landmarks of all strata have to be present in the sampling data set.

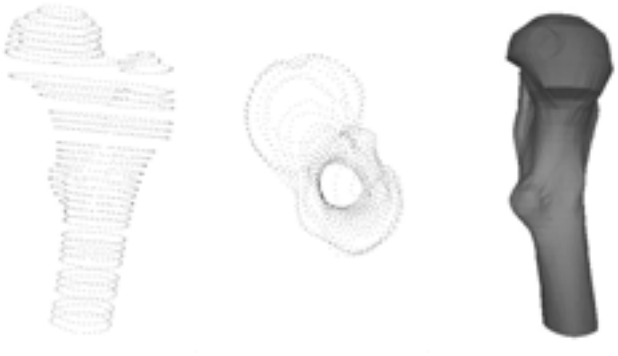

Figure 3–7: *Contour sampling data point set of the femur, the upper extreme of the thy bone. The α-complex geometric model is shown at the right (contour data obtained form the organ data base, Tel Aviv university, Gill Barequet).*

3.4.3 Organisation of the landmarks

Landmark sets may be regularly spaced, organised on a lattice, or irregularly spaced, as a scattered point set. Lattices are taken flexible in this thesis; spacings may differ along different directions, may make jumps along a single directions, may involve spaceas w ell as time dimensions, etc. Probably the best known examples of lattices are the regular rectangular grid and the time series with constant timeinterval. For further background on lattices, see for example [BD74, HM83].

DEFINITION 3.13 (REGULARLY SPACED LANDMARKS)
Landmarks are said to be regularly spaced if their locations match some lattice and irregularly spaced otherwise •

The consequences of regular spacing are severe. Differences in neighbouring distances are removed by a lattice. Obviously, the assumption that $\mathbb{S}$ is in general position does not hold if $\mathbb{S}$ is organised on a regularly spaced lattice and in the context of α-complexes, an $\mathbb{S}$ so organised introduces many degeneracies.

Differences betw een adjacent α-complexes in the α-family can be traced back to variations in distances to the nearest neighbours and variations of weight. Experiment 2.1 in chapter 2 showed that these effects accumulate. In the case of regularly spaced data points (in space and/or time), neighbouring distance variations are eliminated, so theremaining variation must be brought about by the weighting model. Figure 3–8 shows four models, three of which were introduced before. The numerical model is a model derived from the α-complex for numerical computations, such as finite element computations. If also equal weights w erechosen, the α-complex will be degenerate in the sense that faces in the complex all become α-exposed (chapter 2), simultaneously. The α-family then consist of only few members and the modelling flexibility (geometric variation) is largely absent. Therefore, in figure 3–8, regularly spaced points with regular w eights attached is a no-go path, and regularly spaced sample points require unequal weighting. In case of irregularly spaced landmarks and unequal weighting, the number of α-complexes in the α-family will approach the theoretical maximum (chapter 2). Even in the

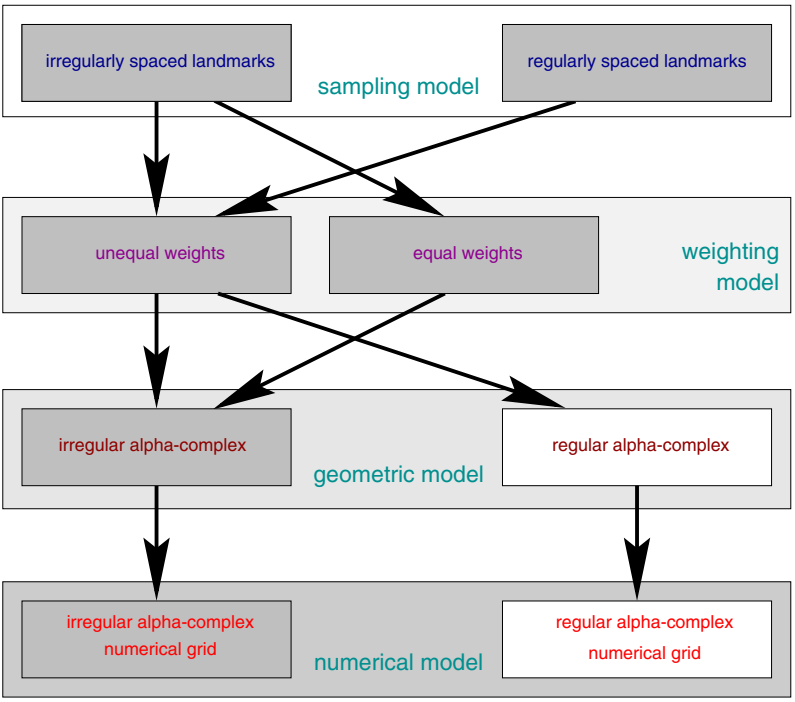

Figure 3–8: *schematic view on the relation between landmark organisation, geometry and numerical model geometry. Gray-ed boxes show the path follow ed with α-complexes. Observe that both irregularly and regularly spaced landmarks can be turned into an α-complex. F or regularly spaced landmarks (e.g., digital pictures), the use of unequal weights is a prerequisite. "Spaced" in this sense also refers to "spaced in time" and "spaced in property-space".*

case of equal weights (e.g., zero weights), spatial variation can be large enough to admit a "rich" α-family.

3.5 Sampling data point set analysis

Analysis of $\mathbb{S}$ is important both in view of further acquisition, for the pre-conditioning of the data and for the design of a proper weight set. The first aspect has been discussed above. The latter t w o aspects will be discussed belw. As a matter of fact, pre-conditioning the data and w eighting are closely interconnected. Not only intuitively, also in a formal sense.

One of the central concepts in spatial analysis is the notion of a configuration. A configuration is defined as follows:

DEFINITION 3.14 (CONFIGURATION)
A configuration of a sampled object is the finite set of all landmarks of that object •

V ariousparameters characterise this configuration. These parameters are the *set parameters*,

common to any set and the more specific *geometric parameters*, typical to geometric sets. To characterise the shape that the landmark set represents, *shape parameters* can be determined. In general, set and shape parameters are real-valued set functions of the form $\mathsf{g} = \Psi(\mathbb{S})$. Compare equation (3–1) and definition 3.3. Generally, pure shape parameters are independent of size, i.e., with $\lambda > 0$:

$$\mathsf{g} = \Psi(\lambda\mathbb{S}) = \Psi(\mathbb{S}) \tag{3–3}$$

whereas set parameters are generally not size independent.

EXAMPLE 3.6 (SET AND SHAPE PARAMETER)
The volume of the convex hull $\mathcal{H}(\mathbb{S})$ is a set parameter but not a shape parameter. The aspect ratio, defined as height divided by width is both a set and a shape parameter •

Set parameters in general can further be divided in *empirical* parameters (observed) and *theoretical* parameters (expected, based on some theoretical model). All these parameters in common give an insight in the spatial point and the associated distribution quality of the data set. So many of these parameters have been proposed that giving an exhausting overview is a bad idea. Rather, a number of typical parameters will be introduced and occasionally given for the data cases to follow in chapter 6. Also, refer to annex D.

3.6 Transformation of the data

3.6.1 Classes of transformations

Transformation is a mathematical term that covers an extensive class of operations. Attention will be restricted here to the pre-conditioning of the landmarks and its impact on the evolvement of the α-complex. This can be done from a domain point of view and from a mathematical point of view. From a domain point of view:

1. *Geometric transformations* apply exclusively to landmark set $\mathbb{S}$.
2. *Property transformations* or *value transformations*[1] always apply to value set $\mathbb{P}_{\mathbb{S}}$.
3. *Weight transformations* always apply to weight set $\mathbb{W}$. Weights can also be seen as a value set, and weighting as a value transformation.

Property and weight transformations will be discussed in greater detail in chapter 4. The former will now be discussed. In other words, the discussion to follow, unless explicitly stated otherwise, applies to Euclidean geometric transformations on landmarks only. From a mathematical point of view, there are three main classes of transformations;

1. The *isometric transformations*.

[1] sometimes called *image transformations*, but this terminology is confusing in this context and will be avoided

2. The wider class of *affine transformations* to which also the linear transformations belong.
3. *Other transformations* that are neither isometric nor affine.

Affine combinations of points were discussed in chapter 2. The properties of these three main classes of mathematical transformations are of particular interest to α-complex modelling. Attention will thereby be concentrated on only two central questions:

1. What impact does the transformation have on the development of the α-family?
2. What impact does the transformation have on the Lebesgue measure?

Finally:

DEFINITION 3.15 (METRIC PROPERTY)
A property is called a metric property if it is left invariant under an isometric transformation, like translation, rotation, etc •

DEFINITION 3.16 (TOPOLOGICAL PROPERTY)
A property is called a topological property if it is left invariant under a homeomorphic, i.e., one-ton-one continuous transformation •

3.6.2 Isometric transformations

Isometries leave Euclidean distances invariant under isometric transformation. Euclidean distance is therefore a metric property under an isometry. Obviously, if weights are not transformed, then also Laguerre distances remain invariant.

DEFINITION 3.17 (EUCLIDEAN ISOMETRIC TRANSFORMATION)
A transformation $\mathsf{T} : S \mapsto U$ *is said to be an isometry (isometric) if it leaves the Euclidean distance between two arbitrary members of* S *invariant, i.e., unchanged* •

An important theorem for Euclidean geometry can now be formulated:

THEOREM 3.6.1 (CLASSIFICATION EUCLIDEAN ISOMETRIC TRANSFORMATIONS)
An isometry is either a translation, a rotation, a reflection, a glide reflection or an identity •

A proof can be taken for example from [Bix94]. Isometries are also known as *rigid motions*. Rigid motions can freely be applied to α-complexes, without any impact on their development or Lebesgue measure. The α-family remains invariant.

A bijection T between $\mathbb{S}$ and $\mathbb{U}$ as a one-to-one correspondence between originals s_i and images u_i. If the mapping from $\mathbb{S}$ onto $\mathbb{U}$ and back is a bijection, the inverse T^{-1} can be shown to exists and both T and T^{-1} are continuous. A proof can be found in almost any textbook on this matter, e.g., see [ND88]. A transformation T from S onto U is called a *homeomorphic translation* (or: *homeomorphism*[2]) if it is bijective and both T and T^{-1} are continuous. Every isometry, for instance, is a homeomorphism. Every rotation, being an isometry, is also a homeomorphism.

[2] do not confuse with another topological characteristic, called a homomorphism between two maps (see e.g., [Mun75, Ch. 8])

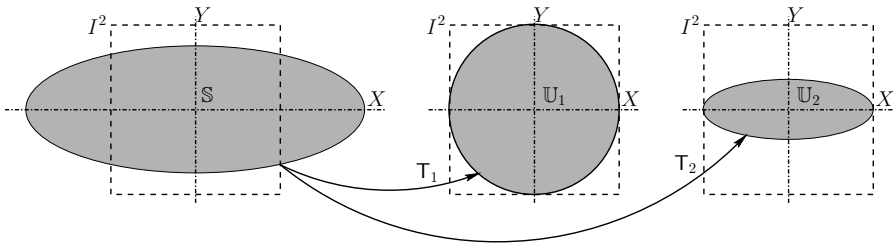

Figure 3–9: *An-isotropic scaling* $\mathsf{T}_1 : \mathbb{S} \mapsto \mathbb{U}_1$ *(left-on to-centre) and isotropic scaling* $\mathsf{T}_2 : \mathbb{S} \mapsto \mathbb{U}_2$ *(left-on to-right).*

A transformation $\mathsf{T} : \mathbb{S} \mapsto \mathbb{U}$ that maps a set $\mathbb{S} \subseteq \mathbb{E}^d$ onto a set $\mathbb{U} \subseteq \mathbb{E}^d$ is said to be an *isotropic scaling* if it multiplies (scales) all coordinates of the originals by a constant real factor λ. A transformation that scales different coordinates differently is called an *an-isotropic scaling.*

EXAMPLE 3.7 ((AN)ISOTROPIC SCALING)
Figure 3–9 shows two different transformations T_1 *and* T_2 *mapping a domain* S *onto* U_1 *and* U_2*, resp. An-isotropic scaling* T_1 *maps the ellipse-shaped domain* $S \subset E^2$ *onto the unit ball and must therefore apply a different scaling* λ_X *and* λ_Y *in* X *and* Y*-direction, resp. More precisely, with* e_X *and* e_Y *being the main radii of the ellipse, we have that:* $\lambda_X e_X = 1$ *and* $\lambda_Y e_Y = 1$ *and* $e_X \neq e_Y$ *in this case. Isotropic scaling* T_2*, on the other hand, scales by a single factor* λ *in both* X *and* Y*-direction, preserving the "shape" of* S*. Now we have that* $\lambda_X e_X = 1$ *but* $\lambda_Y e_Y < 1$*. Both transformations are homeomorphisms, neither of them is an isometry* •

3.6.3 Affine transformations

The latter example provides a good introduction to the next class of transformations, the affine transformations.

DEFINITION 3.18 (AFFINE TRANSFORMATION)
A transformation $\mathsf{T} : \mathbb{S} \mapsto \mathbb{U}$ *is called affine if the members of* $\mathbb{U}$ *can be written as an affine combination of the originals in* S •

DEFINITION 3.19 (LINEAR TRANSFORMATION)
A transformation is called linear if composite effects may be reduced to a cascade of elementary simple transformations, i.e., if: $\mathsf{T}(\lambda_1 \mathbf{s}_1 + \lambda_2 \mathbf{s}_2) = \lambda_1 \mathsf{T}(\mathbf{s}_1) + \lambda_2 \mathsf{T}(\mathbf{s}_2)$ •

If linear, the transformation can be shown to be also affine and a continuous inverse can be shown to exist if the transformation is homeomorphic. Homeomorphism excludes null-transformations which fail to be bijective.

OBSERVATION 3.1 (AFFINE AND LINEAR TRANSFORMATION)
An affine transformation may stretch or shrink a compact original set S *in every direction and translate it, but such that it remains compact. It can be composed of a translation by a translation vector and a linear transformation. If the translation vector is a null vector, then the affine transformation is a linear transformation* •

assuming that the linear transformation is non-singular. The glide (translation) part of an affine transformation, like a rigid motion, has no impact on the development of an α-complex. What remains is a linear transform with impact on both the development of the α-complex and the Lebesgue measure.

EXAMPLE 3.8 (AFFINE AND LINEAR TRANSFORMATION)
Both transformations in figure 3–9 are affine and linear •

3.6.4 Other transformations

Members of the third class are not affine and therefore neither linear nor isometric. No explicite statements can be made upon their impact on the α-family and the Lebesgue measure. Evidently and generally speaking, they cannot be expected to leave the development of the α-family or the Lebesgue measure invariant. Their properties must be evaluated on an individual basis.

Central in the meriting of transformation, irrespective of the class it belong to, is always the notion of *image space* $\mathrm{im}\,\mathsf{T}$ covered by $\mathbb{U}_0 \subseteq \mathbb{U}$ and *kernel* or *nullspace* $\ker \mathsf{T}$. For isometric and affine transformations, it is not difficult to see that $\mathbb{U}_0 = \mathbb{U}$. For the identity transformation, we even have that $\mathbb{U}_0 = \mathbb{U} = \mathbb{S}$. But for other transformations than these, this does not hold true, generally.

With regard to the kernel $\ker \mathsf{T}$, for isometric and affine transformations, the kernel can at most contain a single point. In other words, with isometric and affine transformations, the *dimension* of the kernel, $dim\ \ker \mathsf{T} = 0$, assuming that T is not a null-transformation. This is as expected in the case of a bijective relation and in line with what has been said for the image space. Bijection can be shown to imply that $\ker \mathsf{T} = \{\mathbf{0}\}$. Bijectivity also implies that $\mathbb{U}_0 = \mathbb{U}$ and therefore $dim\ \mathrm{im}\,\mathsf{T} = dim\ U$.

3.6.5 Transformations and the Lebesgue measure

The impact on the Lebesgue measure can be made explicit, under certain limitations and conditions, by estimating the *norm* of the transformation. The discussion here is, for practical reasons, limited to transformations that are at least linear and not null. The *norm of the transformation* is a measure for the impact that transformation has on the domain. The norm indicates an upper bound on the "magnification effect" between any of the images and its original. The norm has two properties that are useful to define when estimating the impact on Lebesgue measures (e.g., [ND88]):

$$\begin{cases} \|\mathsf{T}^k(S)\| & \leq & \|\mathsf{T}(S)\|^k \\ \|\lambda\mathsf{T}(S)\| & = & |\lambda|\ \|\mathsf{T}(S)\| \end{cases} \tag{3–4}$$

In this work, the above norm is called the global norm, and for our purposes, realizing that the Lebesgue measure is position independent, a *local norm* or *Helmertized norm* is defined as follows:

DEFINITION 3.20 (LOCAL NORM OR: HELMERTIZED NORM)
The local norm of a transformation is the norm obtained after Helmertization, i.e., after translating the image $\mathsf{T}(\mathbf{0})$ *of the origin back to the origin, so as to remove the effect of the translation on the norm* •

Determining the local norm is equivalent to determining the norm relative to a translated basis or, equivalently, a local axis system with the same basis vectors as the global. The following may be observed:

OBSERVATION 3.2 (INVARIANCE OF THE LEBESGUE MEASURE)
The impact on the Lebesgue measure is none if the local norm of the transformation is equal to 1. *The reverse is not necessarily true* •

The global norm of an arbitrary isometry is not necessarily 1. Consequently, this also holds for an arbitrary affine transformation and for other transformations. In fact, the global norm is only equal to unity for an identity transformation, for a reflection in a hyperplane through the origin, for translations that resemble a reflection of the supremum in a hyperplane through the origin, and for rotations around an axis through the origin, and a glide-reflection that is a reflection (zero-glide) as above. In many occasions where linear transformations are used, the local norm can be made 1. In the case of isotropic scaling, the local norm is equal to λ and the impact on the Lebesgue measure is given by:

$$\nu_{\mathcal{L}}^{d}(\mathsf{T}(\mathbb{S})) = c\|\lambda^{d}\mathsf{T}\| = c|\lambda^{d}|\ \|\mathsf{T}\| \tag{3–5}$$

3.6.6 Classifying transformations for α-complex modelling

With these definition, it is now possible to further subdivide the geometric transformations in the context of α-complex modelling:

- **Transformations that have no impact on the α-family nor on the Lebesgue measures**

  By far the most important classis formed by the isometric transformations. Neither Euclidian distances not Laguerre distances change. Both these properties are metric and topological properties under these transformations. The local norm of these transformations is equal to 1.

- **Transformations with no impact on the α-family but with impact on the Lebesgue measures of the α-complexes**

  Typical representatives are isotropic scaling, among which isotropic normalisation. Euclidian distances are scaled by a (non-zero) factor $|\lambda|$. The impact on the Lebesgue measure for isotropic scaling is given by eqn. (3–5).

- **Transformations with impact on both the evolvement of the α-complex and the Lebesgue measures**

  Typical representative; gridding and anisotropic scaling. Affine transformations in general, with non-zero glides, belong to this class. The impact of affine transformations on

the Lebesgue measure is given by equation (3–5). Generally, both shape, topology and Lebesgue measures change. If not linear, no explicit statements can be given.

3.6.7 The effect of weighting

So far, transformations were Euclidean transformations, i.e., their properties were discussed in terms of Euclidean metric. How is this when distances are weighted Laguerre distances? After all, weighting can also be regarded as a translation in product space; see figure 3–10.

Consider a transformation that keeps the α-family invariant but not necessarily the Lebesgue measure. For example, assume an isotropic scaling by a factor λ. Regarding the Laguerre distances, two situations may occur:

1. Weight set $\mathbb{W}$ is scaled by a factor λ^2. The Laguerre distances, being a *power distance* are then scaled *conformingly* (e.g., [Kyt98]) and weight is then a metric property under this weight transformation.
2. Weight set $\mathbb{W}$ is scaled by a factor unequal to λ^2. The Laguerre distances may then be modified such that the development of the α-complex is affected. Laguerre distances may become negative, for example. If the development of the α-complexes is indeed affected, the transformation belongs to the third class, described above.

Two examples:

Example 3.9 (weighted lattice)
Figure 3–10 shows a translation T_w by a vector $[\mathbf{0}\ w]^T$, $w > 0$, along the w-axis in positive direction. T_w maps the back-plane grid onto the front grid. For the sake of clarity, the point size has been increased in the front grid, so as to express its increased region of dominance •

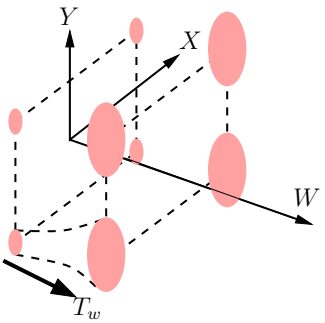

Figure 3–10: *Weighting of a regular grid depicted as a translation in product space $E^2 \times R$. T_w is translated by a vector $[\mathbf{0}\ w]^T$.*

Example 3.10 ((an-)isotropic weighted scaling)
Figure 3–11 shows an weight transformation T_w that is an an-isotropic scaling (centre picture) and isotropic (right picture) both by a factor $\lambda = \frac{1}{2}$. In the latter case, the weight is scaled conformingly, i.e., by a factor $\lambda^2 = \frac{1}{4}$ •

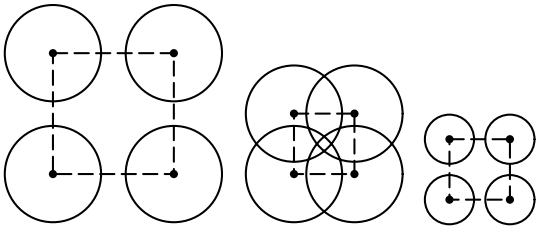

Figure 3–11: *an-isotropic and isotropic weighted scaling in $E^2 \times R$ by a factor $\lambda = \frac{1}{2}$, central and right picture, resp. Weights are depicted by their region of dominance (see chapter 2).*

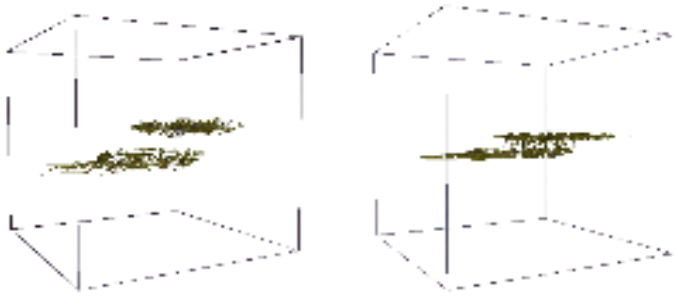

Figure 3–12: *The effect of applying different scale factors in different directions demonstrated here on two adjacent sheet like sand bodies. left: un-scaled, right: scaled with $\mathsf{T}_V = \frac{1}{2}\mathsf{T}_H$. Notice that the α-complex develops differently. In the un-scaled picture, two bodies are well separated, but start to interconnect after scaling, for the same α-value.*

Obviously, all weighted isometric transformations that leave Laguerre distances invariant (i.e., identity transformations), leave α-complexes invariant. In chapter 4 it will become clear that this does not imply that it is also a Euclidean isometry, vice versa. This is almost immediate if one returns to the product space $E^d \times R$ and realizes that Euclidean transformations are transformations that (at least in this thesis) are maps from E^d (on)to E^d, in other words, the weight-coordinate is assumed to remain unaffected. Both domain and image are completely contained in a hyperplane of product space $E^d \times R$ and the transformation does not affect the remaining coordinate. A Laguerre transformation is defined from $E^d \times R$ (on)to $E^d \times R$. It may be broken down in a pure Euclidean transformation that doesn't change weights, and a pure translation or reflection orthogonal to the hyperplane E^d or a combination. See figure 3–10.

Definition 3.21 (Laguerre isometric transformation)
A transformation $\mathsf{T} : \tilde{\mathbb{S}} \mapsto \tilde{\mathbb{U}}$ is said to be an isometry (isometric) if it leaves the Laguerre distance between two arbitrary members of $\tilde{\mathbb{S}}$ invariant •

A number of reasons, however, prevent transformations based on weighted distances from being further treated this way and from this point on, the well established mathematical fundament of linear Euclidean transformations has to be abandoned. Mainly because (see also Annex C):

1. The Laguerre distance is not a metric and it is not a metric property under Euclidean isometric transformations and even not a metric property under Laguerre isometries.

2. Product space $E^d \times R$, endowed with the Laguerre distance is not a metric space and behaves non-Euclidean.

3. As Laguerre distances may become negative, it is unclear (in the scope of this thesis) what the topological consequences are and therefore also whether the Laguerre distance fails to be a topological property.

Actually, all these aspects are inter-related and a result of the nature of the combination space-metric. Further research into the Laguerre transformation seems necessary at this point. This issue is posted as an open problem for further research in chapter 7.

3.6.8 Normalisation

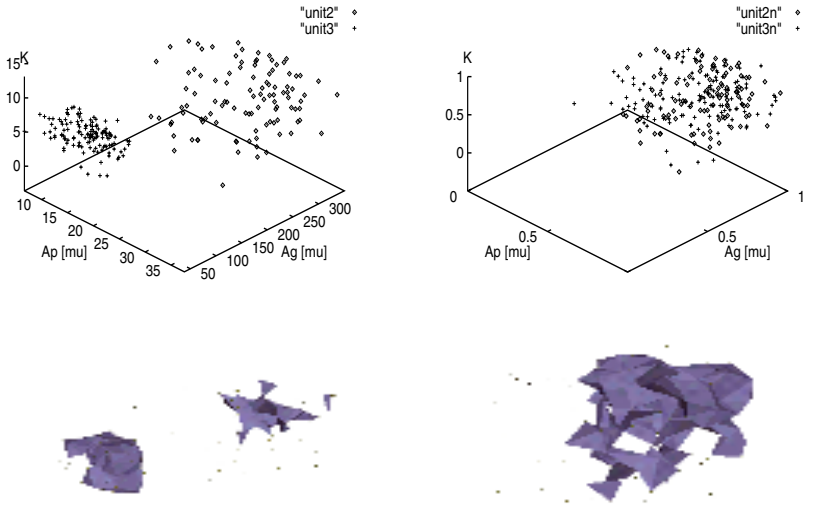

Figure 3–13: *The effect of merging independently normalised data sets. Figures show a tri-variate distribution of permeability K (in Darcy), pore area A_p and grain surface A_g (in μm^2) in an upper part (unit 3) and lower part (unit 2) of a point bar. Pictures at the left show non-normalised data, clearly revealing a clustering in the data. The right-hand side depicts the independently normalised data, resulting in a completely different α-complex. (data samples taken from Martinius, [Mar96] with minor modifications).*

This section on data transformations will be concluded by a discussion of one of the principal transformations in modelling with α-complexes. Normalisation is an affine transformation that causes data, possibly defined on different scales, to become homogeneous in terms of metrics. Normalisation is a common step in shape analysis, and α-complex modelling alike, aiming

to rule out size effects and directional effects. This way, distances between landmarks along different axes can be brought on an equal scale first, before weights are attached. A first step in normalisation is usually an (isometric) translation to the origin of the unit domain, after which the actual scaling takes place. The remainder can be seen as a linear transformation.

If normalisation is an isotropic scaling, then the only effect is that it:

1. Scales the α-spectrum by a factor λ .
2. Scales the Lebesgue measure (d-volume) by a factor $c\|\Pi_{j=0}^{d-1}\lambda_j\| = c|\lambda^d|$.

If an-isotropic, results cannot be stated explicitely. Generally, however, the development of the α-complex and the Lebesgue-measure will be affected. Figure 3–12 illustrates this effect.

There is a second pitfall in normalisation. More precisely, when different sets of landmarks are normalised isotropicly but *independently*.

EXAMPLE 3.11 ((IN)DEPENDENT NORMALISATION)
Let Y_1 and Y_2 be two landmark sets in sample space, with $Y_1, Y_2 \subset S \subset E^d$, that are independently normalised using the following transformations: $\mathsf{T}_1 : Y_1 \mapsto [0,1]^d$ and $\mathsf{T}_2 : Y_2 \mapsto [0,1]^d$. Both normalisation transformations are isotropic and the corresponding scaling factors of T_1 and T_2 are given by:

$$\lambda_1 = \frac{1}{\sup_{j,k}\{|s_{j_k}|\}} , \quad \mathbf{s} \in \mathbb{Y}_1 \tag{3–6}$$

and:

$$\lambda_2 = \frac{1}{\sup_{j,k}\{|s_{j_k}|\}} , \quad \mathbf{s} \in \mathbb{Y}_2 \tag{3–7}$$

resp., where sup *denotes the supremum. Obviously, $0 \leq j < d$. The problem is now apparent: since $\lambda_1 \neq \lambda_2$, in general, the landmark sets are merged, while unequally scaled. Figure 3–13, showing two landmark sets in $\mathbb{E}^3$ of different parts of a single object, shows how clusters of points are completely smeared in the merger* •

Finally, the following observations can be formulated:

OBSERVATION 3.3 (NORMALISATION OF SUBSETS OF LANDMARKS)
Isotropic normalisation of subsets is in itself not a sufficient condition for the development of the α-family based on the union of subsets to be invariant. Normalisation of subsets of landmarks, together forming a set of landmarks can only lead to an invariant α-family if they are all scaled by a common scaling factor. In other words, if isotropy is among dimensions and *subsets* •

3.7 Assigning the weights

Basically, we augment our geometry and/or parameter space with a real valued weight, denoted as h yper-spatial modelling and described in hapter 2. The actual model "ingenuity" is basically in this step, together with any pre-conditioning on the landmarks that might ha vetaken place. The idea is to endow the landmarks with weights suc h that the righ t landmarks connect in the chosen interv alof α and undesirable connections do not show up. Weighting may become a lot easier after applying the appropriate transformations, as the kernel modelsho ws. On the other hand, to some extent, weighting may depend on the spatial scale of the problem. If weighting still does not show the righ tresults, the point process may be modified by "seeding" additional pseudo-landmarks, suc h that the eventual weighting model fits the desired α-complex of the object.

In chapter 6, applications will be discussed in which weights are computed from one or more value sets. Basically, this is a mapping of one or more marked points processes onto a cov ering process with the same poin t process. Weighting is a complicated process and a topic in its own right. It will be discussed in greater detail in chapter 4.

3.8 Inferring a solid object

Once the best-suiting α-complex has been selected, and assuming a d-polytope, w ehav e come to a point that we may wan t to turn the α-complex into one or more connected or disconnected d-faces or d-cells $\mathrm{Conv}\,\mathbb{Y}_j$ or a solid object. The following steps are required for this purpose:

Remov e singular faces singular faces can simply be dropped.

Optionally, remov e tunnels from our final α-complex The only possibility is to triangulate the underlying space $|\mathcal{C}_t|$, using the vertices lying in the border $\mathbb{Y}_t = \{\mathbf{x}|\mathbf{x} \in \mathbb{S} \bigcap \mathcal{H}_t\}$.

Optionally, remov e v oids and pockets from the α-complex Similar.

Compute the underlying space This is basically the space $|\mathcal{C}_\alpha|$ obtained by collecting all the d-simplexes in the complex.

Capture the underlying space in a reduced n umber of d-faces The most straightforward w a y to do this is just to k eep the result from the previous step. In addition, one may wan t to filter off (part of the) internal vertices so as to reduce the storage complexity.

Notice that the pros of α-complex modelling will be partly undone by an all too negligent removal of tunnels, voids, etc. It leads, ho w ever, to a geometry and topology which is somewhat easier to import in many modelling en vironmen ts. It may be a necessary step to obtain seamless integration with existing modelling environments.

3.9 Theoretical analysis

Point processes ha v ebeen in troduced in chapter 2. Time related issues are usually described b y *renewal theory* ([Tij94], with the P oisson process a time dependent problem, and spatial

occupancy issues, such as the region of dominance of a weighted point are conveniently described by a *cover age process* (e.g., [Hal88]). Point processes can be defined over time much in the same fashion as in space. Assume a point set $\mathbb{S} = \mathbb{S}(t)$ for some $t \in (t_0, \infty)$ and assume that sample points are no wobserved on an individual basis at specific moments in time. The constraints that $\mathbb{S}$ is finite and compact posed in chapter 2 remain in place. It makes sense to define each $s(t) \in \mathbb{S}(t)$ as a sequence in time such that time t is strictly increasing:

$$t_0 < t_1 < t_2 < \cdots < t_n \tag{3–8}$$

with:

$$\lim_{n \to \infty} t_n = \infty \tag{3–9}$$

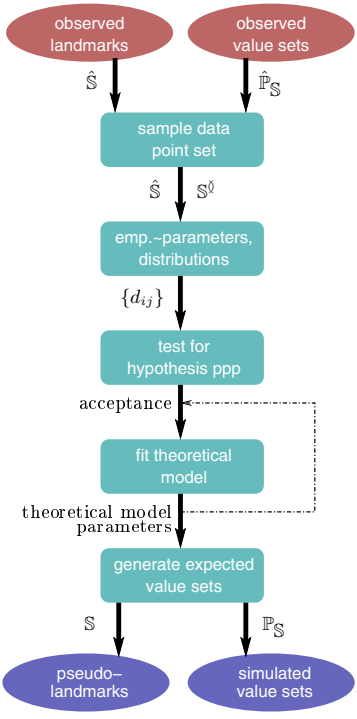

Figure 3–14: *basic steps in theoretical point process model estimation.*

The ordered sequences $s(t) = [s_1..s_n]$ of a single fixed sample point overtime, where s_1 denotes s at t_1, etc., form a marked point process, with the observed value set as the set of marks and the arrival times t_j as events. It makes more sense to study the (theoretical or empirical) point process in spatio-temporal space as an entirely spatial point process. This way,

the generally *simple non-delayed renewal process* is turned into a spatial Poisson point process. In that case, time is also defined on a half-space, i.e., $t > t_0$. For further details, see for example [Sig95, SKM95]. Approaching temporal problems by means of a spatio-temporal sample space carries along the risk that the uni-directional quality of the cause-event-effect and inter-event relations of time gets blurred in the spatio-temporal space. In spatial problems, inter-event relations are usually not uni-directional, whereas problems defined in the time domain, tend to develop inter-event relations that are working away in time only Not backwards.

The *null-hypothesis* of the ppp being (homogenous) Poisson is to be verified and accepted or rejected, according to good statistical practices. The intensity of the Poisson point process (shortly: ppp), is given by $\lambda = \mathsf{E}[\Phi_{\mathbb{S}}([0,1]^{\mathrm{d}})]$. For a homogenous ppp, this λ will be independent of the subset taken from $\Phi_{\mathbb{S}}$. For a true ppp, points are uniformly distributed in space and stationarity and isotropy (or: homogeneity) can be proven. If a sampling window is placed over the sample space and samples are only drawn from the window area, then for a stationary random spatial point pattern, the intensity will be uniformly distributed too. More in detail, with $\Sigma^{(d)}$ a d-dimensional window:

$$\mathsf{E}[\Phi_{\mathbb{S}}(\Sigma^{(\mathrm{d})})] = \mathsf{E}[\mathrm{card}\ \Sigma^{(\mathrm{d})}] = \lambda \nu_{\mathcal{L}}^{d}(\Sigma^{(d)}) = \lambda |\Sigma^{(d)}| \tag{3–10}$$

where $\nu_{\mathcal{L}}^{d}(\Sigma^{(d)}) = |\Sigma^{(d)}|$ is a Lebesgue measure for the window. It is important to notice that stationary Poisson point processes have the so called conservation property:

OBSERVATION 3.4 (POISSON POINT PROCESS CONSERVATION PROPERTY)
A (non-singularly) linearly transformed stationary Poisson point process is again a stationary Poisson point process •

Verification of the null-hypothesis of a ppp is a topic further discussed in annex D.

What theoretical support can be provided by a ppp, fit to an observed point set? More precisely: how can these models be used to determine *estimators* for the expected α, weight, nearest neighbour distances and voids, along with their variances? In this work, two coverage processes are of interest:

- **A coverage with weight-plus-alpha balls in the landmarks**

  This is a coverage with the union $\mathcal{B} = \bigcup_j \mathtt{B}_{w+\alpha}(\mathbf{s}_j)$ of weight-plus-alpha-balls, resembling the space filling diagram $\mathcal{F}(\tilde{\mathbb{S}}) \cong \mathcal{U}_{\alpha}(\tilde{\mathbb{S}})$, as discussed in chapter 2. Refer to figure 2–1. This union has a dual, which is the geometric realisation of the nerve, coinciding with the α-complex as a sub-complex of the regular triangulation for that α.

- **A coverage of the radical centres with equally sized α-balls**

  The radical centres coincide with the vertices of the Voronoi diagram $\mathcal{V}(\tilde{\mathbb{S}})$, as explained in chapter 2. These radical centres $C^{\emptyset}$ become the centres of the coverage process $\mathcal{A} = \bigcup_j \mathtt{A}_{\alpha}(C_j^{\emptyset}$ and the α-balls become the grains.

The latter coverage process is associated with the former in the sense that both are parametrised by α. What does the coverage process tell about the resulting α-complex? What is the expected α for example? The grains of both coverage processes generally:

- **Do not overlap or touch for** $\alpha < \alpha_{\min}$

  No edge between any two nearest neighbours is α-exposed yet.

- **Overlap and touch for** $\alpha_{\min} \leq \alpha \leq \alpha_{\max}$

  Part of the $\mathcal{V}(\tilde{\mathbb{S}})$ is still uncovered but both processes do overlap or at least touch. If not, no α-exposedness could occur and the α-complex could not develop.

- **Completely overlap for** $\alpha \geq \alpha_{\max}$

  No part of the Voronoi diagram is uncovered anymore, i.e., $\mathcal{V}(\tilde{\mathbb{S}})$ is fully covered by $\mathcal{U}_\alpha \bigcup \mathcal{B}_{w+\alpha}(\tilde{\mathbb{S}})$.

With respect to both coverage, the probability of a void of a given size, for a homogenous ppp given by $\mathsf{Pr}[\Phi_{\mathbb{S}}(\mathtt{A}_\alpha) = 0]$ and its complement $1 - \mathsf{Pr}[\Phi_{\mathbb{S}}(\mathtt{A}_\alpha) = 0]$ is of interest, as it denotes the probability of a vacancy, an incomplete coverage, and consequently a hole of either nature in the α-complex. More detailed discussions on this matter and also consequences of inhomogeneous underlying Poisson point processes in chapter 4.

This section is concluded with the definition of the remaining open problem, about the need for full spatial occupancy in an icon and the instantiated objects from that icon. Firstly, it is important to come to a conclusion as to whether a void space be justified from a geological point of view and if so, under what circumstances. If not, what should be done to "repair" the presence of a void. Should it be filled with some appropriate "background" material, like clay or sand, or should it be saturated by a fluid, like water? Secondly, if void space is allowed, how should it be handled in the scope of scenarios and in the modelling framework processes, such as inversion?

3.9.1 Stochastic parameters

Section 3.5 discussed the analysis of a sampling data point set. Now that the ppp has been given a place in the modelling framework, a couple of analysis tools can be added. Annex D provides background on the describing parameters. This section focuses on the meaning of *distance-based* parameters in the analysis process.

Triangulations deliver a nearest neighbour analysis in the sense that $\mathcal{NNG}(S) \subset \mathcal{T}(S)$, and also $\mathcal{LFNG}(S) \subset \mathcal{T}(S)$ where generally, the nearest neighbour graph $\mathcal{NNG}(S)$ and the local-furthest neighbour graph $\mathcal{LFNG}(S)$ generally differ. Recapture from chapter 2 that the important parameters that determine a triangulation and filtered α-complexes, are:

- The number of points per unit (hyper-)volume, expressed by the empirical point density $\bar{\lambda}$. The theoretical counterpart is the point process intensity λ.

- The empirical distribution of the Euclidean nearest neighbour distances, for example, expressed and tied to a location by the geometric Euclidean distance based nearest neighbour graph $\mathcal{NNG}(\mathbb{S})$. The theoretical counterpart is the theoretical k-th nearest neighbour distribution, for example given in [SS94, Ch. 4].

- The distribution of the Euclidean local-furthest neighbour distances, expressed and tied to a location by the geometric Euclidean distance based local-furthest neighbour graph

Estimator		Empirical		Theoretical	
ts density point	density point	empirical point	$\hat{\lambda}$	Poisson point process	λ
Euclidean tances	nearest neighbour distance function	Euclidean nearest neighbour distance $\mathrm{NN}(\mathbb{S})$, $\hat{\mathrm{d}}(\mathbf{s}, \mathrm{NN}(\mathbf{s}))$	density	Euclidean nearest neighbour distance	$\hat{\mathrm{d}}(y)$
graph	bour distance	Euclidean real-furthest neighbour distance $\mathcal{LFNG}(\mathbb{S})$, $\hat{\mathrm{d}}(\mathbf{s}, \mathrm{FN}(\mathbf{s}))$	bour distance	Euclidean k-th nearest neighbour distance	$\mathrm{d}^{(k)}(y)$
bourhood distance Lague meigh	Lague meigh bour distance graph	Lague nearest neighbour $\mathcal{NNG}(\tilde{\mathbb{S}})$, $\hat{\mathrm{d}}(\mathbf{s}, \mathrm{NN}(\tilde{\mathbf{s}}))$			
	coverage	coverage $\hat{\kappa}$, void ratio $\hat{\varepsilon}$			$\mathsf{g}(\kappa)$, $\mathsf{E}[\kappa]$
	α and eight	$\mathcal{V}(\tilde{\mathbb{S}})$ (implicit)			$\mathsf{g}(\alpha)$, $\mathsf{E}[\alpha]$, $\mathsf{g}(w)$, $\mathsf{E}[\mathrm{w}]$

Table 3-2: *empirical ersus theoretical in functions and functionals discussed*

parameters. Interchangeable *further theory and s do not coalesce.*

$\mathsf{g}(y)$ *is a distribution*

hapter 3:

$\mathcal{LFNG}(\mathbb{S})$. The theoretical counterpart is the theoretical local-furthest neighbour distribution that is determined in the k-th nearest neighbour distribution, above.

- The distribution of the nearest neighbour Laguerre distances, expressed and tied to a location by the Laguerre distance based weighted nearest neighbour graph $\mathcal{NNG}(\tilde{\mathbb{S}})$. The theoretical counterpart must be modelled using a Boolean model in which weight is related to the grain size, or a Poisson point process in hyperspace.
- The distribution of the local-furthest neighbour Laguerre distances, expressed and tied to a location by the Laguerre distance based weighted local-furthest neighbour graph $\mathcal{LFNG}(\tilde{\mathbb{S}})$. The theoretical counterpart is the same model as with the nearest neighbour distances.
- The degree of coverage of the Voronoi diagram by the d-ball union $\mathcal{U}(\tilde{\mathbb{S}}) \cong \mathcal{B}(\tilde{\mathbb{S}})$, expressed by the empirical coverage factor $\hat{\kappa}$. The degree of void space, the empirical void ratio $\hat{\varepsilon}$, can be derived from the difference between the convex hull $\mathcal{H}(\mathbb{S})$ and $\mathcal{W}(\tilde{\mathbb{S}})$. The theoretical counterpart being the expected ε.
- A distribution of the Laguerre distance of an arbitrary point to weighted points, among other things an indication for the α-values required for α-exposedness, expressed by the theoretical point-event distance distribution.There if no direct equivalent, but the Voronoi diagram contains this information in an implicit fashion.

Table 3–2 summarises.

3.10 Refining the kernel modelling framework

Figure 3–15 shows the expanded kernel modelling framework, the initial kernel version of which has been presented in section 3.3. Given a MoM on the one hand and the theoretical support and the empirical and theoretical point process analyses on the other hand, the question is how to determinethe α-complex with the best goodness-of-fit. As long as the inversion and the knowledge-based part of the modelling environment (see fig. 3–1) are not ready, visual inspection and human interaction stop the model geodynamic modelling cycle. Present characteristics of the α-complex that can be related to the empirical and theoretical parameters and values, to allow for repair. Repair is basically: first try to modify weights to improve the coverage, adding pseudo-landmarks if needed. As soon as the knowledge-based part is ready, adding more detailed facts and possibly new rules and constraints becomes a third option.

3.11 Dynamic models

So far, object models have been static, i.e., independent of time. In this section, dynamic problems based on α-complexes will be discussed. The use of dynamic models fits in a wider objective, already faintlypainted in chapter 1. Recording and replaying geological evolutionary scenarios must be supported by the α-complexes that represent the objects. The more concrete objective of this section is to abridge the use and definition of landmarks and the α-complexes they set forth and their dynamic behaviour. It has been stipulated before, that dynamic modelling affects geometry, topology and properties. Table 3–3 elaborates on this.

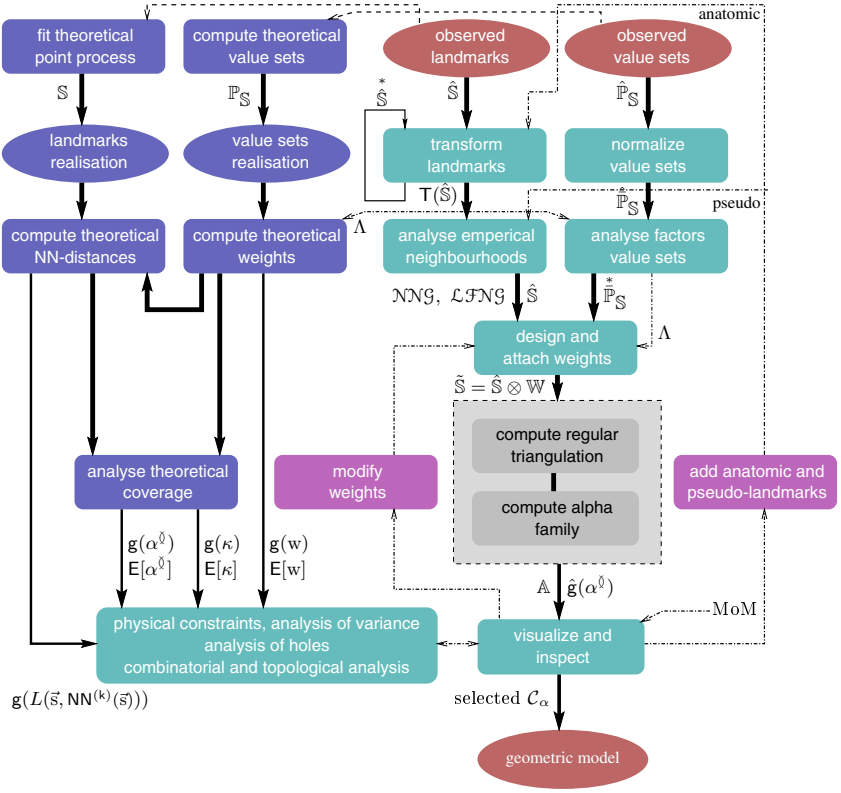

Figure 3–15: *the expanded sequence of steps involved in modelling with α-complexes, some steps may be void. Not shown in this figure is the domain decomposition that can be imposed on S, on the triangulation and on the resulting α-complex.*

Instantiated objects are constructed to receive their dynamic behaviour to both *internal* processes that have been embedded in the icon, to *external* processes that run in the environment and have been embedded in the scenarios and to *external* objects that act upon them.

EXAMPLE 3.12 (PROCESSES)
Internal creep, governed by embedded internal creep model, may cause the object to deform as its overburden increases. The increase of radiogenic heat flow that passes through the object, a process defined in the environment, accelerates the object's plastic deformation. The object may then become hydrocarbon saturated under the influence of a source rock system below, that expels the multi-phase fluid flow containing hydrocarbon and impermeable rock ontop that caps the object, trapping the hydrocarbon •

The unimaginable extent of geological scales also has its influence on the description of dynamic models. Depending on the chosen scale, geological events can take the appearance of discrete instantaneous state changes but at a finer scale, become continuous evolutionary

processes.

EXAMPLE 3.13 (INFILL OF A VALLEY BY A MEANDERING RIVER SYSTEM)
Assume that the infill of a valley by a river system takes $O(10^4)$ A, order of magnitude of ten thousand years. In a geomorphological scenario that studies exactly this infill process, the fluvial sedimentation process studied at a regional scale and within a seasonal time frame is continuous and evolutionary. For a paleological scenario that runs at a continental spatial scale and at a geological era or period time scale, like Miocene, a $O(10^6 - 10^7)$ A-timescale, say, the same sedimentary process is usually beyond the model's time resolution and infill occurs instantaneously
•

Geodynamic objects must therefore be implemented such that they can act and respond to both modelling approaches. From a theoreticalpoint of view, both the continuous evolutionary and instantaneous state change scenarios can be accommodated by a single dynamic model description, but in practice, implementation of such approaches is inconvenient. Therefore, the two descriptions will be treated separately

3.11.1 Continuous evolutionary model

Dynamic models that follow a continuous evolutionary development are commonly described by an analytic model based on a system of linear or non-linear (partial) differential equations. The majority state a boundary value or initial value problem, or a combination thereof. Occasionally, analytical model are used directly for computations. This will not be regarded here. Here, the definition of a numerical model is assumed. The numerical geometric model to be derived from the icon α-complex (see figure 3–8) then becomes usually a model based on one of:

- **Finite element model**

  Faces from the α-complex can be used for the definition of the elements, under certain conditions:

  - Elements are generally 3D.
  - The aspect ratio of the simplices must be reasonable.
  - Element families are not always as mature as quad-like elements, for example regarding the capabilities to handle orthotropic phenomena.

  The honouring of conservation laws, like mass conservation, poses some problems for node-based finite element formulations, occasionally.

- **Finite difference model**

  The problem here is that regridding must usually take place. Finite difference approaches based on simplices were not found in literature.

- **Control volume finite difference model**

  This class of numerical models poses roughly the same problem as the finite element models, but honouring conservation laws can mostly be guaranteed.

There are many variations on these central numerical model descriptions, but the main outline of the problems remains usually valid. With there being a vast amount of literature on these numerical approaches, no further description will be presented here. See for example, general discussions in [Zie83, Str86, Hug87, Sew88, Tay92] and discussion related to the field of natural sciences and earth sciences in particular in [LP82, Aki90, DS90, ZN93, ABBM94, ABBM95].

Introducing dynamics in a finite element model derived from an iconic α-complex means the definition of time dependent landmarks and value sets. Making topology dynamic is hardly or not at all supported by the current generation FEM-codes. The use of α-complex models, with their implicit topology, may change this. One of the cases in chapter 6 demonstrates how. Regarding dynamic geometry, aspect ratio's of elements must remain within safe ranges. Classical themes are always stability and convergence.

3.11.2 Finite state model

In a finite state model, a dynamic system is brought from a stable or unstable state into a (possibly other) stable state, by well-defined planned actions or *events*, triggered to operate upon them. To describe a finite state dynamic model, the approach given in [SH96] is closely followed, except the fact that here a mapping acts on a set rather then on a vector.

Time in the analytic model description will be denoted by t. Time since t_0 in initial value problems will be denoted as $\tau = t - t_0$. The discretized time in a numerical model is denoted by the ordered sequence $t_0, t_1, t_2, .., t_j, t_{j+1}..$ In analytical problems, a time step is denoted by dt, in (iteratively solved) numerical problems by $\Delta t \cong \Delta\tau$.

Long-time dynamic behaviour is modelled in the approach by Stuart and Humphries using invariant sets and limit sets:

DEFINITION 3.22 (INVARIANT SET)
An invariant set is a set which is mapped onto itself •

DEFINITION 3.23 (LIMIT SET)
A limit set is an invariant set that is transformed towards a attractor set, i.e., a set of values towards it is attracted under the ruling dynamics •

EXAMPLE 3.14 (INVARIANT AND LIMIT SETS)
Steady state solutions, periodic solutions and chaotic solutions are instances of invariant sets. Maximum distance solutions, zero-frequency solutions and thermodynamic equilibrium are instances of limit sets •

Let $\mathbb{S}$ denote a compact finite set of landmarks in E^d. Further, let $\mathsf{G} : \mathbb{S}_j \mapsto \mathbb{S}_{j+1}$ be a time discrete mapping process, i.e., a process that sends a set $\mathbb{S}_j$ at time t_j into a set $\mathbb{S}_{j+1}$ at time t_{j+1}, with $t_{j+1} = t_j + \Delta t$ and $j \in \mathbb{N}$. In mathematical terms:

$$\mathbb{S}_{j+1} = \mathsf{G}(\mathbb{S}_j) \tag{3–11}$$

which means that for every vector $\mathbf{s}_j$, the image is given by $\mathbf{s}_{j+1} = \mathsf{G}(\mathbf{s}_j)$. Further, at time $t = t_0$ $\mathbb{S}_0$ is given, $\mathbb{S}_0 = S$. An instance of such mapping process is an erosion process, in this thesis

taking the form of a morphological erosion of landmark set $\mathbb{S}$ by some other set. Erosion will be described, shortly.

The step-wise evolution of the mapping process can be written simply as a half-open time sequence of the form:

$$[\mathbb{S}_0, \mathbb{S}_1, \mathbb{S}_2, .., \mathbb{S}_j, \mathbb{S}_{j+1}, .., \mathbb{S}_\infty) \tag{3–12}$$

that denotes the evolutionary time sequence of unique system states, represented by the time discrete set of landmarks. With $\mathbb{S}$ compact and finite, one demands from G that it leaves $\mathbb{S}_{j+1} = \mathsf{G}(\mathbb{S}_j)$ compact and finite, in other words that every image is again a valid original. This sets forth demands on the norm of the mapping process, to be discussed, shortly. Also, in order for unique mappings (solutions) to exist, G is assumed to be single-valued.

The $\mathbb{S}_0$ is called the *initial value* set or *initial data set*. Equation (3–12) is called a *mapping process* or *iteration*, defined as follows:

DEFINITION 3.24 (TIME DISCRETE MAPPING PROCESS)
A time discrete mapping process, in this work, sends a set of landmarks into a modified set of the same landmarks, according to some mapping definition, defined between discrete time steps from starting time t_0 onwards •

In the above form, $\mathsf{G} : \mathbb{S}_j \mapsto \mathbb{S}_{j+1}$, with $\mathbb{S}_{j+1}$ according to eqn. (3–11), is an *explicit* formulation. Many problems, e.g., non-linear problems cannot be formulated in an explicit form. They can only be formulated in an *implicit* form $\mathsf{H} : \mathbb{S}_j \times \mathbb{S}_{j+1} \mapsto \mathbb{S}_{j+1}$, with $\mathbb{S}_{j+1}$:

$$\mathbb{S}_{j+1} = \mathsf{H}(\mathbb{S}_{j+1}, \mathbb{S}_j) \tag{3–13}$$

Explicit formulations can be derived from implicit and the implicit form is also called the *generalised form*. Typical candidates for explicit and implicit formulations are the *forward Euler* and *Backward Euler*, resp., and the more general Runge-Kutta methods. The norm of a mapping process is given by:

$$\|\mathsf{G}\| = \sup_{\mathbf{s}_j} \frac{\|\mathsf{G}(\mathbb{S}_j)\|}{\|\mathbb{S}_j\|} \tag{3–14}$$

An evolutionary map Γ^n is an n-fold product sequence of mapping processes G_j, i.e., $\Gamma^n = \mathsf{G}_j \circ \mathsf{G}_{j+1} \circ \mathsf{G}_{j+2} \cdots \mathsf{G}_{j+n}$. Assume the norm in any of these mappings is at most $|\gamma|$, i.e., $\|\mathsf{G}\| \leq \gamma$. The norm of the evolutionary map then has the upper bound:

$$\|\Gamma\| \leq |\gamma|^n \tag{3–15}$$

For further details, refer to [Tay92, Ch. 5] and [SH96].

Level	Geometry	Topology	Property	Applications	Time dependencies
6	dynamic	dynamic	dynamic	virtual earth, paleo-reconstruction, modelling, erosion, mining, dilation, closing, complex, fluid dynamics, basin analysis, mechanics	$\mathbb{S}=\mathbb{S}(t)$, $\alpha=\alpha(t)$, $\mathbb{P}_{\mathbb{S}}=\mathbb{P}_{\mathbb{S}}(t)\Rightarrow\mathbb{W}=\mathbb{W}(t)$, geometric, value and weighting transformation
	dynamic	dynamic	static	paleo-reconstruction modelling, simple virtual reality models, basin analysis, fracture studies, mechanical	$\mathbb{S}=\mathbb{S}(t)$, $\alpha=\alpha(t)$, Euclidean geometric transformation
	static	static	dynamic	fault systems studies, simple hydraulic studies, crack propagation, 3D GIS applications	$\mathbb{S}=\mathbb{S}(t)$, $\alpha=\alpha(t)$, $\mathbb{P}_{\mathbb{S}}=\mathbb{P}_{\mathbb{S}}(t)\Rightarrow\mathbb{W}=\mathbb{W}(t)$, (Euclidean) geometric, value and weighting transformation
	dynamic	dynamic	static	migration models, timespan studies, spatial distribution of pollution, parameter density studies, spatial studies	$\mathbb{S}=\mathbb{S}(t)$, $\mathbb{P}_{\mathbb{S}}=\mathbb{P}_{\mathbb{S}}(t)\Rightarrow\mathbb{W}=\mathbb{W}(t)$, (Euclidean) geometric, value and weighting transformation
	static	dynamic	static	value of spatial distributions using time series (e.g. in GIS)	$\mathbb{P}_{\mathbb{S}}=\mathbb{P}_{\mathbb{S}}(t)\Rightarrow\mathbb{W}=\mathbb{W}(t)$, weighting transformation
1	static	static	static	status of a reference, shape reconstruction	

dynamic geometry and topology ... *α-complexes.*

3.11.3 Dynamic geometry

Dynamic geometry is fundamental to the use of instantiated templatised shapes. Now that a description of a dynamic model by means of taking $\mathbb{S} = \mathbb{S}(t)$ has been presented, it is now appropriate to look at the further implications that this may have on the shape. For example, geometric changes may induce topological changes. It has been explained that if the evolutionary map can be characterised as a isometric map, the topology of the α-complex does not change. If, on the other hand, the weighted nearest neighbour distances change an-isotropicly (affinely), the α-value, the α-rank and the topology will generally change.

In the case of shape instantiation from an icon, two further strategies can be followed to handle a dynamic α-complex-based object model:

- **Violate the α-complex**

  Instantiate the icon, transform to fit observed data, keeping the icon's topology. Due to the transformation, the resulting shape may be a simplicial complex but not an α-complex anymore (see also: chapter 2).

- **Keeping the α-complex sane by regeneration**

  Instantiate the icon, transform to fit observed data, but update the topology as required to restore appropriate α-filtration. The result is now an α-complex again, but the topology may differ from that of the icon.

What happens if α is defined as a function in time. i.e., $\alpha = \alpha(t)$? Even if the evolutionary map is equal to an identity, still, the changing α may introduce changes in the topology. This is basically the problem of variational geometry, possibly leading to invalid or undesired topologies. Geometry here is parametrised by α and variational geometry means: changing α. The question as to whether this is a problem depends on the problem at hand.

The effect on the Lebesgue measure is not easily stated in general terms. The discussion on dynamic geometry is concluded by an example, illustrating this.

EXAMPLE 3.15 (COMPACTION PROCESS)
Consider a non-linear isotropic compaction process, given by the evolutionary map $\Gamma^n S_0$ with $S_0 = S$. Let $S_{j+1} = \alpha(t)S$ with $\alpha_{j+1} = 2\alpha_j$. Assume $\alpha(t) \gg w$, thus neglecting the effect of w and $\|\Gamma^n\| \leq |\gamma|^n$. Further, realise that if α doubles, the radius of an α-ball increases by $2^{\frac{1}{2}}$. Then the effect on the Lebesguemeasure of a changing α can be estimated using the inequality $\nu^d_{\mathcal{L}}(\Gamma^n S) \leq |\gamma|^{\frac{1}{2}nd}$. Although true for some $n \in \mathbb{N}$, the tricky part is that $|\gamma|$ is monotonically growing for growingn and unbounded for $n \to \infty$ •

3.11.4 Dynamic topology

In chapter 2 it is has been demonstrated that weight and α have similar effects and that it is the combination of $w + \alpha$ that governs the development of the α-complex. Also take a preview on figure 4–4. The latter shows in fact an accumulation of the two effects, in the sense that $\epsilon(\alpha) = w + \alpha$. Two questions are now important:

1. Is the *whole distribution* of nearest neighbour distances running out of sync with the current α over time? Then remedy by setting $\alpha = \alpha(t)$ and if the divergence is stationary, then in addition or alternatively, an isotropic scaling transformation $S = S(t)$ can be applied. The clue here is to apply global Euclidean transformations.

2. Is the *cover age locally* getting too low or too high? Then remedy by taking $w = w(t)$, thus modifying the local Laguerre distances in the identified neighbourhoods. The clue in this case is to apply local weight transformations.

More concisely, assume a time dependency, i.e., take $\epsilon(w(t), \alpha(t))$. The topology will remain invariant if the time derivative of $\epsilon(w(t), \alpha(t))$ is equal to zero:

$$\frac{d}{dt}\epsilon(w(t), \alpha(t)) = \frac{\partial \epsilon}{\partial w}\frac{dw}{dt} + \frac{\partial \epsilon}{\partial \alpha}\frac{d\alpha}{dt} = 0 \tag{3–16}$$

A trivial way to obtain this is setting $w(t)+\alpha(t) = w+\alpha = c$, another trivial way is to compensate changes in weight by changes in α, an effect already shown by experiment in chapter 2:

$$\frac{\partial \epsilon}{\partial \alpha}\frac{d\alpha}{dt} = -\frac{\partial \epsilon}{\partial w}\frac{dw}{dt} \tag{3–17}$$

From a practical point of view, such schemes are not easily designed for the general case.

3.11.5 Dynamic properties

In this work, a vector of value sets map into a single weight set. In fact, dynamic properties, leading to dynamic value sets and dynamic weight, are the triggers for changes in the shape to occur. This is only a natural consequence of the property-ruled shapes that we encounter for natural objects. If properties become functions in time, so become the corresponding vertices in the parameter space and so becomes their equivalence class membership and so becomes their weight. See chapter 2.

The property-weight relation, as will be explained in chapter 4, can be stated in normalised form:

$$w = \lambda_1 p_1 + \lambda_2 p_2 + \cdots + \lambda_m p_m = \sum_{j=1}^{m} \lambda_j p_j \tag{3–18}$$

such that we have $\sum_j \lambda_j = 1$, for the properties $p_j,\ 1 \leq j \leq m$ in concern. Let the coefficient vector[3] $\Lambda = [\lambda_1, \lambda_2, \ldots, \lambda_m]^T$ denote the relative weights λ_j in equation (3–18). Vector Λ usually results from some data analysis process, typically discriminant and factor analysis (e.g., see [Dav86, Boc96, Mos97]). It states the relative discriminating power of each of the individual properties and it is itself not likely to change over time.

[3] the term: weight vector would be more appropriate, but in this context confusing

Assuming $d\Lambda/dt = 0$, the effect of the property vector $\mathbf{P(t)} = [p_1(t), p_2(t), \ldots, p_m(t)]^T$ on the weight $w(t)$ is zero if:

$$\left\| \frac{dP}{dt}^T \right\| = 0 \tag{3–19}$$

again from a theoretical point of view and complicated to estimate in practice for the general case.

3.11.6 Dilation and erosion

The geodynamic process of deposition and erosion are of paramount importance in the replay of evolutionary geological scenarios. Particularly with sedimentary type of objects primarily focused on in this thesis. From a geological or geomorphological point of view, it is relevant to determine if material sources and sinks are internal to the environment or external. Deposited material may be streamed into the environment as an input flux or may be originating from erosional processes elsewhere within the system. Likewise, eroded material may be exported from the environment. If not, it must be deposited in a sink elsewhere in the environment or remain flowing around.

These geological processes are nicely supported by their morphological abstract counterparts dilation (supporting deposition), erosion (supporting erosion), opening (supporting wear, cracking and separation) and closing (infill of holes). Dilation and erosion are two well understood set operations in mathematical morphology. From a mathematical point of view, an erosion is a mapping for $\mathsf{G}_E : \mathbb{S} \mapsto \mathbb{S} \ominus \mathbb{U}$. It sort of wipes out (erases) landmarks of the eroded object, contained in the pathway of the eroder.

The important aspect here is to establish the capability of α-complexes to support such operation in a natural way. This will be discussed now.

Erosion

As explained earlier, objects are eroded by processes in the environment or by other objects in their vicinity. The latter are called *eroders*.

DEFINITION 3.25 (ERODER)
An eroder is an instantiated object that erodes an adjacent object •

An easy geometric shape of the eroder makes the definition of the erosion mapping process less complicated, but basically, any object represented by any α-complex may become an eroder. The shape of the eroder is then always the α-hull or α-shape $\mathcal{W}_\alpha(S)$. The eroder itself may also become eroded. So in the general case, two objects are both eroder and subject to erosion. This leads to an important observation:

OBSERVATION 3.5 (CHANGING CARDINALITY OF ERODER AND ERODED SHAPE)
Erosion becomes manifest in a changing cardinality $\mathrm{card}\,\mathbb{S}$ *of both the eroder and eroded shape* •

How to deal with vanishing points? As with dynamic geometry, there are basically two strategies:

- **Violate the α-complex**

  For the evolutionary map to remain a bijection, points may not vanish and the cardinalities may formally not alter. Two possible solutions materialise:

  Replace eroded elements by neutral elements Degradate vanishing landmarks and their star to empty sets, i.e., lower their dimension to -1, making them an improper (-1)-face (empty set). This collapses faces to void space. In so doing, the bijection of the evolutionary map can be maintained. It however violates the topology and changes the Lebesgue measures within the α-complexes.

  Translate eroded points Move vanishing points to the new boundary resulting after erosion. Points so moved survive as landmarks. They may be moved until at infinitesimal but non-zero distance from the landmark with which an edge is shared in the complex. If further translation is needed, then both these landmarks will have to move. This keeps the topology of the α-complex invariant, but may no longer correspond to the underlying triangulation criteria (see chapter 2).

- **Keeping the α-complex sane by regeneration**

  Instantiate the icon, erode it and regenerate the regular triangulation after every evolutionary step. Triangulations are bound to change and therefore also the α-complex. The result is a valid α-complex, in contrast with the previously presented solutions.

A third but basically different approach is the following. Eroded landmarks are re-inserted under a closing operation. This mimics the process of relocating eroded material in existing holes. It must then be bound to some material balance. Such a process has not yet been found in literature.

Applying these morphological operations in the context of α-complexes is a subject that is hardly investigated. It deserves much further attention but room to do this in this thesis is lacking. The conclusion is that erosion and the other operations are naturally supported by the notion of evolutionary maps and hence by dynamic shapes represented by α-complexes. For further details, refer to [SS94, App. D] and [SKM95, RW96, DM98, BNKVL99].

Dilation

Dilation is a growth process in which a dilator, following the boundary of the dilated object, wipes out a part of space that is added to the dilated object.

DEFINITION 3.26 (DILATOR)
A dilator is an instantiated object that dilates an adjacent object •

The strategies presented for erosion can basically also be applied to dilation. Degradating points may be replaced by promotion of empty sets (dormant landmarks) to landmarks. Dilation may also be seen as a auxiliary process to implement infill with some *background material* to obtain complete spatial occupancy. Spatial occupancy will be further discussed in chapter 5.

3.11.7 Time series versus 4D models

In the following section, the organisation of landmark set with respect to their time value will be reviewed. Although figure 3–8 keeps its validity for time dependent landmark and value sets, throughout. In many cases, said 4D models are in fact time series. In CAD, models in which the z-coordinate is explicitely defined: $z = \mathsf{F}(x, y)$, are often referred to as 2.5D-models. In the same spirit, one might speak about 3.5D-models, if the time coordinate is explicitely defined in terms of $\mathbf{x}$, disallowing multiple values.

DEFINITION 3.27 (3.5D SPATIO-TEMPORAL MODEL)
A spatio-temporal model is said to be a 3.5D spatio-temporal model if the time coordinate satisfies an explicit definition of the form $t = \mathsf{G}(\mathbf{x})$ •

OBSERVATION 3.6 (UNIQUENESS OF TIME COORDINATE)
The explicit definition of the form $t = \mathsf{G}(\mathbf{x})$ *implies that* $\nexists \mathbf{x} : t = \mathsf{G}(\mathbf{x})$ *not unique* •

If on the other hand the time coordinate can only be given by an implicit relation of the form $\Psi(\mathbf{x}, t) = c$, then the model apparently requires a "full" 4D topology.

DEFINITION 3.28 (4D SPATIO-TEMPORAL MODEL)
A spatio-temporal model is said to be a 4D spatio-temporal model if the time coordinate can be multi-valued •

Generally, 3.5D spatio-temporal models can be supported using time-series of 3Dα-complexes from a 3D icon, i.e., using a time discrete evolution of a mapping process, 4D models must borrow from a (weighted) 4D icon definition $\wp(\tilde{S}) \in (\mathbb{E}^3 \times \mathbb{R}) \times \mathbb{R}$. Without going too deep into all kinds of philosophical details regarding dimensions, this discussion will be concluded by a couple of examples.

EXAMPLE 3.16 (3.5D VERSUS 4D MODEL)
In earthsciences, a frequently encountered geological scenario is the following:

Interval 1: deposition *New material is supplied at the top.*

Interval 2: uplift *The geodesical altitude is increasing.*

Interval 3: erosion *The deposited material is eroded under the influence of environmental processes, such as a glacial climate.*

Interval 4: deposition *New material is deposited again.*

in this case, a true 4D topology is required to adequately model the sequence of events, over time. Depositions at position $\mathbf{x}$ *may originate from more than one era. It may, for example, be deposed during the first period of deposition or during the latter. In this example two time values* t_1 *and* t_4 *project orthogonally onto a hyperplane parallel to the spatial subspace. Equivalently, one may say that a hyperplane parallel to the spatial subspace exists, that intersects the top-most depositions twice* •

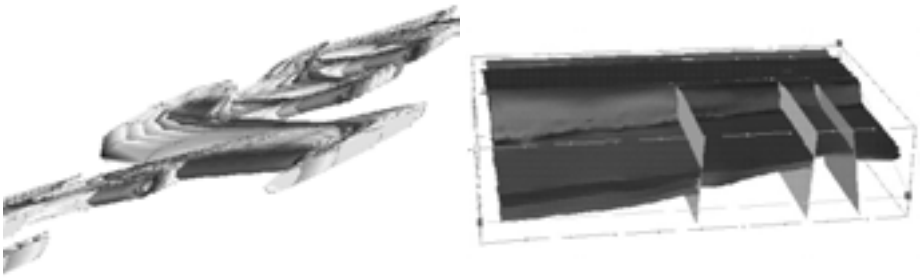

Figure 3–16: *left: projection of a 4D meandering channels into 3D. Right: ZXt-intersection of 4D structural spatio-temporal model. Back-to-front, time increases from $t = -500\ MA$ to $t = 0\ MA$ in the front, with land environment in the back, switching to marine at $t \approx -460\ MA$ and switching back to land at $t \approx -310\ MA$. All along the X-direction, subsidence is rapidly increasing at $t \approx -250\ MA$. The dashed line at the right indicates a linear subsidence model.*

EXAMPLE 3.17 (EROSIONAL CHANNEL OVER TIME)
Consider a "cannibalistic", erosional channel system over time, see figure 3–16, left picture. Of interest is the tracing of materials at all times and at all locations. Such systems cannot be described conveniently in a three dimensional Euclidean space. Reason for this is that the shape carves itself away and its final shape does not adequately model all the deposit material. In other words; it takes a 4D geometric and topological description, rather than a dynamic 3.5D description. In 4D, the shapes is "stretched" along the extra time dimension, such that the cannibalistic effect is removed and the complete shape can be studied at any location in time. Conservation laws are to be honoured at any time, so material conservation is considered over a time cross-section. 4D models are hard to visualise. Figure 3–16, left picture is a view on the projection from 4D into 3D space, more formally: $\mathsf{P} : E^3 x T \rightarrow E^3$ •

EXAMPLE 3.18 (E^2xT STRUCTURAL SUBSIDENCE MODEL)
A structural model evolving over time due to subsidence, compaction, and faulting, is depicted in the right part of figure 3–16. These systems cannot be adequately represented in 3D either. Some aspects of the structural model can conveniently be described by a E^2xT space. The figure depicts an intersection along a hyperplane perpendicular to the Y-axis and parallel to the ZXT-space. The dashed line at the right denotes a linear subsidence model •

3.11.8 Alpha and weight as a function of time

In the previous sections, time dependent forms of α and w have been discussed. It is also relevant to consider α and w in conjunction. For example in the context of geometric constraints. See table 3–4.

	Description
$w(t)$	dynamic weighting, possibly in combination with $\alpha(t)$; generally induced by dynamic value sets $F_S(t)$ of properties $p(t)$
$w(\alpha)$	weight a function in α. Geometric static constraints
$w(\alpha, t)$	weight function in α and t. Geometric dynamic constraints
$w(\alpha(t))$	weight function in time dependent α. Geometric dynamic constraints

T able 3–4: *various dynamic forms of weight.*

Chapter 4

Using weight as a modelling tool

4.1 Overview of this chapter

In this chapter, the use of weighted data point sets as input for α-complexes will be addressed. Weighted points are fundamental to the use of weighted α-complexes, and in fact, as a modelling instrument, they endow α-complexes with practical meaning. Emphasis will be on the mechanism of weighted points and how this mechanism can be applied to pursue the desired α-complex. The basic idea is to use weights to bring the α-complex into a state close to the perceptual target shape and to use α for a lean-to-fat variation within a limited part of the α-family.

For the geometric interpretation of weighted points, understanding the geometry of the ball and sphere is essential; a good portion of this chapter will be devoted to it, starting with section 4.2. There is a wide body of literature available on the geometry of sphere and ball, e.g., [Coo16, Coo24, Bar27, Max52, Sch79]. Unfortunately, much less is known about weighting *strategies*. Moreover, no particular applications of weighted α-complexes were encountered in literature. To date, there is no such thing as a general purpose weighting recipe. To that extend, a few possible problem-dependent approaches will be examined (section 4.6). In the light of subsurface objects, coupling weights to observed physical properties stands out as the most natural and fruitful approach. After all, we found that the shape of observed natural objects is often property-ruled (refer to chapter 3, fig. 3–3). Therefore, most of the attention goes to this approach.

The problem of designing a weight set based on observed physical properties can conveniently be split into two parts:

- **Finding the relative contribution of each property**

  This is basically an instance of a factor or discriminant analysis problem. The relative contribution of each of the selected properties (factors) to the weight is determined in this analysis. The result is a weight set $\bar{\mathbb{W}}$ of *normalised weights*.

- **Scaling the weight**

  The second part is to relate the normalised weights to the nearest neighbour distances to abridge. In this chapter, this problem is translated into an equivalent coverage problem by

the weight-plus-α-balls. Property-derived normalised weights are matched with the nearest neighbour distances by means of *weight transformation*, i.e., translation and scaling mostly. Weight transformation must be such that the desired coverage is obtained and for instance the assumed hole-free regions are indeed fully covered. The result is the final weight set $\mathbb{W}$ to be assigned to $\mathbb{S}$ prior to triangulation.

Techniques and methods for the first part of the problem can be taken from widely available literature on this matter. See for example [Boc96] for a review of recent developments. As indicated, the second part is less well documented. The second part is dominated by the question: how to find the largest α-complex in which no edges are *enforced* by weight alone and a second α-complex which is the smallest hole-free complex. These two complexes define the boundaries of the α-interval within the α-family in which the expected α and α-complex are to be found in practical applications. Boundaries should be such that variation of α provides sufficient lean-to-fat variation within this interval. Recall from chapter 2 that the α-values belonging to the two α-complexes must be equal to $\alpha = \alpha_{\min}$ and α close to $\alpha_{\max}$, resp. See definition 2.14 and observation 2.12. As weight increases, $\alpha_{\min}$ will move towards zero but not reach it. The first edge enters the α-complex as soon as α exceeds $\alpha_{\min}$. The α-complex is guaranteed to be hole-free, by definition, when $\alpha \geq \alpha_{\max}$. Refer to figure 4–1. The forming of an edge occurs when two eight spheres intersect and hole-free can be associated with full coverage by weight-plus-α balls. How exactly, will be discussed further down. The scaling of weight can thus be reduced to a coverage-by-weight problem.

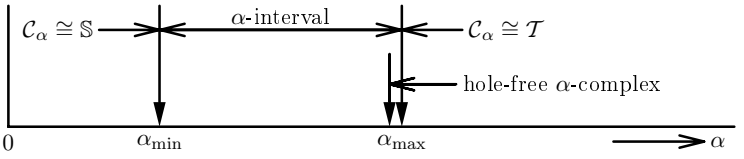

Figure 4–1: *target α-interval for weight transformation of part two, ranging from $\alpha_{\min}$ up to an α close to $\alpha_{\max}$.*

To further unravel the discussion on part two of the weighting, it is appropriate to identify two distinct weight transformation cases to obtain the desired coverage:

- **Case I: isotropic scaling of the property-derived normalised weights**

  The relative distribution of the normalised weights is to be preserved and weights are therefore up-scaled by a global scale factor to match *globally smallest* nearest neighbour distance.

- **Case II: anisotropic scaling of the normalised weights**

  In this case, the relative distribution of the normalised weights will be disrupted and weights are up-scaled to match their *individual* nearest neighbour distance.

Case I applies to property-ruled objects. Case II ruins the idea of a property-ruled geometry, but is the way to obtain a hole-free object. Observe that case II may *follow* case I, either for the whole object or for certain parts. For case II, the Stienen model will be discussed. The Stienen model points out exactly the lower boundary weight corresponding to the local nearest

neighbour distance. Section 4.8 discusses the use of the Stienen model. Unfortunately, there is no clear estimator for the upper boundary.

Up till now, weights were taken scalar by nature. In practical modelling applications however, tying weights to physical parameters such as a fluid flow often requires weights to be defined as *vectors* or *tensors*. This would require an extension to the current definition of the weighted α-complexes and is therefore considered beyond the scope of this thesis. An outlook on the problem and possible further research will be given in section 4.9 by the end of this chapter.

4.2 Weighted points

Weighted points were already briefly introduced in section 2.3 and will be further discussed here. Recall that as far as the geometric interpretation is concerned, a weighted point $\tilde{\mathbf{s}} = (\mathbf{s}, w_s)$ is often represented and interpreted as d-ball or $(d-1)$-sphere centred at $\mathbf{s}$ and having a radius $r = \sqrt{w_s}$. In case $r^2 < 0$ the $(d-1)$-sphere becomes an imaginary sphere (or: *i-sphere*). Imaginary spheres will be discussed a little further, in paragraph 4.2.1. To understand the geometric interpretation of negative weights and the geometric interpretation of *configurations* of weighted points, a suitable formalisation is needed. A convenient form to do so is by borrowing from the geometric description of complex numbers developed mainly at the end of the 19-th- and the beginning of the 20-th century. Refer for instance to [Coo16, Max52, Sch79, Hah94]. Using this formal description, configurations of spheres will be classified and the combined value of $w + \alpha$ will be associated with the resulting classes.

4.2.1 Formalisation of weighted points

Let $z \in \mathbb{C}$ be a complex number, such that $z = x + iy$ and $\bar{z} = x - iy$ is it's *complex conjugate*. Furthermore, let $C = (c_0, c_1)$ be an arbitrary point in $\mathbb{C}$. A (1)-sphere $\mathtt{S}_{\rho^2}(C)$ with radius ρ centred at C:

$$(x - c_0)^2 + (y - c_1)^2 = (z - C)(\bar{z} - \bar{C}) = |z - C|^2 = \rho^2 \tag{4–1}$$

can be represented by a *Hermitian matrix* $\mathbf{S}$ ([Max52, Sch79]). Equation 4–1 can be written in the general form $Kz\bar{z} + Lz + M\bar{z} + N = 0$. By comparing this general form with equation (4–1), a characteristic Hermitian matrix can be found:

$$\mathbf{S} = \begin{pmatrix} K & L \\ M & N \end{pmatrix} = K \begin{pmatrix} 1 & -\bar{C} \\ -C & C\bar{C} - \rho^2 \end{pmatrix} \tag{4–2}$$

representing the sphere. Constant K is real and commonly $K \geq 0$. Constant K may be set to unity, but as for any $\lambda \neq 0$, $\mathtt{S}_1 = \lambda \mathtt{S}_2$ represent the same sphere real, any $K > 0$ will again represent the same sphere. Indeed $C\bar{C} - \rho^2 = |C|^2 - \rho^2$ is real and C and $\bar{C}$ are each others conjugates. The determinant Δ of matrix $\mathbf{S}$ is by definition given by:

$$\Delta = |\mathbf{S}| = K(C\bar{C} - \rho^2 - C\bar{C}) = -K\rho^2 \tag{4–3}$$

Observe that $\Delta \in \mathbb{R}$, as expected.

The cases in which $K = 0$ or $K, L, M, N = 0$ yield a straight line or do not yield a proper circle and are excluded. In line with equation (4–3), it is now possible to derive the following *classification of spheres*:

Class	$\lvert\mathbf{S}\rvert$	$\Leftrightarrow$	Radius ρ
real sphere	$\Delta < 0$	$\Leftrightarrow$	$\rho^2 > 0$
point sphere	$\Delta = 0$	$\Leftrightarrow$	$\rho^2 = 0$
i-sphere	$\Delta > 0$	$\Leftrightarrow$	$\rho^2 < 0$

If $K \neq 0$, then $\Delta = 0 \Rightarrow \rho = 0$ leads to a point sphere.

Example 4.1 (imaginary unit sphere)
The unit sphere $\mathtt{S}_{-1}(0)$ *in* $\mathbb{C}$ *is given by* $z\bar{z} + 1 = 0$. *The Hermitian of this sphere is:*

$$\mathbf{S} = \begin{pmatrix} 1 & 0 \\ 0 & 1 \end{pmatrix}$$

All diagonal elements are real and for all elements: $s_{ij} = \bar{s}_{ji}$, *as expected for a Hermitian matrix. For* $|z| \downarrow 0$, *the sphere goes to a point sphere centred at* $C = (0, 0)$ *or, equivalently,* $C = 0 + i0$ •

Using the above formulation, a *configuration of two real spheres* can now be represented as a *pencil of spheres*. A pencil of spheres $\mathcal{P} = \{\lambda_j \mathtt{S} | \lambda_j \in \mathbb{R}\}$. A pencil of two spheres in E^d is a linear combination:

$$\mathcal{P} = \lambda_1 \mathtt{S}_1 + \lambda_2 \mathtt{S}_2 \tag{4–4}$$

represented in matrix notation by $\mathbf{P} = \lambda_1 \mathbf{S}_1 + \lambda_2 \mathbf{S}_2$. Denote the elements of the Hermitian matrices $\mathbf{S}_1$ by K_1, L_1, M_1, N_1, resp. and likewise for $\mathbf{S}_2$. The determinant of the configuration is then given by:

$$\Delta = |\mathbf{P}| = \begin{vmatrix} \lambda_1 K_1 + \lambda_2 K_2 & \lambda_1 L_1 + \lambda_2 L_2 \\ \lambda_1 M_1 + \lambda_2 M_2 & \lambda_1 N_1 + \lambda_2 N_2 \end{vmatrix} = \Delta_1 \lambda_1^2 + 2\Delta_{12} \lambda_1 \lambda_2 + \Delta_2 \lambda_2^2 \tag{4–5}$$

a quadratic form in the real λ_1 and λ_2 and therefore again $\Delta \in \mathbb{R}$. In equation (4–5), $\Delta_1 = |\mathbf{S}_1|$, $\Delta_2 = |\mathbf{S}_2|$ and $2\Delta_{12}\lambda_1\lambda_2 = (K_1 N_2 + K_2 N_1) - (L_1 M_2 + L_2 M_1)$. Let $\mathtt{S}_1(C_1)$ be centred at C_1 and $\mathtt{S}_2(C_2)$ be centred at C_2, with radii ρ_1 and ρ_2, resp. Then, using equation (4–3):

$$\begin{cases} \Delta_1 &= -K_1^2 \rho_1^2 \\ \Delta_2 &= -K_2^2 \rho_2^2 \\ 2\Delta_{12} &= K_1 K_2 \left[\delta^2 - (\rho_1^2 + \rho_2^2)\right] \end{cases} \tag{4–6}$$

where $\delta^2 = (C_1 - C_2)^2 = |C_1 - C_2|^2$. This leads to the following *classification of configurations of two* real *spheres*:

Class	Description	$\lvert\lambda_1\mathbf{S}_1 + \lambda_2\mathbf{S}_2\rvert$	$\Leftrightarrow$	Radii ρ_1, ρ_2, δ
1.1	no intersection, inside	$\Delta_1\Delta_2 - \Delta_{12}^2 < 0$	$\Leftrightarrow$	$\lvert\rho_1 - \rho_2\rvert > \delta$
1.2	no intersection, outside	$\Delta_1\Delta_2 - \Delta_{12}^2 < 0$	$\Leftrightarrow$	$\rho_1 + \rho_2 < \delta$
2.1	1 point in common, inside touch	$\Delta_1\Delta_2 - \Delta_{12}^2 = 0$	$\Leftrightarrow$	$(\rho_1 - \rho_2)^2 = \delta^2$
2.2	1 point in common, outside touch	$\Delta_1\Delta_2 - \Delta_{12}^2 = 0$	$\Leftrightarrow$	$(\rho_1 + \rho_2)^2 = \delta^2$
2.3	all points in common, complete overlap	$\Delta_1\Delta_2 - \Delta_{12}^2 = 0$	$\Leftrightarrow$	$\rho_1 = \rho_2,\ \delta = 0$
3.1	2 distinct common points, intersection	$\Delta_1\Delta_2 - \Delta_{12}^2 > 0$	$\Leftrightarrow$	$\rho_1 + \rho_2 > \delta$
3.2	2 distinct common points, orthogonal, real	$\Delta_1,\ \Delta_2 \neq 0,\ \Delta_{12} = 0$	$\Leftrightarrow$	$\rho_1^2 + \rho_2^2 = \delta^2$

Figure 4–2 shows these configurations. A few additional remarks can be made with regard to the classification of pairs of spheres:

1. For all classes: an *inequality* with respect to the determinant leads to an *inequality* of δ, ρ_1 and ρ_2, and zero-determinants (*equality*) yield an *equality* in δ, ρ_1 and ρ_2 .

2. For class 2.3, the two spheres coincide completely: their centres coincide and their radii are equal.

3. For class 3.2, if $\Delta_1 > 0$ or $\Delta_2 > 0$, i.e., one of the spheres is an i-sphere, $\Delta_{12} = 0$ still says that the two spheres meet orthogonally, but $\rho_1^2 + \rho_2^2 \neq \delta^2$. Any sphere orthogonal to an i-sphere is itself real ([Sch79, Ch. 1]). This will turn out to be relevant for a regular triangulation whit negative weights.

4. Also for class 3.2, although straight lines have been excluded by stating that $K \neq 0$, it is trivial that every straight line through the centre of a sphere can be considered a sphere of infinite radius intersecting the other sphere orthogonally.

5. Still for class 3.2, a point sphere ($\Delta_1 = 0$ or $\Delta_2 = 0$) can be shown to be orthogonal (refer to [Sch79, Ch. 1]) to a sphere iff completely contained in the circumference of that sphere. The only point of a point sphere is its centre, so this condition is equivalent to the event of the centre of the point sphere lying in the circumference of that sphere. Obviously, this does not give 2 distinct common points, as usual for class 3.2 .

6. If both $\mathtt{S}_1$ and $\mathtt{S}_1$ are point circles (i.e., $\Delta_1 = 0$ and $\Delta_2 = 0$), one cannot discriminate between class 2.1, 2.2 and 2.3 .

Now that a classification for spheres has been established, and one for configurations of two spheres, the questions that remain are:

1. How can the above classification be used in the light of weight-plus-α spheres and balls?

2. How does this formalisation extend to higher dimensions?
3. How does the classification behave under the landmark transformations discussed in chapter 3 and under the weight transformations to be discussed in this chapter?

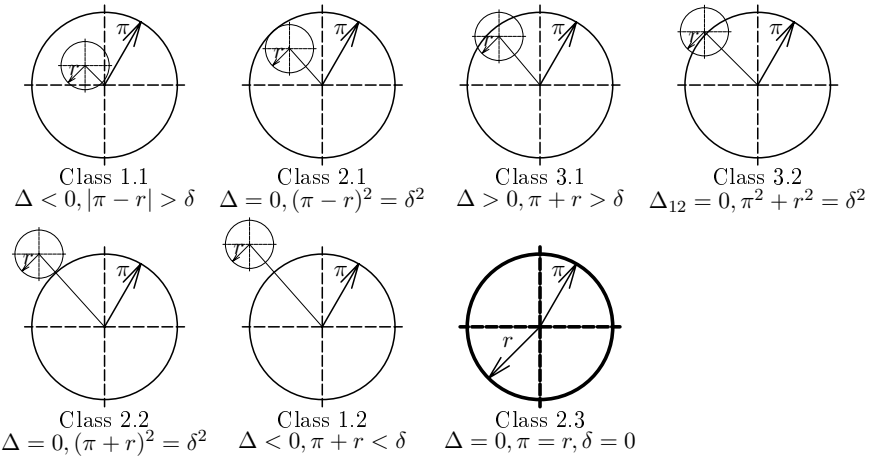

Figure 4–2: *classification of configurations of two real spheres with radii of π and r. In the bottom-right configuration of class 2.3, the two spheres coincide.*

Using the classifications for weighted points

An important role in the classification is apparently played by the joint determinant Δ_{12}, more in particular by the term $\delta^2 - (\rho_1^2 + \rho_2^2)$. In case of orthogonality (class 3.2), this term fades to zero. Substituting w_1 for ρ_1^2 and w_2 for ρ_2^2 (or better: $w_1 + \alpha$ for ρ_1^2 and $w_2 + \alpha$ for ρ_2^2) connects class 3.2 to orthogonality of weighted points and zero Laguerre distance. Furthermore, class 1.1, class 2.1 and class 3.1 correspond to the redundant vertices defined in chapter 2, definition 2.6. Also see observation 2.6. They violate the regularity constraint (definition 2.5) in the regular triangulation and will be dropped. Reducing the weight (except for class 2.3) may lift the regularity violations and cause configurations to flip to another class, e.g., to class 3.2, class 2.2 or class 1.2 . Class 2.2 and 3.2 model the formation of an edge as soon as weight spheres overlap in weight-plus-α covering $\mathcal{B}$. Class 1.1, 2.1 or 2.3 configuration may also occur, but only for non-zero α. Class 3.2 is typical for the formation of an edge in the radical α-ball covering.

Negative weight

The notion of i-spheres can be used in a straightforward manner for the *accumulation* of α and weight, with $\alpha + w$ associated with radius ρ. Call the *combined* effect $\varepsilon(\alpha)$, defined as:

$$\varepsilon(\alpha) = \begin{cases} a + w \ , & \text{for: } w + a \geq 0 \\ i^2(\alpha + w) \ , & \text{for: } w + a < 0 \end{cases} \tag{4–7}$$

As stated in chapter 2, α will be drawn from the ray domain $[0, \infty) \subset \mathbb{R}$.

What is the geometric interpretation of negative weight? A point with a negative weight contains no real points. It has an imaginary marker attached to it, with a negative radius. The distinction to be made with respect to marker radius r in case of negative weights is expressed by ([Ede92]):

$$r = \begin{cases} \sqrt{w}\,, & \text{for: } w \geq 0 \\ i\sqrt{w}\,, & \text{for: } w < 0 \end{cases} \tag{4–8}$$

An alternate approach that circumvents the problem of imaginary-spheres altogether has been proposed in [Ede92]: draw both α and w from the ray domain $[0, \infty) \subset \mathbb{R}^{\frac{1}{2}}$. Let $\alpha' = \sqrt{\alpha}$ and let $w' = \sqrt{w}$. Then inequality $\varepsilon < 0$ reads $\alpha'^2 + w'^2 < 0$, which is never the case. In this case, ε is associated to r and ρ rather than r^2 and ρ^2.

Towards higher dimensions

A sphere in E^d can be described in normalised form by ([Bar27, BP94]):

$$\mathbf{x}^T\mathbf{x} - 2\mathbf{m}^T\mathbf{x} - \varepsilon^2 = 0 \tag{4–9}$$

and relating this to the form $Kz\bar{z} - z\bar{C} - \bar{z}C + C\bar{C} - \rho^2 = 0$ (compare equation (4–1)) is not trivial. No further attempt will be made. A real equivalent of the Hermitian matrix is an orthogonal matrix and a formulation of orthogonality extends into higher dimensions straight away. The fact that $\delta^2 - (w_1 + w_2) = 0$ denotes orthogonality is not limited to any dimension.

4.2.2 The Laguerre fan

This section discusses the *Laguerre fan*. Refer to figure 4–3. The Laguerre fan is defined as follows:

DEFINITION 4.1 (LAGUERRE FAN)
The Laguerre fan is the fan spanned by all positive Laguerre distances of a point relative to a weighted point •

Given a weighted point $\tilde{\mathbf{s}}_1 = (\mathbf{s}_1, w_1)$ and a point $\tilde{\mathbf{s}}_2 = (\mathbf{s}_2, w_2)$. Parametrise their Laguerre distance by a single parameter w_1 and furthermore use as a shorthand notation $L_{12}(w_1) = \delta_{12}^2 - (w_1 + w_2)$. Then :

$$\frac{d}{dw_1}(L_{12}) = \frac{d}{dw_1}\left[\delta_{12}^2 - (w_1 + w_2)\right] = -1 \tag{4–10}$$

so that the Laguerre distance monotonically decreases with a strictly increasing w_1. Moreover, $L_{12} = \delta_{12}^2$ is a global maximum for this configuration and $L_{12} = 0$ is a minimum for positive

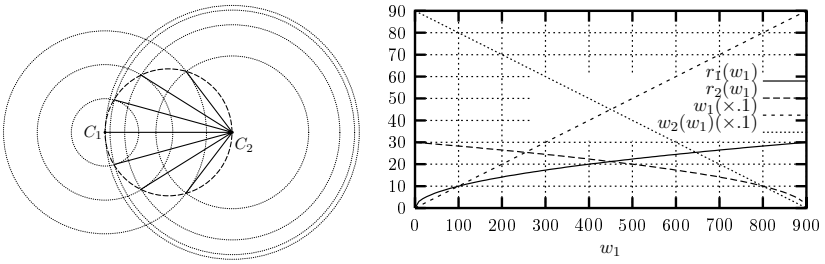

Figure 4–3: *left: Laguerre fan (bounded by the dashed circle) of a weighted point* $(\mathbf{C}_2, 0)$ *relative to a weighted point* $(\mathbf{C}_1, w_1) \in E^2$*, for positive distances. The spheres in the right bundle, centred at* $\mathbf{C}_2$*, are orthogonal spheres to* $(\mathbf{C}_1, w_1)$*. Right: effect of increasing* w_1 *on orthogonal* w_2*, and radii of both spheres.*

distances. The same holds true for L_{12} and w_2. Further, with $r_1 = \sqrt{w_1}$ and $r_2 = \sqrt{w_2}$, we have that:

$$\delta_{12}^2 = r_1^2(w_1) + r_2^2(w_1) \tag{4–11}$$

which is the form of a sphere, so that all intersection points in all members of the bundle lie on a circle, centred half-way of the line carrying $\mathbf{s}_1$ and $\mathbf{s}_2$. Observe the following:

OBSERVATION 4.1 (LAGUERRE FAN)
The sphere bounding the Laguerre fan in E^d *is the smallest* $(d-1)$*-sphere intersecting the centres* $\mathbf{s}_1$ *and* $\mathbf{s}_2$ •

OBSERVATION 4.2 (LAGUERRE FAN AND THALES THEOREM)
The Laguerre fan follows basically from the application of Thales theorem in E^2*, stating that two orthogonally intersecting lines through the centres* $\mathbf{s}_1$ *and* $\mathbf{s}_2$ *(fig. 4–3) lie on a circle with diameter* $\|\mathbf{s}_2 - \mathbf{s}_1\|$ *passing trough both* $\mathbf{s}_1$ *and* $\mathbf{s}_2$ •

4.2.3 The synthesis of α and weight

The role of α and weight w in the development of the α-complex is different. An increasing α causes *all* weight-plus-α balls to grow whereas an *initial* weight only provides a *bias* at a zero α-value. This means that w and α can only be seen in close conjunction. In this section, the relative influence of each will be discussed and contrasted with their joint effect.

Weighting acts as a modelling instrument to shape the desired α-complex. In practice, it is convenient to let some coverage be conquered by α. This is the "lean-to-fat"-variation in the α-interval $[\alpha_{\min}, \alpha_{\max}]$ introduced earlier in this chapter. This way, a *target* α will be chosen which is approximately of the magnitude of w. Call the combined effect ε, like in equation (4–7), so that ε is equal to the square of the radius r of the weight marker. Then for the derivative $\frac{dr}{d\alpha}$:

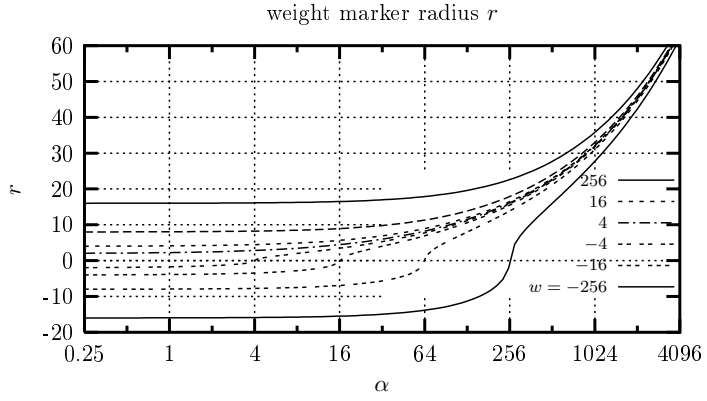

Figure 4–4: *marker radius* $r = \sqrt{\varepsilon}$ *versus* α *for various weights* w*, depicted on a* ^{2}log*-linear scale.*

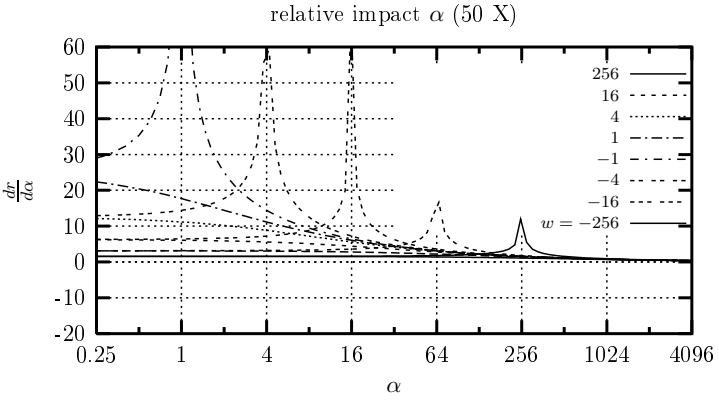

Figure 4–5: *relativ e influence of* α*. The figures show the limited influence for* $\alpha \ll w$ *and* $\alpha \gg w$*. Observe the negative weigh t-curv es and their local maximum for their derivative* $\frac{dr}{d\alpha}$*.*

$$\frac{dr}{d\alpha} = \begin{cases} \frac{1}{2\sqrt{a+w}}\,, & \text{for: } w + a \geq 0 \\ \frac{-i}{2\sqrt{a+w}}\,, & \text{for: } w + a < 0 \end{cases} \tag{4–12}$$

Then clearly, the relative influence of α is small as long as α is small compared to w, i.e., $\alpha \ll w$, strongly increasing when $\alpha \approx w$ and α *completely wipes out* the influence of w when $\alpha \gg w$. Weight is fixed-valued and its effect decays rapidly for increasing α-values. To get a grasp: for a dominance function $d(\alpha)$ with $\alpha_1 = w$ and $\alpha_2 = 10\alpha_1$, radius ε_2, associated with α_2 is equalto $\varepsilon_2 = \frac{1}{2}\sqrt{22}\varepsilon_1 \approx 2.345\varepsilon_1$. For $\alpha_1 = 10w$ and $\alpha_2 = 10\alpha_1$, this reduces to $\varepsilon_2 = \frac{1}{2}\sqrt{22}\varepsilon_1 \approx 0.0000\varepsilon_1$. See figures 4–4 and 4–5. The weight may be chosen such that expected α-value $\mathsf{E}[\alpha]$ and w are approximately on equal scale, in order to experience the effects of both. Local variation depends

on the distribution of the ratio between nearest and local-furthest neighbour distances and the distribution of the local coverage κ. This issue will be further discussed in section 4.6.5 and will give rise to the definition of one of the possible weight transformations to apply.

4.2.4 Incremental weight

Next question to be raised is: can weight be added and subtracted incrementally? In the current definition, α is equal for all members of $\mathbb{S}$. Imagine a set $\mathbb{A}$ of α-values for each individual member of $\mathbb{S}$, although we know all these values are equal. Firstly, notice that the cardinalities of $\mathbb{S}$, $\mathbb{A}$ and $\mathbb{W}$ are equal. Then the Minkowski sum $\mathbb{A} \oplus \mathbb{W}$ reflects the bias w_j plus the increased α for a vertex $\tilde{\mathbf{s}}_j \in \mathbb{S}$. Minkowski set subtraction is defined similarly, but in general, Minkowski set subtraction is not the inverse of a Minkowski set addition (e.g., [SKM95]). Caution should also be taken when considering the reflection of the weight of a weighted set $\tilde{S} = \mathbb{S} \otimes \mathbb{W}$:

DEFINITION 4.2 (SET REFLECTION)
The reflection of a set is obtained by scalar multiplication of all elements by $\lambda = -1$ •

Notation: $\check{\mathbb{S}}$ or simply $-\mathbb{S}$. The reflection of the weight may yield unexpected and undesired side effects.

Minkowski set additions are associative and commutative. As a consequence, building up the weight set from different parts is trivial:

$$\mathbb{S} \oplus (\mathbb{W}_1 \cup \mathbb{W}_2 \cup \ldots \cup \mathbb{W}_m) = (\mathbb{S} \oplus \mathbb{W}_1) \cup (\mathbb{S} \oplus \mathbb{W}_2) \cup \ldots \cup (\mathbb{S} \oplus \mathbb{W}_m) = \bigcup_j (\mathbb{S} \oplus \mathbb{W}_j) \qquad (4\text{–}13)$$

4.3 Centres

For a thorough understanding of configurations of spheres, it is also important to understand the existence and nature of various centres, unique to that configuration. Here, the following centres will be discussed:

Circumcentre: the centre of the circumscribing sphere (figure 4–6).

Centre of simultude: the apex of the single and double tangential conic of two weighted points (figure 4–7).

Radical centre: the single point of intersection of radical planes of pairs of $(d-1)$-spheres, as discussed in chapter 2.

Napoleon centre: an exterior point associated with each $(d-1)$-face in the boundary, in which a sphere can be positioned that intersects that face' vertices orthogonally, as well as the orthogonal radical α-ball (figure 4–11).

The circumcentre in E^d is defined for a configuration of $d+1$ weighted points, in this work. The centre of simultude is a centre belonging to a configuration of two weighted points, the radical

centre and the Napoleon centre generally require more than two weighted points. According to Napoleon's Theorem (e.g., [Hah94]), the Napoleon sphere is only defined for triangles spanned by zero-weight vertices (See figure 4–11). The definition is adapted for weighted vertices. The precise discussion of this configuration will be postponed to section 4.3.

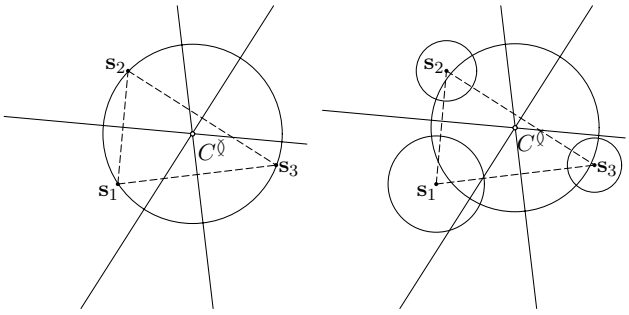

Figure 4–6: *Circumcentre of a configuration of three weighted points in* E^2. *The circumcentre* $C^{\emptyset}$ *is located in the interior of triangle* $\tilde{s}_1\tilde{s}_2\tilde{s}_3$ *iff the triangle is acute. The circumcentre coincides with the radical centre and the circumscribing sphere is equal to the orthogonal radical* α*-ball* $\mathtt{A}_\alpha(C^{\emptyset})$. *Left: zero-weight vertices, right unequal weights.*

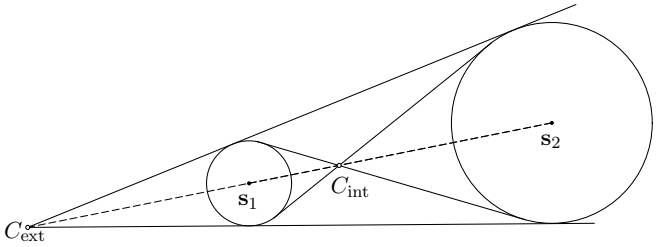

Figure 4–7: *Tangential conic of two weighted points* $\tilde{\mathbf{s}}_1$ *and* $\tilde{\mathbf{s}}_2$. *The external centre of simultude is located on the carrying line through the two points outside the locus of the two points, the internal centre of simultude is also located on that line but in between the two points.*

Circumcentre

The circumscribing sphere of $d+1$ points in d-space can be found in almost any textbook on geometry. Here, this definition for unweighted point is stretched to also cover weighted points. Doing so is more or less trivial if the definition is made the same as an orthogonal sphere centred in the radical centre. The circumsphere is then identical to the radical α-ball. Refer to figure 4–6.

Centre of simultude

The centre of simultude is the apex of the tangential conic of two weighted points, as shown in figure 4–7. In fact two such conics can be drawn: a single conic and a double conic. This yields two centres, an *internal* centre of simultude:

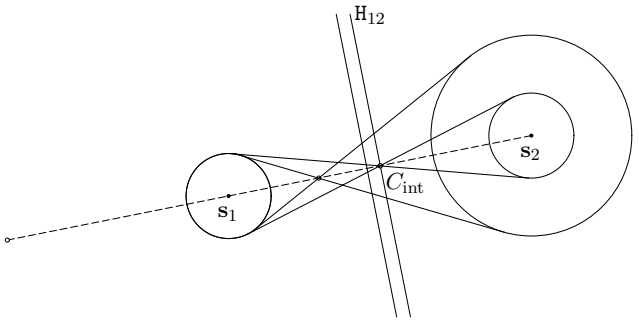

Figure 4–8: *Centre of simultude and the radical plane. Only for two equal-weighted points, the radical plane passes through the centre of simultude* C_{int}.

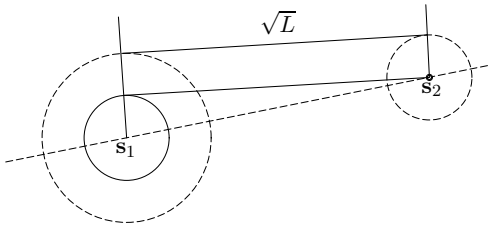

Figure 4–9: *Relation between centre of simultude and the Laguerre distance. Extracting the smallest weight from the greatest and determining the (collapsing internal and external) centre of simultude, gives a chord that corresponds to the geometric representation of the Laguerre distance. This figure also demonstrates that if* $\Delta w_1 = \Delta w_2 \Rightarrow \Delta L = 0$.

$$\mathbf{C}_{\text{int}} = \frac{\mathbf{s}_1\sqrt{w_2} + \mathbf{s}_2\sqrt{w_1}}{\sqrt{w_2} + \sqrt{w_1}} \tag{4–14}$$

located *in between* the two points and defined by the double conic, and an *external* centre of simultude:

$$\mathbf{C}_{\text{ext}} = \frac{\mathbf{s}_1\sqrt{w_2} - \mathbf{s}_2\sqrt{w_1}}{\sqrt{w_2} - \sqrt{w_1}} \tag{4–15}$$

defined by the single conic and located *external* to the locus of the two spheres. The external centre of simultude, defined by equation (4–15) can be at infinity. This is the case for equal-weighted points. In that case, the internal centre lies on the radical plane, see figure 4–8. If one of the weighted points has zero-weight, then the external and the internal centre of simultude coalesce in the centre of that point. The chord from the external centre of simultude reflects the Laguerre distance, in that case. Figure 4–9 demonstrates this.

Radical centre

A line segment along the radical plane spans an edge in a weighted Voronoi diagram. A radical plane satisfies:

$$\mathbf{x} \cdot \mathbf{dx} = \frac{\langle \mathbf{s}_2, \mathbf{s}_2 \rangle - \langle \mathbf{s}_1, \mathbf{s}_1 \rangle - w_2 + w_1}{2} = D \tag{4–16}$$

where D is a term that denotes the position relative to the two weighted points. The radical centre in E^2 can then be computed from the intersection of two such planes:

$$\begin{pmatrix} dx_{21} & dy_{21} \\ dx_{31} & dy_{31} \end{pmatrix} \begin{pmatrix} x \\ y \end{pmatrix} = \frac{1}{2} \begin{pmatrix} D_2 & D_1 \\ D_3 & D_1 \end{pmatrix} \tag{4–17}$$

an equation of the form $Ax = B$. The term dy_{21}/dx_{21} in equation (4–17) denotes the direction of the hyperplane of $\tilde{s}_2$ and $\tilde{s}_1$.

The radical plane does not necessarily pass through the internal centre of simultude C_{int}. This is only true for two equally weighted points. See figure 4–8. In that case, external centre of simultude C_{int} is located in the ideal point at infinity and the other one is on the perpendicular bisector, which in this case coincides with the radical plane. And, hence, the latter passes through the centre of simultude. Refer to figure 4–8.

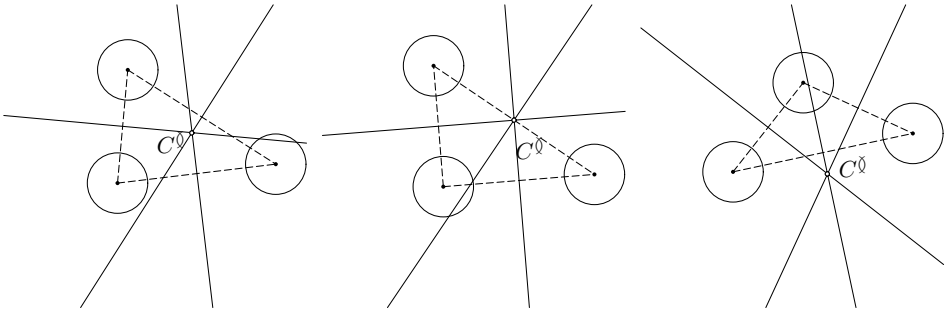

Figure 4–10: *location of the radical centre in E^2 for acute, isosceles and obtuse triangle. With equal-weighted vertices, the centre lies inside if the triangle is acute (left), in the boundary if the triangle is isosceles (centre) and outside an obtuse triangle (right).*

In dimensions higher than 2, multiple shapes of "bad aspect ratio" d-faces exist, such as "slivers", "needles", etc. See [Bak89, BCER95].

Napoleon centre

The Napoleon theorem (e.g., [Hah94]) says the following. Expand each edge of an arbitrary (primal) triangle into an equilateral triangle (gray triangles in figure 4–11, left picture). A positive orientation must be applied (e.g., [Sto91]), to ensure that the apex is outside of the primal

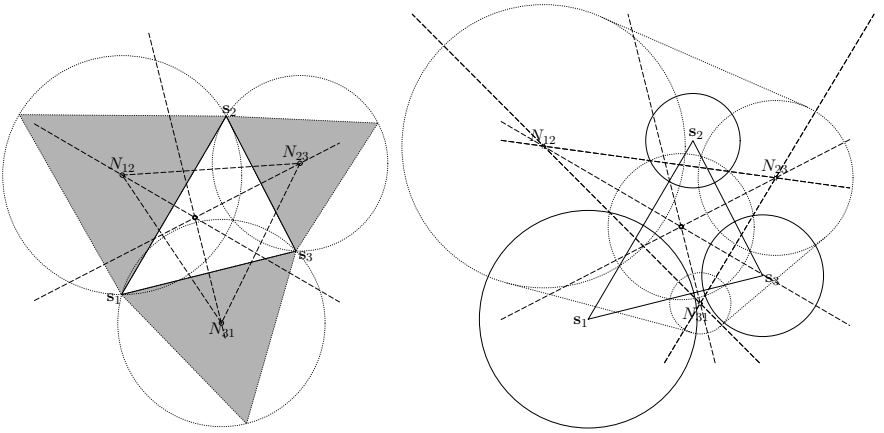

Figure 4–11: *the relation between Napoleon's theorem and obtaining full coverage of the d-simplex. Left: zero-weighted points. Connecting the Napoleon centres N_{jk} gives an equilateral dual triangle (dashed). Right: weighted version, which generally does not yield a regular dual (d)-face. Legs of the (weighted) equilateral triangles have not been drawn.*

triangle. Connecting the circumcentres of these equilateral triangles gives a dual equilateral triangle. Napoleon's theorem holds for acute, isosceles and obtuse triangles. What makes the Napoleon theorem interesting is the fact that it creates a full ball coverage by the Napoleon-spheres in all occasions. Figure 4–11 shows this for a single triangle, figure 4–12 shows this for a triangulation. Full coverage is *not* obtained by the set of dual triangles. Moreover, these triangles do not form a coverage at all, let alone a triangulation.

The situation becomes different when working with weighted vertices (figure 4–11, right picture). The edges of the dual Napoleon triangle are contained in the radical planes of the Napoleon spheres and the orthogonal radical α-ball. The dual triangle connecting the Napoleon centres is no longer equilateral. Even not when working with weighted distances. For weights too high, the Napoleon sphere may become an i-sphere and its geometric interpretation blurs. Many aspects of this coverage remain unclear and this covering is therefore left alone for further research.

4.4 Modelling with weight

This section treats the issue of modelling mechanisms, obtained by manipulating the distribution of weight. The effects of changing distances and weight will be demonstrated by means of "dynamic configurations" of spheres. In the figures used, pairs of spheres will move upward by a fixed step, while changing. This is done for readability. Figures are parametrised by a single parameter t in the following sense: $\mathbf{x}(t) = c_3t^3+c_2t^2+c_1t+c_0$ and also: $w(t) = c_3t^3+c_2t^2+c_1t+c_0$. Example 4.2 illustrates this.

EXAMPLE 4.2 (DYNAMIC CONFIGURATION)
Assume a coordinatesystem in which $x(t)$ increases "to the right" and $y(t)$ runs upward. Let pencil $\mathcal{P}(t) = \lambda(\mathtt{S}_1(t) + \mathtt{S}_2(t))$ be defined as follows. $\mathtt{S}_1(t) = ((-t^2 + t + 10, 5t + 2), 4t^2 + t + 30)$

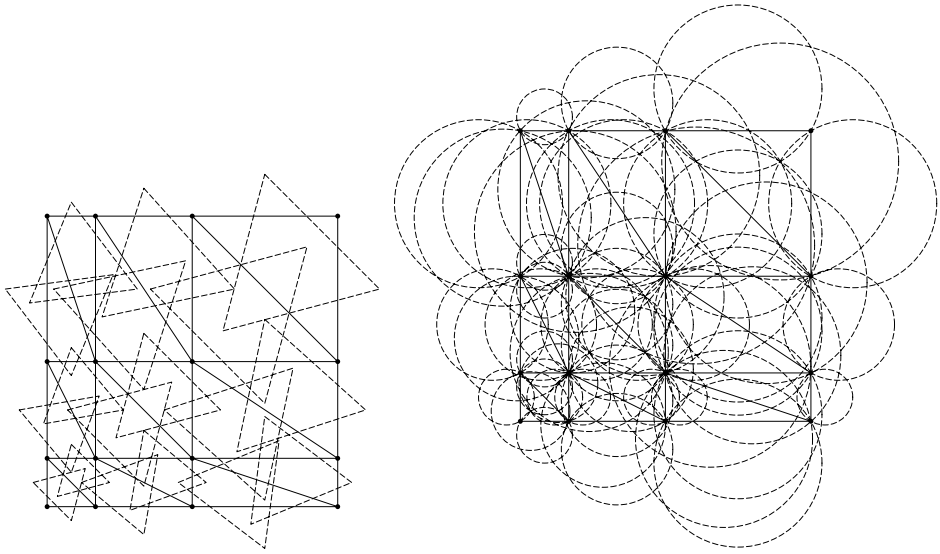

Figure 4–12: *the relation betw een Napoleon's theorem and obtaining full coverage and α-exposedness of the d-simplex, here for a weigh ted triangulation. Left: dual triangle coverage, right: ball coverage. Solid lines depict primals, dashed lines the duals.*

and $\mathbb{S}_2(t) = ((2t^2 - t\sqrt{2} + 30, 5t + 2), 100)$. *The development of this configuration is given for* $0 \leq t \leq 5$. *Notice that the "height" of both spheres is given by the expression* $y(t) = 5t + 2$.

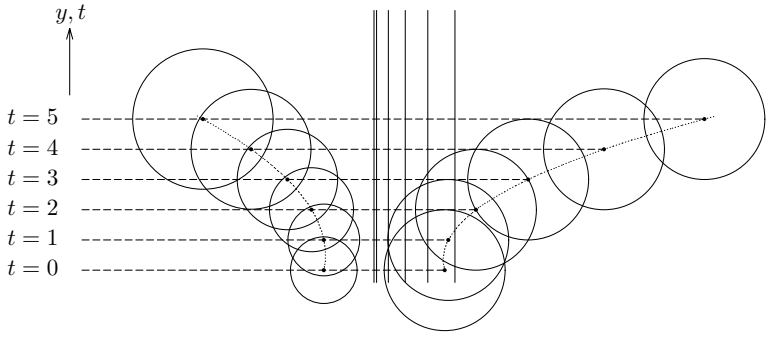

Observe the following. Parameter t runs in the dir ection of y, i.e., upward. The figure shows pairs of spheres, the left of which increases in weight with t, the right of which has constant weight. The location of the spheres diver ge. The radical plane moves to the right as a result of this •

The Laguerre distance $L(\tilde{\mathbf{s}}_1, \tilde{\mathbf{s}}_2) = \langle \mathbf{s}_1 - \mathbf{s_2}, \mathbf{s}_1 - \mathbf{s_2} \rangle - (w_1 + w_2)$ can also be written as $L(\tilde{\mathbf{s}}_1, \tilde{\mathbf{s}}_2) = \langle \mathbf{s}_1, \mathbf{s_1} \rangle + \langle \mathbf{s}_2, \mathbf{s_2} \rangle - 2\langle \mathbf{s}_1, \mathbf{s_2} \rangle - (w_1 + w_2)$. Again, this sho wsthat the movement of points $\tilde{\mathbf{s}}_1$ and $\tilde{\mathbf{s}}_2$ corrected for their joint movement in the same direction is important and on the other hand, their common weight. This is again the distance and the w eigh t. Figure 4–13

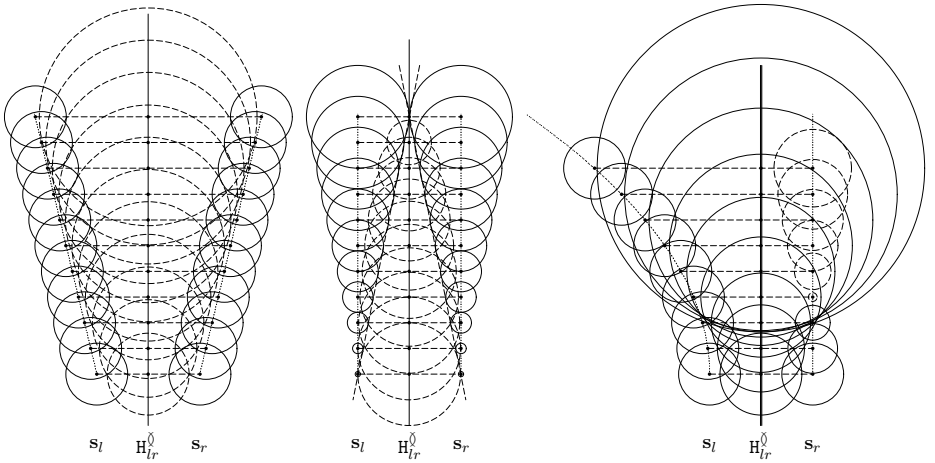

Figure 4–13: *effect of distance and/or weight changes on the configuration of two spheres and the orthogonal α-ball. Changes are such that the radical plane $\mathtt{H}_{12}$ remains fixed. The left picture shows a variation of distance to the radical plane with $\Delta\delta_l^2 = \Delta\delta_r^2 = c_1 t + c_0$. The central picture shows how a quadratic increase of the weight from zero-weight to orthogonality (class 2.2 configuration) acts upon the orthogonal ball. The right picture shows a compensation of a change in $\Delta\delta_l^2$ by a decrease Δw_r of the weight of the right point. Dashed spheres are i-spheres.*

shows the effect of changing these components. To make the figure easier to read, changes are such that the radical plane $\mathtt{H}_{12}$ remains fixed. Let δ_l^2 be the squared distance of point $\mathbf{s}_l$ to the nearest point $\mathbf{s}^{\emptyset}$ in the radical plane $\mathtt{H}_{12}^{\emptyset}$ and let w_l be its weight. Likewise for the right point. The left picture in figure 4–13 shows a variation of distance to the radical plane (location of the centres) such that $\Delta\delta_l^2 = \Delta\delta_r^2 = c_1 t^2$. The central picture shows how increasing the weight by a factor $c_1 t^2$ from zero-weight to a class 2.2 configuration acts upon the orthogonal ball. Distance $\delta_l^2 = \delta_r^2 = 100$ is kept constant. If the weight of both spheres increases by $\Delta w = t^2$, the Laguerre distance to the radical α-sphere becomes zero as soon as we have that $\delta^2 - t^2 = 0$ which occurs for $t = 10$. Increasing the weight up to a class 3.2 configuration (orthogonality) would turn the radical α-sphere into an i-sphere. The right picture of figure 4–13 shows a compensation of a change in distance of the left point by an increase of the weight of the right point, i.e., $\Delta\delta_l^2 + \Delta w_r = 0$. The weight of the right point becomes negative and the sphere becomes an i-sphere as the left point moves away from the radical plane. This relation can be derived from the following:

$$\frac{L_l}{L_r} = \frac{\langle \mathbf{s}_l - \mathbf{s}^{\emptyset}, \mathbf{s}_l - \mathbf{s}^{\emptyset} \rangle - w_l}{\langle \mathbf{s}_r - \mathbf{s}^{\emptyset}, \mathbf{s}_r - \mathbf{s}^{\emptyset} \rangle - w_r} = \frac{\delta_l^2 - w_l}{\delta_r^2 - w_r} = 1 \tag{4–18}$$

and also, to restore this *invariant*:

$$\frac{\Delta L_l}{\Delta L_r} = \frac{\Delta\delta_l^2 - \Delta w_l}{\Delta\delta_r^2 - \Delta w_r} = 1 \tag{4–19}$$

If only the left point $\mathbf{s}_l$ moves and only the right weight changes, then this results in:

$$\Delta\delta_l^2 = -\Delta w_r \tag{4–20}$$

and with equation (4–18) one obtains:

$$\Delta\delta_l(2\delta_l + \Delta\delta_l) = -\Delta w_r \tag{4–21}$$

The Laguerre distance $L(\mathbf{s}_l, \mathbf{s}^{\emptyset})$ is equal to the squared radius of the orthogonal ball in figure 4–13. A change in the Laguerre distance is therefore proportional to a change in the α-value for α-exposedness, vice-versa. The left picture is easily associated with isotropic scaling, the centre with weight transformation still to be discussed and the right picture with the combined and interchangeable effect of distance and weight demonstrated in experiment 2.1. As stated, we do not take into account negative α-values, but in geometric modelling, locally demoting the development of the α-complex is of great practical importance and negative weights are vital for that. Negative weights obstruct the entrance of those vertices and faces into the α-complex until the negative weight is compensated by the α-value and their sum is positive again (section 4.2).

In terms of α-complexes, a great enough negative weight attached to an interior point $\mathbf{s} \in \operatorname{Int}\mathcal{C}_\alpha$ of the α-complex, is a seed for a void, or a pocket that can grow into a void for a greater α. It acts as a white spot that cannot be covered by the α-complex with the current value of α. Figure 4–14 illustrates this phenomenon. The effect of strong enough a negative weight is that it "deflects" the formation of d-faces in a direction radial to the negative weight. Figure 4–15 shows this effect clearly. The stronger the negative weight at the top-right, the more needle-like the triangles get in a diagonal direction, emanating from the negative weight. Apparently, the negative weight seeds a elongated star of d-faces.

Figure 4–14: *the effect of negative weight as a seed for a hole in the interior of an α-complex. In this case, the negative weight has been attached to the centroid.*

4.5 Weighted points as a point process

A set of weighted points can be considered as a marked point process, with the weight balls as markers. If the coverage by weight markers is of interest, the point process can also be considered

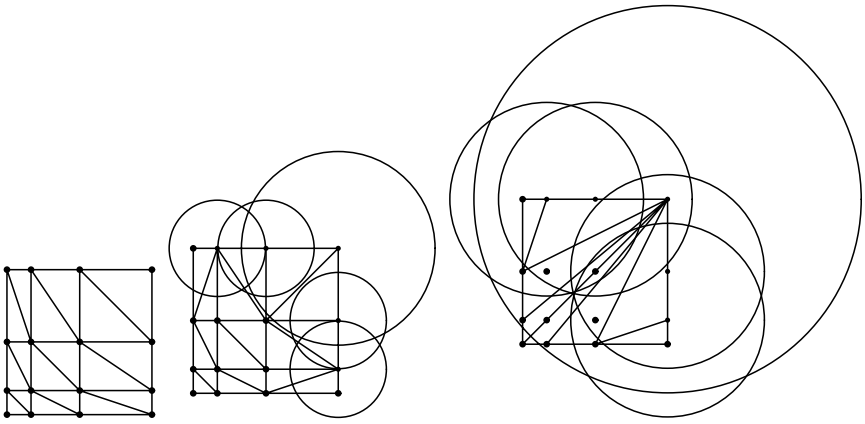

Figure 4–15: *regular triangulations of the same point set for different weight sets. Left: zero-weighted case, centre: weights increase linearly from zero for the lower-left vertices to a much higher value for the upper-right region. Notice that differences show up only where weighs have been changed. Right: overly dominating upper right points, strongly directing the formation of the faces radially out of this region of dominance.*

as a coverage process. Both marked point process and coverage process were introduced in chapter 3. In fact twomarked point processes can be considered. The question may be raised as towhether theseco verage processes lead to the same conclusions for the development of the α-complex. The two coverage processes are:

- **Weight-plus-α markers located in the points $\mathbb{S}$**

  This process reaches full coverage when the markers, growing with increasing α, eventually will have swept out all powercells. This is coverage $\mathcal{B}$ discussed in section 2.3, figure 2–3 show edan example.

- **The α-markers located in the radical centres**

  This is coverage process $\mathcal{A}$, discussed in section 2.3 too. The process reaches full coverage when the α-markers located in the radical centres and growing with increasing α, eventually will have intersected the weight markers in the vertices of $\mathbb{S}$ orthogonally. Refer to figure 2–3 again for an example.

Both processes reach their full coverage for the same α-value, which can be understood with the principle of transfer of dominance to be discussed in the sections ahead. In this work, emphasis is on the first process. This process is easily related to the Stienen model, to be discussed later. The second process will be discussed, where appropriate.

4.5.1 Transfer of dominance

To study the relation between these coverage processes, it is convenient to understand the principle of dominance transfer, coined in [Ede92].

DEFINITION 4.3 (TRANSFER OF DOMINANCE)
Dominance transfer between two weighted points is the transfer of weight of one point onto the other. Let $\tilde{\mathbf{s}}_1 = (\mathbf{s}_1, w_1)$ *and* $\tilde{\mathbf{s}}_2 = (\mathbf{s}_2, w_2)$ *be two different weighted points. Let* $\tilde{\mathbf{s}}_1\prime = (\mathbf{s}_1, w_1 - \Delta w_1)$ *and let* $\tilde{\mathbf{s}}_2\prime = (\mathbf{s}_2, w_2 + \Delta w_1)$. *Then,* $L(s_1, s_2) = L(s_1\prime, s_2\prime)$ •

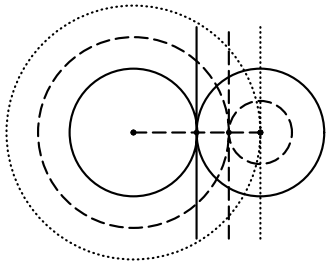

Figure 4–16: *the principle of weight transfer demonstrated. The radical plane moves but the radius of the radical* α*-sphere remains constant.*

The principle is demonstrated in figure 4–16 . Obviously, with transfer of weight, the radical plane moves along, as indicated. Apparently, the weighted distance between two weighted points remains unchanged if the sum of the weight changes is zero, which can be readily seen from the definition of the Laguerre distance. Recall that the weighted distance is zero if two weighted points are orthogonal. Let $\tilde{\mathbf{s}}_1$ and $\tilde{\mathbf{x}}_2$ be orthogonal. Then apparently, orthogonality also occurs for these two points, with weights of $w_1\prime = w_1 + w_2$ and $w_2\prime = 0$, i.e., a *complete transfer of weight* from one point onto the other. Apparently, orthogonality is preserved for these two orthogonal points $\tilde{\mathbf{s}}_i$ and $\tilde{\mathbf{s}}_j$ under a complete transfer of weight from one point onto the other. This leads to the following observation ([Ede92]):

OBSERVATION 4.3 (DOMINANCE TRANSFER OF ORTHOGONAL POINTS)
Assume that two weighted points $\tilde{\mathbf{s}}_i$ *and* $\tilde{\mathbf{s}}_j$ *are orthogonal. After a complete transfer of weight from* $\tilde{\mathbf{s}}_j$ *onto* $\tilde{\mathbf{s}}_i$*, the former must be on the enlarged sphere of* $\tilde{\mathbf{s}}_i$ *and the radius of the enlarged sphere around the receiving* $\tilde{\mathbf{s}}_i$ *must have become equal to the Euclidean distance between the two points* •

Observation 4.3 is illustrated graphically in figure 4–16. Dominance transfer further simplifies the computation of α-exposedness. Sticking to the example of an edge, all weight may be transfered from one vertex onto the other. The Euclidean distance between the zero-weight donor point and the increased sphere of the receiver point is now to be abridged by an α-ball, centred in the intersection point of the radical plane and the carrying line through the two points. Of course, if both vertices have zero-weight, the α-ball will have to cover exactly the Euclidean distance between the vertices. The following observation for α-exposedness of edges is easily verified (fig. 4–16):

OBSERVATION 4.4 (α-VALUE FOR α-EXPOSEDNESS OF AN EDGE)
The α*-value of the minimum-radius* α*-ball, centred in the intersection point of radical plane and edge corresponds to the weight to be* additionally *transfered to the receiver in order to make it intersect the zero-weight donor* •

The first *real* sphere that intersects tw oweighted point orthogonally is important for α-exposedness. If two weighted points already intersect as a class 2.2 type, the α-ball is a null-sphere lying in their intersection point. Recall that this point is also located on the radical axis. Assume the weight of the two points is further increased to a class 3.2 configuration, i.e., to orthogonality. Radical α-balls located inside their intersection interior are imaginary, with $\Delta > 0$. Negative w eight must be transfered in order to restore the class 2.2 configuration. In fact the α-ball located in the intersection point of radical axis and edge determines the weight to be added/subtracted for the points to touch. The following example illustrates this.

EXAMPLE 4.3 (ORTHOGONAL RADICAL α-BALL)
The α for which an edge first becomes α-exposed, can be determined as follows. Define $\alpha = \rho^2$, and weight $w = r^2$, then a weighted point $\tilde{\mathbf{s}}_1 = (\mathbf{s}_1, w)$ is represented by a sphere with radius r and a weighted point $\tilde{\mathbf{s}}_2 = (\mathbf{s}_2, \alpha)$ with weight α is represented by a sphere with radius ρ. We have that:

$$\|\mathbf{s}_1 - \mathbf{s}_2\| - (r_1 + r_2 + 2\rho) = \delta - (r_1 + r_2 + 2\rho) = 0 \tag{4–22}$$

from which we immediately have:

$$\rho = \frac{1}{2}\left[\delta - (r_1 + r_2)\right] \tag{4–23}$$

This concludes the example •

A concluding remark on transfer of dominance. The principle of dominance transfer also holds if dominance becomes a function of weight plus alpha, like in $w(\alpha) = w + \alpha$:

$$(w_i + \alpha) + (w_j + \alpha) = (w_i + 2\alpha + w_j) + (w_j + \alpha - w_j - \alpha) \tag{4–24}$$

4.6 Weighting strategies

A *weighting strategy* is a process to obtaining a weight set $\mathbb{W}$ such that for some $\alpha \in [0..\infty)$ the resulting α-complex is fulfilling all the geometric and topological constraints imposed upon the object's model. See chapter 3. This w asfurther narrow eddo wn,earlier in this chapter, in the sense that with appropriate weighting $\mathsf{E}[\alpha] \in [\alpha_{\min}, \alpha_{\max}]$. But what is a proper strategy to design weight sets accomplishing this? Of course, the answer to this question depends on the *problem* on the one hand and the *modelling objectives* on the other hand. A couple of strategies will now be discussed. Also, refer to [GVdWV00b].

4.6.1 Unstructured weighting

Weight can be assigned on a per-point basis. This form of w eighting will be referred to as *unstructured weighting*. The use of unstructured weighting, applicable to both regularly and

Function	Definition	Function	Definition
gamma(ζ)	$\Gamma(\zeta) = \int_0^\infty e^{-\eta}\eta^{\zeta-1}d\eta, \zeta > 0$	-ln(ζ)	$-\ln(\zeta) = \int_0^\zeta \eta^{-1}d\eta,\ \zeta > 0$
normal(ζ)	$p(\zeta) = \frac{1}{\sigma\sqrt{2\pi}} e^{\frac{(\zeta-\mu)^2}{2\sigma^2}}$	error(ζ)	$\mathrm{erf}(\zeta) = \frac{2}{\sqrt{\pi}} \int_0^\zeta e^{-\eta^2} d\eta$
sign(ζ)	$\mathrm{sign}(\zeta) = \begin{cases} -1 & \text{for } \zeta < 0 \\ 0 & \text{for } \zeta = 0 \\ 1 & \text{for } \zeta > 0 \end{cases}$	bloc k(ζ)	$\mathrm{p}(\zeta) = \begin{cases} 0 & \text{for } \zeta \notin [a,b] \\ 1 & \text{for } \zeta \in [a,b] \end{cases}$

T able 4–1: *natural weigh t functions exhibiting a "cut-off" effect. Use the linear transform* $\zeta = \beta_1\xi + \beta_2$, *with* $\beta_1, \beta_2 \in R$, *to shift and scale of the "cut-off" point.*

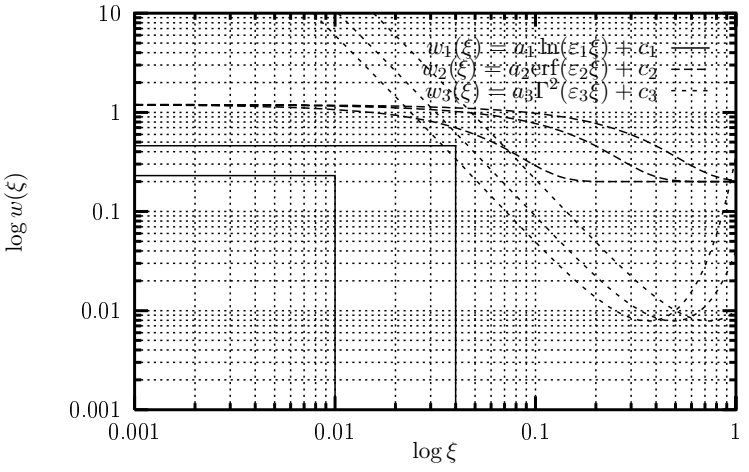

Figure 4–17: *Weight functions with "cut-off" effect.* $w_1(\xi)$ *has upper-bound for* $0 < \xi < \varepsilon^{-1}$. *The rapid weight drop at* $\xi = \varepsilon^{-1}$ *can readily be seen from the figure. V ertices within this* ε^{-1}*-ball cen tred at* $\xi = (0, 0, \ldots, 0)$ *will be attracted to one another, those outside the ball will be distracted for equal values of* α. *Weigh t functions* $w_2(\xi)$ *and* $w_3(\xi)$ *ha ve similar effects.*

irregularly spaced data, is of limited practical value. It is typically used in combination with free-form modelling of simple shapes. T osome extend, the painting (spraying) of weight can be regarded as unstructured weighting. Unfortunately, such tools are still lacking for 3D. A best-practice solution would be the use of sliced data. The comet West case to be discussed in chapter 6 follows this approach.

4.6.2 Weight functions

Weights can also be based upon some function defined over the domain E^d of $\mathbb{S}$, parameter space E^m or subspaces thereof. Generally, a weight function is of the form $\mathbf{g} : E^d \rightarrow R$ and mostly exhibits a sharp "cut-off" effect. Figure 4–17 and table 4–1 show a few such functions. Using weight functions is easily combined with the masking technique, to be discussed in the next section.

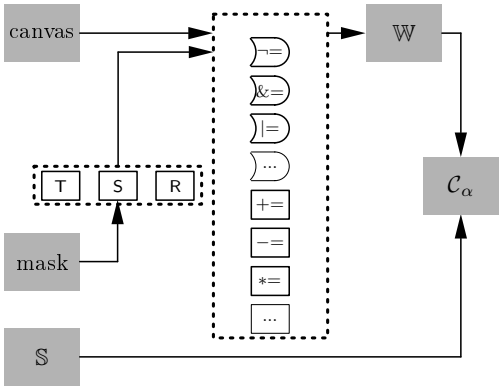

Figure 4–18: *schematic overview of the masking technique; the aim is to compose a weight set* $\mathbb{W}$*, that "highlights" the desired geometry* ($\mathcal{C}_\alpha$) *in the regularly spaced sampling data point set* $\mathbb{S}$*. Starting point is an empty canvas (lattice) of the size of* $\mathbb{S}$*. Successively, masks* (partial, basic weight sets) *are added to the weight set* $\mathbb{W}$ *using transformations and one or more logical or mathematical operations. The Cartesian product* $\mathbb{S} \times \mathbb{W}$ *is then input to* $\mathcal{C}_\alpha$*.*

4.6.3 Masking

A 2-lattice L is a regularly organised subset of $\mathbb{Z}^2$. Each of these points has a location, an ordinal number, and may be assigned one or more values. A lattice with no such value sets assigned yet, is called an empty *canvas*. Let point set $\mathbb{S}$ be organised on a lattice. Consider the following weighting strategy for such a regularly spaced sampling point set $\mathbb{S}$:

Step 1: Create an empty canvas to contain the eventual weight set $\mathbb{W}$ of the size of the data set and initialise the canvas to zero-weight.

Step 2a: Instantiate a (library-based) standard weight mask by generating it with appropriate parameters.

Step 2b: Translate, rotate and scale the mask, as appropriate.

Step 2c: Map the instantiated mask onto the canvas. Mapping onto is essentially a "pixel"-based logical or mathematical operation.

Step 3: Construct the weighted α-complex, based on $\mathbb{S} \otimes \mathbb{W}$.

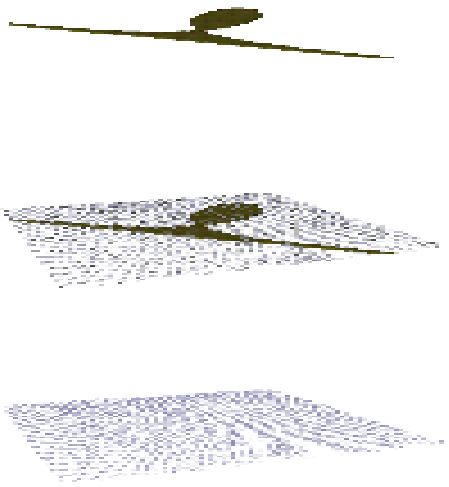

Figure 4–19: *the masking process: the lattice-based regularly spaced set* $\mathbb{S}$*, covering the canvas (bottom), is weighted using predefined masks (middle); here a mask containing Descartes folium. For* $-\infty < t < \infty$*, the folium is given by the parametrised equations:* $x = 3t/(1+t^3)$ *and* $y = 3t^2/(1+t^3)$*. The mask cuts out a singular point at* $(0, 0)$*.*

Repeat steps 2 and 3, as appropriate.

This strategy is referred to as *masking*. Fig. 4–18 depicts this process, and fig. 4–19 shows an example using a mask that cuts out a folium-of-Descartes-shape. In terms of image algebra ([RW96]), a mask consists of a topological space made up by the points in L (or: $\mathbb{S}$), a *value set* $\mathbb{W}$ of values associated with these points and a discrete topology. Incremental weight addition is justified by equation (4–13). Standard masks can be collected in a library. Masks can be based on standard weight function, like the ones in table 4–1. These functions can be taken relative to a point, a line, a plane, etc. Arbitrary constrained weight functions can be compiled using for example Lagrange polynomials. Basically, masking is applicable to regularly spaced landmark sets of any model space dimension E^d, although weight design tools become increasingly sparse for dimensions larger than 2.

4.6.4 Using physical properties

Shape reconstruction is relevant as far as object models are to be derived from real-live counterparts, as advocated in section 3.2. Not only in earth sciences or in clinical analysis, but also for example when a measuring robot establishes the tolerance misfit of a cast-iron part. Often, properties are stored in the form of raw or aggregated data. Sometimes, observed data are encoded in colour encoding systems. Sometimes, a value can be directly sampled in each landmark, sometimes the landmark is inaccessible and some interpolation of the value set is required.

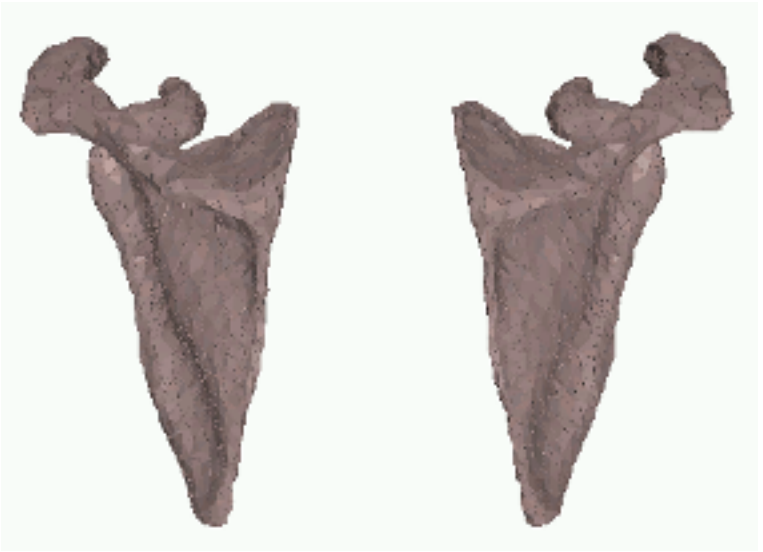

Figure 4–20: *Alpha-complex of the left and right shoulder blade (data set by courtesy of Delft Univ. of Techn., Dep. Elec.Eng., 3434 points). Refer to [GVdWV00b] for details.*

In any case, the exact geometry depends on a number of things. Among others:

- The data observation technique features.
- The "contrast" present or achievable in the data.
- The threshold value chosen to discriminate "background" (embedding environment) from "foreground" (the object).
- The suite of properties observed.

Often, observed sampling data get blurred by noise and other undesired effects. If such features hamper the finding of the right α-complex, filtering away remote areas outside the region of interest is easily accomplished with an AND-mask, i.e., a logical & =-operation. Many algorithms exist in the domain of image analysis to enhance contrast and to find, manipulate and extract features. Refer for instance to [RW96]. Another problem with observed data is the translation of vector- and tensor-properties to scalar, *omni-directional* weights. Averaging is one technique to circumvent this, finding dominant phenomena and fitting weights to them is another approach.

The use of physical properties to determine weights is most relevant and fruitful for natural objects (e.g., [GVdWV00b]). Therefore, this strategy will be given further attention in section 4.7.

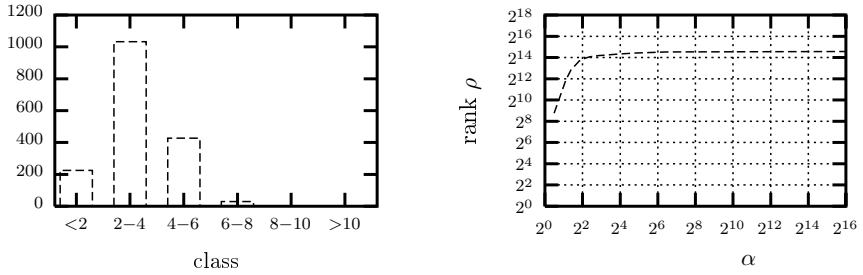

Figure 4–21: *Left: distribution of the nearest neighbour distances of the scapula-sampling data set of fig. 4–20. Right: the increase of α vs. α-rank of the scapula-sampling data set of fig. 4–20.*

4.6.5 Neighbourhood weighting

The weighting strategy based on nearest neighbour distances exploits the complementarity of weight and distance. The goal with nearest neighbour distances based weight assignment is to minimise the variance of the Laguerre distances. This minimisation chokes and moves the target α-interval (figure 4–1) and the expected α-value $\mathsf{E}[\alpha]$. It also affects the formation of the α-family and through this the relation of α vs. α-rank ρ, which is related to the accumulative distribution of the nearest neighbour distances (see fig. 2–10). Generally, the cardinality of the α-family will show only minor changes if at all. Let $\bar{l}$ be the empirical mean Laguerre distance and let l_{ij} denote the empirical variance of the Laguerre distance between $\tilde{\mathbf{s}}_i$ and $\tilde{\mathbf{s}}_j$, given by:

$$(N-1)\tilde{s}^2 = \sum_{i=1}^{N} \left(l_{ij} - \bar{l}\right)^2 \tag{4–25}$$

Minimisation of the empirical variance $\tilde{s}^2$ of the Laguerre distances requires that:

$$min\{\tilde{s}^2\} \cong min\left\{\sum_{i=1}^{N} \left(\delta_{ij}^2 - v_{ij} - \bar{l}\right)^2\right\} \tag{4–26}$$

where $v_{ij} = v_{ji} = w_i + w_j$, making up the matrix $\mathbf{V}$. The value of $\bar{l}$ is not constrained. Further:

OBSERVATION 4.5 (HOMOGENOUS LAGUERRE DISTANCES)
In case of the theoretical minimum variance $\tilde{s}^2 = 0$, all weighted points in $\mathbb{S} \otimes \mathbb{W}$ lie on a hyperplane parallel to E^d •

Figure 4–21 shows the distribution of the nearest neighbour distances for the scapula-sampling data set of figure 4–20. Figure 4–22 shows the initial versus the minimised distribution. An optimal value of the Laguerre variance is generally desirable but insufficient for a optimal or even meaningful α-complex, unless the α-complex coincides with the regular triangulation. The latter can be controlled by the minimum variance weight set. On the other hand, it is not desirable that some faces in the resulting α-complex are *enforced* by the weight alone. It is

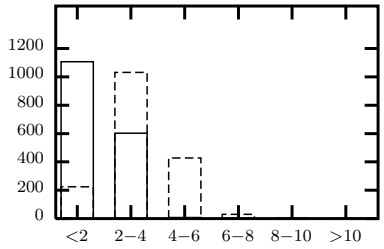

Figure 4–22: *Euclidean (dashed) vs. minimised Laguerre distance distribution (solid) of the scapula sampling data point set.*

therefore a constraint that all the Laguerre distances remain positive, so that the lower boundary $\alpha_{\min}$ of the interval of α as discussed in section 4.1 is also positive. This, in turn, implies that the Euclidean nearest neighbour distance are limiting the weight.

Minimising the dispersion (variance) is quite different from minimising the mean value. Moreover, one may in fact *choose* a target mean Laguerre distance $\bar{l}^*$ and determine the minimised weights against that mean value, obeying the non-negative constraint. It must be noted that the Laguerre distances are not independent. The elements $v_{i,j} = v_{j,i}$ of $\mathbf{V}$ mutually influence one another. Minimisation of the weights on a per-point basis decreases the variance in Laguerre distances, whereas a mere isotropic scaling scales the variance in a global fashion. A translation of the mean Laguerre distance has only limited influence on the variance and non on the coefficient of variation. Further down this chapter, weight transformations will be discussed. It is interesting to contrast Laguerre distance minimisation with weight transformations.

4.7 Physical properties based weighting

In this section the use of physical properties to determine the weight set will be further outlined. First, the estimation of the normalised weights will be treated, followed by the weight transformation of the normalised weights to reach their final values. To support the estimation of this weight transformation, a theoretical model, a ppp, will be fit. This strategy forms a natural link between the observations and measurement of a *physical example* and the optimal fit of some *theoretical model*.

4.7.1 The colour encoding of physical properties

The start of the weighing step is always a data analysis of the value sets $\mathbb{P}_{\mathbb{S}}$, generally one value set per property, see chapter 3. Very often, physical properties are encoded as colour value on some colour scale. The BGR, blue-green-red scale is a frequently used scale, red-white-blue is a common colour scaling for seismics, and of course gray-scaling. If magnitudes of physical parameter values are directly transcribed into colour values, then no information is lost. Provided that the used transcription (in particular, the "clip values") are similar, two colour-scaled maps of physical parameters can be compared one-to-one.

	Homogenous		Clustered	
Statistic	x_1	x_2	x_1	x_2
minimum	2.41537e-04	6.11700e-03	1.49715e-03	6.98440e-03
maximum	9.99460e-01	9.94870e-01	9.95577e-01	9.92220e-01
mean	5.18196e-01	5.02282e-01	5.58130e-01	5.60698e-01
variance	8.47603e-02	8.99756e-02	9.20329e-02	1.12539e-01
standard deviation	2.91136e-01	2.99959e-01	3.03369e-01	3.35469e-01
standard error	2.65770e-02	2.73824e-02	3.16284e-02	3.49750e-02
coefficient of variation	5.61827e-01	5.97193e-01	5.43546e-01	5.98306e-01
skewness	-6.83696e-02	-1.43748e-01	-1.72102e-01	-8.92594e-02
- significance level	2.23607e-01	2.23607e-01	2.55377e-01	2.55377e-01
kurtosis	-1.17019e+00	-1.22903e+00	-1.15783e+00	-1.48348e+00
- significance level	4.47214e-01	4.47214e-01	5.10754e-01	5.10754e-01
weighted sum	6.21835e+01	6.02738e+01	5.13480e+01	5.15842e+01
N		120	92	
diameter		9.99218e-01	9.94080e-01	
orthogonal breadth		9.88753e-01	9.85236e-01	
diameter/breadth ratio		1.01058e+00	1.00898e+00	

Table 4–2: *Descriptive statistics of the homogenous (left) and the clustered ppp (right). The significance levels for skewness is taken* $\sqrt{\frac{6}{N}}$ *and for the kurtosis* $\sqrt{\frac{24}{N}}$.

Quite different is the situation when dealing with an entire palette of colours, that have to be interpreted *by name*. Such a situation occurs for example when observing natural objects using a digital camera. Or, when spotting a comet from an observatory station, with a huge telescope. It is also a prerequisite in our desire to merge all kind of knowledge in primitives. In those instances, physical properties values are *reconstructed indirectly* from this pallete of colours. For example: the ion tail of a comet is pale blue. But what is pale blue.

In fact, this is an instance of a *colour classification problem* or *colour naming problem*, studied for more than a century. There is much to say to this problem, but an extensive discussion is beyond the scope of this thesis. The approach chosen here is to split off *intensity* from *chromaticity* a procedure common in colour research. The CIE chromaticity diagram[1] is consulted for colour naming and composition, where needed. For further details and descriptions, refer to a standard references on colours or computer graphics, like [FvD82, SS87] and for a more mathematically oriented discussion on these colour models, see for example [Lam94].

4.7.2 Point process analysis

In order to find the weight transformation, an analysis must be made of the underlying ppp. Refer to the outline of the modelling steps presented in section 3.9. Here, these steps will be further worked out with the aim to illustrate how to obtain a properly scaled weight set. In the remainder of this section, the analysis of two concrete related point process examples will be taken for illustration. The two processes are depicted in figure 4–23. The processes differ mainly in the degree of clustering. The two processes are defined in two-space, but procedures are similar in higher dimensions. Unfortunately, computation get sometimes complicated in higher dimensions. See e.g. [SKM95] for details.

[1] composed by the Commision Internationale de l'Éclairage (CIE) in 1931, based on panel results

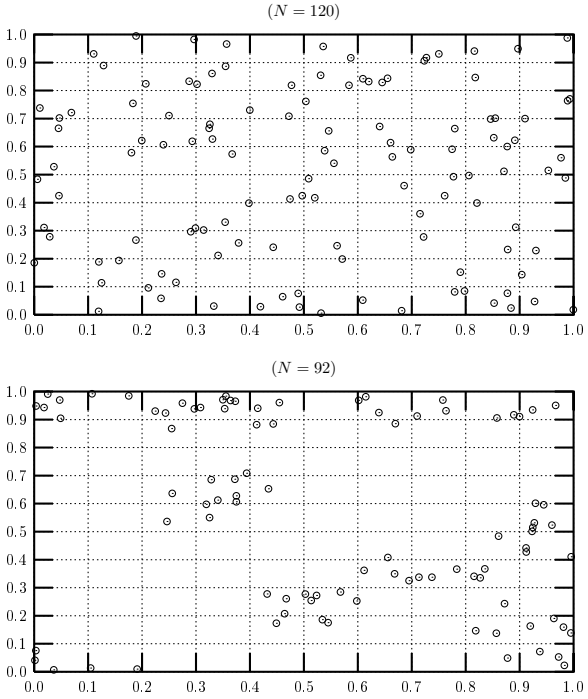

Figure 4–23: *top: homogenous Poisson point process, defined on the 2D unit domain* $[0,1] \times [0,1]$. *bottom: a clustered ppp on same domain. For the* χ^2*-test, the domain is divided in* 3×3 *equal-sized regions.*

Point process homogeneity

The null-hypothesis of homogeneity of the ppp can be verified by a classical *chi-square* test. The graphs $\mathcal{NNG}(\mathbb{S})$ and $\mathcal{LFNG}(\mathbb{S})$ may reveal a first clue of problem spots for weighting. See annex D for further details on the verification of ppp's and the statistics underpinning this. Table 4–2 shows these condescriptive statistics of the homogenous and the clustered ppp in comparison. The results of the χ^2-test will now be discussed first, followed by the nearest neighbour distance analysis.

A simple χ^2-test on the homogenous ppp with $K = 9$ cells shows that while a cell has an expected $\mathsf{E}[\mathrm{k}] = \lambda = 120/9 = 13.33$, the minimum cell contains 10 landmarks and the maximum cell 16. This yields a $\chi^2 = 2.85$ at 8 degrees of freedom. For the clustered ppp, these figure are: $\mathsf{E}[\mathrm{k}] = 10.22$ 4 landmarks and 17 landmarks, and a resulting $\chi^2 = 16.0$. Table 4–3 presents the figures of both ppp's. Notice the significant change of the value of χ^2. We have that for the clustered ppp, $\chi^2_{.05} < \chi^2 < \chi^2_{.025}$, so homogeneity can be accepted not even at a 5% significance level. Compare for the homogenous ppp: $\chi^2_{.95} < \chi^2 < \chi^2_{.90}$. The results of the chi-square analysis may be directly related to the locally expected weight $\mathsf{E}[\mathrm{w}]$ and expected local coverage $\mathsf{E}[\kappa]$.

ST ATISTIC	HOMOGENOUS	CLUSTERED
N	120	92
$\nu_{\mathcal{L}}$	1.00000e+00	1.00000e+00
global λ	1.20000e+02	9.20000e+01
E[k] per cell	1.33333e+01	1.02222e+01
minimum k	1.00000e+01	4.00000e+00
maximum k	1.60000e+01	1.70000e+01
(row,col) of min k	row=0,col=1	row=0,col=1
(row,col) of max k	row=0,col=0	row=2,col=1
χ^2	2.85000e+00	1.60000e+01
DOF ($K = 9$)	8	8

T able4–3: *results of the χ^2-test on the homogenous and the clustered ppp. Left: for the homogenous ppp, right column for the clustered ppp.*

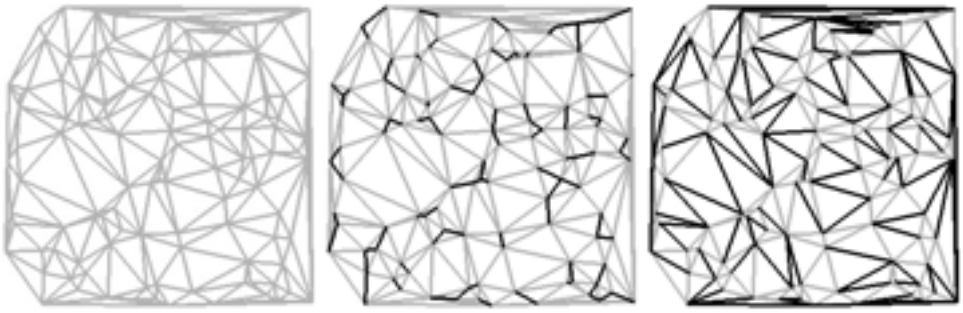

Figure 4–24: *left: triangulation of the homogenous ppp of figure 4–23. Centre: nearest neighbour graph (dark er edges), right: local-furthest neighbour graph (darker edges).*

Neighbourhoods analysis

T o study differen t regions, some sense of neighbourhood must be defined and the definition must be conv enien t in the context of the regular triangulation. Recall that an α-complex is filtered off from a triangulation. The *close d star* $S\bar{t}$ $\mathbf{s}$ of a vertex $\mathbf{s}$ is the subset of the triangulation $\mathcal{T}$ of all closed k-faces incident upon $\mathbf{s}$ and all their sub-faces. See section 2.5. Then for a neighbourhood:

DEFINITION 4.4 (NEIGHBOURHOOD)
A neighbourhood $\mathcal{N}(\mathbf{s})$ *is the spac ecovered by the close dstar* $S\bar{t}$ $\mathbf{s}$ *of* $\mathbf{s}$ •

Among the faces in this $\mathcal{N}(\mathbf{s})$, at least one 0-face can be denoted as the nearest neighbour NN(s) and at least one 0-face as the local-furthest neighbour FN(s). Figure 4–25 shows the distribution of the nearest neighbour distances of the homogenous and a clustered ppp. Figure 4–24 show triangulation and neighbour graphs of the homogenous ppp. In general, nearest- and local-furthest neighbours are not unique. The k-th nearest neighbour is the 0-face in $\mathbb{S} \bigcap St\ \mathbf{s}$ that is the k-th closest to $\mathbf{s}$. $\mathcal{N}(\mathbf{s})$ is conv ex and NN(s) and FN(s) are always contained in the boundary $\partial\mathcal{N}(\mathbf{s})$. Each $\mathcal{N}(\mathbf{s})$ has one or more associated radical centres. A radical centre is *not* necessarily located in $\mathrm{Int}\,\mathcal{N}(\mathbf{s})$; see section 4.3, and figure 4–10.

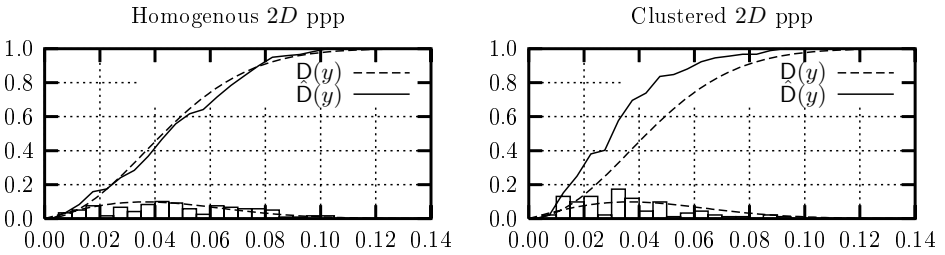

Figure 4–25: *Distribution of the Euclidean nearest neighbour distances of the homogenous and clustered ppp. left: homogenous ppp. Right: inhomogeneous, clustered ppp, in comparison to the theoretical homogenous ppp nearest neighbour distance distribution (dashed). The clustered ppp diverges considerably more from this theoretical distribution than the homogenous ppp. The skewness of the former ppp is higher (i.e., more positive) than the homogenous ppp.*

Statistic	Homogenous	Clustered
N	120	92
NN min	7.61398e-03	9.37712e-03
NN max	1.02002e-01	9.31548e-02
NN mean	4.89148e-02	3.49612e-02
NN s^2	5.51644e-04	3.74663e-04
NN s	2.34871e-02	1.93562e-02
NN $\|s\|$	1.94520e-02	1.52009e-02
NN skewness	1.74291e-01	9.03845e-01
- significance level	2.23607e-01	2.55377e-01
NN kurtosis	-2.70554e-05	-1.43057e-05
- significance level	4.47214e-01	5.10754e-01

Table 4–4: *condescriptive statistics of the nearest neighbour distances of the homogenous and the clustered ppp. Significance levels for skewness and kurtosis as in table 4–2.*

Non-homogeneity and skewness

There is a relation between the skewness of the nearest neighbour distances distribution and the degree of non-homogeneity, here the degree of clustering. Check out table 4–4 and figure 4–25. Skewness is defined as follows:

Observation 4.6 (skewness of a distribution)
Skewness (or: third central moment) is a measure of symmetry for distributions: if non-zero, a distribution is not-symmetric, and if symmetric, a distribution has a zero skewness •

Let $\mathbb{S}$ generate a ppp on some domain D and let y denote the random variable of the Euclidean inter-event distance between a site $s \in \mathbb{S}$ and its nearest neighbour $\mathsf{NN}(s) \in \mathbb{S}$. Then the theoretical distribution function $\mathsf{D}(y)$ (e.g., [Dig83, SKM95]) is given by:

$$\mathsf{D}(y) = 1 - \exp(-\lambda\pi y^2) \;, \qquad y \geq 0 \tag{4–27}$$

and for the corresponding probability density function:

$$\mathsf{d}(y) = 2\lambda\pi y \exp(-\lambda\pi y^2) \tag{4–28}$$

Local coverage

Assume that an initial weight set has been designed and attached to $\mathbb{S}$ and assume all Voronoi cells to be bounded, if needed, by convex hull $\mathcal{H}$. The local coverage $\kappa(\mathbf{s}_j)$ is defined as:

$$\kappa(\mathbf{s}_j) = \frac{\nu_{\mathcal{L}}^d\left(\mathsf{B}_\alpha(\mathbf{s}_j) \bigcap \mathsf{V}(\mathbf{s}_j)\right)}{\nu_{\mathcal{L}}^d\left(\mathsf{V}(\mathbf{s}_j)\right)} \tag{4–29}$$

Further details will be discussed below. In practice, point process statistics point at the same "problem spots".

4.7.3 Combining landmarks and weight

Many times in this thesis, the Cartesian direct product $\mathbb{S} \otimes \mathbb{W}$ has been mentioned. Apart from the values of $\mathbb{W}$, what does this product set look like? and how to create it? Let $\mathrm{card}\,\mathbb{S} = N$ denote the number of landmarks in $\mathbb{S}$. Recall that the rows of the configuration matrix $\mathbf{X}_{\mathbb{S}}$ contain the coordinates of the landmarks and its dimension is therefore $N \times d$. Let m-vector $\mathbf{p}(\mathbf{s}) \in E^m$ be the vector of (scalar) properties measured in point $\mathbf{s}$. These property values may be organised in an $N \times m$-property matrix $\mathbf{P}_{\mathbb{S}}$ in which the j-th row contains the property vector of $\mathbf{s}_j$. The "geometric" space, represented by configuration matrix $\mathbf{X}_{\mathbb{S}}$ may now be augmented by the "property" space, represented by $\mathbf{P}_{\mathbb{S}}$, in the following sense:

$$\mathbf{X}^*_{\mathbb{S}} = \left(\mathbf{X}_{\mathbb{S}} | \mathbf{P}_{\mathbb{S}}\right) \tag{4–30}$$

where $\mathbf{X}^*_{\mathbb{S}}$ denotes the augmented matrix, resulting in a hyper-spatial representation discussed in section 3.3.

Weighting based on physical properties can be regarded as a projection of m property coordinates onto l weight coordinates, i.e., $\mathsf{W} : E^m \mapsto R^l$. Basically, this projection is continuous. Limitations in the current concepts of weighted α-complexes prevent l from being different from 1. Representing weight by a complex rather than a real value has some advantages (e.g., [Ede92, Ede93]). Moreover, further research has to be initiated, into the representation of vectorial and perhaps tensorial weight (for non-scalar properties) by the use of (imaginary) *quaternions* (see chapter 7). In this work, we always have $\mathrm{val} = 1$ so that the set of weights $\mathbb{W}$ can be represented by a n-vector $\mathbf{w}$:

$$\mathbf{w} = \mathbf{P}_{\mathbb{S}}\Lambda \tag{4–31}$$

with:

$$\Lambda = [\mu_1, \mu_2, \ldots, \mu_m]^t \qquad \text{with: } \sum_{j=1}^{m} \mu_j = 1 \tag{4–32}$$

an $m \times 1$-coefficient matrix of the *relative contribution* μ_j of each of the properties on the weight. Storage in an icon of such weight sets must somehow be made size- and scale independent. Normalisation can accomplish this. On instantiation, weight transformations canbe applied to adapt the normalised weight set to the current spacing of the landmarks. First, the determination of the normalised weights will be discussed and then the weight transformation.

4.7.4 Determining the normalised weight

Generally, value sets need to be brought on equal scales by normalisation first, so that they all contribute in equal manners to the normalised weight set $\bar{\mathbb{W}}$. For the elements of $\bar{\mathbb{W}}$:

$$0 \leq |\bar{w}(\mathbf{s})| \leq 1 \tag{4–33}$$

The values of the μ_j's are commonly resulting from a *discriminant* or *principle component* or *factor analysis*. The goal of such operations is generally to investigate or enhance *classifiability*, by which we understand the abilit yto subdivide the data in clusters and classes. Generally, the outcome of the factor analysis does not or only weaklydepend on the configuration of the landmark set. This subject is not further discussed here. A recent overviewon the status of cluster analysis and data classification is given by Bock in Diday et al. ([Boc96]). Clustering in this work is basically distance-based and clustering is therefore *geometric clustering*. We assume the ordinary Euclidean metric applicable to the property space E^m. Morein particular, in this context, a *cluster* is defined as:

Definition 4.5 ((geometric realisation of a) cluster)
Let $\Psi(\mathbf{x})$ be an implicit definition of close dd-volume in E^m. Then a (geometric realisation of a) cluster of geometric data values in a space E^m is defined as a finite compact region $C \subset E^m$ containing data that satisfy some $c_1 \leq \Psi(\mathbf{x}) \leq c_2$, with $c_1, c_2 \in \mathbb{R}$ and $c_1 \leq c_2$ •

Obviously, edges in the nearest neighbour graph $\mathcal{NNG}$ indicate pairs that tend to cluster earlier in a common cluster than pairs in the $\mathcal{LFNG}$ as the mean length of edges in $\mathcal{LFNG}$ is at least the mean length of edges in $\mathcal{NNG}$. For a single property p_k, associate an $N \times N$ dissimilarity matrix Δ with property matrix $\mathbf{P}_{\mathbb{S}}$, for which:

$$\begin{cases} \delta_{ij} \geq 0 & \text{for } i \neq j \\ \delta_{ji} = \delta_{ij} & \text{for all } 1 \leq i, j \leq N \\ \delta_{ii} = 0 & \text{for all } 1 \leq i \leq N \end{cases} \tag{4–34}$$

A subdivision $\mathcal{Y} = \{\mathbb{Y}_1, \mathbb{Y}_2, \ldots, \mathbb{Y}_q\}$ of $\mathbb{S}$ in q clusters is a sub-partitioning if $\forall j,\ 1 \leq j \leq q$:

$$\begin{cases} \mathbb{Y}_j \subset \mathbb{S} \\ \mathbb{Y}_j \neq \emptyset \\ \mathbb{Y}_i \bigcap \mathbb{Y}_j = \emptyset, \quad i \neq j \end{cases} \tag{4–35}$$

If $\bigcup_j \mathbb{Y}_j = \mathbb{S}$ then the sub-partitioning becomes a partitioning. Each partitioning according to this definition, is also a covering of $\mathbb{S}$. In the general case, α-complex $\mathcal{C}_\alpha(\mathbb{S})$ will have m interiors and l exteriors. Each separate sub-complex forms a *clique*. A *clique partitioning* is a partitioning in q clusters which minimises $\sum_{j=1}^{q} \sum_{k,l \in \mathbb{Y}_j} \delta_{kl}$. In other words, a clique partitioning minimises the total dissimilarities among cluster members of the same cluster, for each cluster. Dissimilarity matrix Δ can be reorganised such that Δ_j is its $N_j \times m$ sub-matrix where $N_j = \text{card}\, \mathbb{Y}_j$ is the cardinality of clique. Sub-matrix Δ_j is minimised in the sense that $\sum_{k,l \in \mathbb{Y}_j} \delta_{kl} = \min$. Now let the geometric realisation of a clique partitioning be found by means of a general dimension α-complex in property space. Let $\alpha = 0$. Then the clique partitioning found is the absolute minimum of 0 for $q = \text{card}\, \mathbb{S}$ clusters: each points a cluster. Each row in Δ is a clique sub-matrix Δ_j and all its columns are zero. Now let α increase monotonically. We then have that if $\alpha_2 > \alpha_1 \Rightarrow q_2 \leq q_1$. Let $\mathbf{s}_l = \mathsf{NN(s_k)}$ at distance δ_{kl}. The points cease to exist as a separate clique as soon as α exceeds $\alpha = \frac{1}{4}\delta_{kl}^2$. Let $\mathsf{E}[\delta_{\mathrm{k,NN(k)}}]$ and $\mathsf{E}[\delta_{\mathrm{k,FN(k)}}]$ denote the expected Euclidean distance (mean edge length) to the nearest and the local-furthest neighbour of $\mathbf{s}_k$, respectively. Then, trivially:

$$\mathsf{E}[\delta_{\mathrm{k,NN(k)}}] \leq \mathsf{E}[\delta_{\mathrm{k,FN(k)}}] \tag{4–36}$$

Let $\mathbf{s}_k \in \mathcal{NNG}$ and $\mathbf{s}_l \in \mathcal{LFNG}$. Then, as a result, for any α and any clique $\mathbb{Y}_j$, one has that:

$$\mathsf{Pr}[\mathbf{s_k} \in \mathbb{Y}_\mathrm{j}] \geq \mathsf{Pr}[\mathbf{s_l} \in \mathbb{Y}_\mathrm{j}] \tag{4–37}$$

which re-establishes the indicative capacity of $\mathcal{NNG}$ and $\mathcal{LFNG}$. Finally:

OBSERVATION 4.7 (NORMALISED WEIGHTED POINTS DO NOT LIE ON A HYPERPLANE)
Property-based normalised weighted points lying in augmented space $E^d \times R$ are generally not lying on a common hyperplane •

4.8 Weight transformation

4.8.1 Different approaches

Once the normalised weights have been determined, the individual weights have to be translated and up-scaled so as to reach the desired coverage. The steps involved can be taken from the scheme presented in figure 3–15. The two basic type of transformations are a translation by Δw and a scaling by a real factor. Using observation 4.5 and 4.7, the case I and case II weighting discussed can now be made further precise:

- **Case I: isotropic scaling normalised weights**

  Affine weight transformation: $w(\mathbf{s}) = w_0 + \varrho\bar{w}(\mathbf{s})$, where w_0 is a constant weight. The transformation is composed of a translation by w_0 plus a isotropic scaling by a non-zero real factor ϱ. This scaling preserves the ordering of the normalised weights. The coverage so obtained is at most the coverage of case II, the resulting weight set is an affine variety of the normalised weights.

- **Case II: attracting of the normalised weights to an attractor**

  This is the approach to obtain a desired coverage, for example the one obtained by a Stienen attractor model. In contrast to the first approach, the ordering of the normalised weights is not necessarily being preserved. The coverage so obtained can be determined or at least estimated beforehand, and is a property of the model.

Determining the parameters of case I

The value of w_0 is chosen such that the remaining empirical variance of the nearest neighbour distances is acceptable, which of course depends on the model at hand. Recall that as a result of a case I transformation, variance $\tilde{s}^2$ becomes $\varrho^2\tilde{s}^2$. The variance is directly related to the covariance of the properties that contribute to the normalised weight. The nearest neighbour distance to be abridged by the transformed weight can be divided into three parts:

1. A part to be consumed by the weight translation by w_0 .
2. A part to be consumed by the weight scaling by ϱ .
3. A part to be consumed by varying α .

The sum of the effects of the first two parts defines the boundaries $[\alpha_{\min},\alpha_{\max}]$, but which one contributes what part can still be manipulated. For example, w_0 can be chosen such that $\varrho = 1$, or even less. The discriminating power of the weight vanishes then, however. It has been shown that weighting makes sense only if $\alpha \approx w$.

Using an attractor

Assume a fixed set $\mathbb{Y}$ of points in space $E^d \times R$, with $\operatorname{card}\mathbb{Y} = N$. Further assume that the normalised weights $\bar{\mathbb{W}}$ are transformed such that the set distance $\|\mathbb{Y} - \mathbb{S} \otimes \mathbb{W}\|$ becomes smaller and smaller, until some arbitrary small value. Set distance D, in this context, is defined as:

$$\Delta = \sum_{j=1}^{N} \sqrt{(\tilde{y}_j - \tilde{\mathbf{s}}_j)^2} \tag{4–38}$$

Then, the fixed set $\mathbb{Y}$ is called an *attractor* and $\tilde{\mathbb{S}}$ is attracted by $\mathbb{Y}$. In this work, an attractor will be used in the sense of a *geometric realisation of an attractor*. The attractor that will be discussed for case II transformation is the *Stienen model*. This attractor will be discussed in detail in the next section.

The purpose of a case II weight transformation is chiefly to obtain hole-free (parts of) objects. In that case, the coverage needs to be *complete*, i.e., be $\kappa = 1$. Target is the weight distribution belonging to the moment that points in the α-complex are about to be connected by an edge. This is the point of no enforcement, discussed in the overview of this chapter. A case I weight transformation cranks up the weights up to the point that the first edge is about to enter the α-complex. From that point, attractor models such as the Stienen model may be used to further increase the local weights, while obeying the no-enforcement.

Finally, notice with the latter approach that the normalised weights may as well all be set to unity, or zero, or any other constant value. In that case, in contrast with observation 4.7, they are located on a common hyperplane. The attraction "forgets" their normalised value and maps all domains $\mathbb{S} \otimes \mathbb{W}'$ of original values to the same model-dictated value $\mathbb{S} \otimes \mathbb{W}$. As such, it behaves as a surjection.

4.8.2 The Stienen model

The Stienen model (e.g., [SKM95]) is a Voronoi tessellation $\mathcal{V}(\mathbb{S}$ plus a ball union $\mathcal{B}(\mathbb{S})$ in which balls have maximum radius without overlapping. Weights are such that their spheres touch the nearest radical plane, i.e., the nearest boundary of their Voronoi cell. As a result, spheres of two adjacent Voronoi cells touch at their common cell boundary iff the two are nearest neighbours. The nearest neighbour relation is not symmetrical and as a consequence, not all spheres actually touch their nearest neighbour sphere. See figure 4–26. In the Stienen model, none of the radical centres can be covered and hence, none of the cells can be completely swept out. This means that all local coverage $\kappa_j < 1$. The geometric realisation of the nerve of the Stienen model is a sub-graph of $\mathcal{NNG}$. The Stienen model produces safe lower bound values for the weight set $\mathbb{W}$: all edges become α-exposed for some finite non-negative α, and all first edges in the star $St\,\mathbf{s}$ become α-exposed for minimum α. The latter does of course not imply that all edges become α-exposed for *the same* value of α. Increasing α causes the edges in the star to enter the α-complex one-by-one, until ultimately, the edge with the local-furthest neighbour enters.

Does the Stienen model have an equivalent that may serve as an upper bound $\alpha_{\max}$ for the weight? Unfortunately, no such model was encountered in literature. The radical centres (Voronoi vertices) are the last points of the Voronoi cell to be swept out by the growing spheres $\mathtt{B}_\alpha$. This can be further made precise, in that the radical centre contained in the radical plane of a point $\mathbf{s}$ with its local-furthest neighbour $\mathtt{FN}(\mathbf{s})$ is the very last point being covered as α grows. If weight is increased such that the sphere reaches this point, the entire Voronoi cell will be covered by the sphere, i.e., $\kappa = 1$. This holds for each cell and full coverage will thus be obtained. Unfortunately, this strategy also introduces many redundant points. Also notice that if $\kappa = 1$ in each Voronoi cell, varying α is no longer relevant. In general, assigning weights to points modifies the weighted Voronoi diagram, as it causes radical planes to move. In practice, the size of the weight sphere touching the furthest Voronoi vertex (radical centre) is therefore multiplied by a factor $0 \leq \omega \leq 1$. Of course, ω should be chosen such that the weight is greater than the weight based on the Stienen model. By absence of better terms, *nearest Stienen model* and *local-furthest Stienen model* will be used to denote the models discussed.

If all Voronoi cells incident upon a radical centre have local coverage $\kappa = 1$, that radical centre cannot lie inside a hole. Since all balls $\mathtt{B}_\alpha$ grow in equal amounts as α changes, a hole shrinks so that the radical centre is always in its interior. On disappearance, the hole consists of *only* the radical centre. But for an *arbitrary* radical centre to become covered, it is not necessary

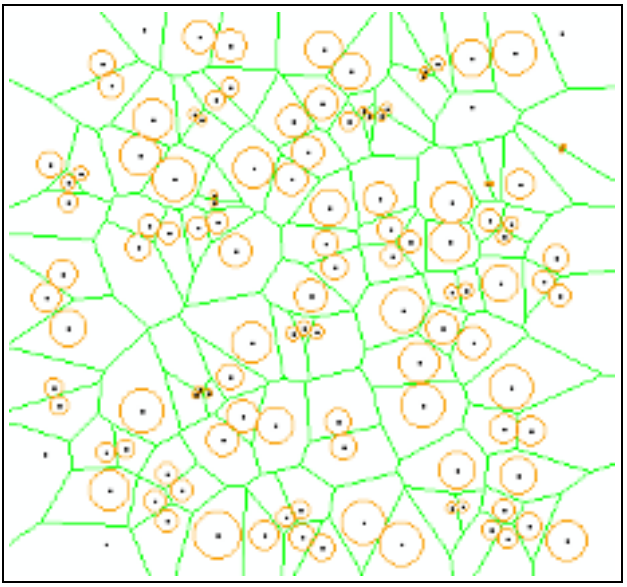

Figure 4–26: Stienen model of the homogenous Poisson point process (figure 4–23). Two spheres may touch at their common cell boundary iff the two are nearest neighbours, but not all nearest neighbour spheres do, due to asymmetry. Observe that none of the radical centres can be covered.

that *all* Voronoicells incident upon a radical centre have $\kappa = 1$. A local coverage $\kappa = 1$ is only reached if also the radical centre with the *local-furthest* neighbour is covered, and not all radical centres are generated by a vertex contained in $\mathcal{LFNG}$. Local coverage is generally *not* independent. In addition, the desired coverage is not necessarily obtained through weight alone. In practice, it is convenient to let some coverage be conquered by α, as discussed. Local variation depends on the distribution of the ratio between nearest and local-furthest neighbour distances and the distribution of the local coverage κ. Variationcanbe equalised by varying local values for ω.

4.9 Towards Vectorial weight

Vectorial weights, in addition to the scalar weights discussed so far, are highly desirable to support the coupling with vectorial properties. A few illustrations: a *potential variable*, such as fluid pressure, may be described just fine by a scalar. Fluid pressure is intrinsically omni-directional (or: undirectional). Radiogenic heat flowfor example, is a *flow variable*, generally described by a *vector field* and a weight set based on it would require weights to be vectorial. Some material properties, such as strains and permeability, or variables such as hydraulic conductivity, are intrinsically *tensorial*, i.e., they are described by a *tensor*. For instance, for a problem in a 3-model space, a tensor can be represented by a 3×3 generally unsymmetrical matrix of tensor coefficients. How to extend the current use and interpretation of weight, in order to accommodate for vectorial and tensorial weight is an open problem. In [AAL+99], skew Voronoi diagrams

have been proposed, using direction-dependent distances and direction-sensitive measure. The approach taken may be a good starting point to further work out the concept of vectorial weight.

Details are left undiscussed and will be posted as an open problem for further research. See chapter 7.

Chapter 5

Alpha complexes as a representation

5.1 Overview of this chapter

In this chapter, α-complexes will be examined with regard to two important aspects: their quality as a *solid object description* and their quality as a *representation scheme*. These two terms will be defined shortly. Where appropriate, a comparison will be made with the more widely applied *faceted boundary representation* (faceted BRep, for short), the *constructive solid geometry representation* (CSG) and the cell(ular) decomposition. As explained in chapter 3, in practical applications, α-complexes may be mixed, merged and converted into other descriptions and representations and finding out about their qualities as such is therefore important. Little is known about α-complexes as a solid object description and as a representation scheme. By side stepping into CSG- and BRep and cell decomposition representations, some reasoning about representation schemes and α-complexes is possible. Much like in the previous chapters, spatial occupancy, holes and singular faces are the leading thread running through this chapter.

The outline of this chapter is as follows. Section 5.2 introduces solid object descriptions and then presents a list of criteria to evaluate such descriptions against. The section concludes with the actual evaluation of the α-complex as an object description. Next, in section 5.3 a similar discussion is being presented with regard to the evaluation of representation schemes against a number of criteria. This section closely follows the expose given by Requicha, in [Req80], Chapter 1, and Kalay, in [Kal89]. Questions concerning the two most important maps, the icon derivation and the primitive instantiation (chapter 3), in relation to variational geometry, are discussed more extensively in section 5.4. Section 5.5 presents a more formal description of holes, their topological relation to the α-complex and their mutual topological relation. Topreserve homeomorphism of the representation maps, a *nil*-icon and a *nil*-object are then introducedn section 5.6. Their roles in originating, transforming and terminating processes of the birth-life-death life-cycle of natural objects is discussed. Finally, set regularisation, important to get rid of singular faces in conversion mappings, is discussed in section 5.7.

5.2 Solid object descriptions

5.2.1 Object descriptions and computer models

So far, four types of models have been discussed: the sampling model, the weighting model, the α-complex model and numerical model, see figure 3–8 in chapter 3. These models were primarily analytical models in the sense that their discussion was not directly targeted at computer implementations. Now, attention turns to the formal description and representation of objects for computer implementation purposes.

DEFINITION 5.1 (COMPUTER MODEL, KALAY, 1989)
Computer models capturing real world objects and phenomena can be regarded as languages of representation composed of symbol structures and syntax rules to manipulate them, assigning a meaning to a collection of symbols and an interpretation in terms of the real world objects they represent •

In this context, instantiated primitives are the symbolic structures and intra- and inter-object constraints are the syntax rules. Emphasis is now on proper ways to describe objects, more precisely, solid objects of general dimension d, with non-empty interior in E^d and in geometric and topological terms. For computer modelling purposes, different approaches exist for that purpose ([Kal89, Zei91, Tay92]). E.g.,

- **Volumetric description**

  The objects' geometries and topologies are described in terms of the *underlying space*, or *(hyper-)volume* or d-volume. Recapture from previous chapter that in general dimension, this volume can be quantified by means of the general dimension Lebesgue measure (e.g., chapter 3).

- **Boundary description**

  The objects' boundaries are described, bounding the objects interiors and separating the interior from the exterior. Recall that in this work, objects are generally no monoliths, but composites, having multiple interiors and exteriors, the number of which may vary with α and vary over time. When partitioned, the objects' internal boundaries, separating the internal cells are also part of this description.

- **Part-whole description**

  In this approach the objects' compositions are described in terms of *primitive* parts and some recipe to assemble them into the aggregation of the model.

This subdivision suggests a much sharper distinction between these approaches than practical implementations admit. The true meaning of the subdivision is chiefly theoretical. In practice, many hybrid approaches exist and software codes may occasionally transcribe one representation into another.

5.2.2 Object description evaluation criteria

In order to evaluate the "fitness for purpose" of α-complexes as a solid object description, criteria are needed that make sense in the context of natural objects. Such criteria have been presented in for example [Kal89, Zei91]. Apart from the general criteria of *well-formedness*, *generality* and *completeness*, the following criteria are of particular interest in this context:

- **Solidity**

  A convex polytope $\mathcal{P}$ (e.g., a simplex), divides space into tw oregions: *interior* $\mathrm{Int}\,\mathcal{P}$ and *exterior* $\mathrm{Ext}\,\mathcal{P}$, separated by *boundary* $\mathrm{Bd}\,\mathcal{P}$. An important question is how and to what extent a description supports this unambiguous division of space and related operations such as point location, that relies entirely on this subdivision.

- **Homogenous dimensionality**

  The issue of homogenous dimensionality is about the boundary-interior topological relation. Homogenous dimensionality is obtained if each face in the boundary $\mathrm{Bd}\,\mathcal{C}_\alpha$ is incident upon the interior $\mathrm{Int}\,\mathcal{C}_\alpha$, in other words: bounds a d-cell.

- **Rigidity**

  Rigidity is obtained when the geometry and topology of the modelled object do not depend on the objects position, i.e., on its location or its orientation in space. If rigid, geometry and topology of the object are left invariant under isometric transformation (see chapter 3).

- **Continuit y**

  Continuity requires that the represented object shall not be composed of disjunct (unconnected) parts.

- **Closure**

  Closure is obtained if none of the k-faces is incident upon a singular face. Forexample, in the case of a triangulated object, when every k-simplex is incident upon exactly $d+1$ $(k-1)$-simplices. If closure is obtained, k-faces can be represented as regularised set (r-sets, to be discussed in section 5.7).

- **Disjunct in teriors**

  The interiors of tw ok-faces f_i and f_j shall be disjunct, i.e., $\mathrm{Int}\,f_i \bigcap \mathrm{Int}\,f_j = \emptyset,\ \forall i,j$.

- **Orientability**

  Full orientabilit yis obtained if all k-faces are orientable, i.e., if their orientation can be told to be positive or negative.

- **Finite time and storage complexity**

  Finite time and storage complexity is obtained if all computer operations involved in storing the objects representation in a computer can be shown to be asymptoticly finite in terms of processing time and storage.

	BRep	faceted BRep	CSG	Cell Decomposition	α-complex
Solidity	yes		yes	yes	only if regularized (Obs. 5.6)
Continuity	yes		yes	yes	only, non-part-b (Obs. 5.9)
Rigidity	yes		yes	yes	(Obs. 5.8)
Homogeneous dimension		only if regularized	yes	yes	if regularized (Obs. 5.1, 5.7)
Closure		only if regularized	yes	yes	only if regularized (Obs. 5.2, 5.10)
Orientability	yes		yes	yes	(Obs. 5.4, 5.12)
Disjunct interior	yes		yes	yes	(Obs. 5.3, 5.11)
Finiteness	yes		yes	yes	(Obs. 5.13, table 2–5)

Table 5–1: *the α-complex compared to BRep, CSG, cell decomposition and faceted BRep description. ... it is only guaranteed to be fulfilled or met after α-value is assumed high enough to allow d-cells to be formed.*

5.2.3 Evaluation of alpha complexes as an object description

A solid object description based on an α-complex as described in this thesis carries the characteristics of:

- **A part-whole description**

  With primitive instancing of k-simplices.

- **A volumetric description**

  By means of a cellular complex, erected by d-simplices (possibly after regularisation, to be explained later).

- **A (faceted) boundary description**

  Built from the $(d-1)$-simplices describing the boundary of the α-complex and spanning its underlying space.

The description that comes closest to α-complexes would be a part-whole description, describing an α-complex as an assembly (complex) of geometric realisations of a single primitive (icon): the k-simplex.

A number of observations are immediately following from the discussion in the previous chapters:

OBSERVATION 5.1 (HOMOGENOUS DIMENSIONALITY AND SINGULAR FACES)
Too low an α-value and the resulting singular faces (chapter 2) present in an α-complex generally violate homogenous dimensionality •

OBSERVATION 5.2 (CLOSURE AND SINGULAR FACES)
Singular faces (chapter 2) present in an α-complex generally violate closure. Removing them generally lifts the violation, provided α is high enough to admit d-cells •

OBSERVATION 5.3 (SELF-INTERSECTION)
The criterion of disjunct interiors also excludes self-intersection •

OBSERVATION 5.4 (ORIENTATION OF HOLES)
Holes are assigned a negative orientation. This follows from an implied positive orientation of the boundary of an object •

OBSERVATION 5.5 (TIME AND STORAGE COMPLEXITY)
Based on the findings of section 2.8, time and storage complexity are finite •

Above, a list of criteria was given for the evaluation of object descriptions. Going down this list, the following evaluation can be made:

OBSERVATION 5.6 (SOLIDITY OF AN α-COMPLEX)
For α-complexes, with their internal voids and possibly singular faces, the solidity-criterion is not necessarily met •

OBSERVATION 5.7 (HOMOGENOUS DIMENSIONALITY OF AN α-COMPLEX)
Provided that α is high enough to permit the forming of d-faces, removal of singular faces ensures homogenous dimensionality and closure •

OBSERVATION 5.8 (RIGIDITY OF AN α-COMPLEX)
The rigidity criterion is obviously met: the α-complex is determined by distance and weight, not by position or orientation. Transformations that can be represented by a homeomorphic mapping do not change the α-complex topology •

OBSERVATION 5.9 (CONTINUITY OF AN α-COMPLEX)
Continuity of the interior cannot be guaranteed, moreover, α-complexes can scatter into many disjunct parts •

OBSERVATION 5.10 (CLOSURE OF AN α-COMPLEX)
For α-complexes, with their singular faces, the closure-criterion is not necessarily met •

OBSERVATION 5.11 (DISJUNCT INTERIORS OF AN α-COMPLEX)
The interior of any two k-faces is always disjunct, as they are faces in the underlying triangulation. This also excludes self-intersection •

OBSERVATION 5.12 (ORIENTABILITY OF AN α-COMPLEX)
Faces of an α-complex are orientable. Voids are commonly attributed a negative orientation, oppositely oriented to the boundary faces •

OBSERVATION 5.13 (FINITE TIME AND STORAGE COMPLEXITY OF AN α-COMPLEX)
For finite complexes, based on a finite compact pointset, finite storage complexity can be shown to exist, as well as finite time complexity for creation, traversal, visiting, removal and linear processingoperations up onthem •

Continuity of the interior cannot be guaranteed. Moreover, α-complexes can scatter into many disjunct parts. This is not necessarily a flaw; it is one of the celebrated features for the modelling purposes in this work and a great advantage for object descriptions with a dynamic topology, subjected to an erosional evolutionary map (see chapter 3). On the other hand, it complicates validity and consistency verifications on the model as well as further operations on the model. With respect to the criterion of well-formedness, it is obvious that continuity is not guaranteed and boundary is generally not connected, only on a part-by-part basis. If the boundary is closed and connected, e.g., close to $\alpha = \alpha_{\max}$, the following holds:

OBSERVATION 5.14 (WELL-FORMEDNESS OF AN α-COMPLEX)
If $\mathrm{Bd}\,\mathcal{C}_\alpha$ can be triangulated (tessellated with triangles), and the boundary is closed and connected, then these twoproperties ensure well-formedness •

As far as completeness is concerned; the data structure storing the α-complex can be easily augmented with auxiliary parameters, like material properties, central moments, etc. The simplex, the basic building block, allows for relatively simple computational schemes, for instance barycentric calculus (e.g., [BP94]).

OBSERVATION 5.15 (COMPLETENESS OF THE α-COMPLEX)
The completeness of α-complexes is comparable to that of triangulations and therefore sufficient in the context of this work •

The above observation is very similar to the characteristics of a cellular decomposition. To a great extent, α-complex object descriptions can be compared to them, assuming the α-complex has dimension d. The only difference is then posed by the singular faces.

The outcome of the evaluation of α-complexes as a solid object description is collected in table 5–1.

5.3 Representation schemes

5.3.1 Representation schemes and computer models

One might say, an object representation is concerned with *what to describe* of a physical object in the model. A *representation scheme* is concerned with the question as to *how to describe this knowledge* in terms of syntax, symbols say, and semantics, rules say. Loosely formulated:

DEFINITION 5.2 (REPRESENTATION SCHEME)
A representation scheme is a way to describe real world objects in a symbolic notation •

Some notations are purely mathematical (abstract representations), some are graphically oriented symbolic notations that can be rendered using a computer. In this thesis, emphasis is on the latter.

Widely used schemes are the Constructive Solid Geometry (CSG), the Boundary Representation (BRep), the cell(ular) decomposition, the spatial enumeration and voxel representation. Every representation has its own characteristics. In a sense, α-complexes can also be seen as a means of representation. Table 5–2 summarises the most important characteristics of the three principle representation schemes CSG, BRep and cell decomposition, setting them off against the α-complex representation. One may also want to review figure 2–1 at this point. Table 5–2 compares the hyper-spatial representation to these three schemes. For further details, see for example [Kal89, Sam90b, Sam90a, Zei91, RNS93, Har96].

At the core of the discussion about mapping and the mathematical aspects of the entire mapping "chain" is the notion of *surjectivity injectivity* and *bijectivity*. The latter one is the easier one to start with: it is simply a one-to-one relation, in which all elements of domain (originals) and co-domain (image) are involved. Figure 5–2, left picture shows a surjective map, the right picture shows an injective map. Either not all the elements in domain $\mathbb{V}$ (surjection) or co-domain $\mathbb{W}$ (injection) are involved, images in the co-domain have multiple originals (surjection), or originals in the domain have multiple images in the co-domain.

Representations can be regarded in the same manner:

DEFINITION 5.3 (MAPPING)
A mapping defined on a set $\mathbb{V}$ *is a function that sends every original member in* $\mathbb{V}$ *into an image in* $\mathbb{W}$ •

OBSERVATION 5.16 (SURJECTIVE MAPPING)
In a surjective mapping, every image has at least one original •

OBSERVATION 5.17 (INJECTIVE MAPPING)
In a injective mapping, every image has at most one original •

	WEIGHTED	FACETED	BREP	CELL DECOMPOSITION	CSG	α-COMPLEX
id shape manifold, and complexshapes	(non-)domain manifold, origin, homogeneous,			complex, separated shapes		non-manifold α-complex,
primitive		k-facet, simple $0 \le k < d$		bounded half-space intersection (parametrized primitive)	d-cell	α-complex
with	graph, polygonal mesh, data structure	incidence, edge, (winged) triangulation, cell-tuple [Bri90], [Wei86]		binary evaluation tree		k-faces [Ede87], face-edge, winged edge, cell-tuple
distance, the Laguerre]	operations, tesselating, tweaking (auk. form) [RW96]	Euclidean (weighted) distance, [OSN93], [Kog94],				α
	geometry-topology separation	yes		no, implicit topology	yes	
and (Λ C) metric Euclidean distance	Chapter 2s Euclidean distance, Laguerre relationship, metric	Euclidean (distance) sets Euclidean		(non-)generalized		
	topology, characteristic	operation of topology, Euler		topology set topology		α-exposedness
	evaluated	yes		optional	yes	
	mixed declarative	procedural declarative	declarative			

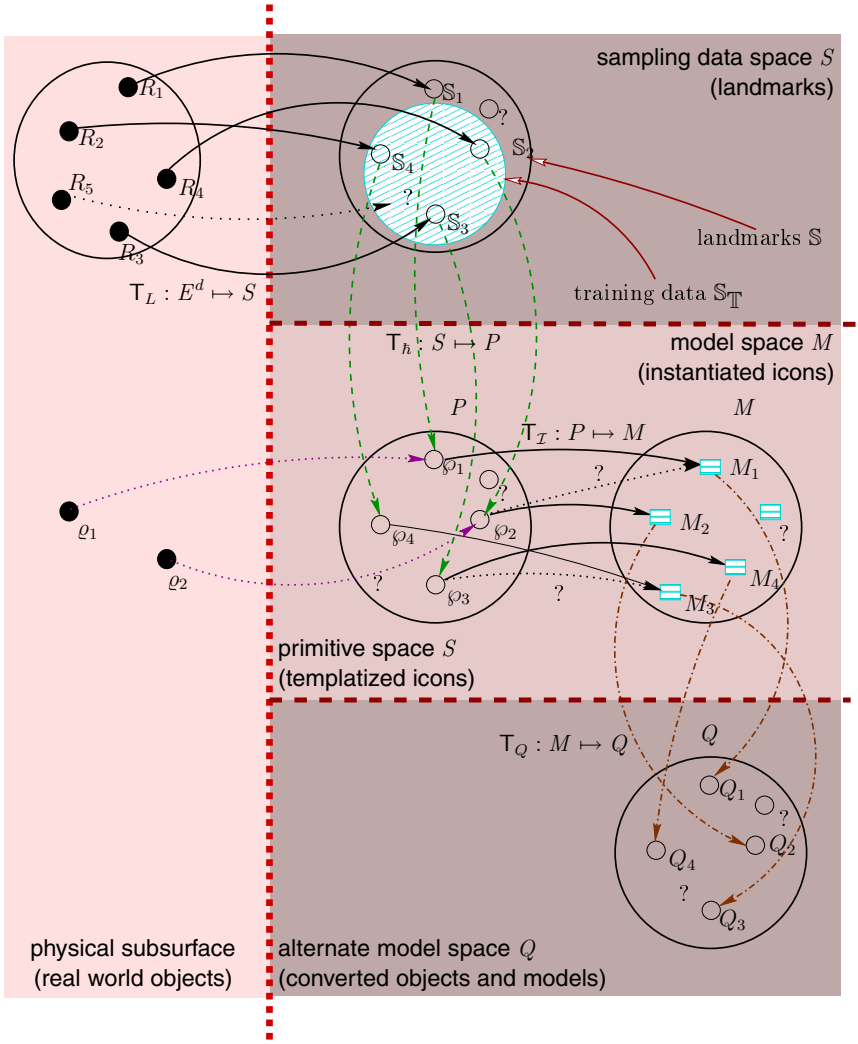

Figure 5–1: *"chain" of representation-to-representation mappings in the hyper-spatial approach. Dotted arrows and question mark-labelled elements refer to the questions raised in the text. Mapping of real w orld objects ϱ_1 and ϱ_2 on to abstract primitives $\wp_1$ and $\wp_2$ would be valid in case of analytical definitions of those abstract primitives. As explained, this is not considered here. The mapping of value sets has been left out, for clarity.*

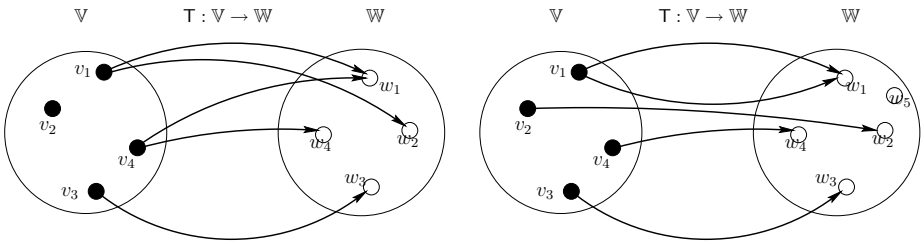

Figure 5–2: *a surjective (left) and injective (right) mapping. Formally the surjection is not a mapping, because not all the originals in* $\mathbb{V}$ *are mapped into* $\mathbb{W}$.

OBSERVATION5.18 (BIJECTIVE MAPPING)
In a bijective mapping, every image has exactly one original and every original exactly one image •

There are many synonyms for bijective mappings, e.g., homeomorphic mapping, isomorphic mapping, invertible mapping.

How does this translate to the problem of mappings in the hyper-spatial mapping chain? As an example, the instantiation mapping $\mathsf{T}_{\mathcal{I}}$ will be considered:

EXAMPLE 5.1 (INSTANTIATION MAPPING $\mathsf{T}_{\mathcal{I}} : P \mapsto M$)
Mapping $\mathsf{T}_{\mathcal{I}} : P \mapsto M$ *maps abstract primitives* $\wp$ *into a model* $M \in \mathcal{M}$*, by instantiation (figure 5–1). When surjective but not injective (and hence not bijective), model components cannot be be uniquely traced back to a single original object and not necessarily all primitives can be instantiated in a model (also see problem 5.1, questions 1 and 2). Such a model may be subject to multiple interpretation, which is generally catastrophic and objetionable. On the other hand, if not all originals in the domain have an image in the co-domain, then apparently, the modelling method does not have the capability needed to cover the entire domain: some objects cannot be described by the modelling representation. If a map does not reach the entire co-domain, then that map is not surjective and therefore not bijective. Apparently, more (other) models of objects can be created than the domain permits. Object models exist that have no original with the corresponding characteristics. This in itself is not a flaw. If models can always be traced back to a single object then apparently, they have at most one primitive as their original and the mapping is an injection. If not an injection, function* T *is formally not even a mapping in the sense of definition 5.3. Only the combination of surjectivity and injectivity yields a crisp and unambiguous one-to-one relation (homeomorphism) between model components and primitives* •

5.3.2 Representation scheme evaluation criteria

Representation scheme evaluation criteria are mostly stated with typical engineering applications in mind. Here, only those criteria will be regarded that are relevant in the context of natural object modelling and α-complexes. Widely agreed such criteria for representation schemes are:

- **Uniqueness**

  Uniqueness refers to the cardinality of all representations that describe the modelled object

under this representation scheme. Uniqueness demands that representations are one-to-one and that mappings from one representation on to another are homeomorphic.

- **Completeness**

  The richness of description, say, in support of operations, analysis and conversions. Completeness inflicts no heavy implications on the mapping, only on the representation. Formally, in conversion mapping, additional information must be "mappable" too.

- **Domain**

  The class of physical objects that can be represented in relation to the class of valid representations the representation scheme can produce. Example 5.1 showed that domain, representations and mapping between them must be compatible. If homeomorphism is to be preserved, then this is a severe requirement.

- **Validity**

  The validity of the objects produced under this representation scheme. The greatest concern in this regard is the variational geometry and the topological variety it can generate. More formally, the instantiated primitives must belong to the *icon variety*, thereby excluding topological variety. In other words, as long as instances remain within the icon variety, they remain topologically equivalent with the icon. As stated, a framework of domain variable and parameter constraints (or: *predicates*) must be defined for this.

These criteria will be applied to the evaluation of α-complexes as a representation scheme.

DEFINITION 5.4 (ICON VARIETY)
The icon variety is the set of valid instantiations that may be generated by the icon by means of parameter variation •

5.3.3 Evaluation of α-complexes as a representation scheme

In literature, representations and mappings of point sets are relatively well understood. Simplicial complexes are less well understood in this regard. See for example [Gib77, PBCF93]. Recall that an α-complex is a simplicial complex (figure 2–1, chapter 2). It can be shown ([EM94]) that an α-complex establishes a unique relation between the data point set $\mathbb{S}$, the α-complex $\mathcal{C}_\alpha$ and its underlying space $|\mathcal{C}_\alpha|$. What is it then, that makes representations based on α-complexes different? Basically the same as what makes simplicial complexes topologically more complicated: holes and singular faces. Holes in this regard, is a general term for a variety of topological features, refer to definition 2.22 and table 2–4 in section 2.7 and table 5–6.

What elements from the mapping chain to evaluate?

The modelling framework presented in chapter 3 contains several representations and mappings thereof. For example the sampling data point set that is meant to represent the anatomic landmarks of a physical object. Basically, not only the α-complex representation is relevant, the "in-between" representation are so too. And also the mapping from one representation to another. A discussion of all these aspects is delicate, however. Therefore, the discussion is narrowed down

to those mappings where α-complexes are most involved, the derivation of icons and the primitive instantiation. Other representations will be considered only within the whole of the mapping chain. If uniqueness is lost as a result of the sampling process, for example, than this also affects the uniqueness of the physical object-α-complex representation as a whole. Those aspects will be discussed. Finally, as long as the complete modelling environment of figure 3–1 is not installed, a "reduced" mapping chain can be sketched, as in figure 5–3. The main difference is in the fact that icons are absent. α-Complexes representing the modelled objects are directly derived from the landmark set. Discussions on the hyper-spatial mapping chain will always trailer a similar look on the reduced chain. So:

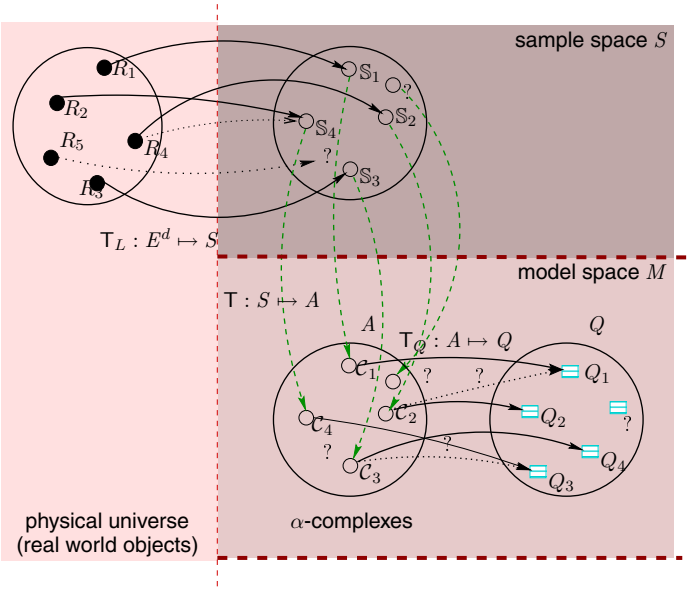

Figure 5–3: *simplified "chain" of representation-to-representation mappings in modelling with α-complexes. The simplification is in the fact that there are no icons. $\mathbb{A}$ is the set of α-complexes, $\mathbb{Q}$ the set of conversions. Dotted arrows and question mark-labelled elements refer to the questions raised in the text.*

- **Hyper-spatial mapping chain cf. figure 5–1**

  This is the full mapping chain, relating α-complexes to physical objects using the following intermediate representations and mappings:

$$\text{physical object } R \overset{\mathsf{T}_L}{\Longleftrightarrow} \text{landmarks } \mathbb{S} \overset{\mathsf{T}_\hbar}{\Longleftrightarrow} \text{icon } \wp \overset{\mathsf{T}_\mathcal{I}}{\Longleftrightarrow} \text{instance } M$$

- **Reduced mapping chain cf. figure 5–3**

  This is the direct usage of landmark sets for α-complex representations of modelled objects, without the use of a collection of icons:

$$\text{physical object } R \overset{\mathsf{T}_L}{\Longleftrightarrow} \text{landmarks } \mathbb{S} \overset{\mathsf{T}}{\Longleftrightarrow} \text{object model } M$$

where icon $\wp$, instance M and object model M are α-complex-based. Mapping T_Q may be follow either of these chains.

Fundamental problem of representation evaluation

The following fundamental problem may now be formulated with respect to α-complex representations of subsurface objects:

FORMULATION 5.1 (α-COMPLEX AS A REPRESENTATION SCHEME)
Assume the existence of a collection of icons representing their shape families and covering the class of subsurface objects to be modelled. Then essential questions with regard to the use of α-complexes as a representationscheme are:

1. *Can* every *subsurface object be represented by the instantiation of some icon, such that it can be made to represent the same object again?*
2. *Can* every *icon be instantiated (within valid constraints) within* any *earth architecture?*
3. *Does any of the mappings allow for the creation of invalid icons or invalid re-instantiations from them?*
4. *How to represent geometricly coupled objects?*
5. *Shall shape families be "orthogonal"? In other words, do the shape families that two icons can generate (their icon varieties) overlap? If so, is there ambiguity then in relating modelled objects back to real world objects?*
6. *What are the consequences of the fact that morphological operationsand transformations that do* not *leave the shape invariant (e.g., erosion), prevent instantiated shapes from being back-tracable to their generating icon?*
7. *After converting a primitive instance into another representation through* conversion, *does the unique relation between the obtained representation and the original object still hold?*

Evaluation of the icon α-complex representation

Triangulations are assumed bounded by the convex hull of the generating point set and therefore having only bounded cells. Evolutionary maps are assumed to be simplicial. Recall that a simplicial map is a homeomorphic map that maps a simplicial complex $\mathcal{C}_1$ through affine transformation on to simplicial complex $\mathcal{C}_2$. Furthermore, assume the availability of suitable observation method. Evaluation of the α-complex representation of the icon shows the following. With respect to the domain:

OBSERVATION 5.19 (PHYSICAL OBJECT)
Physical objects are generally dynamic, not necessarily rigid composite regions, with heterogeneous values in the landmarks and subject to evolutionary maps •

OBSERVATION 5.20 (DOMAIN OF THE LANDMARK SAMPLING REPRESENTATION)
For the class of objects of interest in this work, every physical object can be represented by a finite compact sampling data point set, with arbitrary accuracy •

OBSERVATION 5.21 (HELMERTIZATION OF THE LANDMARKS)
For the class of objects of interest in this work, every family of raw physical shapes and objects can be made to deliver a Helmertized landmark set, possibly empty •

If redundant points are removed, point set $\mathbb{S}_\hbar$ can be shown to be identical to 0-skeleton $F^{(0)}$, obtained by 0-filtration of the α-complex of the icon. See figure 2–13, chapter 2.

OBSERVATION 5.22 (TRIANGULARIZABILITY OF THE LANDMARK SET)
Each (finite and compact) landmark set in non-degenerate position can be triangulated. Every landmark set is thereby the carrier of an equivalence class of triangulations •

The trailing part of this definition points out a problem that shows up later, when *unevaluated representations* will be considered. For a while, this aspect will be ignored. Every convex polyhedron can be triangulated (e.g., [Mun84]). Duplicates and *redundant* points, too close to dominant points must be dropped, singular objects result in a trivial triangulation, i.e., a 0-triangulation or a *nil*-triangulation.

DEFINITION 5.5 (0-TRIANGULATION)
A 0-triangulation consists of a single 0-face (vertex) •

OBSERVATION 5.23 (SINGULAR OBJECT)
Singular (or: minimum) objects, sampled by a single point, result in a 0-triangulation •

DEFINITION 5.6 (*nil*-TRIANGULATION)
A nil-triangulation consists of an empty set •

A *nil*-triangulation may also result from empty Helmertized landmark sets. Empty landmark set are more of theoretical than of practical importance.

OBSERVATION 5.24 (*nil*-OBJECT)
Any nil-object sampled by an empty set result in a nil-triangulation •

instantiated by a *nil*-icon:

DEFINITION 5.7 (*nil*-ICON)
A nil-icon is a templatized empty set, and the only icon having an empty set as its landmarks •

OBSERVATION 5.25 (*nil*-ICON)
Definition 5.7 is not in contradiction with the constraints imposed on $\mathbb{S}$ in section 2.2, chapter 2 •

Finally, with these steps, we have that:

OBSERVATION 5.26 (DOMAIN OF THE ICON α-COMPLEX REPRESENTATION)
The domain of the icon α-complex representation contains the icons of the physical objects given in observation 5.19 •

OBSERVATION 5.27 (COMPLETENESS OF THE ICON α-COMPLEX REPRESENTATION)
The completeness of the α-complex representation of an icon is sufficient. Arbitrary value sets can be stored in a hyper-spatial icon α-complex, along with auxiliary information, in a way compatible with cells in a cellular decomposition •

The validity of an icon α-complex representation assumes that the α-complex is a valid α-complex in terms of geometry and topology and that the icon represented is indeed a valid icon. The geometry of the α-complex is dominated by the landmarks. Assuming a valid landmark set, then this linearly results in a valid geometry. The topology is dominated by weights and α. The topology of the icon must be constrained so that the icon topology represents the "topology" of the physical object. This is assumed to be accomplished by the right coverage by anatomic landmarks and proper weighting, resulting in a properly-chosen icon variety. As stated, a framework of domain variables and parameter constraints (or: *predicates*) must be defined for this purpose.

OBSERVATION 5.28 (VALIDITY OF THE ICON α-COMPLEX REPRESENTATION)
The validity of the icon α-complex representation is generally satisfied by the right coverage by anatomic landmarks, proper weighting and finally a properly-chosen icon variety that covers the raw shape family •

Uniqueness demands that representations are one-to-one and that mappings from one representation onto another are homeomorphic. Unfortunately, the set of landmarks does generally not uniquely represent physical objects. The more landmarks, the less physical objects are being represented:

OBSERVATION 5.29 (UNIQUENESS OF LANDMARK REPRESENTATION)
A set of anatomic landmarks does generally not uniquely represent physical objects. For the limit case where the cardinality of the landmarks goes to infinity, the number of represented physical objects can be reduced to an arbitrary small number •

Observe that by the generation of an α-complex from the landmarks, the non-uniqueness is largely reduced, much as with triangulations. Furthermore, assuming that redundant points have been dropped from the Helmertized landmark set:

OBSERVATION 5.30 (UNIQUENESS OF AN ICON REPRESENTED BY ITS α-COMPLEX)
An icon represented by its α-complex can be uniquely traced back to its generating landmark set, v.v., an icon landmark set generates a unique α-complex •

Evaluation of the instance α-complex representation

Evaluation of the instance α-complex representation proceeds largely along the lines of the icon α-complex representation:

OBSERVATION 5.31 (UNIQUENESS OF AN INSTANCE α-COMPLEX)
Instantiated primitives represented by an α-complexes generated by an icon and belonging to the icon variety can be traced back uniquely to this icon. The icon variety of an icon can uniquely be determined •

Completeness inflicts no heavy implications on the mapping, only on the representation:

OBSERVATION 5.32 (COMPLETENESS OF THE INSTANCE α-COMPLEX REPRESENTATION)
Completeness of the α-complex representation can be compared with that of cellular decompositions •

Domain and validity are the same as that of the icon.

It is also interesting to look at the domain of the model space M. The class of physical objects that can be represented in relation to the class of valid representations that the scheme can produce and mappings between them must be compatible. The α-complex representations of all instantiated icons must be embeddable in model space. But generally, model space will be able to accommodate more α-complexes than the suite of icons can generate. This generally holds for primitive instancing schemes. It makes the mapping between icon domain and domain an injection at best. More on this later. The greatest concern in this regard is the variational geometry and the topological variety it can generate. More formally, the instantiated primitives must belong to the icon variety, thereby excluding topological variety. In other words, as long as instances remain within the icon variety, they remain topologically equivalent with the icon. As stated, a framework of predicates must assure this

As long as the reduced mapping chain is used and landmarks are not Helmertized:

OBSERVATION 5.33 (UNIQUENESS OF AN α-COMPLEX)
α-Complexes can generally not uniquely be traced back to a landmark set •

It is mostly the weight set, possibly causing points to become redundant that ruins the uniqueness. In the process of shape analysis and deriving the icon, these points are carefully removed. Doing so in the reduced scheme is sufficient to re-establish the one-to-one relation between α-complex and landmark set and 0-skeleton of the complex and the landmark set. Further, recall that the representation of physical objects by sample points is generally not unique.

Variations in the α-value, even though constrained, may instantiate a finite family of object models (e.g., figure 1–5). Formally due to their different topologies, this family of models α-complexes cannot be thought of as an equivalent class, comparable with some icon variety. The mapping of the icon on to such an α-complex would not be simplicial in that case. In practice, some limited range of α-variations may be appealing to further match details not shared by the icon with observed data. This would extend model and inversion possibilities. Lean-to-fat variation may be made adaptable after instantiation, so as to honour additional constraining data.

Unevaluated α-complex representation

It has been noticed already that α-complexes are back-traceable uniquely to a Helmertized data point sets and they can be uniquely reproduced from them. This makes an *unevaluated* representation feasible, which reduces storage requirements considerably.

OBSERVATION 5.34 (UNEVALUATED REPRESENTATION)
Alpha complexes can be stored and uniquely reproduced using unevaluated representation by their Helmertized landmark set •

In practice, however, there are two complication. The first complication occurs when equal-length edges occur that may be flipped in the process of triangulation (chapter 2). If the arbitrary choice among equal edges is not preserved (only landmarks are preserved) but reproduced, then the next time (evaluating the unevaluated representation) another edge may be chosen in the triangulation and therefore in the complex, changing the topology. More specifically, two triangulations belong to an equivalence class:

DEFINITION 5.8 (EQUIVALENT TRIANGULATIONS)
Two triangulations are said to be equivalent if they can be made equivalent by topological flips of equal length edges, i.e., if an orthogonal α-ball exists for four weighted vertices. •

See example 5.2 for a sketch. Also, see chapter 2.

EXAMPLE 5.2 (EQUIVALENT TRIANGULATIONS)
Figure 5–4 shows two topologically different but according to the regularity and orthogonality criterion equivalent triangulations. Flipping any of the diagonal edges neither changes orthogonality nor the regularity and any of the 2^9 possible triangulations therefore belong to one equivalence class. •

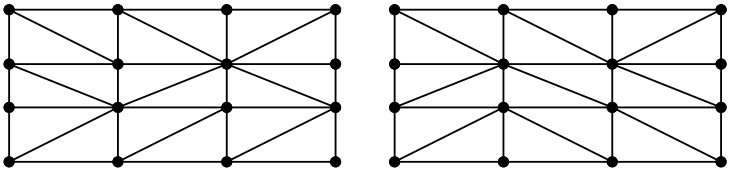

Figure 5–4: *Topologically different triangulations belonging to one equivalence class.*

This problem, which is actually only of theoretical concern, is easily solved. The definitions of equivalent triangulations helps to remedy the problem of different triangulations and the α-complexes they set forth, from the same landmark set of the same icon. By considering the equivalent class rather than the individual triangulation, homeomorphism can be preserved even for unevaluated α-complexes. Like with CSG-representations, this aspect may be exploited in the sense that the representation can be retained in an *unevaluated data structure*:

DEFINITION 5.9 (EVALUATED DATA STRUCTURE)
A data structure is called evaluated if the geometric and topological elements are explicitely stored and immediately available on request, without further operations. •

and evidently, an unevaluated data structure needs processing first. For example, the CSG-tree may need to be evaluated first, before spatial queries on a CSG-representation can be answered.

The second complication is formed by the lack of storage for auxiliary information in the edges, triangles, tetrahedra, etc. In practice, this problem can be solved rather easily ,but part of the storage saving is then undone.

Conversions

A conversion transforms an α-complex representation $\mathcal{C}_\alpha$ of an object model M into another such representation Q (figure 5–1). Its characteristics depend heavily on the target representation of the conversion. If the representation by $\mathcal{C}_\alpha$ and in Q are *homeomorphic*, then a bijective relation can be shown to exist ([Mun84]) and conversion can basically be without loss of information. Topological relations existing in $\mathcal{C}_\alpha$ are then preserved under conversion. This does not necessarily imply a simplicial map.

EXAMPLE 5.3 (CONVERSION)
Consider an α-complex representation $\mathcal{C}_\alpha$ to be converted into a cellular decomposition Q in E^3. Assume α to be high enough to permit the α-complex to contain tetrahedra and assume a hole-free α-complex. The faces in the α-complex are regularised first, thus removing any singular faces. What remains then is a complex of 3-simplices (tetrahedra), themselves composed of k-simplices, $0 \leq k < 3$, all regular or internal (see chapter 2). These regular and internal k-simplices convert one-to-one and back-and-forth continuously onto a tetrahedral cellular decomposition. Once regularised (removing the singular faces) no topological or geometric information is lost in the conversion, i.e., the original α-complex can be readily regained from the cell decomposition after conversion.

On the other hand, assume enough regularity on the simplicial complex to be converted into a hexahedral cellular decomposition. For example, $\mathbb{S}$ is located on some grid. Five or six tetrahedra map onto one hexahedral 3-cell. It is then generally impossible to reproduce the same simplicial complex again, after conversion. Topological information and values have been lost •

OBSERVATION 5.35 (UNIQUENESS OF A CONVERSION)
Generally, multiple conversions exist for a single α-complex and, depending on the type of the conversion, generally, multiple α-complexes lead to the same conversion •

Conversion mappings are all too often not homeomorphic. In particular holes and singular faces that may be present, are often to be skipped from the converted object. This aspect will be discussed somewhat further down. Furthermore, there is not so much more that can be said in general about the conversion representation.

Evaluation of the mappings

Now that the icon and instance representation, plus the landmark representation has been evaluated, it is time to look at the mappings *between* representations. A mapping maps one representation onto another one. A mapping may be examined and evaluated at three levels, as figure 5–5 depicts:

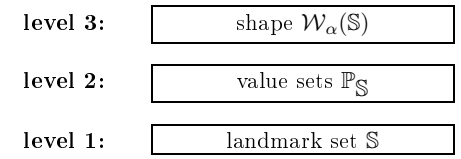

Figure 5–5: *levels of impact of a mapping. Mapping of value sets depends heavily on the value sets themselves. Of interest are primarily level 1 and 3.*

level 1 and level 3, landmarks and shape (fig. 5–5), are of most interest.

The full "chain" of mappings underpinning the hyper-spatial modelling approach is depicted in figure 5–1. The mapping to account for discretisation with finite precision computer internal number representations, like in [Wor92], is not explicitly showed but is assumed to be included in the data sampling step. To structure further discussion, we subdivide the chain into the following maps (refer to figure 3–1 and figure 5–1):

From Map	Aspect	To		Description
$\mathcal{T}_L: \mathbb{E}^d \mapsto S$ physical points	landmarks	R	anatomical landmarks S	observed physical points R are mapped onto sets of anatomical landmarks S
	shape	physical continuum $\mathcal{W}$	raw shape of points $\mathcal{W}(S)$	continuum is represented by point set shape
$\mathcal{T}_h: S \mapsto P$ anatomical landmarks	landmarks	S	Helmertized landmarks $S_\hbar$ of the icon	Helmertized landmarks of family icon are stored, along with α and other parameters
	shape	formalised shape family $\mathcal{W}$	icon shape $\mathcal{W}(S_\hbar)$	shape of landmark sets $S_\hbar$ represents shape family
$\mathcal{T}_P: P \mapsto M$ icon landmarks	landmarks	$S_\hbar$	landmark instance S using linear or other transformation	realisation of family member from icon,
icon shape	shape	$\mathcal{W}(S_\hbar)$	member realisation shape $\mathcal{W}(S)$	shape icon realizes family member
$\mathcal{T}_Q: M \mapsto Q$ instantiated landmarks	landmarks	vertices S	transcribed Q along with	transcription of landmarks realisation shape, k-faces and their topology
	shape	realisation shape family member $\mathcal{W}(S)$	transcribed geometry/topology Q	instantiated shape transcribed in equivalent

Table 5.1: The hyper-spatial transformation mappings taken

- **Landmarking** $\mathsf{T}_L : E^d \mapsto S$

  This is the landmarking mapping of some physical object onto its representing sampling data point set. Data may be added subset by subset, e.g., contours. Multiple such point sets $\mathbb{S}_j$ may exist for a given object. A subset $\mathbb{S}_T$ of point set $\mathbb{S}$ may be set apart as a learning data set, or training data set. The "promotion" of data point sets to training data is in itself a pure subset operation and not a mapping. Data points in $\mathbb{S}$ and $\mathbb{S}_T$ have the same representation and it can be shown that $\mathsf{T}(\mathbb{S}_T \subseteq \mathbb{S})$ has the same characteristics as $\mathsf{T}(\mathbb{S})$.

- **Icon derivation** $\mathsf{T}_\hbar : S \mapsto P$

  In so doing, populating the earth catalogue of abstract primitives $P = \{\wp\}$. This mapping maps sampling data points, the anatomic landmarks $\mathbb{S}$, onto the Helmertized landmark set of the icon in primitive space P. The elements in $\{\wp\}$ are said to form an *alphabet* $\mathcal{A}_\wp$ (definition follows), making up the contents of the earth catalogue. The derivation can, but not necessarily shall be, derived from training data set $\mathbb{S}_T$. Depending on the *orthogonality* (to be discussed, shortly) of the alphabet, zero, one or more data point sets $\mathbb{S}_i$ may map on to the same primitive and zero, one, or more primitives may map back onto a particular data set $\mathbb{S}_i$. At the shape level, the raw shape is mapped onto the icon shape.

- **Primitive instantiation mapping** $\mathsf{T}_\mathcal{I} : P \mapsto M$

  Mapping primitives in icon shape space P onto primitive instances in model space M. The shapes in M will generally form an alphabet $\mathsf{T}_\mathcal{I}(\mathcal{A}_\wp)$ too, with M the set of syntactically correct symbol structures over $\mathsf{T}_\mathcal{I}(\mathcal{A}_\wp)$, that is, the whole of the valid icon varieties. Variational geometry, i.e., variations in geometric parameters that describe how family members relate to the icon, though constrained, may instantiate an infinite cardinality equivalence class of primitive instances of the same icon. As an inadvertent by-product, however, variational geometry may also introduce topological changes, that if occurring, causes them to diverge from the icon. It is assumed here, however, that parameter constraint and internal rules prevent this. This aspect will be further discussed in the next section. Also, see figure 5–6. Scaling, rotation and translation may be applied to send the Helmertized icon landmarks $\mathbb{S}_\hbar$ on to the instantiated shape landmarks $\mathbb{S}$. Meanwhile, at the shape level, the icon shape $\mathcal{W}(S_\hbar)$ is transformed into the instance shape $\mathcal{W}(S)$. The earth catalogue is assumed to form an orthogonal alphabet (see next section). When the icon collection is orthogonal, primitive instances can be traced back uniquely to icons, after instantiation.

- **Conversion mapping** $\mathsf{T}_Q : M \mapsto Q$

  Mapping (a collection of) primitive instances (a model) in M on to some other representation in Q. The mapping and its characteristics largely depends on the target representation of the conversion. If the representation in M and in Q are homeomorphic, then a bijective relations exists and conversion mapping is basically without loss of information and topological relations existing in M are preserved under conversion. An example of a homeomorphic conversion is the simplicial one-to-one map of tetrahedra of the geometric model to the numeric FEM model. An example of a non-homeomorphic representation is a projection from E^d onto E^{d-1}. Multiple conversions in Q may exist for a single model in M and, depending on the type of the conversion, generally, multiple models in M may lead to the same conversion in Q .

Table 5–3 summarises the results. The overall findings on the evaluation of representations plus mappings in the hyper-spatial mapping chain and its reduced form are shown in table 5–4. Table 5–5 compares the α-complex representation with the faceted BRep, CSG and cellular decomposition representations.

What sets out α-complex modelling from BRep and CSG is the capability of handling a large number of cells, singular faces and disjunct parts. For example, inserting massive amounts of cells in a CSG-model is not very convenient. Unless regularised, singular k-faces will cause a CSG-representation to fail on an arbitrary α-complex. For example, when determining the union of a cellular volume with a singular point. An α-complex is not necessarily convex. As a result, boundary representations fail to describe the d-volume of an arbitrary α-complex. The representation that comes closest to what is needed to accurately and unambiguously describe α-complexes would be a part-whole description, built up using instantiated simplices. An α-complex establishes a unique relation between the data point set $\mathbb{S}$, the α-complex $\mathcal{C}_\alpha$ and its underlying space $|\mathcal{C}_\alpha|$.

5.4 Primitive instancing and variational geometry

To formalise the discussion on primitive instancing and the effect that variational geometry has on it, the first thing needed is a definition of a primitive in the context of representations ([Req80, Kal89]):

DEFINITION 5.10 (SYMBOLIC REPRESENTATION A PRIMITIVE)
A primitive (icon) is a symbolic structure composed of landmarks, domain variables, quantifiers, predicates and internal constraints •

A symbolic construct represents objects, environments and processes (forces) that shape them ([Req80, Kal89]).

DEFINITION 5.11 (PREDICATE)
A predicate is an (in)equality bounding (a) variable(s) •

An alphabet can be defined as follows:

DEFINITION 5.12 (ALPHABET)
A (first-order language) alphabet $\mathcal{A}$ *is defined as a composition of finite sets of tokens, i.e., simple variables, domain variables, relational constants and symbols, function constants and symbols, predicates, connectives, quantifiers and punctuation symbols* •

Definition 5.12 can be further sharpened for this context, to a composition of shapes that can be combined into a model according to inter-object constraints Θ bound to some scenario. An alphabet is called orthogonal if:

DEFINITION 5.13 (ORTHOGONAL ALPHABET)
An alphabet is said to be orthogonal if each token generates an expression (or: sentence) that cannot be generated by any other (combination of) token(s), vice versa, each expression can be decomposed uniquely in another ordered sequence of tokens •

PHYSICAL OBJECT	T_L	LANDMARKS S	T_h	ICON α-COMPLEX	T_I	INSTANCE α-COMPLEX
DOMAIN						
physical object c.f. Obs. 5.19	sampling landmarks, non-homogeneous values on landmarks	landmarks, sampling map	Helmertizing landmarks, sampling map c.f. def. 5.4	Helmertized landmarks, variety α-complex	primitive variety, (def. 5.15)	α-complex
UNIQUENESS						
yes	no	no (Obs. 5.29)	if Helmertized (Obs. 5.29)	if orthogonal (Obs. 5.30)	if orthogonal (Obs. 5.31)	yes
UNIQUENESS REDUCED						
yes	no	no (Obs. 5.29)			if redundant points removed (Obs. 5.33, def. 5.8)	yes

Table 5.1: *Evaluation results of the α-complex as a hyper-spatial mapping*

	BREP	FACETED	CSG	CELL DECOMPOSITION	α-COMPLEX
rigid	homogeneous	rigid	homogeneous		
(non-)manifold	manifold	manifold	non-manifold		
lead description, reproducible from CSG-tree			massive description, reproducible from		S
VALIDITY	regularized, set-theoretic				(Obs. 5.25, 5.26)
HOMOGENEITY	homogeneous properties		homogeneous properties		
UNIQUENESS		no			(Obs. 5.27, 5.32)
yes					

tation *compatible* *BREP* *CSG* *cell decomposition* *presen* *tations.*

In this thesis, orthogonality of the alphabet means that models M can uniquely be decomposed into instantiated icons from the alphabet $\mathcal{A}_\wp \cong \{\wp\}$. Finally, for the instantiation mapping $\mathsf{T}_\mathcal{I}$:

DEFINITION 5.14 (INSTANTIATION MAPPING)
The instantiation mapping $\mathsf{T}_\mathcal{I}$ is an operation in which symbolic variables are valuated (given a value), obeying internal and external constraints (syntax Θ) over the generating alphabet •

A model in this sense, is an ordered sequence of shapes, generated from some alphabet of icons (earth catalogue) of which the syntax Θ is given by the inter-object rules in the scenarios of the earth architecture (see chapter 1 and 3). The mapping of hyper-spatial primitives, or icons, into model space (figure 5–1) can be considered as a variant of parametric modelling, using the technique of primitive instancing. See for instance, Requicha in [Req80, Kal89, Zei91, DL91, RNS93, Ram93, SM94, RG96].

DEFINITION 5.15 (VARIATIONAL GEOMETRY)
Variational geometry is a geometric modelling concept by which geometry is manipulated indirectly by the variations of a finite set of geometric parameters •

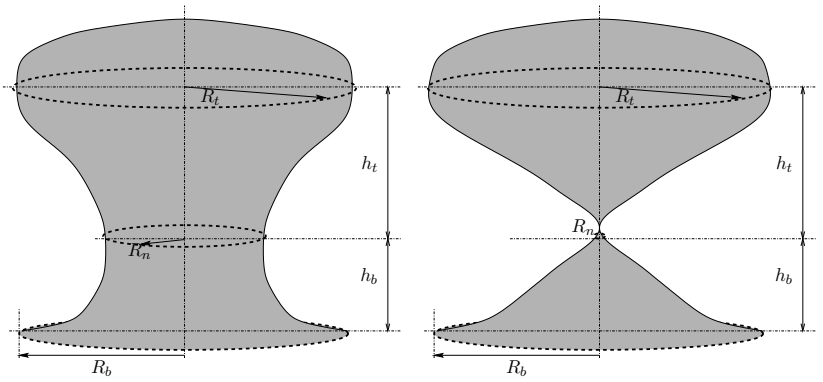

Figure 5–6: *changing topology as a result of geometric variation. Given an abstract primitive salt_dome $\wp_1 = (R_b, R_n, R_t, h_b, h_t)$. If we vary the geometry by decreasing R_n from a given positive value down to 0, the salt dome grows from a manifold object (left) into a non-manifold object (right). What if we have that: $R_b \gg R_n \gg R_t$? Then the shape is more that of a pillow. Variational geometry then leads to variational topology as a by-product. A predicate of the form: $R_n > 0$ may prevent this. A more realistic predicate takes the form: $c_1 \leq \frac{R_n}{R_t} \leq c_2 \ \wedge \ c_3 \leq \frac{R_n}{R_b} \leq c_4$. For the height, something similar can be formulated.*

EXAMPLE 5.4 (VARIATIONAL TOPOLOGY AND ORTHOGONALITY)
The undesirable effect of variational topology that may come inadvertently with variational geometry is shown by figure 5–6. Given an earth catalogue $\mathbb{P} = \{\wp_1 = salt\_dome, \wp_2 = salt\_diapir\}$. These two icons templatize only a minority of the possible salt shapes. [Hal67], for example, described an extensive variety of shapes in the Gulf-South Louisiana Coastal Basin: not only salt domes, but also diapirs, pillows, mono-clines, anti-clines, ridges and massifs •

When the icon collection is orthogonal, primitive instances can be traced back uniquely to icons, after instantiation. But in practice, due to object evolution (deformations and other

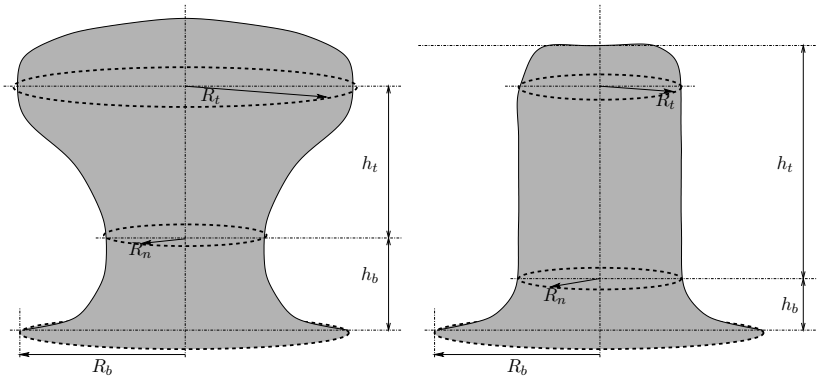

Figure 5–7: *salt dome-salt diapir representation ambiguity due to non-orthogonality; assume two primitives: saltdome* $\wp_1 = (R_b, R_n, R_t, h_b, h_t)$ *and saltdiapir* $\wp_2 = (R_b, R_t, h_b, h_t)$*. The object displayed in the left picture can only be an instance of primitive saltdome* $\wp_1$*. It is only in the iconvariety of the saltdome only. But the object in the right picture, in which* $R_t = R_n$*, cannot be uniquely be traced back to salt_dome* $\wp_1$ *or salt_diapir* $\wp_2$*. It can be an instance of both. A representation scheme that allows for such ambiguity is called an ambiguous representation.*

transforming processes), this may cease to be true for evolutionary maps after some period of evolution. Erosion may vanish an object completely.

If constraining is also to be applied overtime, then two solutions exist, that may be combined:

- **Use spatio-temporal landmarks**

  Spatio-temporal landmarks define landmarks sets that change overtime and in so doing, allow the α-complex they generate to become dynamic.

- **Keep evolutionary maps simplicial**

  This can be done by the use of -1-faces, which allows eroded faces to become empty sets.

Observation 5.36 (spatio-temporal versus spatial constraints)
Evolutionary maps, such as erosion and dilation, may cause shapes to alienate from their instantiating icon. If shapes need to be constrained over time as well, then they need to be instantiated from a spatio-temporal icon rather than from a spatial icon or use nil-simplices to keep maps simplicial •

5.5 A formal description of holes

In this section, two aspects of holes will be discussed in greater detail. Firstly, the description of void space and secondly the topological relations among holes and between holes and shapes. In the former, the exact geometry does matter, in the latter, distances, orientations and locations are irrelevant.

5.5.1 The hierarchy of holes

When an object contains one or more voids, m say, there will be m additional (bounded) exteriors, completely surrounded by the interior. Notice that disjoint exteriors imply multiply connected interiors, vice versa. With a changing α, holes may be transformed into other types of holes, following the hierarchy as in figure 5–8. Observe in this figure that during this traversal (for a growing α), the genus (number of handles) eventually drops to zero, after the last handle has vanished. Recall that when approaching $\alpha_{\max}$, the α-complexs turns hole-free. Also, in this traversal of the hierarchy, multiple steps may be traversed at once, for instance, a tunnel may turn into a void, without ever becoming a pocket and cavities may disappear without ever having had a different anatomy.

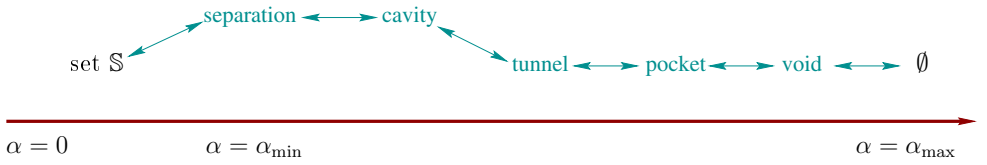

Figure 5–8: *hierarchy of holes, ranked according to the α-value. With increasing α, holes go down the hierarchy from left-to-right. Multiple transitions can take place at a small increment of α.*

The point set $\mathbb{S}$ is one extreme in the α-family, the triangulation is the other extreme. Recall that if these two extrema are neglected, the remaining interval of α is $\alpha \in [\alpha_{\min}, \alpha_{\max})$, the α-interval of figure 4–1. Within this interval, singular k-faces may exist, multiple exteriors may exist and/or multiple interiors. Recall from observation 2.22 that interior $\operatorname{Int} \mathcal{C}_\alpha$ may be a separation, while closure $\operatorname{Cl} \mathcal{C}_\alpha$ is not. Zeid, in [Zei91], distinguishes four classes of polyhedral objects (see table 5–6). Polyhedral objects are planar-faceted objects, with non-curved planar polygonal k-faces. Zeids classification has been expanded by one more class, to support separation (see figure 5–8).

Class	Holes	Genus	Separation	Description
1	no	0	no	simple polyhedra (1 loop, 1 shell, simple k-shell)
2	no	0	no	same, but with inner loops, non-conforming 2-faces
3	yes	0	no	same, with cavities, pockets and voids
4	yes	> 0	no	same, with handles (genus-m polyhedra)
5	yes	> 0	yes	same, separated interior, composite regions [CDFvO93]

Table 5–6: *topological classification of polyhedral objects. For example, a triangulation classifies as a class 1 polyhedral object, an α-complex classifies as a class 5 object. Modified, after Zeid ([Zei91]), class 5 has been added, for separations and composite regions.*

Triangulations, triangulated objects and holes

It can be shown (e.g., [Mun84]) that a every convex polytope can be triangulated. This also holds if the polytope contains holes. At this point, great care is however needed, because there are multiple forms (classes) of triangulations, not all compatible with the triangulation as defined in the context of chapter 2.

FORMULATION 5.2 (TRIANGULATION PROBLEM FORMULATIONS)
Consider two different forms of triangulation problem formulations:

TYPE	TRIANGULATION PROBLEM FORMULATION
Type I	*triangulation* $\mathcal{T}_I(\mathbb{S})$ *of the interior of an object with a given closed boundary triangulation* $\mathcal{T}(\partial\mathbb{S})$. $\partial\mathbb{S}$ *may also define internal boundaries, bounding holes inside the object. Points* $\mathbb{S} \notin \partial\mathbb{S}$ *may or may not become vertices in* $\mathcal{T}_I(\mathbb{S})$
Type II	*triangulation* $\mathcal{T}_{II}(\mathbb{S})$ *of the hole-free interior* $\mathrm{Int}\,\mathcal{H}(\mathbb{S})$ *of the convex hull* $\mathcal{H}(\mathbb{S})$ *of point set* $\mathbb{S}$, *thereby taking each point in* $\mathbb{S}$ *as a vertex in* $\mathcal{T}_{II}(\mathbb{S})$ •

Type I triangulations are often used for FEM mesh generator, for instance. Type I triangulations will not be considered here. A triangulation in this thesis, in accordance with its definition in chapter 2 is always a type II triangulation, bounded by the convex hull.

The underlying space of holes

In the discussion of holes, it is often more convenient to consider α-shapes rather than α-complexes. Recall that their underlying space is identical (chapter 2) and consequently the underlying space of a convex hull and the triangulation thereof is equal too. An α-shape $\mathcal{W}_\alpha$ differs from the convex hull $\mathcal{H}$, the underlying space of the triangulation, by the total amount of space occupied by the various holes. This space is commonly denoted by the term void space[1]:

DEFINITION 5.16 (VOID SPACE)
The void space is the total amount of space, occupied by the union of all holes in an α*-shape* •

If $\alpha \geq \alpha_{\max}$ then the underlying space of the holes is a null-space, as indicated by the empty set in figure 5–8.

The underlying space (or: spatial occupancy) difference between a convex hull and an α-shape is easily established. See also section 2.7 in chapter 2. Let convex hull $\mathcal{H}(\mathbb{S})$ be the convex hull of $\mathbb{S}$ and let $\alpha_{\min} \leq \alpha < \alpha_{\max}$. Furthermore, let $|V_\emptyset|$ denote the underlying space of a hole, no two holes intersect. Holes in E^d are homeomorphic with an open d-ball, so a hole is an open set in this work. For the underlying space the following expression is then obtained:

[1] although the term may be somewhat confusing with the term voids, its use is so common that it will be used here as well

$$|\mathcal{H}| = |\mathcal{W}_\alpha| \bigcup \left| \left(\bigcup_{i=1}^{m} V_{\emptyset_i} \right) \right| = |\mathcal{W}_\alpha| \bigcup \left(\bigcup_{i=1}^{m} |V_{\emptyset_i}| \right) \tag{5–1}$$

Notice that equation (5–1) uses the fact that holes do not overlapand that equation (5–1) can also be written as a function in α. Only for $\alpha \geq \alpha_{max}$ and hence $|\mathcal{W}_{\alpha=\alpha_{max}}| = |\mathcal{T}| = |\mathcal{H}|$, we are guaranteed to have:

$$|\mathcal{H}| = |\mathcal{W}_\alpha| \bigcup (|\ \emptyset\ |) = |\mathcal{W}_\alpha| \tag{5–2}$$

EXPERIMENT 5.1 (UNDERLYING SPACE)
The chalice in figure 5–9 is object of which half the boundary of a 2D-cross section has been sampled (figure 5–9, left picture). Notice thatall sample points are located in the boundary. The boundary was defined from this half outer contour by a rotational sweep over 2π radians. At discretesteps, landmarks were "dropped". The chalice was then modelled by defining its interior as one big pocket, induced by the almost closed boundary. The α-shape is the almost closed boundary in 3D, while α-shape plus pocket plus cavities "surrounding" the chalice fill the convex hull. Remark that instead of a pocket, the interior might also have been defined as a genuine void, using a closed boundary •

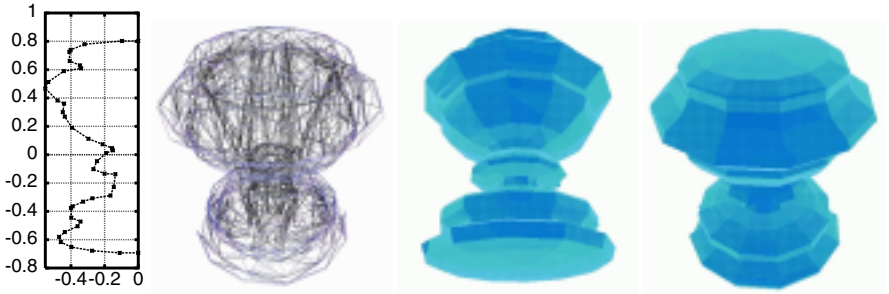

Figure 5–9: *chalice obtained by modelling its interior as a pocket. Left: half a cross-section: all sample points are located in the boundary. Second left: wire-frame representation, showing the "empty" interior. Right: resulting complementary pocket.*

This geometric duality feature is extremely important for the modelling of geometricly coupled shapes, such as immiscible multi-phase rock-fluid systems. Let $\bigcup_{i=1}^{m} |V_{\emptyset_i}| = |\neg\mathcal{W}_\alpha|$ denote the total void space, so that according to equation (5–1), $|\mathcal{W}_\alpha| + |\neg\mathcal{W}_\alpha| = |\mathcal{H}|$. In this formulation, the unary operator $\neg$ denotes the complement of the underlying space of the shape against the convex hull. The total void space $|\neg\mathcal{W}_\alpha|$ can itself be regarded as an α-shape: the dual shape $|\overline{\mathcal{W}_\alpha}|$:

OBSERVATION 5.37 (GEOMETRICLY COUPLED SHAPES AND VOID SPACE)
For a geometricly coupled shape, the total void space $|\neg\mathcal{W}_\alpha|$ of the primal shape $|\mathcal{W}_\alpha|$ defines the coupled dual shape $|\overline{\mathcal{W}_\alpha}|$, v.v. •

$$\begin{array}{lccc} \text{primal shape} & |\mathcal{W}_\alpha| + |\overline{\mathcal{W}_\alpha}| & = & |\mathcal{H}| \\ & + \quad + & & \\ \text{dual shape} & |\overline{\mathcal{W}_\alpha}| + |\mathcal{W}_\alpha| & = & |\mathcal{H}| \\ & || \quad || & & \\ & |\mathcal{H}| \quad |\mathcal{H}| & & \end{array}$$

Primal and dual shapes can be swapped, such that the boundary now belongs to the geometricly coupled dual shape, if also the complement of landmark set $\mathbb{S} \otimes \mathbb{W}$ is taken. For example, with regularly spaced landmarks, by reflecting the weight set in the origin. Furthermore:

OBSERVATION 5.38 (GEOMETRICLY COUPLED SHAPES AND SIMPLICIAL MAPS)
The geometry duality of geometricly coupled objects is preserved under simplicial representation maps $\mathsf{T}_\hbar : S \mapsto P$ *and* $\mathsf{T}_\mathcal{I} : P \mapsto M$ •

In many situations, it is convenient to consider the *void ratio*:

DEFINITION 5.17
The void ratio, denoted by η*, is the ratio between the void space and the underlying space of the* α*-shape* •

in mathematical terms:

$$\eta = \frac{|\neg\mathcal{W}_\alpha(\mathbb{S})|}{|\mathcal{W}_\alpha(\mathbb{S})|} = \frac{|\overline{\mathcal{W}_\alpha(\mathbb{S})}|}{|\mathcal{W}_\alpha(\mathbb{S})|} \tag{5–3}$$

Notice that void space and void ratio are both functions in α and expression (5–3) can also be written as a function in α.

EXAMPLE 5.5 (IMMISCIBLE MULTI-PHASE ROCK-FLUID SYSTEM)
The void space of the rock phase in an immiscible multi-phase rock-fluid system has a dual in the form of the saturated fluid in the rock pores, vice versa, the void space of the fluid geometry is filled with rock. With a set $\mathbb{S}$ *sampling the rock, let* $|\mathcal{W}_\alpha(S)|$ *be the space occupied by the rock and consequently* $|\overline{\mathcal{W}_\alpha(\mathbb{S})}| = |\neg\mathcal{W}_\alpha(S)|$ *denote the void space* $|\bigcup V_\emptyset|$*, in this case the total porespace. The total porespace is also given by* $\phi|\mathcal{H}|$*, where* ϕ *is the porosity. The void ratio* η *is then* $\frac{|\neg\mathcal{W}_\alpha(S)|}{|\mathcal{W}_\alpha(S)|} = \frac{|\neg\mathcal{W}_\alpha(S)|}{|\mathcal{H}(S)|-|\neg\mathcal{W}_\alpha(S)|} = \frac{\phi}{1-\phi}$*. Assume that the saturation is by two immiscible fluid phases, one of which occupies* 70% *of the porespace. Then the fluid content of this fluid amounts to* $0.7|\neg\mathcal{W}_\alpha(S)| = 0.7\phi|\mathcal{H}|$*. The volume of the second fluid is equal to* $0.3\phi|\mathcal{H}|$*. When the porepressure increases,and assuming a fixed outer boundary of the rock for simplicity, the porevolume may increase for example by* 2% *and consequently, the rock volume must change by a growth-factor* $\lambda < 1$*, such that again* $\lambda|\mathcal{W}_\alpha(S)| + 1.02|\neg\mathcal{W}_\alpha(S)| = |\mathcal{H}|$*. The void ratio* η *then changes by a factor* $1.02(1-\lambda)^{-1}$ *. Void ratio* η *is preserved under a linear simplicial mapping* •

5.5.2 Topological relations with holes

For the description of topological relations of objects with their holes, an approach based on the description of topological relations among sets will be used. Refer to Egenhofer et al. (1994) for

a background on the fundamentals of this approach and to Clementini et al. (1995) for a further extension for composite regions. A relation is called symmetric if we have that:

Definition 5.18 (symmetric relation)
A relation is called symmetric if: $\mathbb{X} \Longrightarrow \mathbb{Y}$ *implies* $\mathbb{Y} \Longrightarrow \mathbb{X}$ •

where $\Longrightarrow$ denotes a relation. The following topological relations are defined:

Definition 5.19 (set topological relations)
Two sets $\mathbb{S}_1$ *and* $\mathbb{S}_2$ *have exactly one of the following topological relations:*

- **Set** $\mathbb{S}_1$ **disjoint** $\mathbb{S}_2$

  Sets $\mathbb{S}_1$ *and* $\mathbb{S}_2$ *have no points in common. This relation is symmetric:* $\mathbb{S}_1$ *disjoint* $\mathbb{S}_2$ *implies* $\mathbb{S}_2$ *disjoint* $\mathbb{S}_1$.

- **Set** $\mathbb{S}_1$ **meets** $\mathbb{S}_2$

  The boundary $\partial\mathbb{S}_1$ *and* $\partial\mathbb{S}_2$ *touch (have points in common), but the intersection of the interiors* $\mathrm{Int}\,\mathbb{S}_1$ *and* $\mathrm{Int}\,\mathbb{S}_2$ *is empty. This relation is symmetric.*

- **Set** $\mathbb{S}_1$ **contains** $\mathbb{S}_2$

  Set $\mathbb{S}_2$ *is completely contained in the interior of* $\mathbb{S}_1$*. The boundary of* $\mathbb{S}_2$ *is also lying in the interior of* $\mathbb{S}_1$*. Not symmetric.*

- **Set** $\mathbb{S}_1$ **covers** $\mathbb{S}_2$

  The boundary of $\mathbb{S}_2$ *is partly lying in the interior of* $\mathbb{S}_1$*, partly in the boundary of* $\mathbb{S}_1$*. Not symmetric.*

- **Set** $\mathbb{S}_1$ **equals** $\mathbb{S}_2$

  Interiors $\mathrm{Int}\,\mathbb{S}_1$ *and* $\mathrm{Int}\,\mathbb{S}_2$ *are equal as well as the two boundaries. Symmetric.*

- **Set** $\mathbb{S}_1$ **overlaps** $\mathbb{S}_2$

  Set $\mathbb{S}_1$ *is partly contained in the interior of* $\mathbb{S}_2$*, partly in the exterior of* $\mathbb{S}_2$*. Symmetric.*

- $\mathbb{S}_1$ **inside** $\mathbb{S}_2$

  Set $\mathbb{S}_1$ *is completely contained in the interior of* $\mathbb{S}_2$*. Not symmetric.*

- **Set** $\mathbb{S}_1$ **coveredBy** $\mathbb{S}_2$

  The boundary of $\mathbb{S}_1$ *is partly lying in the interior of* $\mathbb{S}_2$*, partly in the boundary of* $\mathbb{S}_2$*. Not symmetric* •

The possible outcome of these binary topological relations is in $\{\emptyset, \neg\emptyset\}$.

α-shape $\Longrightarrow$ convex hull

First, the relations of an α-shape to the convex hull will be examined. With an α-complex being a sub-complex of the triangulated convex hull, five relations can immediately be dropped:

OBSERVATION 5.39 (IMPOSSIBLE RELATIONS α-SHAPE $\Longrightarrow$ CONVEX HULL)

$$\begin{array}{llll} \mathcal{W}_\alpha & \textit{disjoint} & \mathcal{H} & \Rightarrow \quad \textit{impossible} \\ \mathcal{W}_\alpha & \textit{meet} & \mathcal{H} & \Rightarrow \quad \textit{impossible} \\ \mathcal{W}_\alpha & \textit{contains} & \mathcal{H} & \Rightarrow \quad \textit{impossible} \\ \mathcal{W}_\alpha & \textit{covers} & \mathcal{H} & \Rightarrow \quad \textit{impossible} \\ \mathcal{W}_\alpha & \textit{overlaps} & \mathcal{H} & \Rightarrow \quad \textit{impossible} \end{array}$$

•

leaving only three possible relations. Egenhofer et al. compile a so called *4-intersection matrix* per relation. A 4-intersection matrix is a matrix:

$$\begin{pmatrix} \partial S_1 \bigcap \partial S_2 & \partial S_1 \bigcap \overset{\circ}{S}_2 \\ \\ \overset{\circ}{S}_1 \bigcap \partial S_2 & \overset{\circ}{S}_1 \bigcap \overset{\circ}{S}_2 \end{pmatrix} \tag{5–4}$$

The outcome of these intersections determine the type of relation. Each relation thus has its characteristic matrix, vice versa. Consider the topological set relations $\mathcal{W}_\alpha \Longrightarrow \mathcal{H}$. The 4-intersections are given by table 5–7.

equal	$\partial\mathcal{H}$	$\overset{\circ}{\mathcal{H}}$
$\partial\mathcal{W}_\alpha$	$\neg\emptyset$	$\emptyset$
$\overset{\circ}{\mathcal{W}}_\alpha$	$\emptyset$	$\neg\emptyset$

inside	$\partial\mathcal{H}$	$\overset{\circ}{\mathcal{H}}$
$\partial\mathcal{W}_\alpha$	$\emptyset$	$\neg\emptyset$
$\overset{\circ}{\mathcal{W}}_\alpha$	$\emptyset$	$\neg\emptyset$

coveredBy	$\partial\mathcal{H}$	$\overset{\circ}{\mathcal{H}}$
$\partial\mathcal{W}_\alpha$	$\neg\emptyset$	$\neg\emptyset$
$\overset{\circ}{\mathcal{W}}_\alpha$	$\emptyset$	$\neg\emptyset$

TABLE 5–7: *4-intersections for* $\mathcal{W}_\alpha \Longrightarrow \mathcal{H}$. *Left-to-right:* $\mathcal{W}_\alpha$ *equal* $\mathcal{H}$, $\mathcal{W}_\alpha$ *inside* $\mathcal{H}$ *and* $\mathcal{W}_\alpha$ *coveredBy* $\mathcal{H}$.

Geometricly coupled shape $\overline{\mathcal{W}_\alpha} \Longrightarrow \mathcal{W}_\alpha$

In a dual geometry of geometricly coupled shapes, primal shape $\mathcal{W}_\alpha$ is represented by a union of closed sets (closed bounded interiors), and dual shape $\overline{\mathcal{W}_\alpha} = \neg\mathcal{W}_\alpha$ by a union of open sets, representing the holes (open bounded exteriors). Interiors here are the interior parts of the primal shape. Multiple interiors means that the primal shape may consist of multiple parts. It is illustrative to look into the dual geometry of a geometricly coupled shape, denoted by the relation $\overline{\mathcal{W}_\alpha} \Longrightarrow \mathcal{W}_\alpha$.

FORMULATION 5.3 (TOPOLOGICAL RELATION DUAL GEOMETRY)
The following questions needed to be answered:

1. *Which are the topological relations among the exteriors? In other words, how do the parts of the dual shape relate to each other? How many different relation are possible?*

2. *Which are the topological relations between an arbitrary interior and an arbitrary exterior? In other words, how do parts of the primary shape relate to parts of the dual shape? How many different relation are possible?*

3. *What does the 4-intersection matrix look like for each topological relation combination and what is its dimension?*

The primal shape consists of closed sets. For the dual shape, sets are open and therefore $\overline{\overset{\circ}{\mathcal{W}_\alpha}} = \overline{\mathcal{W}_\alpha}$. Points lying in the boundary belong to the primal shape. In a topological sense, parts of the primal shape may be connected by only a single point, having separated interiors but non-separated closures (Observation 2.22). Primal shapes parts may *meet* in a *singular point* lying in the boundary of both parts. But trivially, for their interiors:

OBSERVATION 5.40 (POSSIBLE TOPOLOGICAL RELATIONS AMONG INTERIORS)
The interiors of the primal shape can impossibly meet, contain, be inside, equal, cover or be cover edby or overlap any other part of the primal shape. The only possible topological relations among interiors is disjoint •

The dual shape consists of open sets. Points lying in the boundary of the closure of the exterior do not belong to the dual shape but to the primal. As a consequence, in contrast to primal shape parts, dual parts cannot meet at all. For the exteriors:

OBSERVATION 5.41 (POSSIBLE TOPOLOGICAL RELATIONS AMONG EXTERIORS)
The exteriors of the dual shape can impossibly meet, contain, be inside, equal, cover or be covered by or overlap any other part of the dual shape. The only possible topological relations among exteriors is disjoint •

more or less trivial and in consistency with the fact that the α-shape is closed and by definition shares no points with its holes:

OBSERVATION 5.42 (TOPOLOGICAL RELATION IN- AND EXTERIORS)
A part of the dual shape (an exterior) an impossibly meet, contain, be inside, equal, cover or be covered by or overlap with any part of the primal shape (an interior), vice versa •

Observation 5.42 implies that the only possible relation $\overline{\mathcal{W}_\alpha} \Longrightarrow \mathcal{W}_\alpha$ is *disploint*, represented by a 4-intersection matrix of only empty set members.

Hole $\Longrightarrow$ convex hull

Attention now turns to individual holes and their relation to the convex hull. This extends the approach in the direction of the approach in [CDFC95]. It is important to understand these relations in conversion mapping and other mappings where holes or the removal of holes plays an important role. A good example is the conversion of the α-complex into a FEM mesh, that generally cannot contain separations, for example. Holes are open sets and their closures may intersect, i.e., they may meet but not overlap:

$$\begin{cases} \operatorname{Bd}\operatorname{Cl}\mathcal{E}_i \bigcap \operatorname{Bd}\operatorname{Cl}\mathcal{E}_j & \neq & \emptyset \\ \mathcal{E}_i \bigcap \mathcal{E}_j & = & \emptyset \end{cases} \tag{5–5}$$

where $i \neq j$, $\mathrm{Bd}\,\mathrm{Cl}\,\mathcal{E} = \partial\bar{\mathcal{E}}$ and the interior of an open set is equal to the open set itself. Holes can be intersected by singular faces. Such singular faces appear as a "spike" intruding the hole. Despite the spike, that is contained in the boundary $\partial\mathcal{W}_\alpha$ of the surrounding α-complex, the hole remains topologically homeomorphic with an open disk. A single hole may also be bisected so that two adjacent holes are formed, the closures of which meet. Figure 5–10 illustrates these cases. Since a hole is covered by an open set, with $i \neq j$, we have that $\mathrm{Int}\,\mathcal{E} \cong \mathcal{E}$, $\mathcal{E}_i \bigcap \mathcal{E}_j = \emptyset$, but $\mathrm{Bd}\,\mathrm{Cl}\,\mathcal{E}_i \bigcap \mathrm{Bd}\,\mathrm{Cl}\,\mathcal{E}_j \neq \emptyset$.

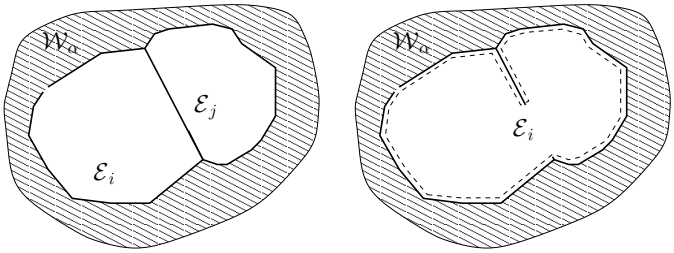

Figure 5–10: *left: the closures of $\mathcal{E}_i$ and $\mathcal{E}_j$ meet. Right: as long as the interiors of $\mathcal{E}_i$ and $\mathcal{E}_j$ are not separated and the bisecting internal boundary separating them is not closed, $\mathcal{E}_i$ and $\mathcal{E}_j$ could be modelled as a single hole. Topologically the open set (dotted line) remains homeomorphic with an open disk, despite the "spike".*

As long as the interiors of $\mathcal{E}_i$ and $\mathcal{E}_j$ are not separated and the bisecting internal boundary separating them is not closed, $\mathcal{E}_i$ and $\mathcal{E}_j$ may be modelled as a single hole. For consistency, however, the hole will be assumed to consist of as many holes as there are d-simplices in the triangulated hole. Doing so greatly facilitates the implementation of simplicial maps. This leads to the following important observation:

OBSERVATION 5.43 (NUMBER OF HOLES IN THE VOID SPACE)
From a topological point of view every d-simplex in the (triangulated) void space is to be considered a separate hole •

Observation 5.43 is immediate if one reconsiders the α-family of a dual geometry. If honoured, a clear split of the set $\mathbb{F}$ of faces of the triangulation $\mathcal{T}(\mathbb{S})$ is obtained:

OBSERVATION 5.44 (α-EXPOSEDNESS AND DUAL GEOMETRY)
Every face that is α-exposed belongs to $\mathcal{W}_\alpha$, as explained in chapter 2, every non-exposed face belongs to $\overline{\mathcal{W}_\alpha}$. For $\alpha < \alpha_{\min}$ the set of faces $\{\sigma^{(k)}_{\mathcal{C}_\alpha}\} = \mathbb{F}$. With α traversing the α-interval $[\alpha_{\min}, \alpha_{\max}]$, a k-face that becomes α-exposed moves from $\{\sigma^{(k)}_{\mathcal{C}_\alpha}\}$ to $\{\sigma^{(k)}_{\mathcal{C}_\alpha}\}$ and as soon as $\alpha \geq \alpha_{\max}$, set $\{\sigma^{(k)}_{\mathcal{C}_\alpha}\} = \emptyset$ and set $\{\sigma^{(k)}_{\mathcal{C}_\alpha}\} = \mathbb{F}$. By definition, faces in $\{\sigma^{(k)}_{\mathcal{C}_\alpha}\}$ are open. When a face becomes α-exposed and traverses from $\{\sigma^{(k)}_{\mathcal{C}_\alpha}\}$ to $\{\sigma^{(k)}_{\mathcal{C}_\alpha}\}$, its subfaces, needed to close the face are already α-exposed (Observation 2.17) and therefore contained in $\{\sigma^{(k)}_{\mathcal{C}_\alpha}\}$ •

5.6 Representing holes

5.6.1 Modelling with *nil*-icons and *nil*-objects

The domain of the α-complex representation scheme is further expanded, if holes can be explicitely represented and treated as part in a bigger assembly. Therefore, a *nil-object* can be used. *Nil*-objects are geometrically and topologically conforming (fitting) to any neighbouring object. As a consequence, *nil*-objects can be inserted in between any two adjacent objects. *Nil*-objects map to background elements ("embedding material") in a conversion mapping onto FEM-models. With this definition of a *nil*-object, consistent spatial occupancy of model space E^d and well-formedness of the modelled object are more easily obtained. Also, homeomorphisms implied by simplicial maps are more easily maintained.

For consistency, abstract primitive space P and its alphabet $\mathcal{A}_\wp$ are therefore augmented with a *nil-icon* $\wp_{nil}$ and a *nil-symbol nil*. The *nil*-icon can also be instantiated $\wp_{nil}$, generating a *nil*-object M_{nil} in model space M. See figure 5–5. A *nil*-icon is generated by an empty landmark set $\emptyset$. A *nil*-icon generates a perfectly "regular" primitive instance, with m dimensions (by the properties of mapping $\mathsf{T}_\mathcal{I}$, but only defines the geometry to be void. When defined as an α-complex, the corresponding simplicial complex $\mathcal{C}_\alpha$ will be the empty set $\emptyset$, the interior $\mathrm{Int}\,\mathcal{C}_\alpha = \emptyset$, the underlying space will be empty, etc. Such an α-complex is obtained by α-filtration from the *nil*-triangulation (definition 5.6). Observe that alphabet, space and syntax remain finite, which is essential.

Advantages and consequences of the introduction of a *nil*-object are:

- **Evolutionary map homeomorphisms**

  Nil-objects may represent void space, occurring for example when objects vanish at the end of their life cycle. This capability is important for the evolution maps to remain simplicial and thereby homeomorphic, e.g., when "iterating back and forth in time" during inversion.

- **Missing tokens in the alphabet**

  During the built-up of the training data set, non-covered real world objects, i.e., object for which there is no icon (yet), can be represented by *nil*-objects, to be refined and redefined later.

- **Alien objects**

  By convention, real world subsurface objects that are not represented by a primitive instance (alien objects) may be represented by a *nil*-object. This way, originating processes and the instantiation of primitives as such can be defined consistently.

- **Consistent spatial occupancy**

  With the definition of a *nil*-object, the spatial occupancy of model space M is easily obtained. *nil*-objects are geometrically and topologically conforming (fitting) to any neighbouring object. By convention, *nil*-objects can be inserted in between any two adjacent objects.

The augmented icon space $\overset{*}{P}$ thus becomes:

$$\overset{*}{P} = P \bigcup \{ \wp_{nil} \} \tag{5–6}$$

The augmented model space $\overset{*}{M}$ becomes:

$$\overset{*}{M} = M \bigcup \{ nil \} \tag{5–7}$$

and also, for the augmented alphabet $\overset{*}{\mathcal{A}}_{\wp}$:

$$\overset{*}{\mathcal{A}}_{\wp} = \mathcal{A}_{\wp} \bigcup \{ nil \} \tag{5–8}$$

and for the augmented syntax $\overset{*}{\Theta}$:

$$\overset{*}{\Theta} = \Theta \bigcup \{ nil \} \tag{5–9}$$

5.6.2 Mapping processes and the *nil*-representation

In chapter 3, the morpho-dynamic processes operating upon instantiated object models have been discussed, mostly in the context of a birth-life-death cycle of dynamic objects in an evolutionary scenario. Here, these processes will be subdivided form a mapping point of view. See table 5–8.

Type of process	Geodynamic process	Morpho-dynamic process	Map
originating	deposition, sedimentation	dilation, closing	$\mathsf{T}_{\mathcal{I}} : nil \mapsto \overset{*}{M}$
transforming	compaction	linear evolutionary map	$\Gamma^n : \overset{*}{M} \mapsto \overset{*}{M}$
terminating	erosion	erosion, opening	$\Gamma^n : \overset{*}{M} \mapsto nil$

Table 5–8: *Originating, transforming and terminating processes that model the birth-life-death life cycle with the use of nil-objects.*

5.7 Set regularisation

Regularisation is a set operation that is used in this work to remove singular parts from objects. Set regularisation is applied to the set covering the underlying space occupied by the object (part). In terms of α-complexes, regularisation can be used to drop singular faces from the complex. The problem of regularisation has considered considerable attention in the realm of CSG implementations.

A *regular open set* and a *regular closed set* are defined as follows:

Definition 5.20 (regular open set)
A regular open set (or: op enr-set) $\mathbb{X}$*, is a set for which* $\mathbb{X} = \operatorname{Int}\operatorname{Cl}\mathbb{X}$ •

and also:

Definition 5.21 (regular closed set)
A regular close dset (or: close dr-set) $\mathbb{X}$*, is a set for which* $\mathbb{X} = \operatorname{Cl}\operatorname{Int}\mathbb{X}$ •

What set regularisation does is shown in figure 5–11.

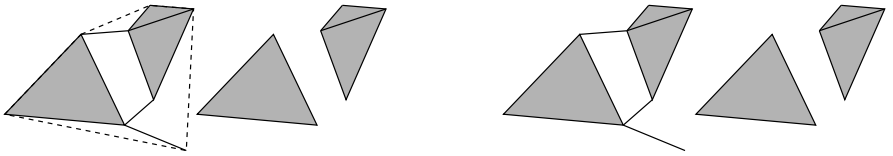

Figure 5–11: *regular open and closed set, obtained by regularisation. Left two pictures: regular open set, right tw o pictures:regular closed set. In this case the regular open and closed sets are equal, although the procedure to obtain them is different.*

Chapter 6

Application cases

6.1 Overview of this chapter

In this chapter, a number of application cases will be presented, by which the α-complex-based modelling approach of the previous chapters will be demonstrated. Cases have been taken from the domain of earth sciences, more in particular subsurface modelling in support of and aiming at the exploration and production of hydrocarbons, ores and minerals and other natural resources. The approach of this thesis is by no means limited to this field of application: see [GVdWV00b] for engineering and design applications and clinical imaging applications. The focal point in the cases is on sedimentary facies (structures) found in fluvial, aeolian and alluvial environments, such as lenses, fans, scroll bars, point bars, channels, river systems, etc. Alpha complex modelling is believed to be best applied there. Section 6.6 therefore also provides some background material on river systems, point bars, etc., as an onset to the cases to follow. Cases in this chapter cover geometric modelling and numerical modelling.

Section 6.2 discusses a first case on the Gulf of Thailand in which the objective is to capture the geometry of subsurface objects embedded in the seismic data. Emphasis in this case will be on landmark set definition and analysis. After the Gulf of Thailand case, the North Sea L8 river system will be discussed in section 6.3. Like in the previous case, seismic goes in and a geometric model comes out. Section 6.4 presents the largest (in terms of data and computing effort) case on the salt pillow or salt dome in the South Marsh Island area, in the Gulf of Mexico. More than anything else, this case uncovers the practical limits of computational efforts with α-complex modelling on todays computer systems.

Having discussed these three seismic-based models, attention is shifted to numerical modelling. Section 6.5 presents a dynamic numerical process model of a barchan dune, evolving over time. The evolutionary map is dictated by erosion, deposition and avalanching processes. This not-too-complicated case paves the way to more complicated models. The geometry is hole free and the only difficulty is formed by the changing topology when avalanching takes place. A more complicated point bar system is discussed in section 6.6. Unlike the former cases, these models are based on stochastic realisations of deterministic models with stochastic input. In fact this case is based on a semi-analytic model, i.e., analytic descriptions, perturbed or augmented by stochastic data. A numerical α-complex-based model of the point bar is presented, that describes coupled single-phase fluid flow with linear stress.

Shape instantiation has been extensively discussed in chapter 3. Section 6.7 presents a case in which the instantiation from the L8-icon will be demonstrated. To demonstrate the model editing capacity, also discussed in chapter 3, section 6.8 discusses the ComeW est case. In this case, the model editing capacity was used to create a 3D-object from various 2D cross sections and views.

Once again and emphaticly, it is brought to the attention that finding the best model or the best modelling method overall is in no case an end in itself in this thesis. The cases presented merely seek to demonstrate and exemplify the techniques developed in the previous chapters.

6.2 The Gulf of Thailand meandering river system

6.2.1 Problem description

The seismic survey of the Gulf of Thailand, as presented by Brown in [Bro96], contains a buried meandering river system at a depth of approx. 196 ms. This buried meandering river system (fig. 6–1) is the subject of this case study. From the mid-Miocene up, i.e., at altitudes above 900 ms, the surveyed area is almost perfectly flat. The time slice containing the meandering river system belongs to this region. Owing to the absence of dips and major phase changes, this case is relatively uncomplicated.

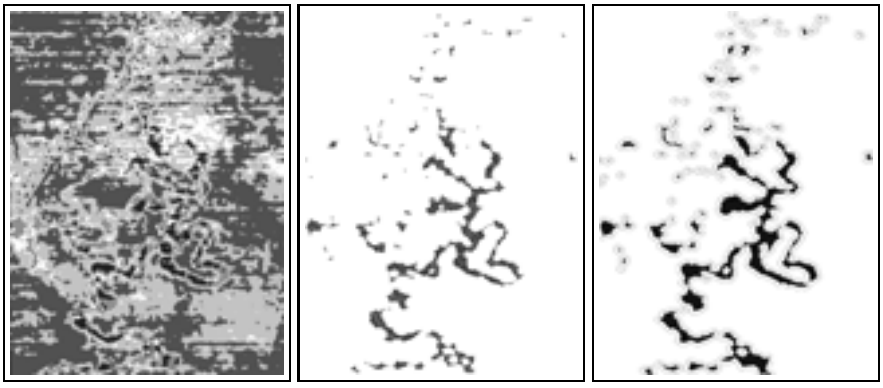

Figure 6–1: *Gulf of Thailand survey, capturing the geometry of a meandering river system, "visible" in a time slice at the left, using an α-complex. The resulting river system geometry is shown in the central and right picture. The captured geometry is parametrisable by varying the α-value. The centre α-complex has a lower α-value yielding a leaner geometry, the right α-complex has a higher α-value yielding a "fatter" geometry (time slice taken from [Bro96])*

6.2.2 Data set

Landmark and value set in most of the cases to be discussed are derived from seismic data. In this thesis, seismic is essentially exploration seismic, i.e., *reflection seismic*, initiated and recorded at the earth's surface. The process of seismic surveying, stripped to its barest essence, consists of the excitation of the subsurface by means of vibration energy sources and collecting the re-

sponse returned from the subsurface by means of *geophones* or *hydrophones*. The hydrophone or geophone records the acoustic pressure or particle velocity in the response signal as a function of travel time. The essentially non-stationary response signal carries information determined by the travelled path through the inhomogeneous subsurface and the location and cause of the reflection. After appropriate stacking and processing, an *acoustic image* can be obtained from the subsurface. Primarily in the space-travel time domain and after a *time-depth conversion* in 2D or 3D space. Generally, the amplitude and the angular information (phase and frequency) of the recorded signal in reflection seismic carries different types of information, revealing different subsurface features. Occasionally, assuming isotropy, pressure wave (or: *p-wave*-) response is separated from shear-wave (or: *s-wave*-) response, each thus providing different types of information.

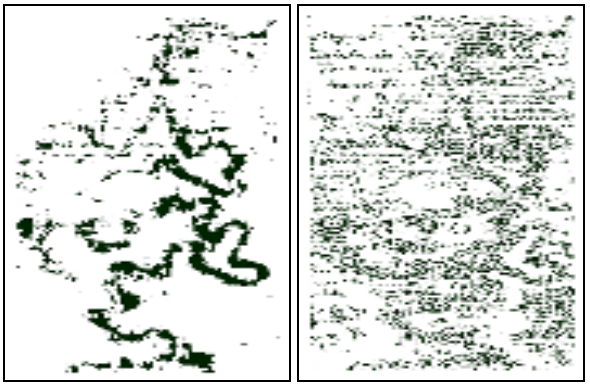

Figure 6–2: *Landmark sets of the Gulf of Thailand case, composed of regularly spaced landmarks plus an amplitude attribute value set. Left: the lower-valued amplitude landmark set, right: the lower- and medium-valued amplitude landmarks. The empirical intensity $\hat{\lambda}$ in the left and the right picture differ.*

Various seismic attributes can be calculated from the actually measured seismic data. In the case studies to follow, both amplitude-related attributes and angular attributes will be used. Attributes used here belong to the class of *instantaneous attributes*. *Edge detecting attributes*, might but will not be used. *Trace attributes*, like average frequency, cannot be used. Instantaneous amplitude and reflection strength can be used in the exploration of bright spots (e.g., the one in the L8 data set, figure 6–9), changes in the amplitude and/or phase generally indicate major lithologic changes and abrupt impedance changes. For further details on practical use and interpretation of seismic, see for example [Bad85, BW85, Bro96].

The data set of the Gulf of Thailand case consists of a single time slice of the survey at a depth of 196 *ms*. Lying above the mid-Miocene unconformity, it is essentially flat. In a time slice, data are regularly spaced. The original landmark set of 2110713 points has been re-sampled to 82800 points, to down-scale the problem to manageable size. The only value set is that of the amplitude attribute shown in figure 6–1, left picture. Basically, all points of the input time slice could be used as a landmark in the α-complex computation. Each weighted according to its attribute value. To save computational effort, points that will be prevented from taking part in the resulting α-complex, may as well be filtered off, at beforehand. In the case studies presented here, this strategy will be followed. So after an initial *subgridding* of the original time slice, reducing the initial 2110713 samples to 82800 samples, the landmark set is further reduced

	Amplitude attribute
nr. of inlines	400
nr. of cross lines	207
nr. of samples	1
wavelet length	unknown
target zone	unknown
inline spacing	unknown
cross line spacing	unknown
sample rate (resampled)	4 ms
survey length	$\approx 12.7\ km$
survey width	$\approx 8.0\ km$
depth	196 ms
nr. of traces	82800
nr. of samples	82800
classified landmarks	$20k$

Table 6–1: *Gulf of Thailand landmark set dimensions.*

by dropping the high-valued amplitude landmarks, the darker landmarks in the left picture of figure 6–1. An additional thinning process cuts landmark set cardinality further down to slightly over $N = 20000$.

The following modelling questions arise:

1. Should medium-valued amplitudes (white-coloured landmarks in left picture of figure 6–1) be classified as belonging to the meandering river system? More specifically, could such values indicate channel sand depositions, such as point pars and scroll bars?
2. Is the hypothesis justified that the channel shows no phase change, i.e., that the entire seismic response of the channel is shown by one and the same class of amplitude values, in this case the lower-valued amplitudes?
3. Could it be that the channels are mud-filled and therefore show a different seismic response than the sandy depositions next to the channels?

These are questions that cannot be answered conclusively without additional data, not available in this case study. Only plausible assumptions can be made in this case and in fact this is what has been done. Assumptions are that:

1. The channel structure is shown entirely by the minimum-valued amplitudes.
2. The channel is assumed to lie entirely in a horizontal plane, at 196 ms, as justified in [Bro96].
3. The channel is assumed to show no phase change.
4. The sand/clay or sand/silt structure depositions, such as point bars and stacked layers in the flood plane are shown in the seismic by medium-valued amplitudes.

To that extent, *peaks*, high-valued amplitude landmarks, will be removed from the landmarks, leaving the medium- and lower-valued amplitudes. Two specific landmark sets were compiled: a lower-valued amplitude landmarks set, and a second set with lower- plus medium-valued amplitude landmarks. Figure 6–2 shows both landmark sets. For the landmark coordinates, inline numbers and cross-line number were taken, yielding a regularly spaced landmark set. To make the landmark sets 3D, landmarks were duplicated with $z = 0$ and $z = 1$ depth coordinates.

STATISTIC	x_1	x_2	x_3
minimum	1.00000e+00	0.00000e+00	0.00000e+00
maximum	2.06000e+02	3.99000e+02	1.00000e+00
mean	1.16696e+02	2.26816e+02	5.00000e-01
variance	2.04090e+03	9.28981e+03	2.50012e-01
standard deviation	4.51763e+01	9.63837e+01	5.00012e-01
standard error	3.12776e-01	6.67307e-01	3.46180e-03
coefficient of variation	3.87129e-01	4.24942e-01	1.00002e+00
skewness	-5.26566e-01	-2.74034e-01	2.04370e-18
- significance level	1.69589e-02	1.69589e-02	1.69589e-02
kurtosis	-2.90963e-01	-4.46459e-01	-2.00019e+00
- significance level	3.39178e-02	3.39178e-02	3.39178e-02
weighted sum	2.43451e+06	4.73184e+06	1.04310e+04

N	20862
diameter	3.99000e+02
orthogonal breadth	1.00000e+00
diameter/breadth ratio	3.99000e+02

Table 6–2: *Condescriptive statistics Gulf of Thailand landmarks set, lower-valued amplitude landmarks only. Higher- and medium-valued amplitude landmarks have been dropped.*

6.2.3 Data analysis

Condescriptive statistics as described in section 3.5 were computed of each of the landmark sets so compiled. Table 6–2 summarises the principle statistics of the lower-valued amplitude landmarks, table 6–3 those of the lower- and medium-valued amplitude landmark set. Comparing the statistics reveals the following more or less trivial features:

- The lower-valued amplitude landmark set has a somewhat smaller variance. The same holds for the coefficient of variation.
- It is also somewhat more skew than the landmark set with medium-valued amplitude landmarks. Skewness is above the adopted significance level of $\sqrt{\frac{6}{N}}$.

Remark that if all points on a grid are accepted as landmark, then spatial statistics become fairly predictable. If specific classes are filtered off (like for instance the lower-valued amplitude landmarks) understanding the statistics becomes more important. Also notice that even if only

Statistic	x_1	x_2	x_3
minimum	0.00000e+00	0.00000e+00	0.00000e+00
maximum	2.06000e+02	3.99000e+02	1.00000e+00
mean	1.10961e+02	1.99932e+02	4.97260e-01
variance	3.10746e+03	1.15738e+04	2.50005e-01
standard deviation	5.57446e+01	1.07581e+02	5.00005e-01
standard error	3.89946e-01	7.52557e-01	3.49765e-03
coefficient of variation	5.02378e-01	5.38090e-01	1.00552e+00
skewness	-2.47033e-01	-3.12217e-03	1.09620e-02
- significance level	1.71347e-02	1.71347e-02	1.71347e-02
kurtosis	-9.73475e-01	-1.06019e+00	-2.00008e+00
- significance level	3.42695e-02	3.42695e-02	3.42695e-02
weighted sum	2.26761e+06	4.08582e+06	1.01620e+04

N	20436
diameter	3.99000e+02
orthogonal breadth	1.00000e+00
diameter/breadth ratio	3.99000e+02

Table 6–3: *Condescriptive statistics Gulf of Thailand landmarks set, lower- and medium-valued amplitude landmarks.*

certain classes are selected as landmarks, their statistics may remain invariant. For instance, the nearest neighbour distances. If selected landmarks are adjacent, forming a contiguous area, their typical nearest neighbour distance will be that of the grid.

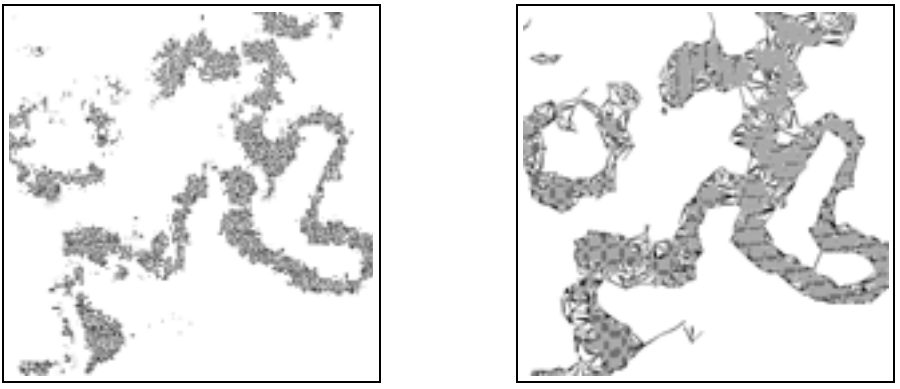

Figure 6–3: *Gulf of Thailand, nearest neighbour (left) and local-furthest neighbour graph (right) of the oxbow region in the troughs-only landmark set.*

Nearest neighbour and local-furthest neighbour analysis

The role of the (weighted) nearest neighbour graph is that it point out the neighbouring landmark in that closed star $St\ \mathbf{s}$ of $\mathbf{s}$ to which $\mathbf{s}$ will be connecting first, sharing a singular edges with it as soon as that edge becomes α-exposed. The local-furthest neighbour graph connects $\mathbf{s}$ with the last neighbouring landmark to which it does connect in the underlying triangulation. These graphs are of great aid in the analysis of weighting problem spots. See chapter 3. Figure 6–3 shows the nearest neighbour and the local-furthest neighbour graph of the oxbow detail of the river system.

6.2.4 Weighting

Weighting is pretty much straightforward in this case. Assigning initial weights is trivial for the lower-valued amplitude landmark set, with only a single value class selected. Weights are assigned values in the range $[0.1, 0.4]$, according to amplitude value and a scaling directly related to the typical grid spacing. In the case of lower- and medium-valued amplitude landmarks, weights are in range $[-0.8, 0.4]$.

6.2.5 Result

The resulting geometric model (family) of the meandering river is shown in figure 6–6, with an intermediate result, triangulation plus α-complex, shown in figure 6–4. Consulting figure 6–6, the lower-valued amplitude landmark set (the upper family) best models the mere channel structure of the river system, as presumed. If more of the flood plane is to be incorporated, medium-valued amplitude landmarks are to be included, as the bottom family in figure 6–6 shows. This family also showsa horizontal line pattern clearly caused by data artifacts. This pattern comes with the inclusion of medium-valued landmarks in the landmark set. Selecting the most appropriate α-value is less trivial. The leftmost family members in figure 6–6 have α-values of $O(10^0 - 10^1)$. More precisely, the third family member from the left of the upper and the lower family have α-values of 17.2 and 9.06, resp., about the maximum that can be accepted with the weights assigned. While the α-family unrolls for growing α in figure 6–6, the river system, being property-ruled, must also be clearly "visible" in property space. Figure 6–5 shows the property space α-complex, projected downfrom the hyper-spatial α-complex in 6-space. The property space α-complex of figure 6–5 shows the following:

- The higher-valued amplitude cluster is well separated from the lower-valued amplitude cluster and the medium-valued amplitude cluster for a large range of α-values.
- The lower-valued amplitude cluster and the medium-valued amplitude cluster are less well-separable, indicating a unsharp transition from channel to channel sand depositions.
- For large values of α, when the property-α-complex approaches the triangulation, the cluster tend to develop a saddle-like shape.
- The diameter of the higher-valued amplitude cluster is small, compared to the diameter of the other clusters.

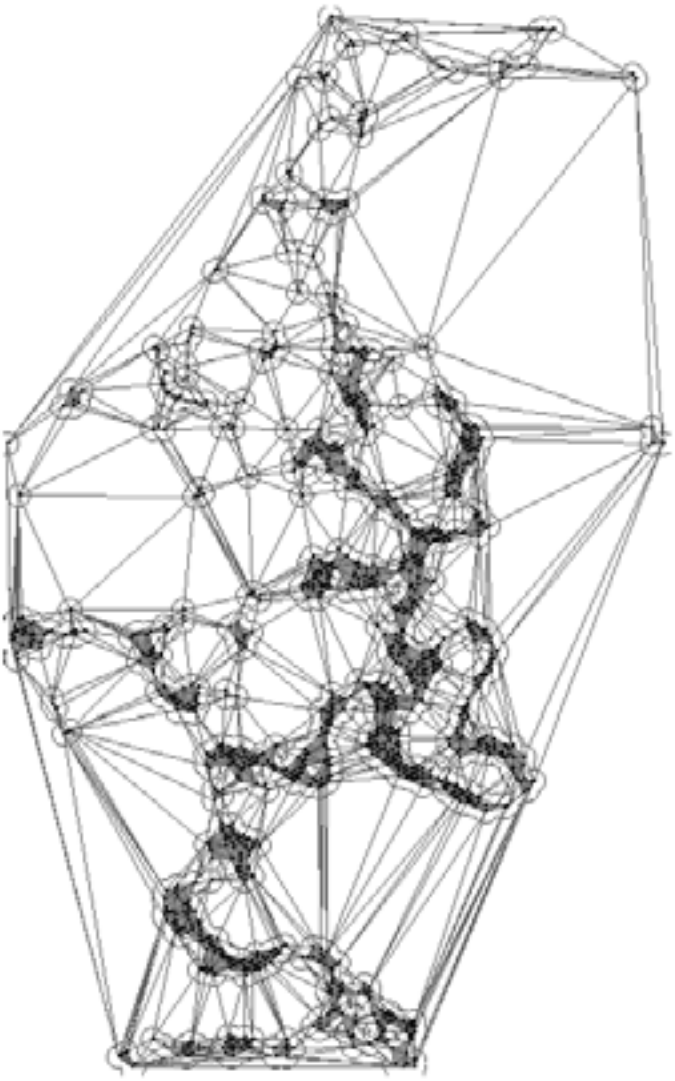

Figure 6–4: *triangulation plus embedded α-complex intermediate result of the lower-valued amplitude landmark set. Observe the sliv er-like triangles near the boundary*

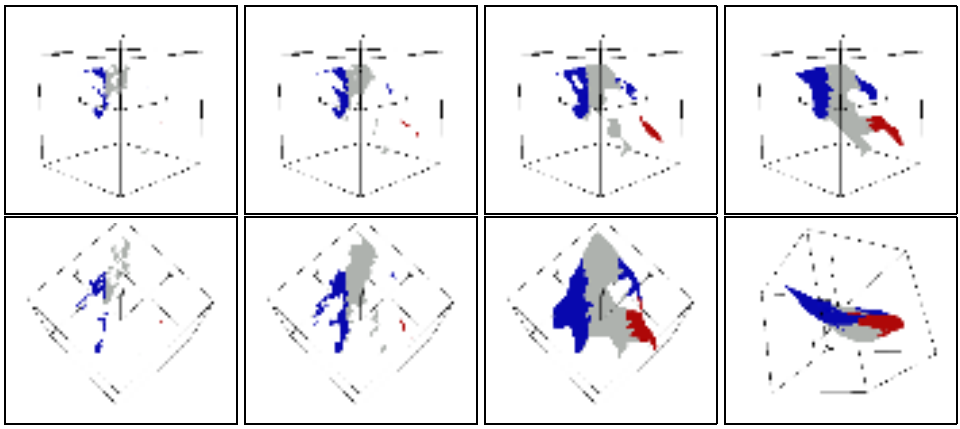

Figure 6–5: *property cube α-complex of the minimum-valued amplitude landmark set of the Gulf of Thailand.*

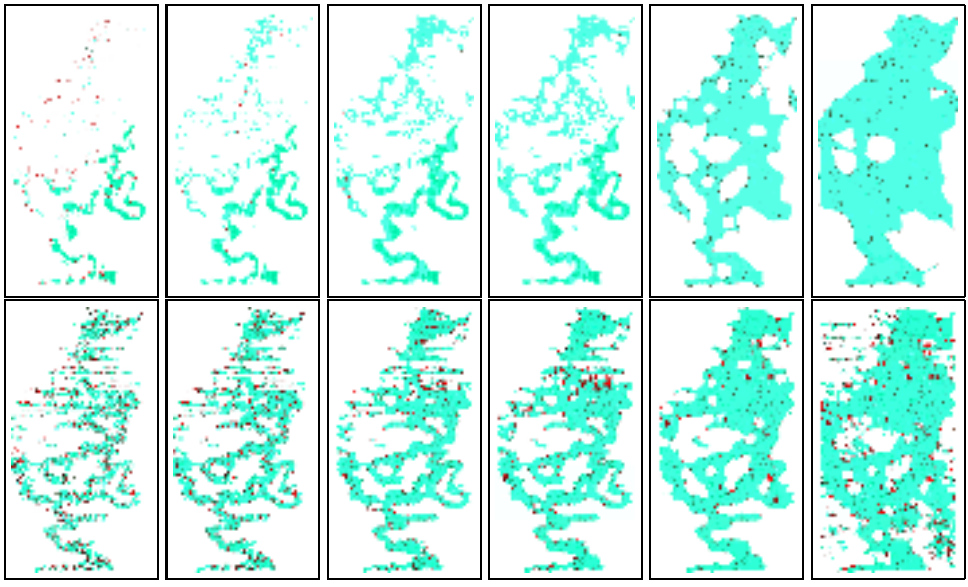

Figure 6–6: *Gulf of Thailand α-complex families: the mildly weighted lower-valued amplitude family on top, and the lower- and medium-valued amplitude family at the bottom.*

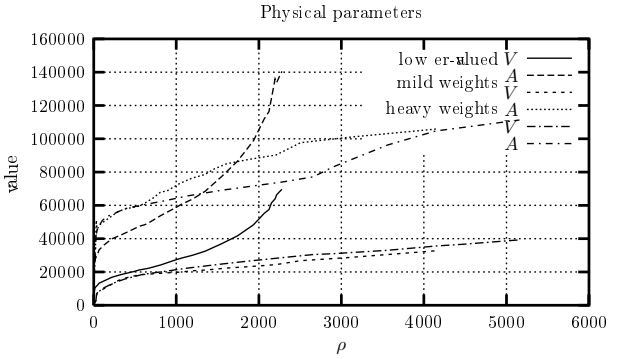

Figure 6–7: *Gulf of Thailand, calculated physical c haracteristics as a function ofα-rank ρ. Mild- and heavy weigh t sets for lo w er- and medium amplitude landmarks create differenα-families, with different α-ranks, as shown.*

- As expected, the range of α-values for which the river geometry and topology appears reasonable, corresponds with the α-value range in which the clusters of the properties are well separable. This appeals to and once more confirms the idea that geometry is property-ruled.

The analysis of singular faces, see figure 6–8, is important in the process of finding the best-fitting α-complex. Singular faces are often rejected b y modellers as topological artifacts, to be duly removed from the model. But within an α-family, singular faces are important gro wth indicators of an object for v arying α. In other words, it reveals the gro wth direction and locations for an increased value of α. This information, combined with a-priori knowledge about the modelled object, may be helpful in finding the appropriate α-value. Finding the best α is a process that is also constrained by physical parameters, suc has total volumes, areas and curvatures. These values may be observed, calculated or statistically estimated. Figure 6–7 shows these constraints as calculated from the α-family.

Discussion

Due to the flatness of the facies and to the absence of phase changes, the single amplitude attribute admits a relatively easy extraction of the target object from its embedding environment. These circumstances are more an exception than a rule, however. In this case, property space was more used as a c heck for the initially assigned weight than a means to find the proper w eights. The reason for this is that the channel is indicated b y a distinct value of the attribute that is easily discovered by the human eye. Generally, this process will be too complicated and a factor analysis in property space is required first. Only after this step, weights can be determined.

Without precise knowledge on the flood plane, the inclusion and promotion of medium-valued landmarks may be argued. Without further constraining data, from a process model simulation, exploration wells, or any other source, no precise estimation can be given for the best α in this regard.

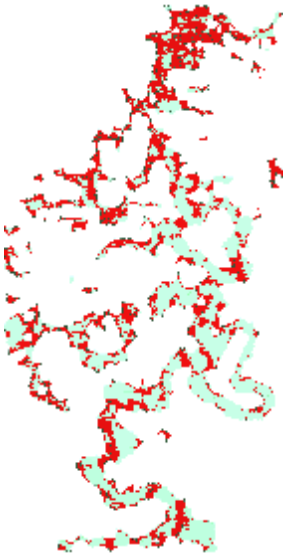

Figure 6–8: *singular face analysis of Gulf of Thailand α-complex. The darker faces are the singular faces, showing the growth trend of the α-complex. Observe for example the oxbow region and compare this to the same region in the nearest- and local-furthest neighbour graph. Also notice the growth trend in the upper part of the river system, as indicated by singular faces.*

6.3 The North Sea L8 meandering river system.

6.3.1 Problem description

The L8 block in the North Sea shows various land-marine coastal fluvial and alluvial environments. This data contains well conserved clinoforms and tidal channels in a deltaic structure. At smaller altitude (approx. 100 ms), the data contains a vaguely showing meandering river system. The river system contains tw o separate channels, stacked on top of each other. The goal of this case study was to capture the geometry of this river. The case is more complicated than the the Thailand case.

6.3.2 Data set

The data set consisted of a carefully interpreted[1] seismic cube and horizons. The seismic cube consists of reflection strength data. The reflection strength is the continuous polarity independent measure of the signals energy defined at any time in the travel time domain. No further seismic attributes are available. In terpretation, as stated, targeted at a target zone way deeper than the river (see table 6–4). F rom this cube, time slices were extracted starting at 96 ms up to 112 ms, at 4 ms sample rate. The time slices are shown in figure 6–9. As with the Thailand case, a further cut of the amount of landmarks is required to match the computational limitations imposed. A

[1] Interpretation by: Sevgi Tigrek, Delft University of Technology

region of interest containing the channel and the surrounding depositions was cut out in each of these time slices and remote regions were clipped away.See for instance figure 6–10. The statistics of the initial landmark set are given in table 6–4. The spacing of the regularly spaced landmark set, after resampling is $37.5 \times 37.5\ m$. The statistics of the reflection strength value set are given in table 6–5.

	Reflection strength
nr. of inlines	211
nr. of cross lines	117
nr. of samples	5
wavelet length	unknown
target zone	$> 1000\ ms$
inline spacing	$37.5\ m$
cross line spacing	$37.5\ m$
sample rate (resampled)	$4\ ms$
survey length	$\approx 7.9\ km$
survey width	$\approx 4.4\ km$
depth	$48 - 148\ ms$
nr. of traces	24687
nr. of samples	123435
classified landmarks	$30k - 67k$

Table 6–4: *North Sea L8 channel landmark set dimensions, after clipping and subgridding from the initial* 211 *inlines by* 1415 *X-lines by* 860 *ms L8 data set. The initial sample rate before subgridding and sampling was* 4 *ms and the initial inline-by-X-line spacing was* $37 \times 12.5\ m$.

STATISTIC	p_1
minimum	-1.27000e+02
maximum	1.26000e+02
mean	5.15782e-02
variance	1.10656e+03
standard deviation	3.32650e+01
standard error	6.46765e-03
coefficient of variation	6.44943e+02
skewness	-3.91431e-02
- significance level	4.76250e-04
kurtosis	3.38240e+00
- significance level	9.51499e-04
weighted sum	1.36442e+06

Table 6–5: *North Sea L8 reflection strength value set statistics.*

6.3.3 Data analysis

Human eye perception is good enough to quickly discover a channel system, but the recognised object is not trivially taken from the data values in this case. The marginal quality of the data

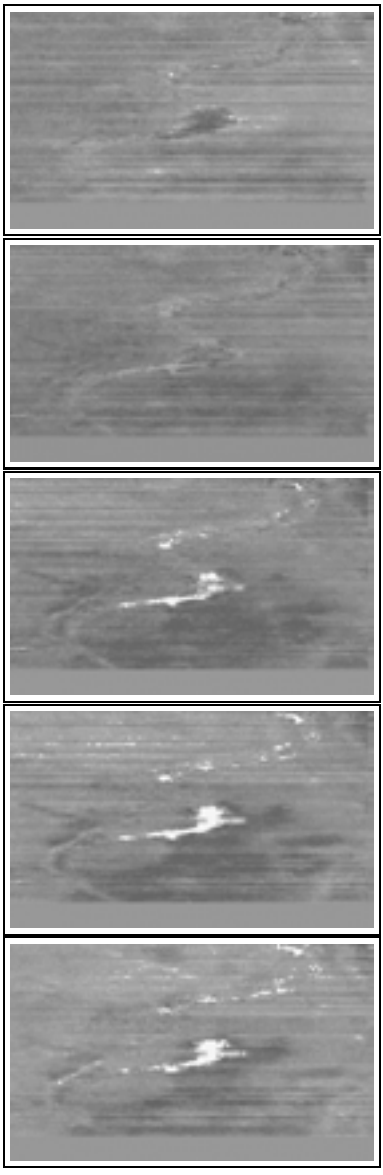

Figure 6–9: *North Sea L8, reflection strength time slices for two-way travel time* $t = 96 - 112\ ms$. *Top:* $t = 96\ ms$, *bottom:* $t = 112\ ms$, *difference* $\Delta t = 4\ ms$. *Observe the bright spot (gas?) in the centre of the data set and also observe the phase changes this spot exhibits over time.*

is in great part due to the fact that the target zone for the seismic was way deeper than the depth of the channels. Unlike the Gulf of Thailand case, the L8 channel shows a number of phase shifts. As a result, there is no obvious relation between the only available attribute and the weight. Phase information is not available as a value set, unfortunately. Nearest neighbour analysis provides only trivial information in this case.

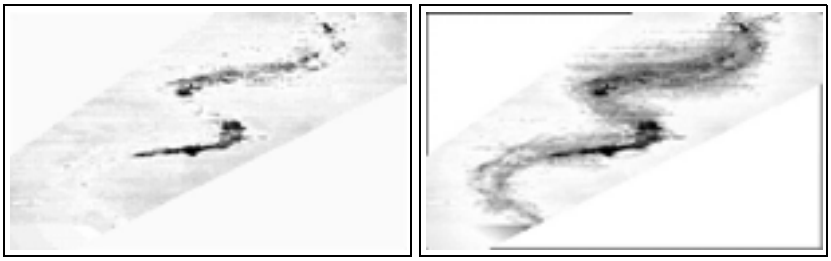

Figure 6–10: *Single attribute-based weight model. Left: phase shifts along the river cause the river geometry in the seismic to be illuminated only partially when only peaks are considered. Also taking into account zero-crossings (right picture), includes a lot of misclassified material. Obviously, the single attribute lacks sufficient discriminating capacity.*

6.3.4 Weighting

Weighting in this case is much more complicated than with the Gulf of Thailand case. There is only a single attribute available, which by itself is not sufficiently discriminating to tell channel or river system depositions apart from embedding material. Adding supplementary attributes and/or phase information would be the appropriate solution, but since unavailable, other strategies have to be developed, based on the only available reflection strength. Three strategies were evaluated(see figure 6–11):

- **Strategy 1: seismic amplitudes only**

  The design of the weights is entirely based on seismic amplitudes, analogous to the previous case.

- **Strategy 2: seismic amplitudes locally at a support model**

  A geometric model is fit across the anticipated channel and attribute values are evaluated a this geometric support model location.

- **Strategy 3: seismic amplitudes and inverse distance-based weights from a support model**

  A (geometric) support model is fitted across the conceptual channel and a inverse distance-based weight estimation takes place, in addition to the local attribute value.

Strategy 1

Unlike the Gulf of Thailand river system, phase changes do play a role in this data. Involving merely the seismic attribute values erroneously classifies data as belonging to the river, v.v.

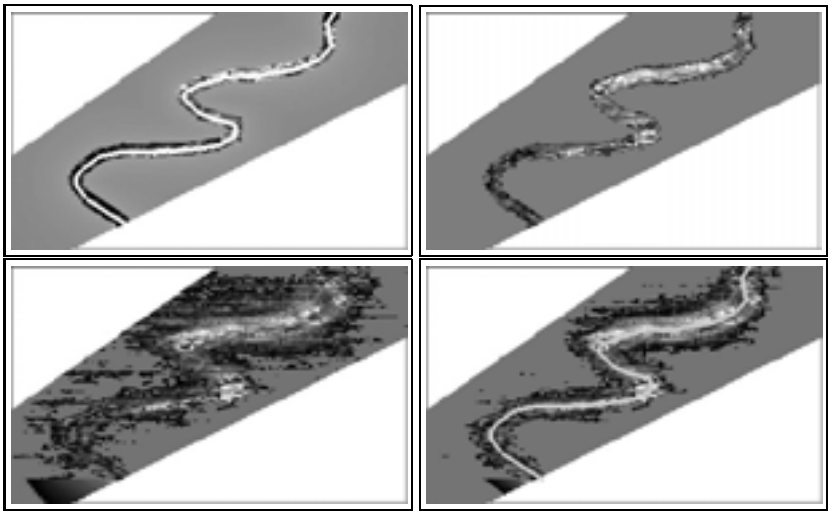

Figure 6–11: *three strategies to obtain a weight model for the L8 river system with only a single weakly discriminating attribute. Top left: the presumed support model, underneath which attribute values are evaluated. The result (strategy 2) is shownat the top right. Bottom left: the result of strategy 1, in which only attribute values are considered. Bottom right, the result of the attribute values plus an inverse distance penalty from a presumed support model (strategy 3).*

Even at the bright spot, the signal changes from trough to peak and back. Channels show peaks, troughs and zero-crossings. Therefore, the discriminating pow er of the seismic amplitude is insufficient to base the weight upon and this strategy has to be rejected. The result of strategy 1 is shown in figure 6–11, bottom left picture.

Strategy 2

Strategy 2 delineates a support model, but evaluates the attributes only at the model location causes the river to be of constant width and neglects its lateral extension. Even if greater channel widths are chosen, then still the variation is largely breached. The support model is shown as a line along the channels main axis in figure 6–11, upper left picture. The result of the strategy 2 evaluation underneath this model in the upper right picture.

Strategy 3

Strategy 3 takes into account both the available reflection strength attribute value and the lateral channel extension. It honours both peaks and zero-crossings, right at the channels' paths as well as fain tly remote from the channels. The further remote from the channel, the greater the distance penalty and the smaller the weight. Details of the distance penalty are discussed below, the result is shown in figure 6–11, bottom right picture.

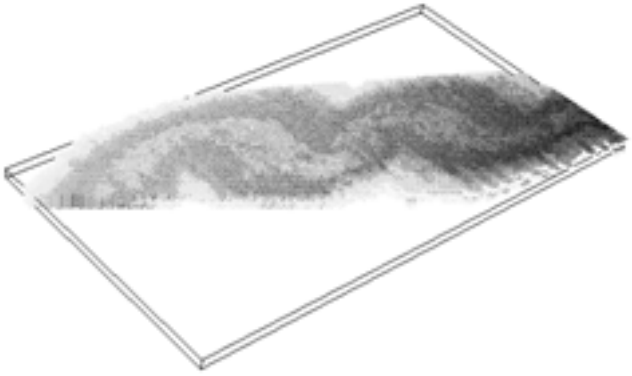

Figure 6–12: *L8, final weighting model. For this regularly spaced landmark set, the channel geometry can easily be recognised in the weight set.*

6.3.5 Result

Strategy 3 appeared to give the best control and the best results. Time slice $t = 104$, the middle time slice of the river system, was used to develop the best inverse distance-based weight functions. Various functions were evaluated. All of the general form:

$$w = \mathsf{g}(p_1) - (\delta - \mu)^m - \frac{(t - 104)}{16} \tag{6–1}$$

where p_1 is the reflection strength, $(\delta - \mu)^m$ is the distance penalty, with δ the shortest distance to the channel central axis and $(t - 104)$ being the "time distance" to the middle time slice. The channel has been assigned a width $2\mu = 24\ m$. Power values $m = 2$, $m = 1.5$ and $m = 1.2$ were evaluated first. Eventually power $m = 1.32$ turned out to give the best result shown in figure 6–11, bottom right picture. Recall from table 6–5 that reflection strength $p_1 \in [-127, 126]$ and the best matching global weight scale factor was set to $\varrho = 0.04$. River channel width $2\mu = 24\ m$ was derived from the top-right river mouth (6–9), which is approximately 60 units, with 1 unit being 12.5 m. The bend at the lower left part (the two branches) span approximately 45 units. Representatives of the resulting α-family are shown in figure 6–13. For the weight component $\mathsf{g}(p_1)$ it is necessary to take into account the phase information. The dominant polarity associated with channel sands across the time slices is negative for $t = 96\ ms$ and then turns to positive for times $t > 96\ ms$. A 3D oblique view of the river is shown in figure 6–14.

6.3.6 Discussion

It is emphasised once more that using a geometric support model is undesirable but caused by the fact that the available attributes lack sufficient discriminating capacity to fully rule out the geometry of the object. The good thing about this case is that it exactly uncovers the limitations of the approach of this thesis. If the quality of the property value sets is poor, then the weight set has only weak *modelling capacity* and without a decisive weight set, the geometry will be vague and with considerable model uncertainty.

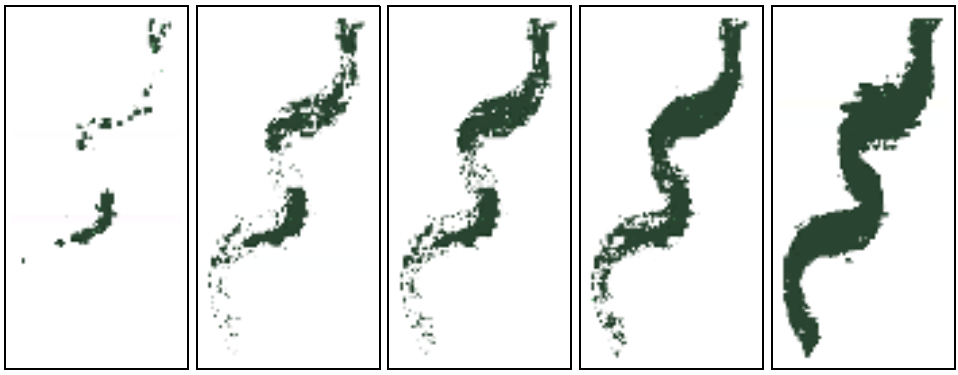

Figure 6–13: *Resulting α-family of the L8 river, based on strategy 3.*

Figure 6–14: *resulting α-complex of the L8 river, 3D oblique view. To indicate the typical size of tetrahedral elements, the figure shows a slightly exploded view. The total number of tetrahedra amounts to* 38835.

Using a support model, however, opens up the road to distance based weighting. The model could be further refined if somehow, the multiple channels could be identified within the bigger picture. Figure 6–14 shows one possible such model, at the right. This model is to be accepted with great caution, as sufficient data are lacking.

6.4 Salt dome in the Gulf of Mexico

6.4.1 Problem description

The South Marsh Island salt dome belongs to the group of salt domes in the Texas-Louisiana Coastal Basin, discovered mainly in the late sixties. The South Marsh Island area is located on the continental shelf in the Gulf of Mexico, west and adjacent to the present day Mississippi delta, approximately in the deepest part of the basin. The basin contains mono-clines, pillows, anti-clines, domes, ridges and massifs, the deepest part contains primarily diapirs and domes. The region consists of a feeding salt layer and younger depositions separated at a depth of approximately 980 ms by a sub-marine canyon. The canyon laps on a steep salt dome, fed by the feeding salt layer (which is not contained in the data). The canyon is in-filled with marine clays. Embedded in the clay are two approx. 250 m wide channels, with only marginal lateral accretion, roughly at the deepest point of the sub-marine canyon. Below the sub-marine canyon, too, channels were reported. Faults radially emanates from the salt dome. The geologic trend is Miocene, late tertiary. This description was largely taken from [Hal67, Ste97]. For further details, see [Hal67].

The true significance of this case is lying in its size. More than the two preceeding cases did, this case approaches realistic dimensions. The model rapidly outgrew the customary workstation configuration. The model of the Gulf of Mexico salt dome was therefore crafted on a SILICON GRAPHICS[2] ONYX2 INFINITEREALITY2E Workstation, equipped with 1 GB of internal memory and four 250 MHz R10000/10010 MIPS processors/FP-processors.

6.4.2 Data set

The sampling data point set consists of 3D seismic data, containing two seismic attributes; instantaneous time dip and reflection strength. In an earlier study, Steeghs ([Ste97]) found that the instantaneous time dip is a good indicator to filter off salt from other lithologies. The landmark set is a slice starting at approx. 500 ms and extending to slightly over 1450 ms. Unfortunately, the top and the foot of the dome are missing in the value sets. Furthermore, the data contain few minor acquisition and migration defects, causing the occurrence of a regular pattern across the data.

The cube consist of 876 inlines, 287 cross-lines and 119 samples. The spatial distribution of the data is as follows. Inline distances are 25 m and cross lines are spaced at 50 m a distance. The sample rate of the data is 8 ms, after resampling from 4 ms. Moreover, the seismic cube was composed from time-migrated 2D-sections and re-sampled by a factor 2 in each direction. The dimensions of the data set taken for this study are given in table 6–6.

The largest model that can be run can be expressed in terms of the number of land-

[2] kindly made available by Silicon Graphics Benelux; see: Acknowledgements

	Reflection strength	Time dip
nr. of inlines	876	876
nr. of cross lines	287	287
nr. of samples	126	119
w a v elet length	unknown	unknown
inline spacing	25 m	25 m
cross line spacing	50 m	50 m
sample rate (resampled)	8 ms	8 ms
surv ey length	21.900 km	21.900 km
surv ey width	14.350 km	14.350 km
depth	$504 - 1456$ ms	$480 - 1480$ ms
nr. of traces	251412	251412
nr. of samples	31677912	29918028
classified landmarks	$140k - 300k$	$50k - 300k$

T able6–6: *Gulf of Mexico South Marsh island salt dome landmark set dimensions. Columns show the specific time dip and reflection strength value set dimensions. T op and foot of the salt dome are missing from the value sets.*

marks filtered off, although the actual memory limitations came from triangulation and α-family-computations. The "original" data set counts $876 \times 287 \times 119 = 29918028$ time dip samples. This landmark set could only be accommodated on the Onyx2 after filtering off landmarks with a normalised time dip in excess of 0.83, corresponding to a time dip value in range $[1.18000 - 1.41774]$ and shadowing the 1 GB internal memory by a 1 GB swapspace, later on expanded once more by some 0.5 GB. The cardinality of this landmark set measures $N = 288417$, i.e., less than one percent! The characteristic dimensions of this landmark set can be found in table 6–7.

	Sampling factor	Spacing factor $[m]$
X-lines	1	$1 \times 50 = 50$ m
Inlines	1	$1 \times 25 = 25$ m
Samples	1	$1 \times 8 = 8$ $ms \approx 8 - 10$ m $(v = 2000 - 2500$ $m/s)$
Time dip	$\bar{\delta} \geq .83$	$2.88417 \cdot 10^5$ landmarks

T able 6–7: *Gulf of Mexico non-resampled instantaneous time dip attribute value set dimensions. A clip level of normalised time dip value $\bar{\delta} \geq .83$ filters off slightly under 300000 landmarks, i.e., less than one percent of the points, yielding the largest possible model that could be run.*

A typical "data voxel" in this case measures approximately $25 \times 50 \times 10$ m, i.e., far from cubic. The following strategies were evaluated to handle this:

- **F urtherresampling**

  This straightforwardly follows the sampling and subgridding that already took place, up to this stage. Aim is to sample such that the data voxel shape becomes more or less cubic.

- **Applying a landmark transformation**

  A landmark transformation may be applied to reshape the data voxel.

Further sampling would imply that inlines and samples have to be dropped. A "112"-resampling variant may be chosen, in which only every second sample is accepted as a landmark. This stretches the depth dimension of the data voxel to $16-20\ m$. Table 6–8 shows the characteristics of this resampling.

	Sampling factor	Spacing factor $[m]$
X-lines	1	$1 \times 50 = 50\ m$
Inlines	1	$1 \times 25 = 25\ m$
Samples	2	$2 \times 8 = 16\ ms \approx 16 - 20\ m\ (v = 2000 - 2500\ m/s)$
Time dip	$\bar{\delta} \geq .83$	$1.45187 \cdot 10^5$ landmarks

Table 6–8: *Gulf of Mexico "112"-resampled instantaneous time dip attribute data cube. A clip level of normalised time dip value $\bar{\delta} \geq .83$ filters off less than half a percent of the points as landmarks.*

Sampling and subgridding this way already excluded some 99.5% from the initial landmark set, however Dropping more samples may cause the sampling to become too crude along the time domain. On the other hand, the salt dome itself does not extend the whole area of the landmark set. Cutting off the dome region itself may bring about a reduction of the landmark set extent down to approximately 47%. The salt area is found in the inline range $[1, 401]$ and this area may be chopped off as the area of interest. With no further resampling (111-configuration), the area measures $401 \times 287 \times 119 = 13695353$ landmarks. This option may be used to allow for a less severe sampling with a lower clip level so that more landmarks are passing the filtration. This would increase the intensity λ of the underlying point process. A "124"-resampling scheme accomplishes an approximately cubic data voxel of $50 \times 50 \times 40m$, allowing the clip level to drop to $\bar{\delta} \geq .6$. See table 6–9:

	Sampling factor	Spacing factor $[m]$
X-lines	1	$1 \times 50 = 50\ m$
Inlines	2	$2 \times 25 = 50\ m$
Samples	4	$4 \times 8 = 32\ ms \approx 32 - 40\ m\ (v = 2000 - 2500\ m/s)$
Time dip	$\bar{\delta} \geq .6$	$3.53946 \cdot 10^5$ landmarks

Table 6–9: *Gulf of Mexico resampling of the instantaneous time dip attribute data cube. A clip level of normalised time dip value $\bar{\delta} \geq .6$ and resampling to data voxels of size $50 \times 50 \times 32\ m$ yields a landmark set of $3.53946 \cdot 10^5$ landmarks.*

Further resampling has also been examined, using the same clip level $\bar{\delta} \geq .6$. A "246"-resampling was created, with the spatial landmark characteristics as given in table 6–10. Resampling beyond the "124"-resampling is acceptable still for the salt dome itself, but too coarse for the rest of the model. As it turns out later, this model contains a sub-marine canyon. This canyon can be missed completely in too coarse a resampling. Of course, the accuracy of the salt dome itself is also limited with a coarse sampling.

Applying a landmark transformation is another option. Landmark transformation should make the data voxel cubic. Reconsider the 111-configuration with a data voxel of dimension $25 \times 50 \times 10\ m$. An anisotropic scaling vector $\mathbf{T} = (2, 1, 5)^T$ would deliver a cubic data voxel

	Sampling factor	Spacing factor $[m]$
X-lines	2	$2 \times 50 = 100\ m$
Inlines	4	$4 \times 25 = 100\ m$
Samples	6	$6 \times 8 = 48\ ms \approx 48 - 60\ m\ (v = 2000 - 2500\ m/s)$
Time dip	$\bar{\delta} \geq .6$	$5.89918 \cdot 10^4$ landmarks

T able 6–10: *Gulf of Mexico resampling of the instantaneous time dip attribute data cube. A clip level of normalised time dip value* $\bar{\delta} \geq .6$ *and resampling to data voxels of size* $50 \times 50 \times 32\ m$ *yields a landmark set of* $5.89918 \cdot 10^4$ *landmarks.*

of dimension $50 \times 50 \times 50\ m$. The transformation needs to be applied prior to the computation of the α-complex and a back transformation by $\mathbf{T}^{-1}$ turns the landmark set back in to normal configuration. Both further resampling and the transformation option have been evaluated.

6.4.3 Data set analysis

Reflection seismic returned by salt structures is intrinsically chaotic. The salt dome flanks are so steep in this case (figure 6–16), that any reflection by them received at the surface is to be mistrusted. Migration effects in this case play an important role. The time dip attribute has been found to indicate the salt fairly well, refer to [Ste97]. But in addition to the salt, the sub-marine canyon also illuminates in this attribute. This clearly shows in the condescriptive statistics for specific altitudes, found in figure 6–15.

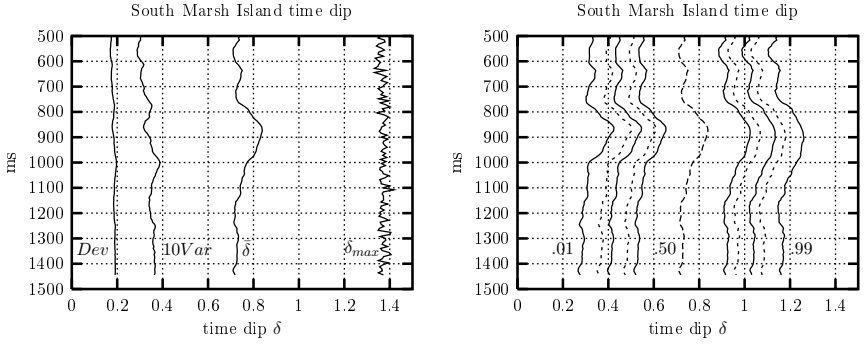

Figure 6–15: *left: primary statistics of the time dip attribute of the Gulf of Mexico in the time domain. Dev and Var are the time slice' empirical standard deviation and variance, resp.,* $\bar{\delta}$ *and* δ_{max} *are the observed mean and maximum time dip, resp. Right: the* 1, 3, 5, 10, 15, 50, 85, 90, 95, 97 *and* 99% *percentiles, resp., from left to right. Observe that in the time window* $800 - 1000\ ms$*, the* 99%*-percentile crosses the* $\delta = 1.2$ *grid line.*

A first analysis of the time tip statistics shows that the range of the time is basically stationary across the time domain. This does not hold for the cen tral moments, mean and variance. The variance is highest at the depth of the sub-marine canyon, approx. at $950 - 1000\ ms$. It is apparent from figure 6–15 that considerable more landmarks are going to be pic ked up in

the time window approx. $800 - 1000\ ms$. It no wbecomes ob viousthat too coarse a sampling that does not properly sample the depth region around this $950\ ms$ zone, can never reproduce this phenomenon.

The landmark set sampling the salt regions produce again a typical nearest neighbour distance that originates directly from the underlying grid, and therefore depends on the data voxel size. As a result, the global scaling factor of the weight transformation can be directly derived from the size of this data voxel.

6.4.4 Weighting

Weighting is a linear combination of attribute values. The tw oattributes available, reflection strength and time dip can be combined as follows:

$$w = w(\delta, p) = \lambda_1 \delta + \lambda_2 p, \quad \lambda_1 + \lambda_2 = 1 \tag{6–2}$$

where $\delta(\mathbf{x}, t)$ denotes the time dip value and $p(\mathbf{x}, t)$ the reflection strength. No improvement is delivered by adding the reflection strength attribute. Replacing reflection strength by instantaneous phase (figure 6–16) doesn't bring an improvement either. As stated, the reflection strength and also the instantaneous phase are much weak erindicators than the time dip and therefore, the normalised weight is approximately equal to the normalised time dip. Instantaneous phase and reflection strength are not independent. Reflection strength and instantaneous phase w ere therefore dropped, leaving only the time dip attribute for weighting.

The time dip is semi positive-definite, in this case in the range $[0.00000, 1.41774]$. With a seismic velocit y$v \approx 2000 - -2500\ m \cdot s^{-1}$, the dimensions of the data voxelsare as indicated in the tables 6–7 to 6–10. The global weight transformation scale factor will be of the same magnitude as the smallest of the inline, cross-line and depth dimensions, usually the latter.

6.4.5 Result

After selecting up to a maximum of approximately $300k$ landmarks from the seismic, and attaching w eights to them, the dedicated "high-end" computer took roughly 5 hours computing time and full memory to prepare the geometric model of the salt dome. A "112"-resampled landmark set turned out to reproduce the salt dome fairly well, too. Coarser resampling produced coarser geometries, as expected, up to inadequate and sometimes unrecognisable geometries beyond a a resampling by a factor 5 of the samples along the traces. River geometries are faintly showing, further statistic analysis must reveal whether their pattern are random or indeed indicate a typical river shape. Such analysis is considered beyond the goal of this case study and has not been carried out, therefore.

6.4.6 Discussion

The salt of the Gulf of Mexico case is geometrically reproduced fairly well. The only "defect" being the sub-marine canyon, also highlighted by the time dip. The combination of reflection

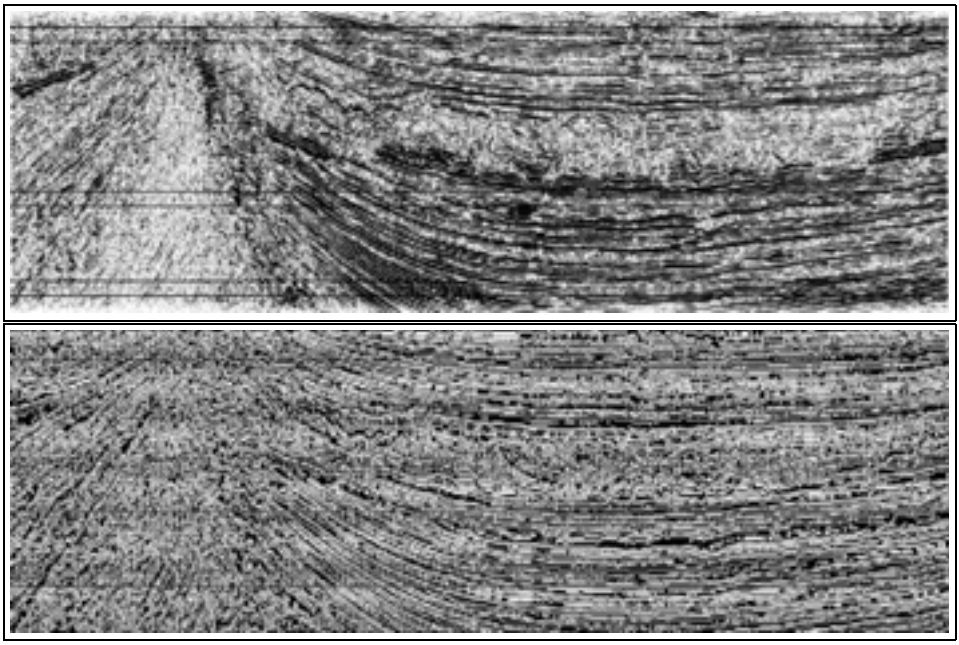

Figure 6–16: *Gulf of Mexico, South Marsh Island, reflection strength and instantaneous phase attribute. These attributes show similar features compared to the time dip and neither of them provides an additional discriminant parameter. The salt dome is at the left part of the figure, the sub-marine canyon runs off from the salt dome flanks, stretching to the right across the middle of the figure.*

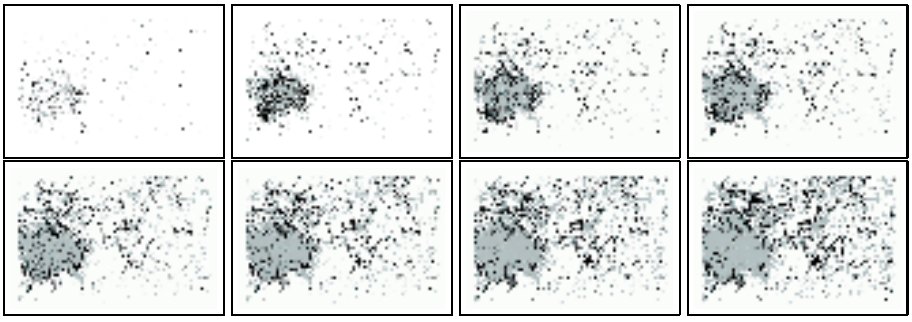

Figure 6–17: *Gulf of Mexico canyon, top view, with at the left the dome, and the time dip illuminating canyon filling the rest of the picture.*

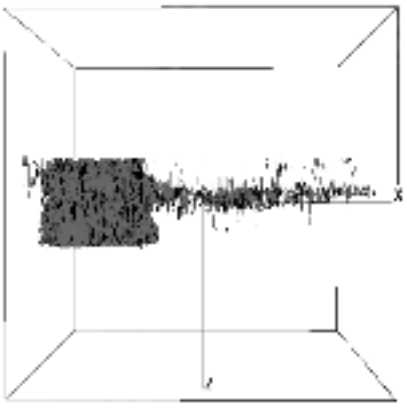

Figure 6–18: *Gulf of Mexico salt dome plus canyon, lateral view. Top and feeding layer are absent in this picture. The sub-marine canyon is clearly visible in the model.*

strength and time dip is not sufficiently discriminant to wipe out the over-exposure of landmarks in the time window $800-1000\ ms$ resulting from the time dip response to the sub-marine canyon.

In this case, the top of the dome (extending above $500\ ms$) and the "feeding" foot were not included. The entire model would have been too big and beyond the computing equipment capabilities. It shows that for practical purposes, the size of the problem that can be coped with is still severely limited. In terms of real-world problems, this case is still to be considered small. A typical E&P-survey will be bigger and will comprise more value sets. Valuesets are not the problem, because turning attribute values into weight takes place in before the α-family is computed and that is where the limitation is. The amount of landmarks that can take part in the computations is too small. It is fair, however, to expect computers to increase over the coming years in such a manner that one million landmarks would be possible within ten years. In addition, domain decomposition techniques can be applied to break down the problem in smaller equivalents. A *cluster of workstations* may then solve the smaller problems in parallel, re-assembling the entire solution afterwards. See chapter 7, where this problem is posted as an open problem for further research.

6.5 A barchan dune

6.5.1 Problem description

A barchan dune is a type of dune resulting from a wind field with a strong current and dominant wind direction, acting on a relatively flat plane with particle sediments, grains, say. See figure 6–

19. Barchan dunes commonly appear in a spatial distribution, with a typical neighbouring scale in the order of $\mathcal{O}(10^1 - 10^3)$ m. Spatial distribution is assumed such that interaction among dunes is only faint and regarding a single dune on a further empty flat is justified. Barchan dunes "live" at the surface but their structural left-overs can also be found in the subsurface.

A barchan dune changes shape and migrates under the influence of the wind induced shear stress acting upon its upper surface. Height and position change gradually, but avalanching may cause abrupt changes in its topography. Here, barchan dunes are assumed to have shapes such that their height to length ratio $L_H/L_e \leq 0.05$. Various models have been proposed for the modelling of morpho-dynamic behaviour of 2D and 3D barchan dune models. In this thesis, a simple morphological process model will be used for a single dune, covering the erosional and depositional process plus the avalanching, taken from Stam [Sta94]. Aim is to evaluate the re-gridding capacity of the α-complex applied. Strictly speaking, triangulations also have this capacity but not the flexibility of α-complexes, for instance in the case of separations and in the context of erosion. The use of α-complexes therefore applied to a much wider class of dynamic behaviour, compared to triangulations. Moreover, icons of dunes are based on α-complexes. Emphasis will be on the handling of the topology avalanching stage. Avalanching will be induced merely on the basis of shear stress conditions, so that avalanches show up at unidentified moments in time. This way, evolution of the dune may be simulated in a single-stage, uninterrupted simulation, without any intervention.

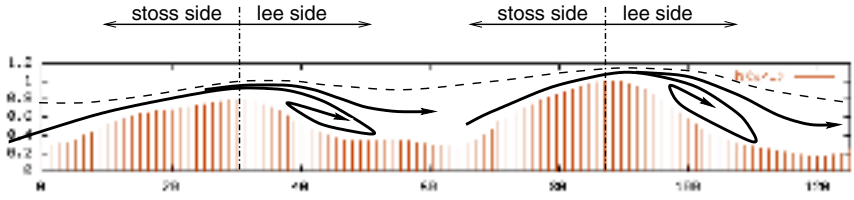

Figure 6–19: *Process model of the barchan dune. The dashed line marks the zone in which the wind velocity profile builds up. Outside this zone, the wind field is assumed undisturbed. At the stoss side, erosion takes away grainy sediments, to be deposited again at the lee side. The top of the dune accretes at the right and upwards. Avalanching discontinuously reduces height and slope.*

A one-dimensional process model

Consider a topographic surface plane described by a Cartesian coordinate system in E^3, in which positions are denoted by location vector $\vec{x}$. The shearing wind across the topography of this plane causes sediment particles to be transported by saltation. The sediment transport capacity, denoted by the vector function $\mathbf{q}(\vec{x}, t)$ in space and time, can be considered as a function of the wind induced shear stress $\tau(\mathbf{x}, t)$:

$$\mathbf{q}(\mathbf{x}, t) = F(\tau(\mathbf{x}, t)) \tag{6–3}$$

Furthermore, mass conservation (or: *sediment-continuity*) demands that:

$$\rho \frac{\partial h}{\partial t} + \nabla \cdot \mathbf{q} = R(\mathbf{q}) \tag{6–4}$$

where:

h	=	topographic height $[m]$
t	=	time $[s]$
ρ	=	sediment density $[kg \cdot m^{-3}]$
$\mathbf{q}$	=	sediment transport capacity vector per unit length $[kg \cdot m^{-1} \cdot s^{-1}]$
$R(\mathbf{q})$	=	sediment influx $[kg \cdot m^{-2} \cdot s^{-1}]$

Consider the one-dimensional form of equation (6–4):

$$\rho \frac{\partial h}{\partial t} + \frac{\partial q(x,t)}{\partial x} = R(q) \tag{6–5}$$

with the one-dimensional sediment transport equation given by:

$$q(x,t) = F(\tau(x,t)) \tag{6–6}$$

A simple $1D$-model can be obtained by adopting Bagnold's sediment transport equation (e.g., [Sta94]), for $1D$ of the form $q(x,t) = C_B \tau(x,t)^{\frac{3}{2}}$. Bagnold grouped a number of grain and other constants in the so called Bagnold constant C_B, dimension $[s^2 \cdot m^{\frac{1}{2}} \cdot kg^{-\frac{1}{2}}]$. An expression for wind induced shear stress $\tau(x,t)$ is not readily found. A linearised model can be obtained by assuming a linear relation between transport and shear stress with a linear correction term for the topographic height:

$$\tau(x,t) = \tau_0 + \tau_1(x,t) \approx \tau_0 + C_1 h(x,t) \tag{6–7}$$

where C_1 is a constant. Assuming a relatively smooth topography with small curvatures, the shear stress can be written as the above linear combination, where τ_0 is a constant for the shear stress, and τ_1 represents a correction term for the height, depending on place and time. An estimation of the cut-off error due to the linearisation can be taken from [Sta94, Ch. 4]. The assumed linear relation for the linearised sediment transport yields:

$$q(x,t) = C_B \tau_0^{\frac{3}{2}} + \frac{3}{2} C_B \tau_0^{\frac{1}{2}} \tau_1(x,t) = C_B \tau_0^{\frac{3}{2}} + \frac{3}{2} C_B C_1 \tau_0^{\frac{1}{2}} h(x,t) \tag{6–8}$$

Hence, one ends up with:

$$\frac{\partial h}{\partial t} + \frac{3}{2} \frac{C_B C_1}{\rho} \tau_0^{\frac{1}{2}} \frac{\partial h}{\partial x} = \frac{C_2 + C_B C_3 \tau_0^{\frac{3}{2}}}{\rho} + \frac{3}{2} \frac{C_B C_1 C_3}{\rho} \tau_0^{\frac{3}{2}} h \tag{6–9}$$

In equation (6–9), the term $\frac{3}{2}\frac{C_B C_1}{\rho} = v$ denotes the dune *migration velocity* in $[m \cdot s^{-1}]$ and term $\frac{3}{2}\frac{C_B C_1 C_3}{\rho}\tau_0^{\frac{3}{2}}$ is known as the *dune amplitude growth factor*. For positive right-hand side $R(q)$, for instance for the one-dimensional model:

$$R(q) = C_2 + C_3 q(x,t)) \tag{6–10}$$

the crest of the dune will move in de direction of the wind, the dune will increase height and the lee-side slope will become steeper. A valanching (to be discussed, shortly) is bound to occur. Figure 6–20 shows the dune evolution for a constant wind during $10^6\ s \approx 12$ days.

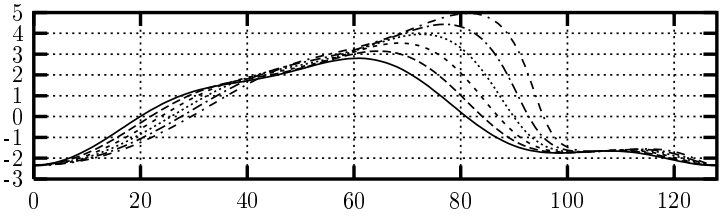

Figure 6–20: *evolving barchan dune during $t = 10^6\ s \approx 12$ days simulation time. The direction of the wind is left-to-right, constant strength. Observe that the crest of the dune moves right, increases height and that the steepness of the slip-face, the lee-side slope, increases over time.*

Avalanching, or *land-sliding*, is a complicated phenomenon that occurs frequently in nature. In this case, avalanching is assumed to take place along a planar slip-face. Let $\mathbf{s}$ denote a unit vector along the slip-face (see fig. 6–21) and $\mathbf{g}$ be the gravity vector. Then in the case of the evolving dune, the term $\mathbf{g} \cdot \mathbf{s}$ increases as the slope gets steeper due to sedimentation. In contrast, the shearing resistance that can be delivered by the interlocking grains remains constant. When roughly equal, a zone of slope instability appears and a slight disturbance may trigger the avalanche. Once started, moving grains affect other grains in the slip-face and as a result, grainy material slides down the slip-face, leaving the slope at a decreased angle, known as the angle of repose γ_r. At this steepness, stability has returned and the process of deposition and angle increase starts all over again, heading for the next avalanche. Figure 6–21 sketches this.

Emphasis will be on the handling of numerical complications due to avalanching. In the case of the barchan dune model, using an α-complex has hardly any decisive advantages over for example a triangulation. Except for the handling of separations and holes. To explore the capacity of an α-complex in numerical modelling, the relatively simple application of the barchan dune has been selected as a first case.

6.5.2 Data set

The process model is used to generate landmarks for the evolutionary landmark set. More precisely, the process model predicts the 1D dune profile over time, according to equation (6–5). The resulting evolution of the dune profile has been adopted for a finite thickness around a centralcross section of the barchan dune. The profile defines the *topography* of the dune, a reference plane chosen at an arbitrary altitude below the dune profile defines the dune "bottom"

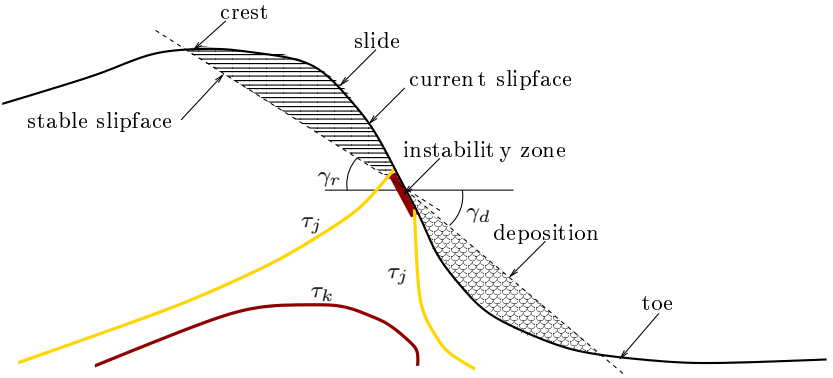

Figure 6–21: *sketch of the anatomy and principle of an avalanche. Observe the zone of instability, bounded by the contours of τ_j hitting the slope, inducing the avalanche. For mass conservation, the sliding volume must be equal to the deposited volume. Also notice that avalanching prevents the dune from growing to infinite height.*

plane. The begin and end plane of the dune topography are chosen remote from the dune itself, to minimise the local effects of boundary conditions. The interior space between the so defined boundaries is then populated with grid nodes laid out with a regular spacing. Altogether, after triangulation, this yields a quasi-$3D$ cellular complex, from which α-complexes can be filtered off. The quasi-$3D$ model strikes out most of the hairy details of a true $3D$ model, and grasps *quod est demonstrandum* equally well. Value sets are not generated: the dune material can be considered homogenous and unsaturated.

6.5.3 Data analysis

The typical nearest neighbour distance is in this case directly tied to the step size Δx at which the dune profile is being computed and populated. In this case, $\Delta x = 1\ m$ or, equivalently, $\Delta x/L = 0.01$, where L is the length of the dune (figure 6–19). Notice that the so generated landmark set is formally not a Poisson point process and landmarks are not randomly distributed in space.

6.5.4 Numerical model

A 4-th order Runge-Kutta scheme has been used to solve equation (6–4). A central difference scheme can be followed to find spatial derivative $\frac{\partial}{\partial x}h(x,t)$. The grainy material is assumed unsaturated so that the effective stress is equal to the total stress. A further assumption is that in the slip-face, the role of the normal stresses is minor, so that the critical stress $\tau_{crit} = c + \sigma_n \tan\phi \approx c$, where c denotes the *apparent cohesion* resulting from grain interlocking. The apparent cohesion can be taken from diagrams existing for various grainy and other materials, e.g., see [Bru79].

The numerical model aims at the computation of the shear stress along the slope, and predicts the instability zone in this slope. This zone is assumed to become unstable when the

shear stress right beneath the surface exceeds some critical value, i.e., when $\tau \approx \tau_{crit}$. Avalanching may then start in this zone. The instability zone is centred around the steepest point. As soon as a certain fraction ϵ of the slope has become unstable in the model, an avalanche is said to take place. The movement of the grains in an avalanche is assumed kinematically determined by the angle of repose.

An α-complex has been used to describe the numerical model. An α-complex, in terms of numerical computing, is generally an *unstructured grid*. The finite element method (FEM) was chosen as the analysis method to apply. A simple linear-elastic tetrahedral element with nodal displacements as degrees of freedom. The set of k-faces $\{\sigma_{\mathcal{C}_\alpha}^{(k)}\}$ of an arbitrary α-complex, as outlined in figure 2–13 in chapter 2, cannot be inserted straightforwardly into a regular FEM-code. Before we can run a finite element analysis (FEA) on an α-complex, three major problems, directly owing to the composition of the set of faces $\{\sigma_{\mathcal{C}_\alpha}^{(k)}\}$, have to be resolved:

1. The removal of singular faces.
2. The problem of separated interiors.
3. The problem of sliver-like d-faces.

Singular faces

Obviously, in a FEA formulation, we want to end up with only complete d-faces. Complete in the sense of *topologically complete*: a complete d-simplex with all its sub-faces. In customary FEA-approaches, singular faces need to be removed first. For any value smaller than $\alpha_{\max}$, there is a chance that such singular faces occur. The physical meaning of singular faces is unclear. From a modelling point of view, they show how the α-complex tends to grow if α is slightly increased. Removal of singular faces is trivial and causes no further problems, which is easy to understand in conjunction with the embedding-approach to be discussed now.

Embedding the α-complex

For $\alpha < \alpha_{max}$, α-complex $\mathcal{C}_\alpha$ is not necessarily connected. To circumvent this problem, we explored the fact that triangulation and α-complex share the same faces. Which implies that an α-complex can always be *embedded* in a triangulation, in accordance with Observation 2.9. A triangulation is connected. This approach will be further explained, shortly.

Slivers

Slivers are simplices with very bad aspect ratios, or shape parameters. For example, a tetrahedron with one edge that is extremely small compared to its other edges. Slivers are primarily developed near the boundary of the convex hull of $\mathbb{S}$ and enter the α-complex at the highest values of α just prior to reaching $\alpha_{\max}$. Figure 6–22 sketches this.

Slivers are hardly ever present in the α-complex itself, but they are present in the embedding triangulation of course. They must be removed from the triangulation if the FEM-code repulses them. In the vast majority of cases, this can be done without the risk that separations reappear. More on this, shortly.

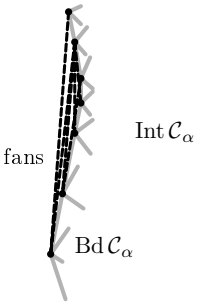

Figure 6–22: *the generation of slivers near the border of the convex hull when α approaches $\alpha_{\max}$, when an increase of α allows "fans" in the triangulation near the border of its convex hull to enter the α-complex.*

Figure 6–23: *fragment of the barchan dune grid at time $t = 0$ s. The form of the dune is easily recognised in the grid. The grid contains two fans along the top boundary with (necessarily) a elevation of the profile (to the right of the toe of the slip face) separating them. Decreasing $\alpha_{\max}$ a bit will easily remove the slivers adjacent to the slip face.*

The embedding approach

A new approach has been developed to run FEA over α-complexes, that overcomes the problems of singular faces, separations and slivers, identified in the previous section. The outline of this approach is as follows. Firstly, tetrahedra of the α-complex model ("foreground material") are turned into tetrahedra FEM-elements. This α-complex of the object is embedded in the hosting triangulation ("background material") that acts as the embedding environment (or: "bulk"). After applying suitable boundary and/or initial conditions, computations can be started. Since dealing with a 3D-model, the d-face is a tetrahedron, but the approach applies to d-simplices of any dimension. The approach developed here exploits the fact that an α-complex is a subcomplex of the triangulation. A triangulation, which is a cellular decomposition *continuum*, can always be input to an FEM-code, and *boundary conditions* can be attached to its boundary faces. Rather than taking the bulk at $\alpha_{\max}$, we lower α somewhat to get rid of slivers. More in detail, the steps to follow are:

Step 1: select an embedding background α-complex

Compute the α-family and select an embedding background α-complex close to the triangulation. Select the largest sliver-free α-complex. Possibly a trial-run may be needed to find out which tetrahedra can be accepted by the FEM-code, and which cannot. If the shape-test is explicitly indicated, a preprocessing step may be conducted, before submitting the model to the FEM-code. Once a bulk-α-complex has been found acceptable,

background material properties (or: "bulk"-properties) are assigned to the elements of the embedding α-complex.

Step 2: determine the boundary of the embedding background α-complex

If $\alpha \leq \alpha_{max}$, this boundary is no longer the boundary of the convex hull of $\mathbb{S}$. We also assumed that the background α-complex is connected and hole-free and therefore has no internal boundaries. Compute the normals of all the triangles in the boundary of this α-complex, in order to find out how boundary conditions need to be attached to the embedding α-complex.

Step 3: select the foreground α-complex

Select the α-complex representing the foreground material of the modelled object. In this case, this is the α-complex that best represents the barchan dune. Assign foreground material properties to the object model α-complex. Next, "inject" this complex into the embedding background-complex, i.e., for each tetrahedron in the foreground α-complex, locate the corresponding tetrahedron in the embedding background complex, and flip the background material properties to foreground properties. If applicable, initial conditions may be assigned after this step.

Step 4: run the FEA-analysis

Run the FEA-analysis and optimise the α-complex as appropriate. If modelled objects erode, foreground material may decay into background material. If completely eroded, only background material is left. Accreting material may cause background material to turn into foreground material, up to a complete disappearance of the background material.

A few additional words will be spent now on the selection of background material properties. In order not to (significantly) influence the results, background material properties must be "neutral": an order of magnitude more permeable, stiffer, conducting, etc., which depends on the physics underpinning the model.

6.5.5 Results

The dune evolution was simulated over 1 million seconds, at a time step $\Delta t = 1000$ s. A value of $C_B = 0.867\ s^2 \cdot m^{\frac{1}{2}} \cdot kg^{-\frac{1}{2}}$ was specified for the Bagnold constant, which is relatively high but speeds up the evolution. A value of $\tau_0 = 0.150\ Pa$ has been used. Further, regular unsaturated dune sand parameter values were taken. Given the value of $h(0,t)$, a compatible transport $q(0,t)$ at $x = 0$ can be computed from $C_B(\tau_0 + C_1 h_0)^{\frac{3}{2}}$, for the non-linearised version of equation (6–9). At the toe-side (figure 6–21) of the dune, at $x = L$, the boundary condition inflicted is that $\left[\frac{\partial}{\partial x} h(x,t)\right]_{x=L} = 0$.

Selecting the embedding background (step 1) is trivial in this case. As revealed by figure 6–23, slivers occur near the slip face (and also near the stoss side not shown in this figure). Lowering α delivers an embedding environment that in this case is nearly identical to the dune α-complex (step 3) itself. Moreover, since the dune α-complex contains no separations, embedding is not even necessary in this case. Embedding a hole- and sliver-free α-complex in *itself* is by no means in contradiction with the embedding approach outlined. Finding the "right" α-value (step 3), comes down to match the volume of the α-complex with the volume estimated by equation (6–8).

At every 0.2 Ms (1 $Ms = 10^6$ $s \approx 12$ days), the shear stress has been recomputed. Figure 6–24 shows the results.

As the dune evolves, the steepness of the slip face increases and the crest of the dune rises and rises. The critical shear stress contour moves from the bottom of the dune, under the lower part of the slip face, upwards. See figure 6–24. When it reaches the slip face, the critical shear stress seeds a zone of instability, as sketched in figure 6–21 and easily identified in figure 6–24. At some point, avalanching will occur along a not necessarily flat plane more or less parallel to the slip face, along which the shear stress between grains surpasses the critical value for slope stability. The movement of the sediment in the avalanche is kinematically bound to take place along this plane. The FEM-computations aim at the finding of this sliding plane and the moment of reaching the critical value. When surpassed, the avalanche takes place in the model, i.e., grid points of the affected area "slide downhill" along the plane, towards the toe of the dune, until the moving mass comes to rest at the toe of the dune. The sediment-transport, meanwhile continues and the process repeats if the conditions tell so.

In the process of avalanching mass conservation needs to be obeyed. The density of the downhill deposited material is assumed similar to the sliding material uphill, so mass conservation comes down to volume conservation. A "residue"-approach has been followed: when assigning new locations to the displaced material, we laid out new grid nodes at preferred, evenly spaced locations. To maintain this approach, a certain *mass residue* may result after the processing of the avalanche. The residue of the current step will be equalised in the next avalanche and in the long run, the residue will be kept close to zero. No aggregation of residue is allowed.

The process of erosion/deposition, shear-stress computations and avalanching takes place in a single continuous non-interrupted cycle made possible by the capacity of the α-complex to re-grid, to uniquely restore its topology on the basis of distances between points.

6.5.6 Discussion

The stress model maintained over time identifies the occurrence of avalanches. Avalanches change the topology of the numerical model. Due to the capacity of an α-complex to reconstruct its topology, the erosion, shear stress computations and handling of avalanches can be processed in a single non-interrupted iterative computation, allowing an evolutionary process model to evolve by uninterrupted time-stepping. The use of an α-complex is an effective solution to the regridding problem in modelling phenomena such as the avalanching: grid nodes may freely roll down the slip face, after which re-computation of the complex follows. In this case, a re-triangulation might have accomplished the same result, but generally, an α-complex allows for a much wider class of topological changes to occur, up to complete separations. The embedding approach allows such models still to be captured in a single numerical model. This opens up new possibilities for birth-life-death type of models, such as deposition/erosion models and dynamic topology models in general. Not discussed here, but certainly a topic for further research is the use of control volume finite difference methods instead of finite elements.

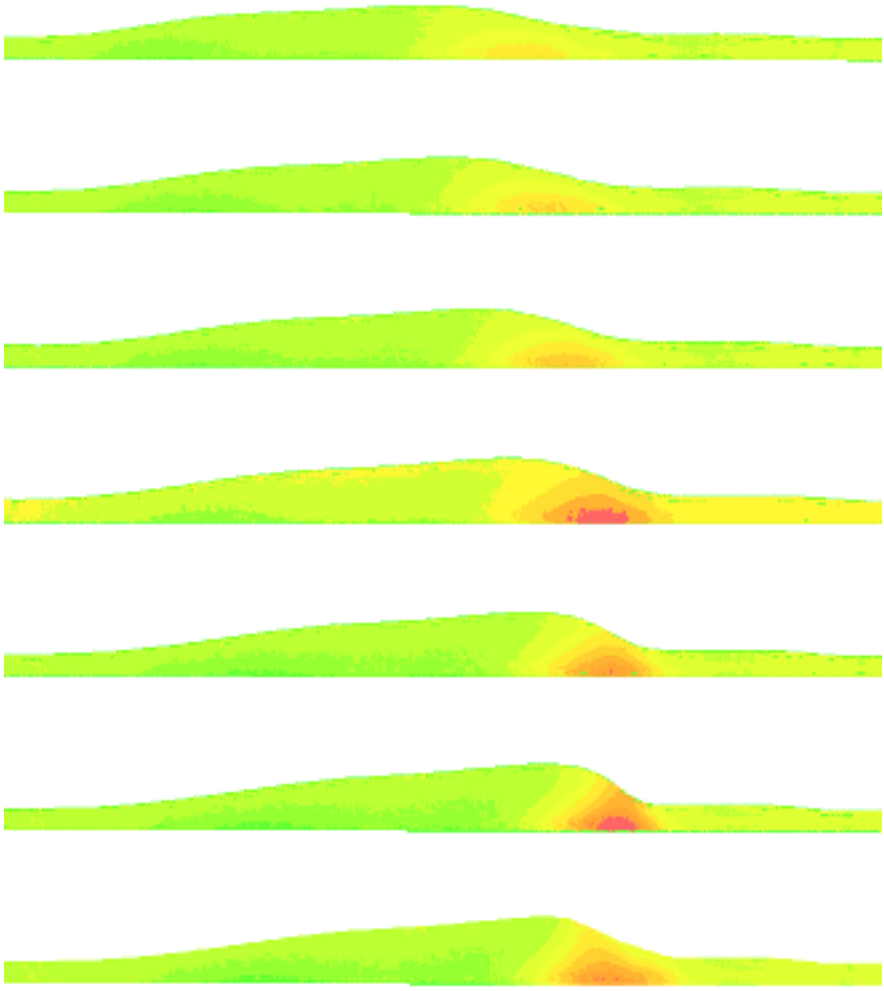

Figure 6–24: *top-to-bottom: time series of dune evolution. Pictures depict the shear stresses τ_{xy} at $t = 0\ s$ at the top to $t = 1\ Ms$ $(10^6\ s)$ at the bottom. The bottom two picture show the handling of the avalanche. The pictures top-down show how the instability zone slowly builds up. The second picture from the bottom shows the shear stresses right before avalanching takes place. The instability zone is easily identified. The bottom picture shows the shear stresses right after avalanching has taken place.*

Figure 6–25: *Example of the complex, partly labyrinthine, partly jig-saw morphology of a meandering river system. Picture shows a* 2.3×2.6 *km area of the Milhako river, Alberta, Canada. Observe the frequently reworked depositions (*scrollbars*) on the river banks at the inner bends. Also the clay-/mud-filled "dead" river channels, abandoned after a short cutting "neck chute". The point bars form a labyrinth of permeable flow-channels and are able to trap hydrocarbons. Well design and reservoir simulation is a tedious task in such a reservoir. Photo taken from Allen (1985). Copyright ©: Alberta Energy Company. Reprinted with permission.*

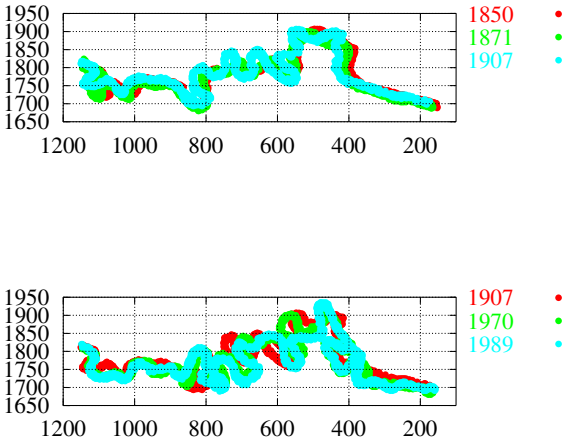

Figure 6–26: *The river Bollin, near Wilmslow, Cheshire, Northwest England, as observed over a time frame of nearly one-and-a-half century, from* 1850 *up to* 1990. *Top: development during the late 19th century, bottom: evolution during the 20th century (data taken from [BHTP92]).*

6.6 Modelling point bars

6.6.1 Meandering river systems

River system can be subdivided in many respects. One such subdivision sets braided river systems apart from meandering river systems. Under certain conditions, river systems start to meander, mostly when they have become *mature* ([RS80]), i.e., in their middle section. Sinuosity can be low or relatively high and may alter on a given part of the river during its lifetime. Upstream, when in their youth, rivers are often running on gravel beds and sediment load is often relatively coarse rock debris. This part of the river system can be characterised as gravel-rich and low sinuosity. Most rivers systems in their maturity tend to migrate towards mixed sediment load systems, in which sand from erosion, downstream transported rock material and finer clay, mud or silt material is found in some mix, and sinuosity will generally be higher. At this stage, river systems will be denoted as sandy fluvial systems, to be offset from gravelly or bouldery systems.

Many process-models have been developed to model the process of meandering and their evolvement in time. For instance [WR69, CG76, Mia78, Wal80, RS80, All85, Ric87, DS90]. A recent state-of-the-art can be taken from [BHTP92]. The models developed so far take many input parameters on alluvial plane topography and river geometry, discharge, sediment load and characteristics, climate, etc., but it is now recognised that additional *human factors*, such as land use, urbanisation and engineering measures, must be known to come up with reasonable simulation results. See for instance Hooke and Redmond in [BHTP92]. In this thesis, such models are left undiscussed further. An important parameter thereby is the "erodibility" of the

river banks versus the erodibility of the river bed. It is assumed here that the river banks erode easily enough to allow meanders to grow. In that case, meanders tend to grow outward and downstream in various fashions, meanwhile depositing material in their inner bends. Coarser material at the foot of the inner bend, finer material more upward. The outwardly accreting inner bend is known as a *point bar*. When the discharge regime changes, the formation of the current point bar may come to an end and another point bar, with slightly different configuration, grow path, steepness, etc., may start to grow where the former point bar terminates. This way, a so called *composite point bar* may be formed, as a succession of various individual point bars in the same meander. Figure 6–27 sketches this process.

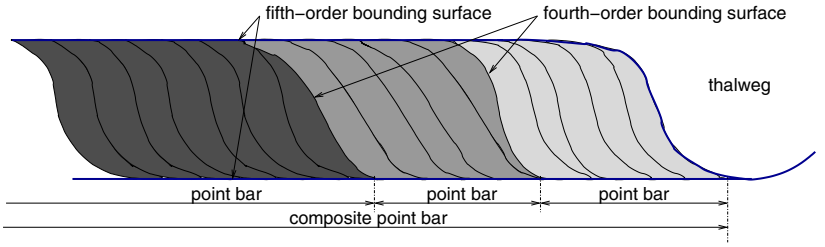

Figure 6–27: *Sketch of a composite point bar, consisting of a succession of individual point bars separated by third- and fourth-order boundary surfaces and bounded by fifth-order surfaces.*

A common value for the migration velocity of meanders is $\mathcal{O}(10^0 - 10^1)\ m/A$, but it depends on many parameters. The curvature of the meander increases until the neck breaks trough ("neck shute"). This leaves behind a mud-filled dead channel, or *oxbow lake* which by itself may gives room to a renewed extension of a meander. Once in a while, usually seasonal, the river will be flooding and the entire alluvial plane or river valley will be flooded by commonly fine grain material such as fine sand or clay. If seasonal, often multiple (composite) point bar systems can be found: a low discharge point bar system and a flooding discharge point bar system, in which the tidal area of the low discharge point bar often gets carved by small scale chutes and cut-off channels and lobes. In this case, those features will be neglected. Also, paleosol and lag depositions will be neglected. Vegetation and other influences often create a usually carbonate paleosol on top of the composite point bar. At the toe of the point bar, at the river bed, coarse rock material that cannot go into suspension, will be deposited. This may create a distinct thin layer of relatively coarse material. To sweep off unnecessary details, it will be ignored in this case study.

In a longer time frame, the river may form an alternate *avulsion point*, i.e., choose an entirely other branch or *thalweg* (figure 6–27). Assuming a net influx of sediment, the valley in which the river bed is located will tend to fill up by the stacking layers of river depositions, deposited in the various *geomorphic cycles*. Meanwhile, meandering avulsion and other processes and events may cause erosion to occur. As a result, the topology may become extremely complicated. A real-world example can be taken from figure 6–25, which shows a 2.3 by 2.6 km area of the Milhako river, Alberta, Canada and from figure 6–26, which maps the development of meanders of the river Bollin, recorded over a longer period. Most of the river system features discussed here can be recognised in this picture.

Point bars are of interest to the oil- and gas industry because when buried, they may form structural traps for hydrocarbons. The result is a channel system of dead and connected channels

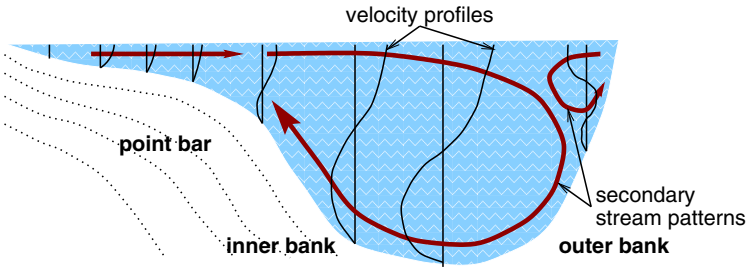

Figure 6–28: *Secondary flow in meander cross section, with velocity profiles. Left: point bar in the inner bend. The top of the point bar is commonly finer material, deposited in ripple lamination, the lower part if commonly coarser material, deposited as trough-shaped cross-stratified sets.*

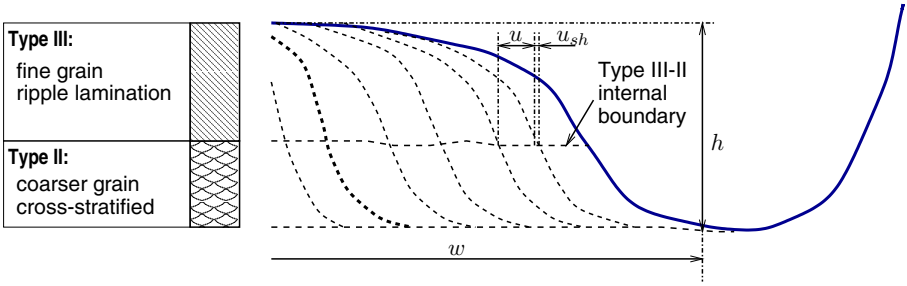

Figure 6–29: *point bar flow types. The flow type III top of the point bar consists of finer material, deposited in ripple lamination, the low erpart, flow type II, consists of coarser material, deposited as trough-shaped cross-stratified sets.*

of more or less permeable sands, covered and dissected by impermeable clay or silt sheets. To model such a reservoir, for instance for infill drilling, is beyond today's technical reach. In the case to be discussed here, a simple geometric point bar model is a first objective. The geometric point bar model will be obtained by stochastic simulation. Next, fluid flow simulations are to be conducted in the direction of the meander and perpendicular to the meander. Finally, erosion will be inflicted on the point bar and fluid flow computations will be repeated to study the effect. The numerical modelling of the point bar, though much more complicated, builds upon the results of the barchan dune. Without the approach outlined in section 6.5.4, numerical computations as to be carried out here would not have been possible.

6.6.2 Data set

The landmark and value sets were constructed using a Monte Carlo technique on measured data from fluvial outcrop studies of the Tortola fluvial system in the Loranca Basin in Central Spain by Martinius in [Mar96]. Characteristic dimensions and rock/grain parameters were drawn from these outcrop studies. The composite point bar of the medial area, ("type B, geomorphic zone 3") served as a model for the point bar. Its parameters were input in a point process resulting in a stochastic landmark set and the resulting α-complex will further be used as a basis for fluid flow computations. Figure 6–29 sketches the two *flow unit* types constituting the point

bar: the *genetic type* point bar is further subdivided in flow unit types, according to litho-facies, petrographic (internal) boundary surfaces, permeability distribution and gamma-ray response. Table 6–11 captures the geometric parameters for both flow unit types.

			Sand		Silt	
Parameter	Symbol	Unit	II	III	II	III
thickness	$\bar{u}$	m	5.8	5.8	0.12	0.12
	Δu_{max}	m	1.7	1.7	0.04	0.04
width	$\bar{W}$	m	68.0	68.0	68.0	68.0
	ΔW_{max}	m	26.1	26.1	26.1	26.1

Table 6–11: *Characteristic parameters of the Type II and III flow unit type. Refer to figure 6–29 for the definition of the thickness and width. No parameter values were found on the thickness of the separating clay/silt sheet u_{sh}.*

The landmark set of the point bar has been stochastically simulated by drawing samples from a type III flow unit on top of a type II unit. Starting at some geological age A_0, the composite point bar starts to accrete with a point bar plus silt drape per seasonal cycle T_{cyc}, in which one period of failing discharge and one period of high discharge are adjoint. The seasonal cycle parameters used in the simulation are $T_{cyc} = 0.001\ kA$ and for avulsion $T_{avul} = 1.000\ kA$. Meanders were assumed symmetric and an arc can be specified around this axis of symmetry over which the point bar deposits. The following parametric function was used to describe the basic point bar shape in a two dimensional cross section (see figure 6–30):

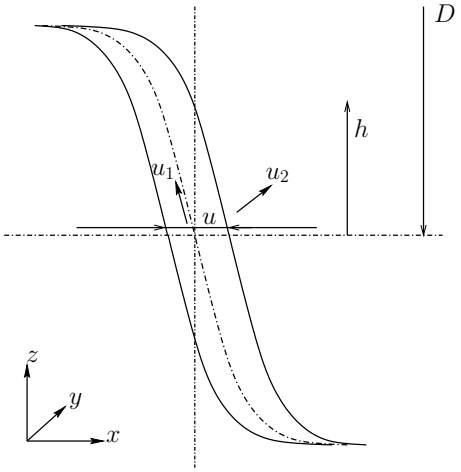

Figure 6–30: *sketch of the point bar model anatomy used for stochastic simulation. For an explanation of the parameters, see text.*

$$\mathbf{x}(\mathbf{u}) = (u_1, u_2, -h\ \mathrm{erf}(\tan\beta\ u_1 + u) + D) \tag{6–11}$$

where:

h	=	height of the point bar $[m]$
β	=	slope of the point bar $[rad]$
u	=	thickness of the point bar at central altitude $[m]$
u_1	=	trajectory coordinate along bottom-to-top central axis in the cross section $[m]$
u_2	=	trajectory coordinate along the outer boundary of the point bar, orthogonal to the cross section $[m]$
D	=	depth of the point bar $[m]$

In equation (6–11), u, u_2, h and D are assumed to be constant over time, but $u_1 = u_1(t)$. A "slab" of landmarks is created this way, later on to bended and confined according to the meander geometry. Furthermore, if $u_1 > \rho(u_{1_{max}} - u_{1_{min}})$, the sample is assumed to lie above the internal bounding surface between unit type II and type III and belong to unit III. Next, a standard uniform random number r is drawn on the domain $[0, 1)$, and stochastic deviation is added as follows:

$$x_i = x_i + (2r - 1)n_{i_{max}} \tag{6–12}$$

where $n_{i_{max}} = f_i(Var(x_i))$, in other words, the maximum stochastic deviation is determined by the implied variance in that direction.

The value sets are primarily composed of petrophysical properties. In a Monte Carlo-based stochastic realisation as for the geometry, samples are drawn from the distributions given in [Mar96].

			Sand		Silt	
Parameter	Symbol	Unit	II	III	II	III
permeability	K	D	1.7	3.7	0.090	0.124
	ΔK_{max}	D	0.8	1.2	0.008	0.10
porosity	$\bar{R}$	[.]	0.102	0.102	0.51	0.51
	ΔR_{max}	[.]	0.06	0.06	0.22	0.22

Table 6–12: *Characteristic parameters of the Type II and III flow unit type. Effective permeability K is obtained from vertical and horizontal permeabilities found from Darcy's law and single-phase fluid flow simulations on a homogenised grid. Refer to [Mar96, App. I] for details.*

6.6.3 Data analysis

The petrophysical parameters turn out to be distributed according to a lognormal distributions. In the stochastic simulation, random uniform samples are therefore drawn and "weighted" against a lognormal distribution, before transformation: accept if $f(u) <= \text{lognormal}(u, 1., .01)$, reject otherwise, with:

$$f(u) = \frac{1}{\sigma u \sqrt{2\pi}} e^{\frac{-(\ln(u)-\mu)^2}{2\sigma^2}} \tag{6–13}$$

Figure 6–31 shows a clear separation of the property clusters (in property space) of the type III and the type II flow units. Although pore surface A_p and grain surface A_g are not independent

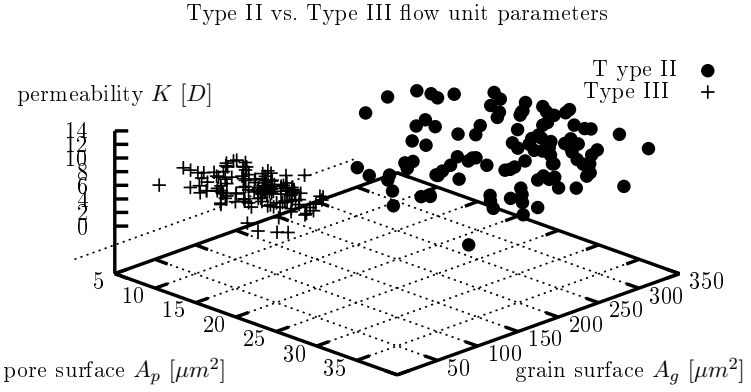

Figure 6–31: *Petrophysical parameters of flow unit type II and III. Cross plot of effective permeability K against pore surface A_p and grain size A_g. Pore surface is defined as a surface within a certain measurement area. Porosity as a fraction can be obtained by linear transformation.*

and probably their dimensionless ratio A_p/A_g should be considered instead. The differences in permeability are relatively small, which should be kept in mind for the fluid flow numerical model to be developed.

The bounding surfaces of third-, fourth- and fifth-order are believed to form impermeable baffles, kinematically restricting the fluid flow ([Mar96, pg. 36]). The internal bounding surfaces are partly formed by silt drapes and mud/clay sheets, deposited in times of flooding and paleohydrodynamic changes. The result is a system of permeable (upward-fining)sandstone embedded in mud- and siltstone. The progradation and retrogradation of the river system, along with a corresponding change of geomorphic conditions, is believed to play an important role in the eventual connectivity of the labyrinthinestructure of channels ([Mar96, General conclusions])

6.6.4 Weighting

The weight is taken dependent on the position within the point bar. Let $\bar{u_1}$ denote a normalised parametric variable on the domain $[-1, 1]$ running along the central line bottom to top along the cross section of the sandy point bar and the silt drape. The shape of the point bar is such that it confines as $|\bar{u_1}|$ increases, that is, when moving away from the central altitude towards top or bottom. The same is true for angle ϕ moving away from the central hart line of the meander, where the point bar has its greatest thickness. The normalised weighting here is done by means of a weight function:

$$w(u_1, \phi) = \cos\phi - |\bar{u}_1| + C \tag{6–14}$$

where C is a constant, and the global weighting is done according to properties: higher weight for silt, lower for sandThe intention is to "highlight" the silt drapes. Notice in equation (6–14)

that the cosine is an even function. For a height h of the point bar, with $h = 0$ for $u_1 = 0$, we have that $\bar{h} \in [-1, 1]$ and $\bar{u}_1 = -1 \Leftrightarrow \bar{h} = -1$, $\bar{u}_1 = 0 \Leftrightarrow \bar{h} = 0$ and $\bar{u}_1 = 1 \Leftrightarrow \bar{h} = 1$. The stochastic realisations of the weight "profiles" for the normalised weight along the normalised height within the point bar and the normalised angle around the centaxis of the meander is shown in figure 6–32 and 6–33, resp.

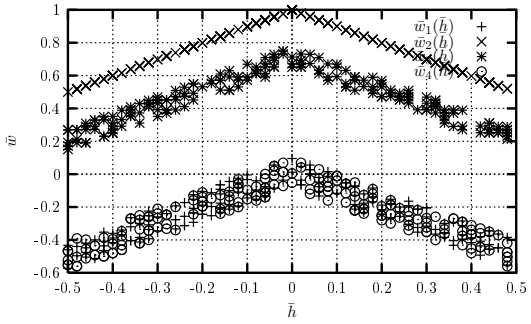

Figure 6–32: *relative weight distribution $\bar{w}(\bar{h})$ over point bar height h, at relative height h_{-1}, h_0, $h_{.75}$ and $h_{.95}$. Weight changes smoothly over the relative heights.*

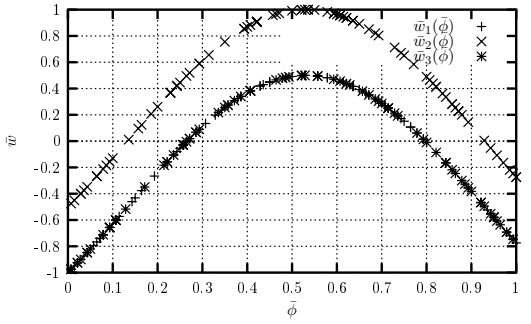

Figure 6–33: *relative weight distribution $\bar{w}(\bar{\phi})$ over point bar angle ϕ. The relative weights at three three characteristics angles are shown: $\bar{w}_1$ at $\phi_{-\pi/2}$, $\bar{w}_2$ at ϕ_0 and $\bar{w}_3$ at $\phi_{\pi/2}$.*

6.6.5 Geometric modelling results

Figure 6–34 shows the cross sections of the point bars so obtained. Appropriate transformations can bend them into the "arc" of the meander. Figure 6–35 shows the final result. The right picture in figure 6–35 clearly reveals the silt drapes, defining the inner flow channel structure.

6.6.6 Numerical modelling results

Like with the barchan dune, the embedding approach outlined in section 6.5.4 has been followed. The objective was to find a plausible inner structure for the point bar, subjected to overall constraints, focusing on fluid flow computations. Meanwhile, a more comprehensive understanding

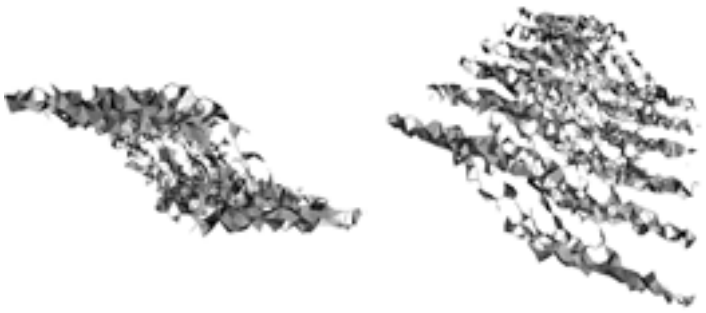

Figure 6–34: *Resulting α-complex of a 2D point bar cross section (left), and a series of such cross sections (right).*

Figure 6–35: *α-complex of a point bar system. Left: oblique view, right: cross section. Observe the silt drapes in the cross section.*

should be gained of the physical meaning of tunnels, pockets and voids. This lead us to work out two further approaches:

A clay bulk complex with a sandy complex injected

Tunnels, pockets and voids represent barriers, plugs, clay inclusions, etc. This approach is fine for the secondary flow directions, but less meaningful for the principle flow directions.

A sandy bulk complex with a clay complex injected

Tunnels, pockets and voids now represent high permeable channels. From a computational point of view, this is the preferred approach for principle flow directions.

The selection of an appropriate approach will also be directed by the kind of input data available.

First, an overall velocity field was computed for simple fluid flow across the monolithic point bars at regional scale. This gave an indication of the Darcy velocities, water pressures, and hydraulic conductivities for the point bars as a whole. Then, the internal structure of the point

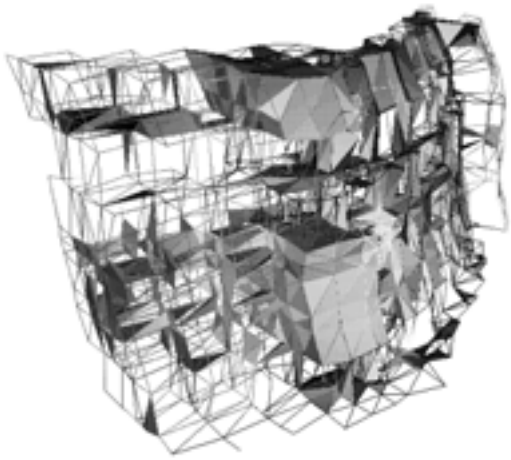

Figure 6–36: *injected, heavily eroded sand point bar for fluid flow computation on a stochastic point bar α-complex. Shown are the tetrahedra plus the singular edges, removed before the actual FEM-computations commence.*

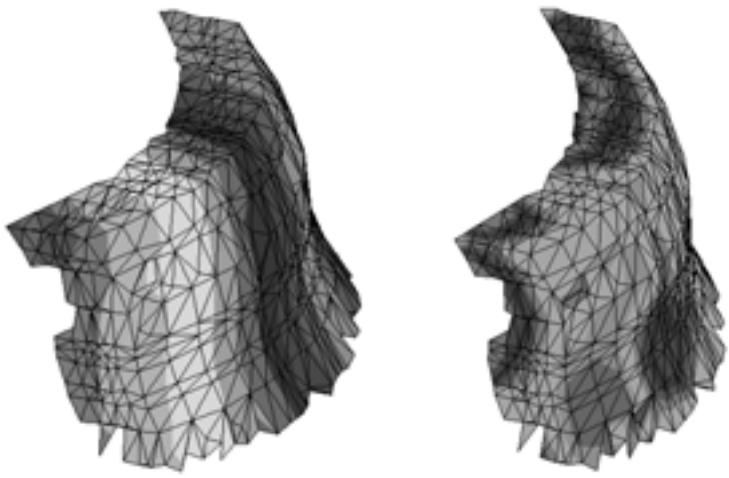

Figure 6–37: *fluid flow computation on a synthetic point bar α-complex. The point bar has been created by "injecting" a heavily eroded sand α-complex into a clay bulk. Left: pressure distribution in x-direction, parallel to the point bar's internal structure, right: pressure distribution in y-direction, perpendicular to the internal structure.*

bars was refined by stochastic simulation of the silt drapes. For various values of α, conductivities were re-computed, imposing the overall regional ("up-scaled") conductivity as a physical constraint. Next, the fine-scale conductivities were computed using a commercial finite element code, employing combined linear stress/single phase fluid flow computations. The commercial code, not by any means designed to be fed with awkward FEM-grids, acted repulsively on the injected α-complex. Prescribed grid element aspect ratio tests are way too restrictive for this kind of numerical models. The most effective solution would be to lift the input restrictions. This was not feasible, however. Therefore, the model has to be adapted. The geometric model had to be modified such that the most critical parts were eliminated. The modified α-complex "injected" is shown in figure 6–36. The results of fluid flow computations, the pressure distribution in x-direction, parallel to the point bar's internal structure, and the pressure distribution in y-direction, perpendicular to the internal structure, are shown in figure 6–37.

6.6.7 Discussion

Using the parameters collected on outcrops, the defined stochastic simulation model appears to be able to generate fairly realistic point bar models, from a geometric point of view. Deterministic process models can be found in literature, though, but stochastic models were not found. The initial problems with the numerical simulation are entirely due to the severe shape aspect ratio constraint imposed on the numerical grid elements. The constraints are imposed with in mind, freely generated grids in typical engineering problems. Relaxing the constraints is one way to get around (not possible in this case), using an alternate FEM-code is another. FEM codes used for this purpose were by no means meant to cope with geometries of this nature. It would therefore be interesting to evaluate alternate FEM approaches, such as the edge element, dual grid approach proposed in [Bos98]. This aspect will not be discussed any further in this thesis. Rather, it will be posted as an open problem in chapter 7.

One may further raise the question of finding some optimal α-value, related directly to the computed hydraulic conductivity. As might be expect, it turned out to be impossible to find an optimal α for both the horizontal and the vertical conductivity. Optimisation is only possible for a combination.

6.7 The L8-icon shape family instantiation

6.7.1 Problem description

This case is a bit of a bold one among the others in this chapter. This case seeks to demonstrate the shape family instantiation from the L8-icon. This is an important building block in the modelling framework introduced in chapter 3. For a quick glance, review figure 3–2. Given an icon, derived as discussed in chapter 3, instantiate a shape family using affine and shear transformations.

6.7.2 Resulting L8 shape-family

Figure 6–38 shows a linearly (affinely) transformed shape family, figure 6–39 a sheared family of a section of the L8 meandering river icon. The central shape is always the icon. Shapes along

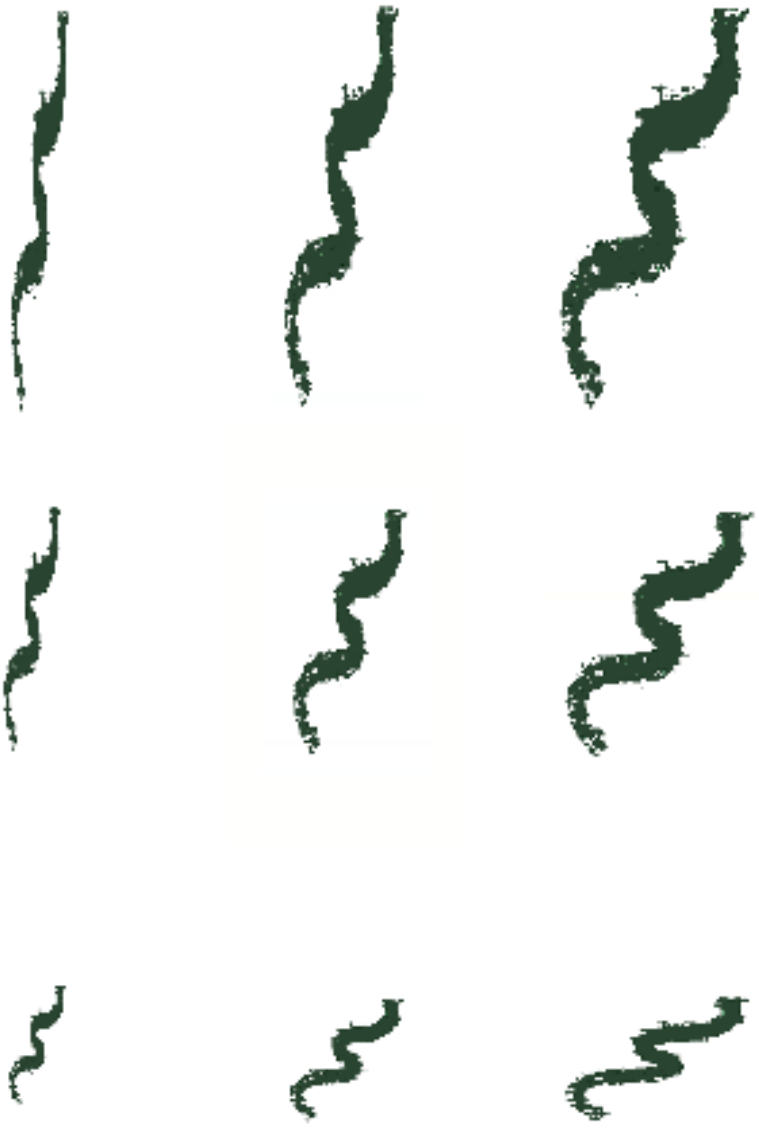

Figure 6–38: *linearly (affinely) transformed shape family of a section of a meandering river, transformed by a scaling transformation. The centre shape is the icon, left-to-right is a scaling of X by a factor .5, 1. and 2.,resp., bottom-to-top is a scaling of Y by a factor .5, 1. and 2., resp. Icons on the diagonal bottom-left to top-right have identical shape as the icon.*

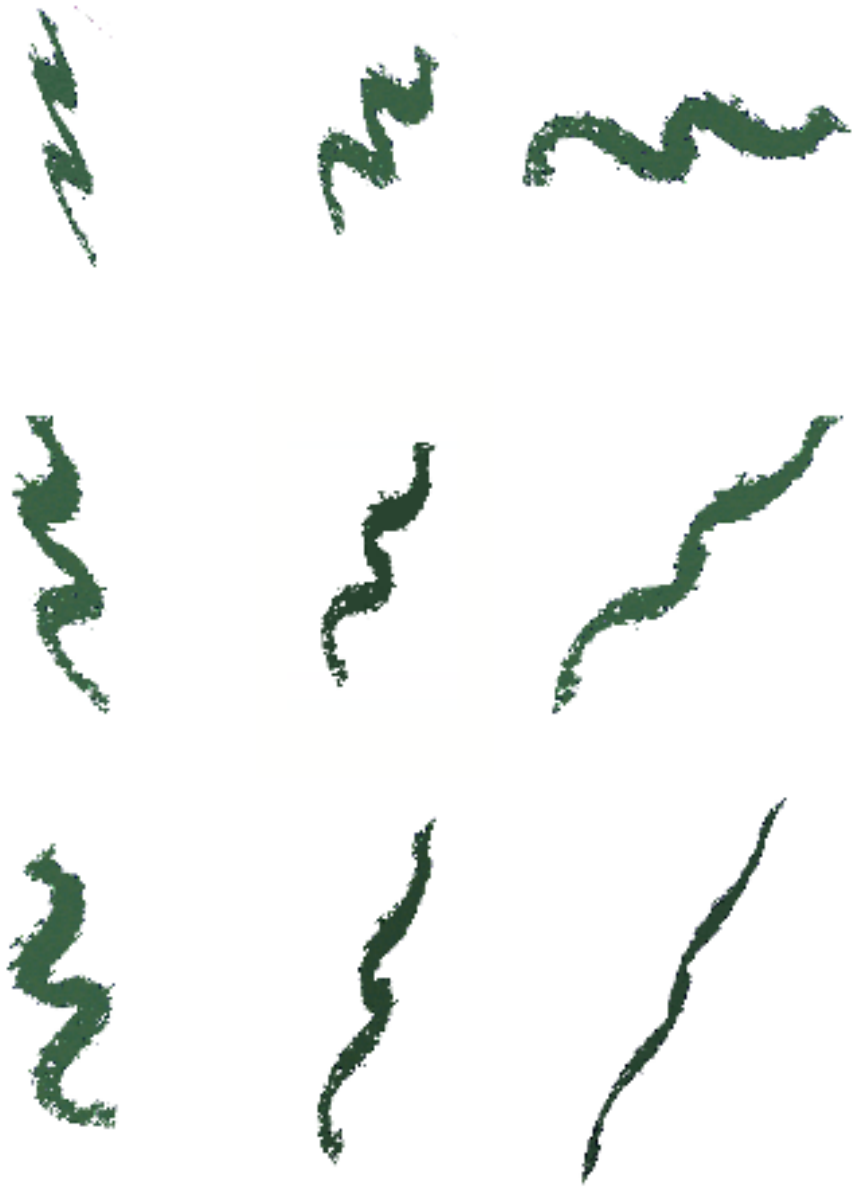

Figure 6–39: *transformed shape family of a section of a meandering river, transformed by a shear transformation. The centre shape is the icon, left-to-right is a shearing along the X-axis b y*$-60°$, $0°$ *and* $60°$, *resp., bottom-to-top is a shearing along the Y b y*$-60°$, $0°$ *and* $60°$, *resp. None of the shapes (except the icon itself) is identical to the icon shape.*

the diagonal (bottom-left to top-right) are always transformed isotropicly, i.e., the same for X and Y. Only the shapes along the diagonal in figure 6–38 have the same shape as the icon. All other instantiated shapes diverge from the icon shape.

6.7.3 Discussion

Figure 6–38 and figure 6–39 show the diversity that can be obtained by geometric transformation alone. This case demonstrates the basic principle of shape parametrisation and primitive instancing discussed in chapter 3. Indeed, the icon parametrises en entire family of river shapes. The eventually applied family members are to be further constrained by additional data and physical constraints. Applying transformation matrices rather than the (continues) transformation mapping further enhances geometric modelling flexibility, provided such detailed constraints are available.This issue will not be further discussed here.

6.8 The Comet West

6.8.1 Problem description

A comet is an irregularly shaped natural object of frozen gas and rocky debris, orbiting around the sun. A comet has a focal bright approximately 10 km wide kernel, called the *nucleus*. When approaching the sun, a comet develops three tails: the bright[3] *coma*, a large trailing cloud of diffuse material, the pale-blue *ion tail* of ionised plasma, and the yellowish *hydrogen envelope*, with hydrogens that escaped the comet's gravity. The Comet West[4] has been observed by various observers during its bright appearance in 1976. See figure 6–40, left picture.

Emphasis in this case will be on the model editing capacity as discussed in chapter 3. Model editing will be applied to significantly modify the initial result.

Figure 6–40: *α-complex of the Comet West. Left: as observed. Centre: nucleus (gray-scale weighting, with threshold: 0.4). Right: ion tail, obtained by extraction of the blue cluster points shown in figure 6–41.*

6.8.2 Data set

The data set was composed from the many digital pictures disclosed through the Internet. One of the major challenges was the uniformation of the colour encoding of the observations. The

[3] the colour actually depends on the observation and recording methods

[4] named after the astronomer West, who first described his observation of the comet.

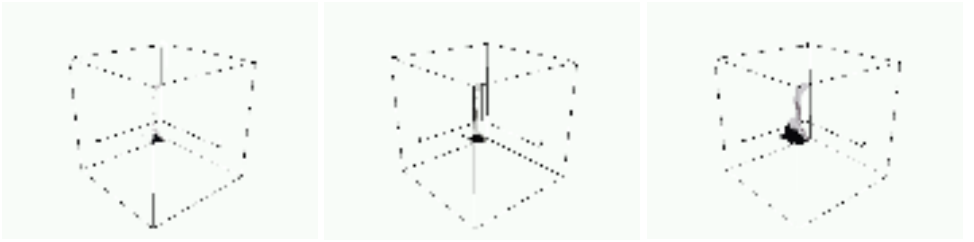

Figure 6–41: *α-complex of the colour spectrum property space. X-axis represents red, Y-axis green and Z-axis blue. Clusters represent different parts of the comet. Dark cluster represents the blue ion tail. The α-value increases left-to-right. Separation is weak and clusters concentrate around the gray-diagonal.*

eventual value set $\mathbb{P}_{\mathbb{S}}$ was composed of the spectral content of the light emitted by the comet. Using a named colour model (section 4.7.1), the *ion tail* was encoded pale-blue and the hydrogen envelope and dust tail where coloured white, with a yellow component for the hydrogen content. The resulting data set contained only data in 2-space E^2.

6.8.3 Data analysis

Spectral contrast is very weak and clustering is bad: figure 6–41 depicts the normalised property space in the unit cube, looking down the gray-scale diagonal. Nonetheless, three "clusters" are visible: a blue cluster (dark) representing the ion tail and the edges of the dust tail, a gray cluster along the main diagonal representing the dust tail and a rest cluster (nucleus, coma, dust tail). Due to the "pale" colours, the property values tend to accumulate around the main diagonal. Contrast cannot be enhanced without modification of the observed value sets.

6.8.4 Weighting

Cluster members, i.e., landmarks, were extracted from the landmark set $\mathbb{S}$ by membership of the clusters in property space. The blue ion tail cluster for example, is composed of exactly those landmarks making up that tail. See figure 6–40, right picture. The nucleus was found by extracting landmarks of which the properties showed a very low hydrogen content. See figure 6–40, central picture.

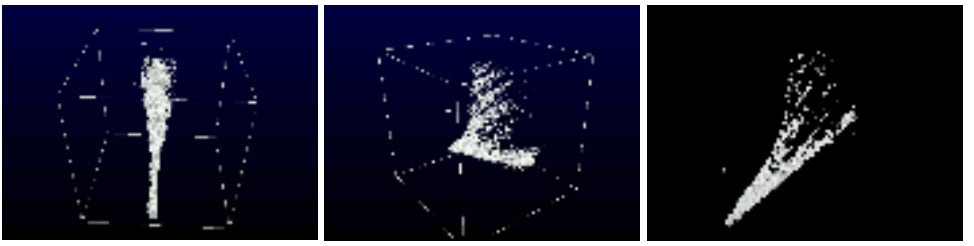

Figure 6–42: *3D α-complex of the Comet West, reconstructed from cross sections, that were edited using fig. 6–40 as a template. Dust and ion tail have been extended and modified (the claim that the model fits the observations must be abandoned).*

6.8.5 Result

The model of figure 6–40 was created by hyper-spatial modelling, with the property space spanned by the spectral content of the light emitted by the comet. How to come from a 2D-model to a model in 3D? With only data available in 2D, no 3D model could be made without *editing*.

6.8.6 Editing the result

The coma was in part reconstructed from various pictures, using "paint-brushes" to spray landmarks on cross sections. In this case, a paint-spray tools could be modified such that the intensity λ and the area could be tuned. Property values were then interpolated/extrapolated from the value sets available for the cross sections. The initial result of figure 6–40 was taken as a template for further editing. Figure 6–42 shows the eventually acceptedresults.

6.8.7 Discussion

In many aspects, this case uncovers the limits of this approach. In the first place the problem of compiling property value sets from various sources, some of which suffer from the named colour problem (section 4.7.1). In the second place the limits imposed by the working with observed properties with only little contrast. Clustering in this case is extremely weak and as a result so are the tail boundaries. As expected with property-ruled objects.

On the other hand, the model editing capacity could be demonstrated quite conveniently with this case. It is not very complicated to evaluate various scenarios. Unfortunately, suitable tools for editing are still lacking. A spraying tool like the one used here is not bad a first attempt.

Chapter 7

Conclusions and recommendations

7.1 Conclusions

7.1.1 The concept of an α-complex

In this thesis, α-complexes have been merited in the context of their anticipated role in the modelling framework discussed in chapter 3. This modelling framework targets at the reconstruction of natural objects. The storage of icons in a catalogue of template objects is foreseen. Natural objects are generally too complex to describe them analytically. Sampling point sets are therefore the only way to represent observed objects. This concept is also known as morphological landmarking and the sampling points are called landmarks. For most modelling purposes, representing an object by landmarks is inadequate. Many purposes require a solid object description. A solid object description is a prerequisite for topological queries, most numerical computations and simulation. Alpha complexes turn out to be able to abridge the gap between point sets and solid objects and appear to be ideal for accreting and eroding objects. Such objects are frequently encountered in nature. The use of α-complexes on this type of objects reduces the problem of the dynamic geometry and topology across the full deposition-erosion cycle to the definition of a dynamic point set. Its implicit topology can cope with any topological change, no matter in how many parts the objects scatters, persisting to keep its modelling flexibility. To further enhance modelling flexibility, particularly in the presence of regularly spaced landmark sets, weighted α-complexes were used, generated by weighted landmarks. In a neighbourhood of high weights, the α-complex tends to develop at lower α-values, whereas negative weights discourage the α-complex to develop.

7.1.2 The use of α-complexes to implement icons

In this thesis, the idea of icon shapes, primitives carrying the parametrised anatomy and dynamics of families of natural objects, has been presented. Its application has been demonstrated primarily on subsurface objects, a class of natural objects. In addition to the conceptual capacities just mentioned, α-complexes can be defined in general dimension, which makes them well-suited for hyper-spatial modelling. Hyper-spatial modelling is a modelling approach in which geometric space is augmented with property space. Additional a-priori knowledge and constraints that can

be transcribed into landmarks or property values can be merged. Cluster analysis and factor analysis may help to build property space and the augmented landmarks may be stored in a single icon α-complex. Projections plus intersections and cluster-membership allow landmarks representing embedded objects)parts) to be extracted from a larger set, or embedded objects from their embedding background. Furthermore,icon objects can be endowed with process definitions and internal constraints, enabling them to act as process models. Dynamic modelling of α-complex models is conveniently supported by morphological set operations on the generating landmark set, such as dilation and erosion. The result is an evolutionary map, driven by a morphological process. Instantiation of parametrised objects is a matter of creating the object from an icon, by assigning actual values to its parameters, assigning a location, an orientation and a size. Deformation can be accomplished with transformations, such as reflection, scaling, shearing, etc. If required, additional observed data can be used to serve as an attractor that further shapes the instantiated primitive. An inversion-based forward modelling scheme can also be imposed.

The derivation of icon has been based upon the principles of shape analysis and shape matching, which is maturely developed. Two approaches to instantiation have been discussed in this thesis. One approach constrained to generate objects with a topology similar to the icon, i.e., objects within the linear icon variety. Another approach relaxes these constraints and allows the topology of the instantiated object to diverge from the icon's topology. Keeping within the icon variety ensures the instantiation mapping to remain homeomorphic. On the other hand, the second approach gives room to a more flexible instantiation and a wider family of shapes.

7.1.3 The design of weight sets

Weighting has been one of the key issues in this thesis. For natural objects, weights can be derived from a well-chosen combination of discriminating observed physical properties. This is not the only possible approach but for natural objects in general, it is the most intuitive and fruitful approach. Determining the weights has been treated as a two-stage problem: determining the normalised weights and a weight transformation. The accumulation of the relative contributions of the normalised properties in property space leads to the normalised weights. Normalised weights can be stored within the icon, independent of the landmark spacing. Weight transformation relates the normalised weights again, accounting for the actual nearest neighbour distances. Commonly, the relative distribution of weight found in this normalised weight set is to be preserved in the weight transformation, obeying the property-ruled nature of the object under creation. Weight transformation is therefore mostly isotropic and determined by the globally smallest nearest neighbour distance. To obtain a hole-free object or a hole-free region, weight transformation may be taken one step further: an attractor, such as the Stienenmodel may be used to define the locally largest possible weights.

Theoretical support by a coverage process was found to provide valuable insight in the initial design and incremental improvement of the weights. After fitting of a theoretical model to the observed empirical point process, many more quantitative estimations can be determined to aid in the process of weighting. Most underlying point processes are Poisson point processes, with some degree of clustering. An analysis of the nearest neighbour and the local-furthest neighbour distances provides quantitative information on the local Laguerre distance to be abridged by weight. In fact this problem was turnedinto a coverage problem and the quantitative information on the local coverage was used. Transformations can sometimes be used to improve the

spatial distribution of the landmarks, prior to weighting. For instance, landmarks with strongly directional patterns were found to be ill-suited and transformation can be applied to entirely or in part eliminate the improper spatial distribution. Accumulating effects of transformations and weight require detailed knowledge of the underlying sampling data set and modelled object. When applying transformations, it is important to understand the effect on the Lebesgue measure and on the development of the α-complex with varying α. Weighting has an *omni-directional* effect, ignoring tensor-like and vector-like phenomena. The lack of support for vector and tensor-like phenomena is something to be improved by future research.

7.1.4 Alpha complexes as a formal object description

The ability to handle singular faces and disjunct parts in object descriptions based on α-complexes is both a strength and a complication: it provides modelling flexibility during the modelling process, but at the same time, it complicates the formalisation of certain parts in the modelling framework, particularly in conversions. Holes and geometrically coupled complementary objects, such as fluids in pore space, are inherently defined, along with the object itself. An α-complex may violate the criteria of continuity, solidity, closure and homogeneous dimensionality, but regularisation and the background-embedding approach, as with the dune and the point bar case, can be followed to remedy this. The introduction of the related *nil*-object greatly aids in achieving homeomorphic maps. The α-complex as a representation scheme is unambiguous but not unique. Validation is generally expensive.

7.1.5 Numerical modelling with α-complexes

Running numerical computations over an α-complex does not require a transcription between the geometric model and a numerical model. But turning an α-complex into a numerical model for FEA does, however, require a solution for three problems: singular faces, separations and slivers. In this thesis, a framework has been developed that circumvents these three problems by exploiting the fact that α-complex and triangulation of the same point set share faces. This allows for an embedding of the α-complex in the always connected triangulation. Taking an α-complex close to the triangulation rather than the triangulation itself is generally sufficient to remove all or enough of the slivers to make the numerical grid acceptable for FEM-computations. Slivers, like obtuse triangles, turn out to be generated mostly in the boundary region and for α-values close to $\alpha_{\max}$. The evolving barchan dune model of section 6.5 demonstrated the use of this framework in an evolutionary process model, including topological changes due to avalanching. Due to the capacity of an α-complex to reconstruct its topology, the erosion, shear stress computations and handling of avalanches can be processed in a single non-interrupted iterative computation, allowing an evolutionary process model to evolve by time-stepping without human intervention. The use of an α-complex is an effective solution to the regridding problem in modelling phenomena such as the avalanching, particularly when separations and holes may be expected.

7.1.6 Computational demands

Generally, detailed models require vast amounts of data and large computers to process them. For simple models ($O(10^2)$ to $O(10^3)$ landmarks), results show that implementations can generally

be made fast enough for interactive use. For more complex and bigger problems ($O(10^4)$ to (10^6) landmarks), storage becomes increasingly critical. The largest model, the Gulf of Mexico salt dome, had almost $3 \cdot 10^5$ landmarks and took more than 1 Gb internal memory and 5 to 6 hours of dedicated processing time on a powerful 4-processor ONYX 2 SILICON GRAPHICS "high-end" computer. This case points out the current limits which are fairly restrictive, still. With the advent of faster computers with more memory this limit is believed to be lifted soon. Additionally, domain decomposition, not discussed in this thesis, can help to break down the problem in smaller sub-problems and have multiple smaller computers compute the solution in parallel. The necessary methods, techniques and tools to implement such solutions are already available. Storage requirements can be reduced by exploiting the fact that α-complexes can be stored as unevaluated object descriptions, i.e., the complex itself can be uniquely be reproduced from the set of landmarks alone.

7.1.7 General conclusion

All in all, this makes α-complexes a suitable candidate to serve as a storage container for icons in a convenient manner. As such, α-complexes have been proven to be formal (chapter 2), mature, widely applicable (chapter 6) and robust (chapter 5) enough to serve as the *container object* to capture the icon shape as discussed in chapter 3. Although some improvements are feasible, a weighting approach has been developed (chapter 4) that is powerful yet flexible enough for the purposes defined in the scope of this thesis. The use of α-complexes offers good possibilities for knowledge-based modelling and variational geometry. Crisp measures-of-merits and cost function are mostly lacking, for natural objects, and topological constraints are often undefined. With the help of physical constraints such as mass and volume, fairly realistic geometries and topologies can be obtained following the approach as outlined in chapter 3 and applied in chapter 6.

7.1.8 An outlook on longer-term perspectives

The idea of creating a lively collection of interconnected co-existing natural objects (shapes) is steadily growing towards reality. In the century lying ahead, technical developments in the area of distributed computing are foreseen to become common ground and sound enough to facilitate the technical environment. A modelling system like this has all the characteristics needed for concurrent subsurface modelling, which, in turn, is believed to bring about important cost savings for the E&P-industry. Meanwhile, the search for appreciable definitions and design of shapes can take place, with enhanced domain analyses and object-oriented techniques as a starting point. For shapes based on α-complexes, the key step is to establish a relation relating geophysical properties to the value of α and the corresponding weight set. Enhanced computing capabilities will do the rest.

At the end of the day, natural object models comprise more then just geometry and topology and there is a strong urge for natural object model editing to be brought up to a higher level of abstraction. Pure geometric modelling shall be replaced by geological modelling, biomedical modelling, etc. Geometry and topology shall be *modelling proœss output* rather then *user input*. The process of "translating" model updates into required geometric and topological modifications first, before evaluating *the effect* of these changes in terms of geology, biometrics, etc. is error-prone and simply too time consuming. Geological modelling ought to take place on the basis of geological concerns, manipulating geological parameters only. Within the domain of geological

modelling, geometry and topology are mere derivatives.

It is exactly this philosophy that underpins the idea of *parametric modelling* and *knowledge-base d* modelling. P arametric (v ariational) modelling is based on capturing the characteristic features in a few determinant parameters. Geometry and sometimes also topology may alter by v ariation of these parameter values. V ariational geometry topology and functional characteristics cannot be seen in isolation: one affects the other. Important here is the fact that, within the limits set by a n t work of in ternal and external constraints, geometry and/or topology changes imposed by the variation of a limited set of parameters, can bring about well-determined changes in functional haracteristics (see e.g., [Kal89]).

Knowledge-based modelling proceeds solely in terms of knowledge-based and cased-base reasoning and *sc enario development*. The geometry and topology is generated only just prior to representing models and results. As a matter of fact, the user is hardly given a position therein to directly manipulate the geometry or topology. Modelling with *hyper-spatial primitives*, though akin to parametric modelling, tries to emphasise more on knowledge modelling, b y embedding (aggregated) property values and a-priori knowledge. An abstract primitive is a symbolic construct ([Req80, Kal89]) composed of domain variables, quantifiers, predicates and constraints, and it is in representation schemes that symbolic variables are valuated (given a value), obeying rules and constraints.

7.2 Recommendations for improvements and further research

7.2.1 Planned data acquisition

All too often, sampling is a single step process, without sufficient knowledge of the expected objects being sampled. Ideally, sampling is driven by an early model, that is further refined using *planned ac quisition* of further samples. The practical value for today's oil exploration at large may be argued. Seismic acquisition in regional surveys for instance, is mostly a one time v ent, "bulk"-type acquisition. Nevertheless, planned acquisition approaches ha v e been introduced, for example in in tegrated hydrocarbon reservoir management approaches. Reservoir management targets at the monitoring of production characteristics such as pressure depletion, over time. This dynamic modelling approach relies on an in tegrated data acquisition, notably 3D or 4D seismic plus well logs. Keywords here are rapid model update and low-cost. F or a practical approach, refer for example to Pink in [Pin93].

The idea of planned data acquisition (e.g., [Tay92]) is basically to start with a limited detail model of the object, based on a preliminary sampling data set, a-priori knowledge, a h ypothesis, or a combination of these. Next, an acquisition plan is generated or refined as new constraining data is brought in, after which this cycle is repeated. The difficulty of implementing a planned data acquisition is more in the finding of a measure-of-merit, MoM for short (Taylor, in [Tay92]; see fig. 3–1), objective functions and cost functions that assist in conv erging to the best among the suite of possible solutions for the object's geometry. It is therefore necessary to have a measure of the "distance" betw een a template object and the actual object. The Procrustes distance is commonly used for this purpose, e.g., [SKM95, DM98]. This subject further remains un-addressed here.

First goal is the aggregation of the anatomic landmark set. Anatomic landmarks are usually extracted from a *set* or family of identical sampled objects. In the parlance of scheme 3–

1, identical objects represented by training data. By definition, the landmarks are present in all of the family members, and therefore also in the icon. In the identification process of anatomic landmarks, salient features ought to be preserved. To facilitate comparison, the family members are normalised first, i.e., their centres of gravity are translated to the origin first and their mean distance relative to this common origin is normalised by scaling.

Various approaches exist for the estimation of landmarks. To paint the idea, an outline of the approach can be found [BT00]. This method seems applicable to a broad class of natural objects. Brett and Taylors automated landmarking approach is centralised around the building of a binary tree of which each node contains the merger of shapes contained in the left and right branch. Merging in this context, means that pairs of corresponding landmarks have been identified and positioned in a way that interpolates both shapes best. More in particular, the leaves contain the observed family members, and the root contains the mean shape of the entire family. The root contains the landmark set that survived in the propagation from observed family members all the way up to the root. This common set of anatomic landmarks propagates back down the branches to the observed objects. An estimate of the misfit of the individual set of anatomic landmarks from the aggregate set in the root is a goodness-of-fit measure for that individual family member against the aggregate shape. The root shape is the natural but not necessarily the only candidate for an icon. Brett and Taylor show that following their approach, roughly ten percent of the observed points make it into the final root anatomic landmark set. They also found that errors introduced on relatively smooth objects tend to swing up and may be inadvertently identified as landmarks.

Planned acquisition involves the observation of these points on a physicalobject in the first place. The observed object takes the role of a new family member. Even if all anatomic landmarks have been measured for an observed shape, further observations may assist in the finding of the exact geometry of the object. Formally these observations cannot be regarded as anatomic landmarks anymore, because they are not found profoundly enough on the other family members. Such observations may nevertheless be necessary for a further hovering of the reliability of the model. Of course, weighting model and planned acquisition go together hand in hand.

The open problem of planned acquisition in combination with landmarking consists of the following questions:

Open problem 7.1 (Planned acquisition in landmarking)

7.1a What is a proper start, in terms of anatomic landmarks, or initial reliability, for an initial model to base further acquisition upon?

7.1b How are holes "detected" by a stepwise refined acquisition approach? Moreover, how to resolve the issueof ambiguous topology?

7.1c Weighting model and planned acquisition go together hand in hand. Can the derivation of weights be directlycoupled to the coarse model at the basis of planned acquisition?

7.1d Planned acquisition for a dynamic model is still a problem. Moreover, optimising objective and/or cost functions at any time is difficult and highly problem-dependent. How to tackle the issue of time dependentgeometry evaluation in a general sense?

7.1e Should the merger of pseudo-landmarks be included? What if pseudo-landmarks become disqualified by later anatomic landmarks?

7.2.2 Shape uncertainty and uncertainty shapes

In this thesis, weight are primarily linked to physical properties. Uncertainty in the physical properties thus propagates to uncertainty in the weight and finally to uncertainty in the geometry. In many modelling approaches and evaluations, uncertainty is a key factor, for instance in Decision Support Systems (DSS) and Economic and Risk Management (ERM) systems. Representing spatial uncertainty is an important step. Instead of physical properties, weights can be coupled to uncertainty. Doing so opens up the road to a ordered family of shapes, ordered by (un)certainty. Such families can represent stochastic geometries. Remark that the members of such a family may again show holes and separations if uncertainty goes down to zero. Geometric constraints may be the result of economic or business constraints. For instance, by a financing company accepting no uncertainty less than 34% or a governmental agency accepting no volumetric estimation involving material with a porosity of less than $0.28 + 0.06$. Numerical computations may be needed to aggregate uncertainty across the shape.

The following open problem can be defined:

OPEN PROBLEM 7.2 (UNCERTAINTY SHAPES)
Given a shape, represented by an α-complex, such that in every of its vertices the uncertainty of the geometry is given. Then:

7.2a How to determine an uncertainty shape with a given maximum level of uncertainty, based on these values?

7.2b How to aggregate uncertainty across k-faces? How to aggregate uncertainty across separated parts?

7.2c How to interpret the topology of uncertainty shapes? What is for instance the meaning of holes that may be made arbitrarysmall or may be made to disappear by increasing α? Should uncertainty shapes for DSS-es and ERMs fulfil certain topological constraints in order to be meaningful?

7.2d With uncertainty coupled to weights, what is the meaning of α?

7.2e How to couple the ordered α-family of uncertainty shapes to planned acquisition (Open problem 7.1)?

7.2f Which topological queries are required for modellers to interpret the uncertainty shapes?

7.2g How to insert statistical a-priori knowledge and constraints?

7.2h How to treat anisotropic uncertainty distributions?

7.2i How to process and store the results of numerical computations?

7.2j How to compute difference among two shapes within a family? Which norm is to used for that? How to visualise uncertainty "distances"?

For an introduction of decision analysis and risk analysis, see for instance [Meg84, New75].

7.2.3 Shape analysis

In chapter 3, shape analysis has been introduced for the derivation of icons from observed landmark sets. It is unclear to what extend the orientation of subsurface shapes plays a role in their classification. It is quite common for subsurface properties to differ considerably in horizontal and vertical direction, or in conformal direction (in the plane of deposition) and perpendicular.

OPEN PROBLEM 7.3 (ORIENTED VERSUS NON-ORIENTED SHAPE)
The question may be raised, from an earth science point of view, as to whether subsurface shapes can be classified, irrespective of their orientation.

The open problem consists of the following questions:

7.3a With processes significantly influenced by orientation, can internal processes and constraints of subsurface shapes be considered identical irrespective the direction of gravity forces? For example: is a sufficiently tilted cap rock a trap?

7.3b How to identify features that somehow are related to the orientation? Consider for example a tilted block of compacted rock.

7.3c Can size equip a shape with different behaviour? How small a trap should still be seen as a trap?

Regarding open question 7.3a: in the further research into this matter it appears to make sense to include the possibility of vectorial weights, to be discussed below. See open problem formulation 7.4. Regarding open question 7.3b: here, *scale-space analysis* may be helpful. Fundamental approaches can be taken from [Lin94, SNFJ97]. Also see [Ogn94, AK95] and for further background on applications refer to [Wan83, Ran87, Hel94]. For the impact on the α-complex definition, also refer to [MD00].

7.2.4 Generalisation of weights

For α-complexes to have increased practical meaning in subsurface modelling, the current concept needs to be endowed with a *generalised weight vector*: $g : E^d \rightarrow R^m$. Practical forms being, for example: $g : E^3 \rightarrow R^3$, a vector field $\mathbf{w}(\mathbf{x})$ of weight vectors in 3-space, or $g : E^3 \rightarrow R^2$, with g adding a weight in gravity direction and one perpendicular to this direction. For every data vector, consisting of a geometry in E^3, with an additional parameter space constituted by k (pseudo-)parameters, each of which may be a scalar, a vector or a tensor:

$$\mathbf{x}^{(d)} = \Big(\overbrace{\underbrace{\mathbf{x} = (x, y, z)}_{location}, \underbrace{\mathbf{p}_1 = (p_{1,1}, p_{1,2}, \ldots, p_{1,l})}_{parameter\ subspace\ 1}, \cdots, \underbrace{\mathbf{p}_k = (p_{k,1}, p_{k,2}, \ldots, p_{k,m})}_{parameter\ subspace\ k}}^{d\ dimensions\ for\ geometry + k\ independent\ parameter\ (groups)}\Big)$$

delivering a weight vector:

$$\mathbf{w}^{(d)} = \Big(\overbrace{\underbrace{\mathbf{w} = (w_x, w_y, w_z)}_{location}, \underbrace{\mathbf{w}_{p_1} = (w_{p_{1,1}}, w_{p_{1,2}}, \ldots, w_{p_{1,l}})}_{parameter\ subspace\ 1}, \cdots, \underbrace{\mathbf{w}_{p_k} = (w_{p_{k,1}}, w_{p_{k,2}}, \ldots, w_{p_{k,m}})}_{parameter\ subspace\ k}}^{d\ dimensions\ for\ geometry + k\ independent\ parameter\ (groups)}\Big)$$

Potential variables, such as fluid pressure, may be described just fine by a scalar. Fluid pressure is intrinsically omni-directional (or: undirectional). Radiogenic heat flow for example, is a *flow variable*, generally described by a *vector field* and a weight set based on it would require weights to be vectorial. Apart from potential variables, represented by scalars, there also exist *vector potentials*. The edge-element method, a FEM-variant, is based on the vector potential. See for instance [Bos98]. Some material properties, such as strain and permeability, or variables such as hydraulic conductivity, are intrinsically *tensorial*, i.e., they are described by a *tensor*. For instance, for a problem in 3-model space, a tensor can be represented by a 3×3 generally unsymmetrical matrix of tensor coefficients. Refer for instance to [Bra47] for a general background introduction.

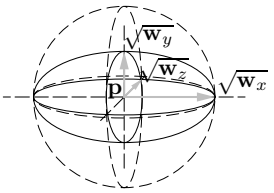

Figure 7–1: *geometric interpretation of vectorial weight, using an ellipsoid. As a reference, the 2-sphere with* $\varepsilon = \sqrt{\mathbf{w}_x}$ *has been added.*

How to extend the current use and interpretation of weight, in order to accommodate for vectorial and tensorial weight? A weight value $\mathbf{w}$ is called vectorial if its values can be represented by a vector, defined in some vector space and similarly, a weight value is called tensorial if its values can be represented by a tensor, defined in some vector space. Vectorial weights can be accommodated for using ellipse geometry (figure 7–1). A classification as discussed for spheres in section 4.2 could be implemented using quaternions, a generalisation of a complex number. More in particular using *imaginary quaternion*, with a zero real part and for instance three imaginary parts. An i-quaternion is defined as: $q = r + ip_1 + jp_2 + kp_3$, with $r = 0$. Like with the sphere, p_1, p_2, p_3 are associated with the radii along the main axes (see figure 7–1) and each of the radii may be negative, independent of the others. Background material on quaternions can be found in [Sho85, SM86, NM88], the majority of which is targeting at the application to rotation vectors. A fundamental discussion into the matter of using *spatial complex coordinates* and quaternions can also be taken from [Nee97].

Projective geometry may used to map an ellipse geometry on a ball or sphere geometry. In a more general context, $(d-1)$-spheres and $(d-1)$-ellipsoids can be regarded as *central conic sections*; sections obtained by intersecting a central conic. The geometric properties, tangential chords, to the ellipse need to be described, so as to establish orthogonality of two ellipses, paving the way to the definition of *skew regular triangulations*. *Inversion* seems to be an important linking concept between spheres and ellipsoids and their orthogonality. In [AAL+99], skew Voronoidiagrams have been proposed, using direction-dependent distances and direction-sensitive measure. The approach taken may be a good starting point to further workout the concept of vectorial weight. Also refer to [vdW73, Sha77, SK79, Hua81, Mun84, Oda88, Sto91, Bix94, KK96, Bix98].

Open problem 7.4 (Generalisation of weight)

7.4a Is it necessary to generalise weight into general *dimension? Or would a vectorial and/or a tensorial weight description in* 3*-space* R^3 *be sufficient?*

7.4b Apart from flow variables and potential variables, the use of vector potential variables has been suggested. See for instance [Bos98]. How to treat these variables and how to merge them in the concept of generalised weight?

7.4c The concept of quaternions seems limited to the use in 3-space only. Mainly in relation to its geometric interpretation and description of the ellipsoid geometry. If weight is generalised to R^d, how can its implementation be supported by quaternions?

7.4d Can a d-ellipse, parabolic, hyperbolic, in general, an section through a $(d+1)$-conic be interpreted geometricly as a vectorial weight? Can projective geometry be used to come to a formulation by Hermitian matrices, like in section 4.2 (also see [Hua81])?

7.4e Can this be extended to tensorial weight?

7.4f Can operation upon them be supported by projectivetransformations?

7.4g To that extent, can homogenous coordinates or Plücker coordinates be used to reach to simpler and less computational formulations?

7.2.5 Composed weight functions

Weights and their effect can be stacked, i.e., with $g : E \to R$ and assuming a 1-dimensional case, with $g = f_1 \circ f_2 \circ \cdots \circ f_p$ we have that for a vertex x_i, the weight is given by a function:

$$w_i = f_1(x_i) + f_2(x_i) + \cdots + f_p(x_i) = \sum_{l=1}^{p} f_l(x_i) \tag{7–1}$$

This may be a powerful approach to analyse and design the effects of weighting. It enables to *fit* a weight (composed) function to user defined *constraints* that must be honoured. Certain *basic weight functions* γ_l may be designed, of which the effect is well understood. Choosing a *linear combination* of such basic functions may provide the desired effect. Let $W = \{w_i\}$ be a set of prescribed weights, i.e., for all vertices $x_i \in \mathbb{X}, 1 \leq i \leq \operatorname{card} \mathbb{X} = N$, one may write for $w(\mathbf{x}) = \Gamma^{(p)}(\mathbf{x})$, the p-order linear combination:

$$w(x) = \begin{cases} \sum_{l=1}^{p} a_i \gamma_l(x_i) & \text{, such that} \\ w_i & \text{for } \forall x = x_i \in \mathbb{X} \end{cases} \tag{7–2}$$

with $a_i \in \mathbb{R}$ being some real coefficient. For these basic weight functions $\gamma_l : E^d \to R$ the use of *Lagrange polynomials* [LP82, Zie83, Hug87] may be considered.

The following open problem can be formulated.

Open problem 7.5

7.5a Are Lagrange polynomials indeed the most appropriate class of functions to apply for the basic weight functions? With multi-dimensional solutions in mind, should tensor-product splines be considered?

7.5b Can the curve fitting approach be generalised into general dimension hyper-surface fitting?

7.5c How can the approach be combined with the masking weighting strategy described in section 4.6.3?

7.5d Is there a motivation to couple weight functions with their counterparts in FEM element definitions?

7.2.6 Transformations of weighted points

There seems to be no mathematical foundation for weight transformations, like there is for linear Euclidean transformations. Mainly because (see also Annex C):

1. the Laguerre distance is not a metric and it is not a metric property under Euclidean isometric transformations and even not a metric property under Laguerre isometries
2. product space $E^d \times R$, combined with the Laguerre metric is not a metric space and behaves non-Euclidean
3. as Laguerre distances may become negative, it is undefined (in the scope of this thesis) what the topological consequences are and therefore also whether the Laguerre distance fails to be a topological property

Actually, all these aspects are inter-related and a result of the nature of the combination space-metric.

To answer these questions, one approach might be to study the Laguerre transformations. See for example [Coo16, Ch. VIII–XI]. In chapter 4 attention has been restricted to underlying weighting effects, and weighting strategies. Open problem formulation 7.6 will further give directives for future research into this matter.

OPEN PROBLEM 7.6
The description of this open problem borrows heavily from [Coo16, Ch. VIII-XI]. Transformations that impact on the weight-sphere of a weighted point are in fact sphere transformations. Spherical transformation in Cartesian space are always conformal and may be decomposed in inversions and reflections. Dualities can be established between spherical and Laguerre transformations by mapping them into an augmented spherical space. Set $\tilde{S}$ can be approached by a convex set circumscribed by an oriented sphere (see also [Sto91]) that is completely on one side of a set of oriented tangent hyperplanes (along which the power is measured, chapter 2). A duality so found is that every Laguerre transformation can be decomposed into four (if direct, i.e., acting on a sub-group) or five (if indirect) Laguerre inversions. A direct Laguerre transformation can be described as a rigid motion (translation, rotation or screw about a real axis) in an augmented spherical space, like a penta-spherial or hexa-spherical space, obtained from the original space by adding improper points at infinity. Dualities can then be established between invariant in the original space and the augmented spherical space.

The open problem consists of the following questions:

7.6a Can Laguerre transformation be formulated in general dimension? One of the problems may be that a generalisation of problem descriptions based on complex numbers into general dimension raises many practical problems. One strategy is the use of quaternions, *e.g., [NM88]. Quaternions have their limitations, however*

7.6b Is it possible to augment space E^d such that it obtains a properly defined associated augmented spherical space?

7.6c Do real rigid motions exist in augmented spherical space that are homeomorphic, apart from the identity transformation?

7.6d If it were possible to conveniently define transformations in the augmented spherical space by means of (decomposed) Laguerre of which the invariants are well understood, what does this mean in the light of classifying transformations like above?

7.6e Is it possible to find explicit formulations for the real and the imaginary part of the norm of the transformation?

7.2.7 Handling void space in an icon

Model building using instantiated objects means populating model space with autonomous objects the shapes of which do not conform. Inevitably, space between them is not occupied by some objects. On top of that, instantiated objects may themselves have holes. The generalised problem of handling void space in geometric and numerical modelling and its interpretation in a physical sense requires further research. The following open problem can be formulated.

OPEN PROBLEM 7.7 (HANDLING VOID SPACE)
Assume a model space to be populated with instantiated objects from icons.

7.7a Can void space be justified from a (geo)physical point of view?

7.7b If not, should it be filled with some appropriate "background" material, like clay or sand, or should it be saturated by a fluid, like water?

7.7c If void space is allowed, how to handle void space in the anticipated inversion?

7.7d Dilation may also be seen as a auxiliary process to implement infill with some background material *to obtain complete spatial occupancy. What is the relation of dilation with item 7.7b?*

7.2.8 Modelling erosion processes

Eroding faces may be associated with improper empty set *nil*-faces. In fact this is what has been suggested to keep evolutionary maps homeomorphic. Infill of holes is handled by *nil*-faces covering the hole. Alternately, eroded landmarks can be re-inserted under a closing operation. This mimics the process of relocating eroded material in existing holes. It must then be bound to some material balance. Such a process has not yet been found in literature.

The following open problem can be formulated.

OPEN PROBLEM 7.8 (RE-INSERTING ERODED LANDMARKS)
Assume a model space to be populated with instantiated objects from icons, all objects represented by α-complexes.

7.8a Can void (model) space be justified from a (geo)physical point of view? How does fluid expulsion and transfer take place? What boundary conditions are defined then?

7.8b If not, should it be filled with some appropriate "background" material, like clay or sand, or should it be saturated by a fluid, like water? What properties do such materials have?

7.8c If void space is allowed, how to handle void space in the anticipated inversion?

7.8d If infill with eroded landmarks takes place, how can evolutionary maps be kept homeomorphic?

7.2.9 Constraints

Constraints can be subdivided in a variety of ways; equalities and inequalities, inter- and intra shape, hard, soft, etc. Thanks to the hyper-spatial approach, physical constraints can be translated into *geometric* constraints: points that need to be honoured, or relative positions that need to be honoured. For instance volumetric constraints, time constraints, parameter constraint *(attractors)* parameter dependencies, etc.

Each shape instantiated from a primitive has to obey the intra-shape constraints; internal rules framing the initial and any of the future states during the evolvement of an object. Inter-object constraints are defined *among* shapes; in which order of appearance they may be instantiated, which shape counteracts to which, which *parent shape* gives birth to which *child shape*, which shape can modify processes in other shapes, etc.

The definition and implementation of constraints is still a very active research area. See for instance [Mes89, FBMB90, Aki90, DL91, Kum92, TS92b, Tsa93, FH97]. This certainly also holds for the solving of a set of constraints. The subject, challenging as it may seem, has not been discussed in this thesis. It will remain as an open problem for future research.

OPEN PROBLEM 7.9 (GEOMETRIC AND TOPOLOGICAL CONSTRAINTS)
In many practical situations, it is convenient to be able to impose geometric and topological constraints on the α-complex, independent of the α and weight set chosen.

The open problem consists of the following questions:

7.9a Can geometric constraints be successfully defined in the form: $\Psi(\alpha, w) = c$, e.g., $\alpha + w \geq c$, with c a given constraint?

7.9b Can topological constraints be successfully defined in terms of α-exposedness, and when stated in the form of the previous question: $\alpha + w \geq c$ with $c = \alpha_{exp} + w$, can they be satisfied simultaneously?

7.9c Can constraints be defined time dependent? E.g., in the form: $\Psi(\alpha(t), w(t)) = c(t)$

7.9d If constraints can be defined time dependent, how to keep them satisfied under erosion?

7.9e The effect of weight cannot be directed along one specific edge, but works across the entire topological star. How to satisfy conflicting constraints along different edges in the same star?

7.2.10 Numerical modelling

Further research should target at more complicated erosional models. At some point, the use of control volume finite difference methods (CVFD) may be preferred over the FEA. Node-based FEM methods may sometimes lead to inaccuracy, such as a loss of mass. This is generally unacceptable. Face-based FEM methods can be stated such that this flaw does not occur. Primal and dual grids, associated with nodes and faces, respectively, can be combined. Bossavit ([Bos98]) for instance, suggests to use approximate formulation on primal and dual grid and to combine the exact formulations of both grids. Bossavit uses metric-less topological formulations and uses the *hodge*-operator to couple them. One of the difficulties to overcome is to handle improper dual elements near the boundary of the completion of triangulations. Another problem is the vulnerability for slivers and needle-like elements. For instance in E^2, this implies a triangulation with only acute triangles, so that radical centres are guaranteed to be inside the triangle and dual edge representing flow variables are guaranteed to intersect their primal edges orthogonally.

The following open problem can be defined.

OPEN PROBLEM 7.10

7.10a Can the formulation be further be optimised for simplicial elements?

7.10b How to guarantee triangulations containing no obtuse triangles?

7.10c How to "repair" failing dualities in the improper faces gained from the completion of a triangulation?

7.10d How to copy with holes and evolutionary maps from a numerical point of view?

7.10e Can the formulation as described above be combined with the background embedding approach? Can metrical properties also be formulated in a dual sense?

7.2.11 Development of a ShapeEditor

A major problem to be solved is the development of an intuitive ShapeEditor. Editing of shapes will be at a different level of abstraction, compared to geometric modelling. Rather than modifying the geometry, so as to end up with the desired implicit changes of the geology, end users will now work on the geology directly, manipulating constraints, parameters, etc. Up-scaling, meshing, boundary conditions, interpolations, etc. will all be hidden in the shape, by the domain expert.

What still remains to be done is the design of a suitable end user level ShapeEditor, a tool that can easily modify an already existing shape thereby verifying active constraint and modifying adjacent shapes, wherever applicable. Furthermore, a sample data set will have to be compiled, capturing all characteristics needed for the derivation of shapes. The use of case-based reasoning is anticipated.

The following open problem may be formulated.

OPEN PROBLEM 7.11 (SHAPEEDITOR)

7.11a How to implement visualisation and selection of landmarks from hyper-space to the modeller?

7.11b Once landmarks have been selected, how to perform an incremental triangulation and α-complex computation?

7.11c How to present the icon variety to the modeller?

7.11d How to display internal constraints?

7.11e Should landmark selection be restricted to anatomic landmarks or does it also include pseudo-landmarks?

7.11f How to visualise the shape under creation?

7.11g How to feed the shape under creation with planned acquisition (open problem 7.1). Can the planned acquisition plan be replayed by the ShapeEditor?

7.2.12 Percolation problems

A *multi-phase system* is a system in which various phases of possibly multiple components may co-exist in thermodynamic equilibrium. A three-phase system for instance may be composed of a water phase, an oil phase and a gaseous phase, in each of which water plus hydrocarbon components may be contained, in some stable or unstable composition. Such a system may for instance flow through the void space of some porous medium. Numerical models exist to predict the transport through such media, based on Darcy's law. Various workers used Poisson Voronoi diagrams to (stochastically) model a porous medium (e.g., see [OBSC00, pp. 301–306]). It would be interesting to compare this approach with results obtained using an α-complex pore space geometry description.

Open problem 7.12

7.12a How to map a multi-phase system to the dual-shape description as described in chapter 5? How to split up the fluid and gaseous phases?

7.12b There must be a relation between the number of handles (tunnels) and the permeability. What is this relation?

7.12c Can more accurate computation be made by considering the joint probabilities of solid phases and fluid phases within the framework of dual shapes?

7.12d Is it advantageous to define a multiply complementary geometrically coupled shape, rather than just a dual, for multi-phase systems?

7.2.13 Domain decomposition

Methods and techniques to apply domain decomposition on the computation of an α-family are in fact all presented and understood already. A domain decomposition decomposes the problem domain in a number of smaller identical problems. A *cluster of workstations* may then solve the smaller problems in parallel, re-assembling the entire solution afterwards. This would allow bigger problems to be handled faster, while saving expenditures in computer platforms.

Open problem 7.13

7.13a Divide-and-conquer algorithms on triangulations need to be revised in the light of this application. See for instance [Ede87, Goo87, Buc88].

7.13b Design similar algorithms to merge partial α-complexes

7.13c Design strategies to handle weight effect on internal domain boundaries.

7.13d Design strategies for numerical computations on sub-domains.

7.13e Design strategies for asynchronically running initial value numerical computations on sub-domains.

7.13f Design algorithms to spread the computational effort and balance the computational load.

7.2.14 Data on natural objects

A final remark on sampling data. Surprisingly few suitable sampling data point sets were encountered on subsurface objects and natural objects in general. In the medical research scene, there is an organ database, created by Gill Barequet, at the Tel Aviv University. No equivalent was found for natural objects or subsurface objects. Having such data sets would greatly facilitate further research like the cases described in chapter 6.

Annex A

Mathematical concepts

A.1 Overview

This annex will briefly introduce the mathematical concepts underlying an α-complex. The discussion presented here should be sufficient to understand the broad merits of α-complexes. Nomenclature can be taken from the Nomenclature overview up front of this thesis. Terminology is explained in annex B, see for instance table B–1. For aspects left untouched, and for more detailed treatise, the reader is referred to the following standard references. Algebraic and geometric topology: Van der Waerden, [vdW73], Semple and Kneebone, [SK79], Munkres, [Mun75],[Mun84]. For computational and combinatorial geometry: Preparata and Shamos, [PS85], Edelsbrunner, [Ede87], Stolfi, [Sto91], Boehm and Prautzsch, [BP94], Hartwig, [Har96], De Berg et al., [dBvKOS97], simplicial complexes: Giblin, [Gib77], Nagata, [Nag83], Munkres, [Mun84], Paoluzzi, Bernardini, Cattani and Ferrucci, [PBCF93] and more specifically, for α-complexes, [Ede92], [Mue93], Edelsbrunner and Mücke, [EM94]. Background on topological graphs and related topics can be found in Giblin, [Gib77] and Gross and Tucker, [GT87] and Thulasiraman and Swamy, [TS92a], background on weighted Voronoi diagrams can be found in Aurenhammer, [Aur87b], Edelsbrunner, [Ede92], and Boehm and Prautzsch, [BP94]. For point process and mathematical morphology, refer to: [Dig83], [SS94], [SKM95], [BNKVL99] and [OBSC00]. For clustering, classification and factor analysis, refer to: [Mos97] and to [Boc96]. A recent survey paper on shape matching was presented by Veltkamp and Hagedoorn in [VH01].

A.2 Sets, domains and co-domains

A **set** is an unordered collection of unique entities drawn from some common universe of discourse. Discussions in this thesis involve numbers drawn from the following sets:

$\mathbb{N}$	the set of natural numbers
$\mathbb{Z}$	the set of integer numbers
$\mathbb{R}$	the set of real numbers
$\mathbb{Q}$	the set of rational numbers
$\mathbb{C}$	the set of complex numbers

Elements of a set are either enumerated, like in:

$$\mathbb{S} = \{s_1, s_2, s_3\} \tag{A–1}$$

described by means of some (in)equality) or equivalence class, like:

$$\mathbb{Y} = \{s \in \mathbb{S} \mid c_1 \leq s_i \leq c_2\} \tag{A–2}$$

for some suitable c_1, c_2, and:

$$\mathbb{Y} = \{s \in \mathbb{S} \mid s_i \text{ an extreme point}\} \tag{A–3}$$

A set is called **closed** (**open**) if it contains (does not contain) the points of its boundary. An open set is denoted as $\mathring{\mathbb{S}}$, a closed set as $\bar{\mathbb{S}}$ and the boundary by $\partial\mathbb{S}$. The **set complement** $\mathrm{Compl}\,\mathbb{S}$ is composed of all elements in the universe of discourse *not* belonging to $\mathbb{S}$. If a set $\bar{\mathbb{S}}$ is closed, its complement $\mathrm{Compl}\,\mathbb{S}$ is open, vice versa. The **closure** $\mathrm{Cl}\,\mathbb{S}$ is the smallest closed set containing set $\mathbb{S}$. A set is said to be **bounded** if all of its members can be contained in a finite radius ball and a set is called **compact** if it is bounded and closed. A set is called **finite** if its **cardinality**, the number of elements, is in set $\mathbb{N}$ of natural numbers. Notice that a compact set is not necessarily finite. A set is called **symmetric** if $\mathbb{S} = -\mathbb{S}$. The **reflection of a set** $-\mathbb{S}$ (or: $\check{\mathbb{S}}$) of a set $\mathbb{S} \subset \mathbb{E}^d$ is obtained by scalar multiplication with $\lambda = -1$:

$$-\mathbb{S} = \{-s \mid s \in \mathbb{S}\} \tag{A–4}$$

A set is said to be **convex** if all its members can be written as convex combinations (see further down) of its boundary members. Every subset of a convex set is again a convex set and the closure of a convex open set is also a convex set.

A **Minkowski set addition** of two finite sets $\mathbb{S}_1$ and $\mathbb{S}_2$ is given by:

$$\mathbb{S}_1 \oplus \mathbb{S}_2 = \{s_1 + s_2 | s_1 \in \mathbb{S}_1, s_2 \in \mathbb{S}_2\} \tag{A–5}$$

and the corresponding **Minkowski set subtraction**:

$$\mathbb{S}_1 \ominus \mathbb{S}_2 = \{s_1 - s_2 | s_1 \in \mathbb{S}_1, s_2 \in \mathbb{S}_2\} \tag{A–6}$$

One has, with a third finite set $\mathbb{S}_3$:

$$\mathbb{S}_1 \oplus (\mathbb{S}_2 \cup \mathbb{S}_3) = (\mathbb{S}_1 \oplus \mathbb{S}_2) \bigcup (\mathbb{S}_1 \oplus \mathbb{S}_3) \tag{A–7}$$

and with $\mathbb{S}_1 \subset \mathbb{S}_2$:

$$\mathbb{S}_1 \oplus \mathbb{S}_3 \subset \mathbb{S}_2 \oplus \mathbb{S}_3 \tag{A–8}$$

In general, Minkowski set subtraction is *not* the inverse of a Minkowski set addition.

A set is a **regular open set** if:

$$\mathbb{S} = \overline{\overset{\circ}{\mathbb{S}}} \tag{A–9}$$

and a **regular closed set** if:

$$\mathbb{S} = \overset{\circ}{\overline{\mathbb{S}}} \tag{A–10}$$

and furthermore:

$$\bar{\mathbb{S}} = \overset{\circ}{\mathbb{S}} \bigcup \partial\mathbb{S} \tag{A–11}$$

So one has that:

$$\overset{\circ}{\mathbb{S}} \subseteq \mathbb{S} \subseteq \bar{\mathbb{S}} \tag{A–12}$$

A **relation** maps **originals** from a **domain** onto their **images** belonging to some **co-domain**. Domains and co-domains are covered by sets and relations may take the form of:

$$\mathsf{H} : S \mapsto (0..1] \tag{A–13}$$

where, in equation (A–13), H is the relation, S is the domain to draw the originals from and *interval* $(0..1]$ is the co-domain. **Intervals** are either **open**, **half-open** or **closed**. Relations are also defined betw een the set cov ering the domain and the set cov ering the co-domain. In this w ork, intervals are mostly defined on $\mathbb{N}$, $\mathbb{R}$ or $\mathbb{C}$:

$$\begin{array}{lrcl} \text{open:} & (r_1, r_2) & = & \{r \in \mathbb{R} \mid r_1 < r < r_2\} \\ \text{half-open:} & [r_1, r_2) & = & \{r \in \mathbb{R} \mid r_1 \leq r < r_2\} \\ \text{half-open:} & (r_1, r_2] & = & \{r \in \mathbb{R} \mid r_1 < r \leq r_2\} \\ \text{closed:} & [r_1, r_2] & = & \{r \in \mathbb{R} \mid r_1 \leq r \leq r_2\} \end{array} \tag{A–14}$$

Let a **set function** $\mathsf{T} : \mathbb{V} \mapsto \mathbb{W}$ be defined on a domain set $\mathbb{V}$, that assigns a value in co-domain set $\mathbb{W}$ to members in $\mathbb{V}$. One also sa ysthat $w \in \mathbb{W} = \mathsf{T}(v \in \mathbb{V})$ is the **image** of the original v. If all members $v \in \mathbb{V}$ are assigned an image in $\mathbb{W}$ b y the function, then the function is called a **mapping** from $\mathbb{V}$ **in to** $\mathbb{W}$.

A function is called an **injection** of $\mathbb{V}$ **into** $\mathbb{W}$ if every image $w \in \mathbb{W}$ has at most one original $v \in \mathbb{V}$. If all members $w \in \mathbb{W}$ are an image of at least one original $v \in \mathbb{V}$ then the function is called a **surjection** of $\mathbb{V}$ **onto** $\mathbb{W}$. If a function is both an injection and a surjection, then every image has exactly one original, v.v. Such a function is called a **bijection**.

Let $\mathsf{T} = \mathsf{T}_1 \circ \mathsf{T}_2 \circ \cdots \circ \mathsf{T}_m$ be a **chain of** m **set functions** $\mathsf{T}_i : \mathbb{V}_i \mapsto \mathbb{W}_i$, $1 \leq i \leq m$, with $\mathbb{W}_j = \mathbb{V}_{j+1}$. Then:

$$\forall i : \mathsf{T}_i \text{ a bijection } \Rightarrow \mathsf{T} = \mathsf{T}_1 \circ \mathsf{T}_2 \circ \cdots \circ \mathsf{T}_m \text{ a bijection} \tag{A–15}$$

and:

$$\exists i : \mathsf{T}_i \text{ not a bijection } \Rightarrow \mathsf{T} = \mathsf{T}_1 \circ \mathsf{T}_2 \circ \cdots \circ \mathsf{T}_m \text{ not a bijection} \tag{A–16}$$

An **order relation** (or: simple order, or: **linear order**) on a set $\mathbb{X}$ is a relation for which:

$$\begin{array}{lrcl} (i) & x \neq y & \Rightarrow & x \lhd y \vee y \lhd x, \forall x \in \mathbb{X} \\ (ii) & \neg(x \lhd x) & \forall x \in \mathbb{X} & \\ (iii) & x \lhd y & \wedge \; y \lhd z \Rightarrow & x \lhd z \end{array} \tag{A–17}$$

where the operator $\lhd$ denotes the order relation. One of the principle order relations is the "less than" order relation $<$. According to this definition, the relation $\leq$ is not an order relation, as it violates (ii). A **partial order** is a relation, denoted b y $\preceq$ for which:

$$\begin{array}{lrcl} (i) & x \preceq x & \forall x \in \mathbb{X} & \\ (ii) & x \preceq y & \wedge \; y \preceq x & \Rightarrow x = y \\ (iii) & x \preceq y & \wedge \; y \preceq z & \Rightarrow x \preceq z \end{array} \tag{A–18}$$

A **strict partial order** is a relation, denoted by $\prec$ for which

$$\begin{array}{lll} (i) & \neg(x \prec x) & \forall x \in \mathbb{X} \\ (ii) & x \prec y \quad \wedge \quad y \prec z & \Rightarrow x \prec z \end{array} \tag{A–19}$$

A.3 Points, vectors and spaces

Let E^d denote a d-**dimensional Euclidian space**, for some $d \geq 0$. Then in this thesis, this d-space can be written as:

$$E^d = \prod_{k=1}^{d} R_k = \underbrace{R_1 \times R_2, \ldots, \times R_d}_{d \text{ dimensions}} \tag{A–20}$$

Given a **point** $\mathbf{x}$ in E^d. P oin t $\mathbf{x}$ can be represented b y its d-**tuple of coordinates** in E^d, $\mathbf{x} = (x_1, x_2, \ldots, x_d)$, b y its **coordinate vector** on some natural basis $\mathbf{x} = (x_1, x_2, \ldots, x_d)$, or, equivalently, in **matrix representation** b y $\mathbf{X} = [x_1, x_2, \ldots, x_d]^T$. The abov e representations will be used interchangeably.

Expanding space E^d with the real number space R yields a **Cartesian product space** $E^d \times R$ and representations for a point $\mathbf{x}$ become $(d+1)$-tuples ov er this Cartesian product. Let $\mathbb{S} \subset \mathbb{E}^d$ and a $\mathbb{W} \subset \mathbb{R}$. F ora pair of equal cardinality sets $\mathbb{S} \in \binom{\mathbb{E}^d}{N}$ and $\mathbb{W} \in \binom{\mathbb{R}}{N}$, so that card $\mathbb{S} =$ card $\mathbb{W} = N$, one obtains a set of N **ordered 2-tuples**:

$$\tilde{\mathbf{s}} = (s_1, s_2, \ldots, s_d, w) \cong (\mathbf{s}, w) \in \mathbb{S} \otimes \mathbb{W} \tag{A–21}$$

where $\otimes$ indicates an **ordered Cartesian product**. In the sequel, the tilde-notation will often be dropped, as in general, data points may be assumed to be alwa ys weighted.

The points $\mathbf{x}$ of a set $\mathbb{X} = \{\mathbf{x}\}, \mathbb{X} \subseteq \mathbb{E}^d$ are said to be **in general position** if every subset $\mathbb{Y}_j$, $\mathbb{Y}_j \subseteq \mathbb{X}$, card $\mathbb{Y}_j \leq d+1$ is geometrically independent. A set $\mathbb{X} \subseteq \mathbb{E}^d$, with $\mathbb{X} = \{\mathbf{x}_1, \mathbf{x}_2, \ldots, \mathbf{x}_d, \mathbf{x}_{d+1}\}$ is said to be **geometrically independent** if:

$$\left.\begin{array}{rcl} \sum_{i=1}^{d+1} a_i \mathbf{x}_i & = & 0 \\ \sum_{i=1}^{d+1} a_i & = & 0 \end{array}\right\} \Rightarrow \forall i : a_i = 0 \tag{A–22}$$

When in general position, all **positively oriented** k-simplexes have a positive determinant and hence a positive length, area, volume, etc. Let a point $\mathbf{x}_i$ be given b y it's coordinate vector

$\mathbf{x}_i = (x_{i,1}, x_{i,2}, \ldots, x_{i,d})$. Then the **orientation** of a $(d+1)$-sequence $(\mathbf{x}_{i_0}, \mathbf{x}_{i_1}, \cdots, \mathbf{x}_{i_d})$ of points in $\mathbb{X}$ is positive, if:

$$\Delta = \det \begin{pmatrix} x_{i_0,1} & x_{i_0,2} & \cdots & x_{i_0,d} & 1 \\ x_{i_1,1} & x_{i_1,2} & \cdots & x_{i_1,d} & 1 \\ \vdots & \vdots & \ddots & \vdots & \vdots \\ x_{i_d,1} & x_{i_d,2} & \cdots & x_{i_d,d} & 1 \end{pmatrix} > 0 \qquad \text{(A–23)}$$

If $\Delta < 0$ then the orientation is said to be negative and if $\Delta = 0$, i.e., if the $d+1$ points lie in a single hyperplane, the orientation is not defined. Also, with $\mathbb{Y}_i = \{y_1^{(i)}, y_2^{(i)}, \ldots, y_{d+1}^{(i)}\}$ and $\mathbb{Y}_j = \{y_1^{(j)}, y_2^{(j)}, \ldots, y_{d+1}^{(j)}\}$, $\mathbb{Y}_i \neq \mathbb{Y}_j$, there exists a $\delta > 0$ for which $|y_k^{(i)} - y_k^{(j)}| < \delta$, for $1 \leq k \leq d+1$. Apparently, when in general position, no $k+1$ vertices lie in a common $(k-1)$-dimensional flat.

A **topological space** is a mathematical abstraction of a space. A topological space X is said to be **metric** (metrizable), with a metric $\mu(\mathbf{x}_1, \mathbf{x}_2)$ iff for all $\mathbf{x} \in \mathbb{X}$:

$$\begin{cases} \mu(\mathbf{x}_1, \mathbf{x}_2) \geq 0 \ \wedge \ \mu(\mathbf{x}_1, \mathbf{x}_2) = 0 \Leftrightarrow \mathbf{x}_1 = \mathbf{x}_2 & \text{positive definiteness} \\ \mu(\mathbf{x}_1, \mathbf{x}_2) = \mu(\mathbf{x}_2, \mathbf{x}_1) & \text{symmetry} \\ \mu(\mathbf{x}_1, \mathbf{x}_3) \leq \mu(\mathbf{x}_1, \mathbf{x}_2) + \mu(\mathbf{x}_2, \mathbf{x}_3) & \text{triangle inequality} \end{cases} \qquad \text{(A–24)}$$

Euclidean space exploits a **Euclidean metric**, a measure which defines the distance between any two points $\mathbf{x}_1$ and $\mathbf{x}_2$ along a line connecting them, by:

$$d(\mathbf{x}_1, \mathbf{x}_2) \cong \|\mathbf{x}_1 - \mathbf{x}_2\| = \langle \mathbf{x}_1 - \mathbf{x}_2, \mathbf{x}_1 - \mathbf{x}_2 \rangle^{\frac{1}{2}} = \sqrt{\sum_i (x_{1_i} - x_{2_i})^2} \qquad \text{(A–25)}$$

where $\langle ., . \rangle$ denotes the **standard dot- or inproduct**.

A **σ-algebra** is a system of sets and subsets that is closed under basic operations, like union, intersection, complement, etc. The **power set** is an example of of a maximal σ-algebra and the family of **Borel sets** $\mathcal{B}^{(d)}$ is another important one. The family of Borel sets form the smallest σ-algebra on E^d that contains all open subsets on E^d. It is strictly smaller than the power set and it can be constructed by basic operations from open subsets. As new open subsets can be added, it can be made to contain all closed (compact) subsets. Point set $\mathbb{S}$ is a subset of a Borel set. Let μ be a **measure** on X and let Σ be a σ-algebra on that space. A measure $\mu^{(d)}$ on (X, Σ) is a function $\mu : \Sigma \mapsto [0, \infty]$ such that:

$$\begin{cases} \mu(\emptyset) & = & 0 \\ \mu\left(\bigcup_{j=1}^{\infty} V_j\right) & = & \sum_{j=1}^{\infty} \mu(V_j) \end{cases} \tag{A–26}$$

Being a measure, $\nu(\mathbb{Y}_j) \geq 0, \quad \forall \mathbb{Y}_j \subseteq \mathbb{S}$. A **locally finite measure** can be defined on a hypercube by:

$$\nu_{\mathcal{L}}^{(d)}(I) = (v_0 - u_0)(v_1 - u_1) \cdot \ldots \cdot (v_{d-1} - u_{d-1}) \tag{A–27}$$

where $I = [0,1]^d$ is the unit d-cube. The **Lebesgue measure** $\nu_{\mathcal{L}}^{(d)}(I)$ is a measure thatcan be constructed from this unit cube according to eqn. (A–26). It can be regarded as a generalisation of the length and it is usually defined by considering a half-open interval covered by smaller half-open interval. It resembles the length for $d = 1$, the area for $d = 2$ and the volume for $d = 3$. In general in this thesis, it also resembles the d-volume or hyper-volume in general dimension. Let $\mathbb{Y}_i, \mathbb{Y}_j \subseteq \mathbb{X}$ be different subsets of $\mathbb{X}$ so that $i \neq j \Leftrightarrow \mathbb{Y}_i \bigcap \mathbb{Y}_j = \emptyset$. The Lebesgue measure $\nu(\mathbb{X})$ is set function for which:

$$\begin{cases} \nu(\emptyset) \; = \; 0 \\ \nu(\mathbb{Y}_j) \; \geq \; 0, \quad \forall \mathbb{Y}_j \subseteq \mathbb{X} \\ \nu\left(\bigcup_j \mathbb{Y}_j\right) = \sum_j \nu(\mathbb{Y}_j) \end{cases} \tag{A–28}$$

Euclidean metric forms a Lebesgue measure, the Laguerre distance not, see annex C. The Lebesgue measure has the following properties. Let $\mathsf{T}_{\equiv}$ denote an isometry and $\mathbb{S}$ denote a Borel set. Then, under transformation $\mathsf{T}_{\equiv} : \mathbb{S} \mapsto [0, \infty)$, with corresponding transformation matrix $\mathbf{T}_{\equiv}$, we have for the Lebesgue measure:

$$\nu_{\mathcal{L}}^{(d)}(\mathbf{T}_{\equiv}\mathbb{S}) = \nu_{\mathcal{L}}^{(d)}(\mathbb{S}) \tag{A–29}$$

and also, for a subset $\mathbb{Y} \subseteq \mathbb{S}$:

$$\nu_{\mathcal{L}}^{(d)}(\mathbb{Y}) \leq \nu_{\mathcal{L}}^{(d)}(\mathbb{S}) \tag{A–30}$$

A **Radon measure** is a measure that is finite for every bounded set. A Lebesgue measure is also a Radon measure. See [SKM95]. Therefore, with $\mathbb{S}$ a bounded Borel set:

$$\nu_{\mathcal{L}}^{(d)}(\mathbb{S}) < \infty \tag{A–31}$$

Euclidean space is a **vector space**, allowing, among others, for vector addition and scalar multiplication, resp defined as:

$$\mathbf{x}_1 + \mathbf{x}_2 = (x_{1_0} + x_{2_0}, x_{1_1} + x_{2_1}, \ldots, x_{1_{d-1}} + x_{2_{d-1}}) \tag{A–32}$$

and, with $\lambda \in \mathbb{R}$:

$$\lambda\mathbf{x} = (\lambda x_0, \lambda x_1, \ldots, \lambda x_{d-1}) \tag{A–33}$$

A.4 Flats, planes, linear varieties and subspaces

A **hyperplane** is a $(d-1)$-dimensional flat, spanned by $d+1$ points in general position, that bisects d-space into two half-spaces with dimension of at most d. In 2-space, for example, a hyperplane is a 1-flat (a line) and in 3-space it is a 2-flat (a plane). According to the above definition, hyperplanes are always considered "flat", i.e., not skew or curved. A bisecting hyperplane can also be obtained by a $(d-1)$-sphere of infinitely large radius with the interior and exterior of the corresponding d-ball on either side. A hyperplane satisfies the implicit equation:

$$\mathtt{H} = \{\mathbf{x} \in \mathbb{E}^d \mid \langle \mathbf{x}, \mathbf{a} \rangle = c \} \tag{A–34}$$

for some $\mathbf{a} \neq \mathbf{0}$. Two such hyperplanes $\mathtt{H}_1$ and $\mathtt{H}_2$ are **parallel** if:

$$\mathtt{H}_1 = \{\mathbf{x} \in \mathbb{E}^d \mid \langle \mathbf{x}, \mathbf{a} \rangle = c_1 \} \tag{A–35}$$

and:

$$\mathtt{H}_2 = \{\mathbf{x} \in \mathbb{E}^d \mid \langle \mathbf{x}, \mathbf{a} \rangle = c_2 \} \tag{A–36}$$

for some $c_1, c_2 \in \mathbb{R}, c_1 \neq c_2$. If hyperplanes are not parallel, a number of them can be arranged (positioned in space) such that they fully wrap (bound) a part of space. For example, $d+1$ such hyperplanes (no two parallel) suffice to span a d-**cell** $\sigma^{(d)}$. Their intersection:

$$\bigcup \left(\bigcap_{j=0}^{d} \mathtt{H}_j \right) \;=\; \partial\sigma^{(d)} \tag{A–37}$$

An **open half-space** satisfies the general implicit definition:

$$\Psi(\mathbf{x}) < c \tag{A–38}$$

and, accordingly, a **closed half-space**:

$$\Psi(\mathbf{x}) \leq c \tag{A–39}$$

Let hyperplane $\mathtt{H}$ be given by the equality $\langle \mathbf{x}, \mathbf{a} \rangle = c$. An open half space $\mathtt{H}^- \subset \mathbb{E}^d$ is defined as:

$$\mathtt{H}^- = \{ \mathbf{x} \in \mathbb{E}^d \mid \langle \mathbf{x}, \mathbf{a} \rangle < c \} \tag{A–40}$$

and analogously, for an open half space $\mathtt{H}^+$:

$$\mathtt{H}^+ = \{ \mathbf{x} \in \mathbb{E}^d \mid \langle \mathbf{x}, \mathbf{a} \rangle > c \} \tag{A–41}$$

the border being formed by the hyperplane $\mathtt{H}$ for which $\Psi(\mathbf{x}) = c$. Points in $\mathtt{H}^-$ are said to lie **beneath** $\mathtt{H}$, points in $\mathtt{H}^-$ lie above or **beyond** $\mathtt{H}$. Observe that this imposes an **orientation** on $\mathtt{H}$. An **open (closed) half-space** is that part of space that lies on one side of (or on) a hyperplane.

A **support plane** of a convex set is a tangential plane to that set, such that the intersection of the tangential plane and the convex set is only a single point. For every point in the boundary $\partial\mathbb{S}$ of a convex set $\mathbb{S}$ there exists a support plane and a convex set intersected by a hyperplane is a compact flat (possibly reduced to a single point). In the latter case, the hyperplane is a support plane.

A **radical plane** between two weighted points $\mathbf{s}^-$ and $\mathbf{s}^+$ is a hyperplane of points at equal weighted distance to these two points:

$$\Psi(\mathbf{x}) = L(\mathbf{s}^-, \mathbf{x}) - L(\mathbf{s}^+, \mathbf{x}) = 0 \tag{A–42}$$

where $L(\mathbf{s}^-, \mathbf{x})$ is the Laguerre weighted distance of a point $\mathbf{x}$ relative to point $\mathbf{s}^- \in \mathtt{H}^-$ and $\mathbf{s}^+ \in \mathtt{H}^+$ to be discussed later.

A **convex combination** of m points $\mathbf{p}_j \in \mathbb{E}^d$ is a linear combination $\lambda_1\mathbf{p}_1 + \lambda_2\mathbf{p}_2 + \cdots + \lambda_m\mathbf{p}_m$ with each $0 \leq \lambda_j \leq 1$ and the sum of all coefficients $\lambda_j = 1$. Let $\mathcal{H}(\mathbb{S})$ denote the convex hull of the points $\mathbf{p}_j$. The **convex hull** is the set of all convex combinations of $\mathbb{S}$. A point $\mathbf{x}$ belonging to this hull can then be written as:

$$\mathbf{x} = \lambda_0(\mathbf{x})\mathbf{s}_0 + \lambda_1(\mathbf{x})\mathbf{s}_1 + \ldots + \lambda_{m-1}(\mathbf{x})\mathbf{s}_{m-1} \tag{A–43}$$

The scalar coefficients $\lambda_j(\mathbf{x})$ are sometimes called the **convex coordinates** or **barycentric coordinates** of point $\mathbf{x}$ with respect to the convex hull $\mathcal{H}(\mathbb{S})$. Related to convex coordinates is the concept of **linear varieties** Consider for instance a closed edge $\mathbf{s}_i\mathbf{s}_j$. An arbitrary point $\mathbf{x}$ on the edge can be given in parametric form by:

$$\mathbf{x} = (1 - \lambda)\mathbf{s}_i + \lambda\mathbf{s}_j \tag{A–44}$$

with $0 \leq \lambda \leq 1$. This is a direct consequence of the fact that the edge is a convex set. A subspace that can be written in the form of equation (A–44) is called an **affine linear subspace**. This generalises to general dimension. All affine linear subspaces are convex sets.

A *lattice* is a collection of locations in a space of which the distance of two adjacent points along one direction fits some regular pattern.

A.5 Transformations

A **transformation** $\mathsf{T} : \mathbb{S} \mapsto \mathbb{U}$ is a mathematical operation defined on all elements of a set $\mathbb{S}$ of originals, called the **domain**, creating a second, basically different set $\mathbb{U}$ of transformed originals, called **image** or **range**. A **translation** (or: **glide**) transformation is a move of all points by an equal vector $\mathbf{u}$. A **rotation** is a revolution over some angle and around some axis of revolution. A **reflection** transformation is a perpendicular mirroring of each point in a hyperplane or an intersection of at most d such hyperplanes. Changing the sign of the x_0-coordinate of all points, for instance, is a reflection in a hyperplane perpendicular to and crossing the origin of the X_0-axis. A **glide reflection** is a reflection followed by a translation by a vector lying in the reflection hyperplane. A transformation is said to be an **identity transformation** if it leaves position (i.e., location and orientation), size and shape invariant and a transformation is said to be an **isometry** (or: **isometric transformation** or: **rigid motion**) if it leaves the Euclidean distance between two arbitrary members of $\mathbb{S}$ invariant, i.e., unchanged. If an isometric transformation contains an invariant point (a *centre*), then it must be a rotation or a reflection. If such an invariant point does not exist, then it must be a translation or a glide-reflection. If all points are invariant points, then it must be the identity transformation, by definition.

A transformation $\mathsf{T} : \mathbb{S} \mapsto \mathbb{U}$ is a **linear transformation** if:

$$\mathsf{T}(\lambda_1\mathbf{s}_1 + \lambda_2\mathbf{s}_2) = \lambda_1\mathsf{T}(\mathbf{s}_1) + \lambda_2\mathsf{T}(\mathbf{s}_2) \tag{A–45}$$

An **affine transformation** is a transformation that can be composed of a translation by a translation vector and a linear transformation. If the translation vector is a null vector, then the affine transformation is a linear transformation.

The **image space** $\mathbb{U}_0 \subseteq \mathbb{U}$ of transformation T, denoted by $\mathrm{im}\,\mathsf{T}$, is the part of co-domain $\mathbb{U}$ that can be "reached" by transformation T. The **kernel** or **null space** $\mathbb{S}_0 \subseteq \mathbb{S}$ of transformation T, denoted by $\ker\mathsf{T}$, is the part of domain $\mathbb{S}$ that is mapped onto the null-vector $\mathbf{0}$ under

transformation T. The **norm of a transformation** T, denoted $\|\mathsf{T}\|$, is the supremum of the ratio betw een a norm of the image and that of its original. With $\mathbf{s} \neq \mathbf{0}$:

$$\|\mathsf{T}\| = \sup_{\mathbf{s}_j} \frac{\|\mathsf{T}(\mathbf{s})\|}{\|\mathbf{s}\|} \tag{A–46}$$

F urther, $\|\mathsf{T}\| \geq 0$ and $\|\mathsf{T}\| = 0$ only for the null-transformation. F urthermore:

$$\begin{cases} \|\mathsf{T}^k(S)\| & \leq & \|\mathsf{T}(S)\|^k \\ \|\lambda\mathsf{T}(S)\| & = & |\lambda| \, \|\mathsf{T}(S)\| \end{cases} \tag{A–47}$$

T ransformation norm $\|\mathsf{T}\|$ can be computed from the eigenvalues of a system of the form $A = \mathbf{T}\Lambda\mathbf{T}^T$, where $\mathbf{T}$ is a matrix called the **transformation matrix**, representing the transformation. F or details, refer for example to [Str86].

A.6 Representations and maps

A **representation** is a symbolic construct composed using the **letters** of an **alphabet** $\mathcal{A}_\wp$ and some **syntax** Θ. An alphabet $\mathcal{A}_\wp$ is a finite set of symbols $\{\wp\}$. An element $\wp \in \mathcal{A}_\wp$ is called a letter or a **token**. A **map** $\mathsf{T} : V \mapsto W$ transforms one representation V into another representation W. A **mapping c hain** is a sequence $\mathsf{T} = \mathsf{T}_1 \circ \mathsf{T}_2 \circ \cdots \circ \mathsf{T}_m$ of maps T_j. A map(ping) is called a **surjectivity , injectivity and bijectivity**, resp. if:

$$\forall w \in W : \exists v \in V : t(v) = w \;\Rightarrow\; \mathsf{T} : V \to W \text{ surjective} \tag{A–48}$$

and:

$$\forall v \in V : w_1 = w_2 \Rightarrow v_1 = v_2 \;\Rightarrow\; \mathsf{T} : V \to W \text{ injective} \tag{A–49}$$

$$\forall v \in V : \exists w \in W : w = T(v) \wedge \forall w \in W : \exists v \in V : w = T(v) \;\Rightarrow\; \mathsf{T} : V \to W \text{ bijective} \tag{A–50}$$

Also, see section A.2. A map is called a **homeomorphic map** (or: **homeomorphism**) if it is a bijective map, and consequently, a map $\mathsf{T} : V \mapsto W$ is homeomorphic, it can be shown that $\ker \mathsf{T} = \{\mathbf{0}\}$ and $\operatorname{im} \mathsf{T} = W$. A map is called a *nil*-map $\mathsf{0}$ if:

$$\forall v \in V : \mathsf{0}(v) = \mathbf{0} \tag{A–51}$$

A.7 Graphs

A **graph** $\mathcal{G} = \{\mathbb{S}, \mathbb{F}\}$ is a set of **v ertices**(or: **nodes**) S and a set of **edges** (or: **arcs**, or: **faces**) F connecting them. A **finite graph** is a graph composed of a finite set of vertices and edges. If edges represent relations betw een nodes that are not symmetric, edges are directed, constituting a **directed graph**. Assume $\operatorname{card}\mathbb{S} \geq 2$. The **nearest neighbour graph** $\mathcal{NNG}(\mathbb{S})$ connects each member in $\mathbb{S}$ to another member in $\mathbb{S}$ that is:

(*i*) connected by an arc in triangulation $\mathcal{T}(\mathbb{S})$

(*ii*) closest-by

A **local-furthest neighbour graph** $\mathcal{LFNG}(\mathbb{S})$ connects each mem ber in $\mathbb{S}$ to another member in $\mathbb{S}$ that is:

(*i*) connected by an arc in triangulation $\mathcal{T}(S)$

(*ii*) furthest apart

In a **geometric graph**, edge lengths are representing some distance between the nodes and the nodes represent points in space. A geometric graph is said to be a **simplicial geometric graph** if it contains no self-loops or multiple edges among any pair of nodes. If based on the Euclidean metric, nearest neighbour and local-furthest neighbour graph as used in this work are finite directed geometric graphs.

An **incidence graph** $\mathcal{IG} = \{\Sigma, I\}$ is a graph in which the collection $\Sigma = \{\sigma^{(k)}\}$ of k-simplices, $-1 \leq k \leq d+1$, is represented as nodes and **incidence relations** $I = \{deg(\sigma^{(k)})\}$ as edges. Also, refer to annex B.

A.8 Balls and spheres

Given a Euclidean d-space E^d, and $\varepsilon \in \mathbb{R}$, $\varepsilon \geq 0$ a real number. Then an **open** d-**ball** $\overset{\circ}{\mathtt{B}}{}_{\varepsilon}^{(d)}(\mathbf{c})$ with radius $\sqrt{\varepsilon}$ and centred at $\mathbf{c}$ is the set of points $\mathbf{x} \in \mathbb{X} \subseteq \mathbb{E}^d$, for which in Cartesian coordinates:

$$\overset{\circ}{\mathtt{B}}{}_{\varepsilon}^{(d)}(\mathbf{c}) = \{\mathbf{x}, \mathbf{x} \in \mathbb{X} \subseteq \mathbb{E}^d \mid \langle \mathbf{x}-\mathbf{c}, \mathbf{x}-\mathbf{c} \rangle - \varepsilon < 0\} \tag{A–52}$$

while a **closed** d-**ball** $\bar{\mathtt{B}}_{\varepsilon}^{(d)}(\mathbf{c})$ with radius $\sqrt{\varepsilon}$ and centre $\mathbf{c}$ is the set of points $\mathbf{x}$ belonging to $\mathbb{E}^d$, for which:

$$\bar{\mathtt{B}}_{\varepsilon}^{(d)}(\mathbf{c}) = \{\mathbf{x}, \mathbf{x} \in \mathbb{X} \subseteq \mathbb{E}^d \mid \langle \mathbf{x}-\mathbf{c}, \mathbf{x}-\mathbf{c} \rangle - \varepsilon \leq 0\} \tag{A–53}$$

Note that, by definition, an open d-ball is (covered by) an open set and a closed d-ball is a closed set. Moreover: $\mathrm{Int}\,\mathtt{B} \cong \overset{\circ}{\mathtt{B}}$, $\mathrm{Cl}\,\mathtt{B} \cong \bar{\mathtt{B}}$, and $\mathrm{Bd}\,\mathtt{B} \cong \partial\mathtt{B}$.

A $(d-1)$-**sphere** $\mathtt{S}_\varepsilon^{(d-1)}(\mathbf{c})$ with radius $\sqrt{\varepsilon}$ and centred at $\mathbf{c}$ is the set of points $\mathbf{x} \in \mathbb{X} \subseteq \mathbb{E}^{\mathrm{d}}$, for which:

$$\mathtt{S}_\varepsilon^{(d-1)}(\mathbf{c}) = \{\mathbf{x}, \mathbf{x} \in \mathbb{X} \subseteq \ E^d \mid \langle \mathbf{x}-\mathbf{c}, \mathbf{x}-\mathbf{c}\rangle - \varepsilon = 0\} \tag{A–54}$$

Notice that $\mathtt{S}_\varepsilon^{(d-1)}(\mathbf{c}) = \partial\mathtt{B}_\varepsilon^{(d)}(\mathbf{c})$. Furthermore, $\mathtt{S}_\varepsilon^{(d-1)}(\mathbf{c})$ can be written in normalised form:

$$\mathtt{S}_\varepsilon^{(d-1)}(\mathbf{c}) = \{\mathbf{x}, \mathbf{x} \in \mathbb{X} \subseteq \mathbb{E}^d \mid \mathbf{x}^T\mathbf{x} - 2\mathbf{c}^T\mathbf{x} + \|\mathbf{c}\|^2 - \varepsilon = 0\} \tag{A–55}$$

Let line $\mathtt{L}$ belong to a pencil through point $\mathbf{x}$ and be given by $\mathbf{y} = \mathbf{u}\lambda$, such that $\mathbf{u}^{\mathbf{T}}\mathbf{u} = 1$. Line $\mathtt{L}$ enters sphere $\mathtt{S}$ for $\lambda = \lambda_1$ and leaves sphere $\mathtt{S}$ at a point on $\mathtt{L}$ where $\lambda = \lambda_2$. Let line $\mathtt{L}$ belong to a pencil of lines through point $\mathbf{x}$, given by $\mathbf{v} = \mu\mathbf{u}$, with $\mathbf{u}^T\mathbf{u} = 1$. The power of $\mathbf{x}$ with respect to the $(d-1)$-sphere is given by the product of $\mu_1\mu_2$ and in the two points $\mathbf{p}$ and $\mathbf{p}\prime$, $\mu_1 = \mu_2 = \pi^2$. This classical problem is also known as the *circle intersection chord*-problem and $\mu_1\mu_2 = \pi^2$ is also known as *Vieta's formula*. For a proof of the fact that power π^2 does not depend on the heading of line $\mathtt{L}$, see for example [Max52, Ch. V], for a sphere in E^2. A proof for a general dimension $(d-1)$-sphere was not found but follows readily from generalisation into general dimension.The normalised equation for $\mathtt{S}$ (see equation (A–55)), takes the form:

$$a\lambda^2 + b\lambda + c = 0 \tag{A–56}$$

where:

$$\begin{cases} a = & \mathbf{u}^T\mathbf{u} = 1 \\ b = & 2\left(\mathbf{x}^T - \mathbf{c}^T\right)\mathbf{u} \\ c = & \mathbf{x}^T\mathbf{x} - 2\mathbf{c}^T\mathbf{x} + \|\mathbf{c}\|^2 - \varepsilon \end{cases} \tag{A–57}$$

This is an ordinary quadratic equation in λ which has two real roots $\lambda_{1,2}$ if $D = b^2 - 4ac > 0$, i.e., if $\varepsilon > 0$. If $\varepsilon < 0$, roots will be *imaginary*, associated with a negative weight $w = -\varpi = i^2\varpi$ where $\varpi > 0$ and $i^2 = -1$. A sphere with $\varepsilon < 0$ is called an **i-sphere**. The **power of a point x** has the following geometric interpretation ([Aur87b],[Ede92],[BP94]). With point $\mathbf{x}$, a point in $\mathbb{X} \subseteq \mathbb{E}^d$ and $\bar{\mathtt{S}}_\varepsilon^{(d-1)}(\mathbf{c})$ a closed $(d-1)$-sphere in E^d, the power of $\mathbf{x}$ with respect to $\bar{\mathtt{S}}_\varepsilon^{(d-1)}(\mathbf{c})$ is the square of the distance $\pi = d(\mathbf{x},\mathbf{p}) = \|\mathbf{x}-\mathbf{p}\|$, with $\mathbf{p}$ being a contact point of a line through $\mathbf{x}$, touching the sphere. Point $\mathbf{p}'$ is the other tangent point, and for $\mathbf{p}$ one may also read $\mathbf{p}'$, so $\pi = d(\mathbf{x},\mathbf{p}) = d(\mathbf{x},\mathbf{p}')$. If radius ε of $\bar{\mathtt{S}}_\varepsilon^{(d-1)}(\mathbf{c})$ grows, such that a point $\mathbf{x}$ becomes contained in the border $\mathrm{Bd}\,\bar{\mathtt{S}}_\varepsilon^{(d-1)}(\mathbf{c})$ of the sphere or in the interior $\mathrm{Int}\,\bar{\mathtt{S}}_\varepsilon^{(d-1)}(\mathbf{c})$ of the sphere, then its power

becomes zero, and negative, resp. According to equation (A–53), a **weighted closed d-ball** $\tilde{\bar{\mathtt{B}}}^{(d)}_{w_c}(\mathbf{c})$ can now be defined as a d-ball with radius $\sqrt{w_c}$, centred at point $\mathbf{c}$, of which the interior consists of points having a non-positive power with respect to $\mathtt{B}$:

$$\tilde{\bar{\mathtt{B}}}^{(d)}_{w_c}(\mathbf{c}) = \{\mathbf{x}, \mathbf{x} \in \mathbb{X} \subseteq \mathbb{E}^d \mid \langle \mathbf{x}-\mathbf{c}, \mathbf{x}-\mathbf{c}\rangle - w_c \leq 0\} \tag{A–58}$$

For a negative weight $w_c = -\varpi = i^2\varpi < 0$, $\tilde{\mathbf{c}} = (\mathbf{c}, w_c) = (\mathbf{c}, -\varpi)$ can be interpreted as an i-sphere (d-ball) centred at $\mathbf{c}$ with radius $-i\sqrt{\varpi}$. Often in geometry, therefore, weighted points are treated as d-balls.

A **pencil of two spheres** in E^d is a linear combination:

$$\mathcal{P}(\mathtt{S}_1, \mathtt{S}_2) = \lambda_1 \mathtt{S}_1 + \lambda_2 \mathtt{S}_2 \tag{A–59}$$

The Lebesgue measure (or: d-volume, or: hyper-volume) of a d-ball $\mathtt{B}^{(d)}_R$ with radius $r = \sqrt{R}$ is given by:

$$\nu^{(d)}_{\mathcal{L}}(\mathtt{B}^{(d)}_R) = e^{\pi R}\left[1 + \mathrm{erf}(r\sqrt{\pi})\right] \tag{A–60}$$

For further details and proofs, see [DFM90].

A.9 Weighted triangulation

A **d-triangulation** is a **tessellation** of d-space with non-overlapping d-simplices as building blocks. As such, it is obviously also a simplicial complex and a **cellular complex** (or: **cell(ular) decomposition**). In a topological sense, a tessellation of non-overlapping cells is also a **cover**. The intersection of two of its simplices, if non-empty, is also a face of the triangulation, along with all its subfaces. A topological space is said to be **triangularizable** if it admits one or more triangulations. More details on triangularizability can be taken from [Sha77], for example. More in particular, every **convex polyhedron** can be triangulated (e.g.,[Mun84]), and being a polyhedron, every convex polytope and therefore every convex hull can so too. They are triangularizable topological spaces. Every k-simplex, $0 \leq k \leq d$ is again a convex hull and a polytope.

Various **weighted distances** exist (see [Aur87a]):

Name ([Aur87a])	Definition
Laguerre weighted distance	$\|\tilde{\mathbf{x}} - \tilde{\mathbf{s}}\|_L = \|\mathbf{x}-\mathbf{s}\|^2 - w_s$
associative weighted distance	$\|\tilde{\mathbf{x}} - \tilde{\mathbf{s}}\|_a = \|\mathbf{x}-\mathbf{s}\|^2 - w_s^2$
muliplicative weighted distance	$\|\tilde{\mathbf{x}} - \tilde{\mathbf{s}}\|_m = \|\mathbf{x}-\mathbf{s}\|^2 / w_s$

In this thesis, only the *Laguerre distance* will be considered. The **Laguerre distance** is defined as:

$$L(\tilde{\mathbf{s}}_i, \tilde{\mathbf{s}}_j) = \langle \mathbf{s}_i - \mathbf{s}_j, \mathbf{s}_i - \mathbf{s}_j \rangle - (w_i + w_j) = \\ \|\mathbf{s}_i\|^2 + \|\mathbf{s}_j\|^2 - 2\langle \mathbf{s}_i, \mathbf{s}_j \rangle - (w_i + w_j) \quad \text{(A–61)}$$

Two weighted points $\tilde{\mathbf{x}}_i$ and $\tilde{\mathbf{x}}_j$ are said to be **orthogonal** if $L(\tilde{\mathbf{x}}_i, \tilde{\mathbf{x}}_j) = 0$.

A simplex is called **regular** if all vertices except the ones belonging to the simplex have positive weighted distances to each of the vertices in the simplex. In other words:

$$\forall \tilde{s}_i \in \tilde{S} - \tilde{Y}, \forall \tilde{y}_i \in \tilde{Y} : L(\tilde{s}_i, \tilde{y}_i) > 0 \quad \text{(A–62)}$$

where $\tilde{Y} \subset \tilde{S}$. Moreover, a d-simplex contained in the regular triangulation must fulfil two conditions:

- **1. Regularity:**

  The simplex must be a *regular* simplex.

- **2. Orthogonality:**

  A $(d-1)$-sphere must exist, centred in the radical centre, that meets all the simplex' weighted vertices orthogonally.

A.10 Weighted Voronoi diagram

A **weighted Voronoi diagram** (or: **power diagram** or: **Dirichlet complex** or: **Laguerre diagram**) $\Pi(\tilde{\mathbb{S}})$ of a finite set of weighted points $\tilde{\mathbb{S}}$ is a space partitioning dividing E^d in a cell complex such that for every $\mathbf{s}_i, \mathbf{s}_j \in \mathbb{S}, i \neq j$, $\mathtt{V}(\mathbf{s}_i)$ defines a **Voronoi cell** for which:

$$\mathtt{V}(\mathbf{s}_i) = \{\mathbf{x} \in \mathbb{E}^d \mid \langle \mathbf{x} - \mathbf{s_i}, \mathbf{x} - \mathbf{s_i} \rangle - w_i < \langle \mathbf{x} - \mathbf{s_j}, \mathbf{x} - \mathbf{s_j} \rangle - w_j \} \quad \text{(A–63)}$$

An (open) Voronoi cell $\mathtt{V}(\mathbf{s}_j)$ generated by a point $\mathbf{s}_j$ contains all the points beneath all members in an arrangement $\mathcal{A}(\mathtt{H})$ of hyperplanes of $\mathbf{s}_j$:

$$\mathtt{V}(\mathbf{s}_j) = \bigcap_j \mathtt{H}^-_{\mathbf{s}_j} \quad \text{(A–64)}$$

by virtue of which one may also write for the (closed) Voronoi cell:

$$\mathtt{V}(\mathbf{s}_i) = \{\mathbf{x} \in \mathbb{E}^d \mid L(\mathbf{s}_i, \mathbf{x}) - L(\mathbf{s}_j, \mathbf{x}) \leq 0\} \tag{A–65}$$

for all $\mathbf{s}_j \neq \mathbf{s}_i$.

A **radical (hyper)plane** is the hyperplane of equal powers with respect to two weighted points. Representing weighted points as $(d-1)$-spheres $\mathtt{S}_1(\mathbf{c}_1)$ and $\mathtt{S}_2(\mathbf{c}_2)$, $\mathbf{c}_1 \neq \mathbf{c}_2$. With normal equations:

$$\mathbf{x}^T\mathbf{x} - 2\mathbf{c}_1^T\mathbf{x} + \|\mathbf{c}_1\|^2 - \varepsilon_1 = \mathbf{x}^T\mathbf{x} - 2\mathbf{c}_2^T\mathbf{x} + \|\mathbf{c}_2\|^2 - \varepsilon_2 \tag{A–66}$$

for the radical hyperplane:

$$\mathtt{H} = \{\mathbf{x}, \mathbf{x} \in \mathbb{E}^d \mid 2(\mathbf{c}_2 - \mathbf{c}_1)^T\mathbf{x} - \left[\|\mathbf{c}_2\|^2 - \|\mathbf{c}_1\|^2 - (\varepsilon_2 - \varepsilon_1)\right] = 0\} \tag{A–67}$$

With equations (A–35) and (A–36) it is obvious that if $\varepsilon_2 - \varepsilon_1$ changes, the radical plane translates along a normal vector of the radical plane, taking a new parallel position. Independent of the weights, $\mathtt{H}$ is perpendicular to the line segment connecting the centres of both weighted points. Also $\mathtt{S}_1 \cap \mathtt{S}_2 \neq \emptyset \Rightarrow \mathtt{H} \cap \mathtt{S}_1 \neq \emptyset$ and $\mathtt{H} \cap \mathtt{S}_1 \neq \emptyset \Rightarrow \mathtt{H} \cap \mathtt{S}_2 \neq \emptyset$. Generally, in E^d, k hyperplanes in general position intersect in a single $(d-k)$-flat. If radical hyperplanes intersect in a single (0)-flat, a point, this point is called the **radical centre**. For a radical centre $C^{\mathtt{V}}$:

$$C^{\mathtt{V}} = \mathtt{H}_1^{\mathtt{V}} \bigcap \mathtt{H}_2^{\mathtt{V}} \bigcap \cdots \bigcap \mathtt{H}_m^{\mathtt{V}} = \bigcap_{j=1}^{m} \mathtt{H}_j^{\mathtt{V}} \tag{A–68}$$

Permutations of the ordered pairs of 2 out of $d+1$ points generate m radical planes, with:

$$m = \binom{d+1}{2} = \frac{(d+1)!}{2!(d+1-2)!} = \frac{1}{2}\frac{(d+1)!}{(d-1)!} \tag{A–69}$$

which generally do *not* form a simple arrangement because such radical planes are not in general position. By definition, the k-faces, $k < d$, of a Voronoi diagram are contained in the radical planes separating the region of dominance of the corresponding weighted points. The line segments between weighted points bisected by a radical plane, are edges in the regular triangulation, see for example [Ede92] or [Ede93]. More in particular, with $0 \leq k \leq d$, if the Voronoi cells of $k+1$ weighted points have a point in common then this point is a radical centre and the $k+1$ points form a k-simplex in the dual regular triangulation.

A.11 Simplicial complex and skeletons

A **finite simplicial k-complex** $\mathcal{C}(\mathbb{S})$, with $\mathbb{S} = \bigcup \mathbb{Y}_j$ is a connected or unconnected collection of simplexes (or: simplices), with $0 \leq k \leq d$, all satisfying tw o properties:

$$\begin{cases} \sigma_{Y_j}^{(k)} \in \mathcal{C} & \Rightarrow \sigma_{Y_j'}^{(k-1)} \in \mathcal{C}' \subseteq \mathcal{C} \\ \sigma_{Y_j}^{(k)} \in \mathcal{C},\ \sigma_{Y_j'}^{(k-1)} \in \mathcal{C}' & \Rightarrow \mathcal{C} \cap \mathcal{C}' = \emptyset \vee \mathcal{C} \cap \mathcal{C}' = \mathcal{C}' \end{cases} \tag{A–70}$$

Apparently, every subface of a simplex needs to be in $\mathcal{C}$ too, and ev ery subcomplex $\mathcal{C}' \subseteq \mathcal{C}$ is itself also a simplicial complex. A simplicial complex may degenerate to a point set, a linear graph, etc., having a highest dimension $m < d$.

A subcomplex $\mathcal{K}^{(k)}(\mathcal{C})$ of $\mathcal{C}(\mathbb{S})$ containing all l-faces $0 \leq l \leq k$, is called a **k-skeleton**. The 0-skeleton $\mathcal{K}^{(0)}(\mathcal{C})$ is the set of vertices $\mathbb{S}$ itself and 1-skeleton $\mathcal{K}^{(1)}$ is a "wireframe" of the simplicial complex $\mathcal{C}$. The **closed star** $\bar{St}\,\mathbf{s}_j$ of v ertex $\mathbf{s}_j$ in $\mathcal{C}(\mathbb{S})$ is the subset of all (closed) faces of $\mathcal{C}$ incident upon $\mathbf{s}_j$. Similarly, an **open star** (or simply: star) $St\ \mathbf{s}_j$ of v ertex$\mathbf{s}_j$ is the union of all in teriors of the subset of faces of $\mathcal{C}$ incident upon $\mathbf{s}_j$. The difference between open and closed star:

$$Lk\ \mathbf{s} = \bar{St}\ \mathbf{s} - St\ \mathbf{s} \tag{A–71}$$

is called the link $Lk\ \mathbf{s}_j$ of $\mathbf{s}$. The star of vertex $\mathbf{s}_j$ is the union of all points $\mathbf{x}$ defined b y some conv ex combination for which $\lambda_j(\mathbf{x}) > 0$. The link $Lk\ \mathbf{s}_j$ of a vertex $\mathbf{s}_j$ is not necessarily connected.

A.12 Alpha complex

An **α-complex** $\mathcal{C}_\alpha$ is a one-parameter finite simplicial k-complex. As such, it is also a subcomplex of the regular triangulation $\mathcal{T}$, which is a d-simplicial complex. A **weight-plus-alpha ball** is defined as follows:

$$\mathtt{B}_{w_c+\alpha}^{(d)}(\mathbf{c}) = \{\mathbf{x}, \mathbf{x} \in \mathbb{X} \subseteq \mathbb{E}^d \mid \langle \mathbf{x} - \mathbf{c}, \mathbf{x} - \mathbf{c} \rangle - (\alpha + w_c) \leq 0\} \tag{A–72}$$

With $\alpha \in [0..\infty)$, $\mathtt{B}$ has a "start"-radius of $\sqrt{w_c}$ and grows proportional to $\sqrt{\alpha}$ as α increases from a very small value to $\alpha_{\max}$.

Let $\sigma_{Y_j}^{(k)} \in \mathcal{C}_\alpha$ denote a k-simplex belonging to the α-complex $\mathcal{C}_\alpha(\mathbb{S})$ and $\mathbb{Y}_j \subseteq \mathbb{S}$. Assume that for every such $\sigma_{Y_j}^{(k)}$ there exists an α-ball in the radical centre $C^{\emptyset}$ of $\mathbb{Y}_j$. A k-simplex $\sigma_{Y_j}^{(k)}$, formed b y $k+1$ points $\mathbf{x}_i \in X$ is **α-exposed** if with an empty α-ball in its radical centre:

$$L(\mathbf{x}_i, C_Y^{\emptyset}) = \begin{cases} 0 & , \quad \forall \mathbf{x}_i \in \mathbb{Y}_j \qquad \text{(orthogonality)} \\ > 0 & , \quad \forall \mathbf{x}_i \in \mathbb{S} - \mathbb{Y}_j \qquad \text{(regularity)} \end{cases} \tag{A–73}$$

A **weighted alpha complex** $\mathcal{C}_\alpha(\mathbb{S})$ is a subcomplex of the regular triangulation $\mathcal{T}(S)$, containing all α-exposed k-faces of $\mathcal{T}$. Notice that equation (A–73) defines exactly those faces of the regular triangulation $\mathcal{T}$ that are α-exposed. Also notice that if $\sigma_{Y_j}^{(k)}$ is made up of zero-weight points, then the $k+1$ vertices $\mathbf{x}_i \in \sigma_{Y_j}^{(k)}$ will be contained in the boundary $\operatorname{Bd}\mathtt{A}$ and $\operatorname{Int}\mathtt{A} = \emptyset$. The follo wing also holds:

$$\alpha_i \leq \alpha_j \quad \Rightarrow \quad \mathcal{C}_{\alpha_i} \subseteq \mathcal{C}_{\alpha_j} \tag{A–74}$$

For sufficiently low a value of α, i.e., for $\alpha < \alpha_{\min}$, the α-complex $\mathcal{C}_\alpha = \mathbb{S}$. This complex is growing, with increasing value of α, into triangulation $\mathcal{T}$, and the **underlying space** $|\mathcal{C}_\alpha|$ into the convex hull $\operatorname{Conv}\mathbb{S} = \mathcal{H}(\mathbb{S}) = |\mathcal{C}_{\alpha_{\max}}|$.

Let $\mathcal{Y}$ be a cover of E^d. Then the nerve $\mathcal{N}_{rv}\mathcal{Y}$ is an abstract simplicial complex composed of the collection of non-empty intersections of subsets of cover $\mathcal{Y}$:

$$\mathcal{N}_{rv}\mathcal{Y} = \{\mathbb{X}_1, \mathbb{X}_2 \subseteq \mathbb{Y} \mid \mathbb{X}_1 \bigcap \mathbb{X}_2 \neq \emptyset \} \tag{A–75}$$

The **geometric realisation of the nerve** of the weighted V oronoidiagram is the regular triangulation. F urthermorefor a $\mathbb{X}_2 \subseteq \mathbb{X}_1$:

$$\mathbb{X}_1 \in \mathcal{N}_{rv}\mathcal{Y} \;\Rightarrow\; \mathbb{X}_2 \in \mathcal{N}_{rv}\mathcal{Y} \tag{A–76}$$

An **α-parametrised Voronoi cell** can be described by:

$$\mathtt{V}_\alpha(\mathbf{s}_j) = \mathtt{B}_{w_j+\alpha}(\mathbf{s}_j) \bigcap \mathtt{V}(\mathbf{s}_j) \tag{A–77}$$

and, with $\mathtt{H}_{ij}^{\emptyset}$ denoting the radical plane of ordered pair $(\mathbf{s}_i, \mathbf{s}_j)$, so that $\mathtt{V}(\mathbf{s}_j)$ is given by $\mathtt{V}(\mathbf{s}_j) = \bigcup_k \mathtt{H}_{jk}^{\emptyset-}$, one has that:

$$\mathtt{V}_\alpha(\mathbf{s}_j) = \mathtt{B}_{w_j+\alpha}(\mathbf{s}_j) \bigcap \left(\bigcup_k \mathtt{H}_{jk}^{\emptyset-} \right) \tag{A–78}$$

and the part of the Voronoidiagram swept out for the given value of α by ball union $\mathcal{B}$, one obtains:

$$\mathcal{U} = \bigcup_j \left\{ \mathtt{B}(\mathbf{s}_j) \bigcap \left(\bigcup_k \mathtt{H}_{jk}^{\bar{\emptyset}-} \right) \right\} \tag{A–79}$$

Without providingall the details: the geometric realisation of the nerve of the α-parametrised ball union is an α-complex. For details, refer to [Ede92] and [Ede93].

Generally, an α-complex contains l-skeletons, with $0 \leq l \leq d$. The k-faces contained in α-complexes may be **singular**, **regular** or **interior** for a specific value of α. Let $0 \leq j < m \leq d$ and let $\sigma^{(j)}, \sigma^{(m)} \in \mathcal{C}_\alpha$. Now we can tell singular k-faces apart from regular ones, as follows [EM94]:

$$\begin{cases} \sigma_{Y_j} \in \mathrm{Bd}\,\mathcal{C}_\alpha \ \wedge \ \sigma_{Y_j} \notin \sigma_{Y_m} & \rightarrow \text{singular face} \\ \sigma_{Y_j} \in \mathrm{Bd}\,\mathcal{C}_\alpha \ \wedge \ \sigma_{Y_j} \in \sigma_{Y_m} & \rightarrow \text{regular face} \end{cases}$$

A face in the interior of $\mathcal{C}_\alpha$, i.e., $\sigma_{Y_r} \in \mathrm{Int}\,\mathcal{C}_\alpha$, is classified as interiorface.

The set $\mathbb{A}$ of all ordered pairs $(\rho, \mathcal{C}_\alpha(\mathbb{S}))$ denotes the finite set of α-complexes of set $\mathbb{S}$, called the **α-family**, and 2-tuple $(\rho_i, \mathcal{C}_\alpha(\mathbb{S})) \in \mathbb{A}$ denotes a member of that set. Here, ρ is a unique index into the α-family, such that:

$$\rho_i < \rho_j \quad \Rightarrow \quad \alpha_i < \alpha_j \tag{A–80}$$

and:

$$\rho_i < \rho_j \quad \Rightarrow \quad \mathcal{C}_{\alpha_i} \subset \mathcal{C}_{\alpha_j} \tag{A–81}$$

whereas in general, for $\alpha_i < \alpha_j \Rightarrow \mathcal{C}_{\alpha_i} \subseteq \mathcal{C}_{\alpha_j}$ doesn't always yield a proper subcomplex. Observe that whereas α only allows for a partial ordering of the α-family, ρ allows for a *strict partial ordering* using a linear order relation "<". Notice also that this definition allows a topological sort of the set $\mathbb{A}$, according to the index ρ.

A **signature** [EM94] (for positive α-values) is a function $\mathsf{S} : [0, +\infty) \rightarrow D$, providing a value for a specific property.

Weights can be generated on a per point basis, they can also be generated as a function. We will refer to such functions as **weighting functions**, of the form $\mathsf{f} : E^d \rightarrow R$. Weights are called **unstructured weights** if two arbitrary functions values (function images) $\mathsf{f}(\mathbf{x}_1)$ and $\mathsf{f}(\mathbf{x}_2)$ have auto-covariance $Cov_{xx}(\mathbf{x}_1, \mathbf{x}_2) \rightarrow 0$.

A.13 Polyhedral objects

A topological space P is a k-**polyhedron** if there exist a collection of l-simplices $\sigma^{(l)}$, $0 \leq l \leq k$, and a set $\mathbb{F}$ of faces of those simplices such that the polyhedron is entirely erected by the faces in $\mathbb{F}$. A polyhedron is the polytope of a simplicial complex. A k-polytope $\mathcal{P}^{(k)}(\mathbb{S})$ is a bounded k-polyhedron. With $\mathbb{Y}_i = \{y_1^{(i)}, y_2^{(i)}, \ldots, y_{d+1}^{(i)}\}$ and $\mathbb{Y}_j = \{y_1^{(j)}, y_2^{(j)}, \ldots, y_{d+1}^{(j)}\}$, $\mathbb{Y}_i \neq \mathbb{Y}_j$, there exists a $\delta > 0$ for which $|y_k^{(i)} - y_k^{(j)}| < \delta$, for $1 \leq k \leq d+1$. Every polytope is a compact topological space. If a polytope spanned by a set $\mathbb{S}$ is convex and free of holes, it coincides with the convex hull $\mathcal{H}(S)$. A **convex hull** of a point set $\mathbb{S}$ is the smallest convex set that contains $\mathbb{S}$. A convex hull of a finite point set is a compact space. If two points $\mathbf{p}_i$ and $\mathbf{p}_j$ of a convex set $\mathcal{H}(\mathbb{S}) \subset \mathbb{E}^d$ belong to $\mathcal{H}(S)$, then also all points lying on the straight line segment $\mathbf{p}_i\mathbf{p}_j$ are part of $\mathcal{H}(\mathbb{S})$ which, by itself, is a sufficient condition for a set to be convex. The intersection of a support plane and a convex hull is always an (extreme) member of $\mathbb{S}$. A point $\mathbf{x}$ belongs to the convex hull of $\mathbb{S}$ if $\mathbf{x}$ can be written as a convex combination in the m vertices of $\mathbb{S}$:

$$\begin{pmatrix} \mathbb{S} \\ \mathbf{1}^T \end{pmatrix} \Lambda = \begin{pmatrix} \mathbf{x} \\ \mathbf{1} \end{pmatrix} \tag{A–82}$$

i.e., finding a solution vector Λ of which the m elements $\lambda_i \geq 0$ and $\mathbf{1}^T\Lambda = 1$. This makes a system of $d+1$ linear equations, with m unknowns. Λ is unique if the $\mathrm{card}\,\mathbb{S} \leq d+1$, i.e., if $\mathbb{S}$ spans a simplex and not unique $\mathrm{card}\,\mathbb{S} > d+1$.

A.14 Morphology

A finite **configuration space** $\mathbb{S} \subset \mathbb{E}^d$ is the space of all possible landmark coordinates. A **configuration** is now described by its **configuration matrix** $\mathbf{X}_\mathbb{S}$, an $N \times d$-coordinate matrix of the form:

$$\mathbf{X}_\mathbb{S} = \begin{pmatrix} x_{0,0} & x_{0,1} & \cdots & x_{0,d-1} \\ x_{1,0} & x_{1,1} & \cdots & x_{1,d-1} \\ \cdots & \cdots & \cdots & \cdots \\ x_{N-1,0} & x_{N-1,1} & \cdots & x_{N-1,d-1} \end{pmatrix} \tag{A–83}$$

When in general position, this matrix is assumed to have full rank. For a lattice, the configuration matrix reduces to:

$$\mathbf{X}_{\mathbb{S}} = \begin{pmatrix} x_0 & x_1 & \cdots & x_{d-1} \\ x_0 & x_1 & \cdots & x_{d-1} + \Delta_{d-1} \\ x_0 & x_1 & \cdots & x_{d-1} + 2\Delta_{d-1} \\ \cdots & \cdots & \cdots & \cdots \\ x_0 & x_1 & \cdots & x_{d-1} + (N-1)\Delta_{d-1} \\ \cdots & \cdots & \cdots & \cdots \\ x_0 + (N-1)\Delta_0 & x_1 + (N-1)\Delta_1 & \cdots & x_{d-1} \\ x_0 + (N-1)\Delta_0 & x_1 + (N-1)\Delta_1 & \cdots & x_{d-1} + \Delta_{d-1} \\ x_0 + (N-1)\Delta_0 & x_1 + (N-1)\Delta_1 & \cdots & x_{d-1} + 2\Delta_{d-1} \\ \cdots & \cdots & \cdots & \cdots \\ x_0 + (N-1)\Delta_0 & x_1 + (N-1)\Delta_1 & \cdots & x_{d-1} + (N-1)\Delta_{d-1} \end{pmatrix} \tag{A–84}$$

For a regular square grid, for which $\Delta_j = \Delta$, starting in the origin, so that $x_i = 0$ for all $0 \leq i < d$ this can be further simplified.

Affine transformations can now be written in matrix notation as

$$\mathsf{T}(\mathbf{X}_{\mathbb{S}}) = \mathbf{T}_G + \mathbf{X}_{\mathbb{S}}^T \mathbf{T} \tag{A–85}$$

where $\mathbf{T}_G$ is an $N \times d$ glide or translation matrix and $\mathbf{T}$ is a $d \times d$ square **transformation matrix** associated with transformation T. Further dimension analysis learns that with $\mathbf{X}_{\mathbb{S}}$ being $N \times d$ and assuming that $dim\ \mathrm{im}\,\mathsf{T} = N$ and therefore $\mathsf{T}(\mathbf{X}_{\mathbb{S}})$ is an $N \times d$ matrix. Equation (A–85) is the expression for a general affine transformation. We now have the following special cases:

- **Linear transformation**

  If $\mathbf{T}_G = \mathbf{0}$ then T is linear.

- **Rotation**

  If $\mathbf{T}_G = \mathbf{0}$ and $\mathbf{T}^T\mathbf{T} = \mathbf{I}$, or equivalently: $\mathbf{T}^{-1} = \mathbf{T}^T$, then T is orthogonal and T is a rotation.

- **An-isotropic scaling**

  If $\mathbf{T}_G = \mathbf{0}$ and $\mathbf{T} = \Lambda\mathbf{I}$, then T is an an-isotropic scaling.

- **Isotropic scaling**

  If $\mathbf{T}_G = \mathbf{0}$ and $\mathbf{T} = \lambda\mathbf{I}$, then T is an isotropic scaling.

- **Identity transformation**

  If $\mathbf{T}_G = \mathbf{0}$ and $\mathbf{T} = \mathbf{I}$, then T is an identity transformation.

where $\mathbf{I}$ is the identity matrix and Λ is a diagonal matrix, $\Lambda = diag\ \mathbf{T}$. Kernel $\ker \mathsf{T} \subset \mathbb{S}$ is the set for which: $\ker \mathsf{T} = \{\mathbf{s} \in \mathbb{S} \mid \mathsf{T}(\mathbf{s}) = \mathbf{0}\}$. One also has that $\ker \mathsf{T} = \mathsf{T}^{-1}(\mathbf{0})$. For the image $\mathrm{im}\,\mathsf{T} = \{\mathsf{T}(\mathbf{s}) \mid \mathbf{s} \in \mathbb{S}\}$. It can be shown (e.g., [Str86]) that for T:

$$\begin{aligned} &(i) \quad \mathsf{T}\ \textit{an injection} \iff \ker \mathsf{T} = \{\mathbf{0}\} \\ &(ii) \quad \mathsf{T}\ \textit{a surjection} \iff \mathrm{im}\,\mathsf{T} = \mathbb{U} \end{aligned} \tag{A–86}$$

with which the combination (i) and (ii) for a bijection is immediate.

Shape matching seeks to map the observed landmark set, represented by configuration matrix $\mathbf{X}_{\mathbb{S}}$ onto the configuration matrix $\mathbf{X}_{\mathbb{S}_\wp}$ of the icon, and shape instantiation does the reverse. So, for example for shape instantiation, find a T, represented by matrix $\mathbf{T}$, such that:

$$\mathbf{X}_{\mathbb{S}_\wp} \mathbf{T} = \mathbf{X}_{\mathbb{S}} \tag{A–87}$$

where $S_\wp$ is the landmark set of the icon. Assume $dim\ \mathrm{im}\,\mathsf{T} = dim\ \mathbb{S} = d$. This is in line with the fact that T is homeomorphic, so $\mathsf{T}(\mathbf{X}_{\mathbb{S}})$ and $\mathbf{X}_{\mathbb{S}}$ have similar dimensions and the rank of matrix $\mathbf{T} = d$. Also, since $\mathbb{S}, \mathbb{U} \subset \mathbb{E}^d$ both $\mathbb{S}$ and $\mathbb{U}$ have the same (Euclidean) vector norm. Finally, $\mathbb{S}$ has been assumed compact and finite, and with **scale parameter** $|\lambda| < \infty$, $\mathbb{U}$ is also compact. Given an affine transformation, as in equation (A–85). A **Helmertized norm** $\|\mathsf{T}\|_\hbar$ is then defined by:

$$\|\mathsf{T}\|_\hbar = \sup_{\mathbf{s}_j} \frac{\|\mathsf{T}(\mathbb{S})\|_\hbar}{\|\mathbb{S}\|} = \sup_{\mathbf{s}_j} \frac{\|\mathbf{X}_{\mathbb{S}}^T \mathbf{T}\|}{\|\mathbb{S}\|} \tag{A–88}$$

and the impact on the Lebesgue measure is given by:

$$\nu_{\mathcal{L}}^d(\mathsf{T}(\mathbb{S})) = c\|\lambda^d \mathsf{T}\|_\hbar = c|\lambda^d|\ \|\mathsf{T}\|_\hbar \tag{A–89}$$

A **shape** $\mathcal{W}(\mathbb{S})$, generated by landmark set $\mathbb{S}$ is a set function for which:

$$\begin{cases} \mathcal{W}(\lambda\mathbb{S}) \cong \mathcal{W}(\mathbb{S}) \\ \mathcal{W}(\mathbb{S} + \mathbf{y}) \cong \mathcal{W}(\mathbb{S}) \end{cases} \tag{A–90}$$

A **shape function** g is a real-valued function $\mathsf{g} : E^d \mapsto R$ of the form $\mathsf{g} = \mathsf{G}(\mathbb{S})$.

A.15 Point process

Let $\Phi_{\mathbb{S}}(\mathbf{x})$ be a **Poisson point process** on $\mathbb{S} \subset \mathbb{E}^d$ with intensity λ. Then:

$$\lambda = \frac{\mathsf{E}[\Phi_{\mathbb{S}}(\mathsf{B})]}{\nu_{\mathcal{L}}^{d}(\mathsf{B})} \tag{A–91}$$

where $\mathsf{B} \subset E^d$ is some window on E^d. If $\Phi_{\mathbb{S}}(\mathbf{x})$ is stationary, then:

$$\lambda = \mathsf{E}[\Phi_{\mathbb{S}}([0,1]^{\mathrm{d}})] \tag{A–92}$$

Let $\Phi_{\mathbb{S}}(\mathbf{x})$ be stationary, with intensit yλ and let $\mathsf{T} : E^d \mapsto E^d$ be a non-singular linear transformation, defined by:

$$\mathsf{T}(\Phi_{\mathbb{S}}(\mathbf{x})) = \{\mathbf{x}\mathbf{T} : \ \mathbf{x} \in \Phi_{\mathbb{S}}\} \tag{A–93}$$

Then, by virtue of the **conservation property**, we have that:

$$\Phi_{\mathbb{S}}(\mathbf{x}) \ \textit{stationary} \ \Rightarrow \ \mathsf{T}(\Phi_S(\mathbf{x})) \ \textit{stationary} \tag{A–94}$$

and the **transformed in tensity** is given by:

$$\lambda_{\mathsf{T}} = \det \ \mathbf{T}^{-1} \tag{A–95}$$

The probability of a **v oid space** of the size B_α is giv en by:

$$\mathsf{G}_V(\alpha) = \mathsf{Pr}[\Phi_{\mathbb{S}}(\mathsf{B}_\alpha) = 0] \tag{A–96}$$

and as a consequence, the probability of α-ball contact of an α-ball centred in a radical cen tre with radius $\sqrt{\alpha}$ is:

$$\mathsf{G}_\emptyset(\alpha) = 1 - \mathsf{Pr}[\Phi_{\mathbb{S}}(\mathsf{B}_\alpha) = 0] \tag{A–97}$$

F or a stationary Poisson process, these probabilities are:

$$\mathsf{G}_V(\alpha) = \mathsf{Pr}[\Phi_{\mathbb{S}}(\mathtt{B}_\alpha) = 0] = \exp(-\lambda\nu_{\mathcal{L}}^d(\mathtt{B}_\alpha)) \tag{A–98}$$

and:

$$\mathsf{G}_\emptyset(\alpha) = 1 - \mathsf{Pr}[\Phi_{\mathbb{S}}(\mathtt{B}_\alpha) = 0] = 1 - \exp(-\lambda\nu_{\mathcal{L}}^d(\mathtt{B}_\alpha)) \tag{A–99}$$

A.16 Objects and systems

A **dynamic system** can be described as a time series of system states for some discrete $t \geq t_0,\ t_j = t_0 + j\Delta t$. Let $\mathbb{S} \subset \mathbb{E}^d$ be a compact finite set of landmarks, let $\Sigma = \{\mathbb{S}\}$ be the set of all possible landmarks and let $\mathsf{G} : \mathbb{S}_j \mapsto \mathbb{S}_{j+1}$ denote time discrete mapping process. Further, let $t_{j+1} + \Delta t = t_j$ and $j \in \mathbb{N}$. Then an **explicit mapping process**:

$$\mathbb{S}_{j+1} = \mathsf{G}(\mathbb{S}_j) \tag{A–100}$$

such that $\mathsf{G}(\mathbb{S}_j) \in \Sigma$ and:

$$\mathbb{S}_{j+1} = \mathsf{G}(\mathbb{S}_j) = \bigcup_{\mathbf{s}\in\mathbb{S}_j} \mathsf{G}(\mathbf{s}) \tag{A–101}$$

where $\mathbb{S}_j$ is the set at discrete time $t_j = t_0 + j\Delta t$. $\mathbb{S}_0$ is the initial data set. A **step-wise evolution** of the mapping process can be written as a time sequence:

$$[\mathbb{S}_0, \mathbb{S}_1, \mathbb{S}_2, .., \mathbb{S}_j, \mathbb{S}_{j+1}, .., \mathbb{S}_\infty) \tag{A–102}$$

where landmark set $\mathbb{S}_j$ represents a unique solution. An **explicit formulation** $\mathsf{F} : \mathbb{U}_j \mapsto \mathbb{U}_{j+1}$ is giv en by the form:

$$\mathbb{U}_{j+1} = \mathsf{F}(\mathbb{U}_j) \tag{A–103}$$

and an **implicit formulation** $\mathsf{H} : \mathbb{U}_j \times \mathbb{U}_{j+1} \mapsto \mathbb{U}_{j+1}$ is given by:

$$\mathbb{U}_{j+1} = \mathsf{H}(\mathbb{U}_{j+1}, \mathbb{U}_j) \tag{A–104}$$

equivalent to the general form:

$$\Psi(\mathbb{U}_{j+1}, \mathbb{U}_j) = c \tag{A–105}$$

Assume an explicit mapping process given by $\mathbb{S}_{j+1} = \mathsf{G}(\mathbb{S}_j)$ and an implicit mapping process by $\mathbb{S}_{j+1} = \mathsf{H}(\mathbb{S}_{j+1}, \mathbb{S}_j)$. Then an **explicit F orward Euler solution** of $\mathbb{S}_{j+1}$ is:

$$\mathbb{S}_{j+1} = \mathbb{S}_j + \Delta t\ \mathsf{g}(\mathbb{S}_j) + O(\Delta t^2) \tag{A–106}$$

and an **implicit Backward Euler solution** for $\mathbb{S}_{j+1}$ by:

$$\mathbb{S}_{j+1} = \mathbb{S}_j + \Delta t\ \mathsf{h}(\mathbb{S}_{j+1}) + O(\Delta t^2) \tag{A–107}$$

with $\mathsf{g}(\mathbb{S}_j)$ a set derivative function $\frac{d\mathbb{S}}{dt}(t)$ defined by:

$$\frac{d\mathbb{S}}{dt} = \lim_{\Delta t \to 0} \frac{\mathbb{S}_{j+1} - \mathbb{S}_j}{\Delta t} \tag{A–108}$$

and $\mathsf{h}(\mathbb{S}_{j+1})$ defined likewise. In all these formulations, $\mathbb{S}_0 = \mathbb{S}$ is the initial data set. The **norm of an evolutionary mapping** process is given by:

$$\|\mathsf{G}\| = \sup_{\mathbf{s}_j} \frac{\|\mathsf{G}(\mathbb{S}_j)\|}{\|\mathbb{S}_j\|} \tag{A–109}$$

An **evolution semigroup** or **evolution map** $\Gamma^n : E^d \mapsto E^d$ is a n-times product of maps G_j, i.e.,:

$$\Gamma^n = \mathsf{G}_j \circ \mathsf{G}_{j+1} \circ \mathsf{G}_{j+2} \cdots \mathsf{G}_{j+n} \tag{A–110}$$

and with $n, m \in \mathbb{N}$ and $\mathbb{S}_0 = \mathbb{S}$, an **action of evolution map** Γ^n is defined by:

$$\mathbb{S}_{n+m} = \Gamma^n \mathbb{S}_m = \Gamma^m \mathbb{S}_n = \Gamma^{n+m} \mathbb{S}_0 = \Gamma^{n+m} \mathbb{S} \tag{A–111}$$

Semigroup $\Gamma^0 = \mathsf{I}$ is an identity transformation. Let $|\gamma|$ define an upper bound on the norm of $\|\mathsf{G}\|$, i.e., $\|\mathsf{G}_k\| \leq \gamma, \forall j \leq k \leq j + n$. Then we have for the norm of the evolutionary map:

$$\|\Gamma\| = \sup_{\mathbf{s}_j} \left\{ \frac{\|\mathsf{G}(\mathbb{S}_j)\|}{\|\mathbb{S}_j\|} \; \frac{\|\mathsf{G}(\mathbb{S}_{j+1})\|}{\|\mathbb{S}_{j+1}\|} \; \cdots \; \frac{\|\mathsf{G}(\mathbb{S}_{j+n})\|}{\|\mathbb{S}_{j+n}\|} \right\} \leq |\gamma|^n \tag{A–112}$$

Let a **weight function** $\mathsf{w} : R^m \mapsto R$ be given by:

$$\mathsf{w} = \lambda_1 p_1 + \lambda_2 p_2 + \cdots + \lambda_m p_m = \sum_{j=1}^{m} \lambda_j p_j \tag{A–113}$$

with $\sum_j \lambda_j = 1$. Furthermore, let $\Lambda = [\lambda_1, \lambda_2, \ldots, \lambda_m]^T$ denote the **relative weights**, assumed constant. $\mathbf{P}(t) = [p_1(t), p_2(t), \ldots, p_m(t)]^T$ is a vector function in time. Then:

$$\frac{d}{dt}\mathsf{w}(P(t)) = \lambda_1 \frac{\partial \mathsf{w}}{\partial p_1}\frac{dp_1}{dt} + \lambda_2 \frac{\partial \mathsf{w}}{\partial p_2}\frac{dp_2}{dt} + \cdots + \lambda_m \frac{\partial \mathsf{w}}{\partial p_m}\frac{dp_m}{dt} = \Lambda \left[\frac{dp_1}{dt}, \frac{dp_2}{dt}, \cdots, \frac{dp_m}{dt} \right]^T \tag{A–114}$$

Weight function $\mathsf{w}(t) = \Lambda \mathbf{P}^T(t) = c$ iff:

$$\left\| \frac{d}{dt}\mathbf{P}^T \right\| = 0 \tag{A–115}$$

For a discrete **finite state dynamic model**, described in **state space** P, let δ denote a **discrete time event time metric**, and let the pair (P, δ) form a metric space. Further, let $D_0(t)$ denote a start scenario at absolute time t. An **erosion function** $\mathsf{Q}_E(\alpha)$ for an **eroded shape** $\mathcal{W}_\alpha(\mathbb{S})$ by an **eroder shape** $\mathcal{Z}_\alpha(\mathbb{Y})$, $\mathbb{S}, \mathbb{Y} \subset \mathbb{E}^d$, is defined as:

$$\mathsf{Q}_E(\alpha) = \mathcal{W}_\alpha(\mathbb{S}) \ominus \breve{\mathcal{Z}}_\alpha(\mathbb{Y}) = \mathcal{W}_\alpha(\mathbb{S}) \ominus \mathcal{Z}_\alpha(\breve{\mathbb{Y}}) \tag{A–116}$$

where $\breve{\mathbb{Y}} = -\mathbb{Y}$ is the reflection of $\mathbb{Y}$ in the origin. A **dilation process** $\mathsf{Q}_D(\alpha)$ is defined by:

$$\mathsf{Q}_D(\alpha) = \mathcal{W}_\alpha(\mathbb{S}) \oplus \breve{\mathcal{Z}}_\alpha(\mathbb{Y}) = \mathcal{W}_\alpha(\mathbb{S}) \oplus \mathcal{Z}_\alpha(\breve{\mathbb{Y}}) \tag{A–117}$$

If T_T denotes a translation along some path, then $\mathcal{Z}_\alpha(\mathsf{T}_T(\mathbb{S}))$ shall denote the shape $\mathcal{Z}_\alpha$ during its glide along the path. In other words:

$$\mathsf{T}_T(\mathbb{S}) = \{\lambda \mathbf{s}\mathbf{T}^T | \mathbf{s} \in \mathbb{S},\ 0 \leq \lambda \leq 1\} \tag{A–118}$$

With this description of a moving eroder, the erosion results in an eroded shape $\mathcal{W}_\alpha$ based on an eroded set $\mathbb{S}_E$, for which:

$$\mathbb{S}_E = \{\mathbf{s} \in \mathbb{S} \mid \forall \mathbf{y} \in \check{\mathbb{Y}}, \mathbf{s} - \mathbf{y} \in \mathbb{S}\} \tag{A–119}$$

and analogously:

$$\mathbb{S}_D = \{\mathbf{s} + \mathbf{y} \mid \mathbf{s} \in \mathbb{S}, \mathbf{y} \in \check{\mathbb{Y}}\} \tag{A–120}$$

The **opening** Q_O of an eroded shape $\mathcal{W}_\alpha(\mathbb{S})$ by an eroder shape $\mathcal{Z}_\alpha(\mathbb{Y})$, $\mathbb{S}, \mathbb{Y} \subset \mathbb{E}^d$, is defined by:

$$\mathsf{Q}_O = \mathsf{Q}_D \circ \mathsf{Q}_E \tag{A–121}$$

and the **closing** Q_C by:

$$\mathsf{Q}_C = \mathsf{Q}_E \circ \mathsf{Q}_D \tag{A–122}$$

Minkowski set additions are associative and commutative. As a consequence, building up the weight set from different parts over time is trivial:

$$\mathbb{A} \oplus (\mathbb{W}_1 \cup \mathbb{W}_2 \cup \ldots \cup \mathbb{W}_m) = (\mathbb{A} \oplus \mathbb{W}_1) \cup (\mathbb{A} \oplus \mathbb{W}_2) \cup \ldots \cup (\mathbb{A} \oplus \mathbb{W}_m) = \bigcup_j (\mathbb{A} \oplus \mathbb{W}_j) \tag{A–123}$$

and:

$$\mathbb{S}_1 \oplus \mathbb{S}_3 \subset \mathbb{S}_2 \oplus \mathbb{S}_3 \tag{A–124}$$

A.17 Asympthotic time and storage complexity

Let $c, c_1, c_2 > 0$ and $n_{min} > 0$ and assume functions $\phi(n), \gamma(n)$ in n. Then the **asympthotic upper bound complexity** $\mathcal{O}(\phi(n))$ is given by the inequality:

$$\mathcal{O}(\phi(n)) = \{\gamma(n) \mid |\gamma(n)| \leq c\phi(n), \forall n > n_{min}\} \tag{A–125}$$

the **asympthotic lower bound complexity** $\Omega(\phi(n))$ by:

$$\Omega(\phi(n)) = \{\gamma(n) \mid \gamma(n) \geq c\phi(n), \forall n > n_{min}\} \tag{A–126}$$

and the **asympthotic exact complexity** $\Theta(\phi(n))$ by:

$$\Theta(\phi(n)) = \{\gamma(n) \mid c_1\phi(n) \leq \gamma(n) \leq c_2\phi(n), \forall n > n_{min}\} \tag{A–127}$$

Notice that these inequalities actually denote *equivalence classes* rather than exact solutions.

Annex B

Terminology and parlance

B.1 Overview

This annex provides some structure to the terminology and parlance practised in this thesis. Most of the terminology originates in the domain of combinatorial geometry and topology. Most of the terminology deals with simplicial complexes, polyhedra and configurations or *arrangements* of lines, planes, spheres, etc.

Mathematical background and definitions are not provided in this annex. These can be found in annex A. Furthermore, the use of terminology regarding earth sciences is mostly restricted to the cases presented in chapter 6 and is therefore defined and explained in this chapter, not here.

B.2 Subfaces, faces and superfaces

A point, a line, a surface, a volume, $\cdots$, a *hyper-volume* are geometric elements having topological counterparts called a vertex, an edge, a 2-face, a 3-face, $\cdots$, a k-face, where k refers to an arbitrary dimension in range $-1 \leq k \leq d$. Dimension -1 may seem somewhat odd at first, its role is explained in the text of the chapters. From a topological point of view, a k-face may be contained in the boundary of a $(k+1)$-face. For instance, an edge, a 1-face, may bound a 2-face, e.g., a triangle. In that case, the k-face is called a *subface* of the $(k+1)$-face and the latter is a *superface* of the k-face. Some sub- or superfaces are also known by alias terms, mostly only in a special context. Principle terms have been collected in table B–1.

In this thesis, faces are mostly but not exclusively simplices. A *simplex* is the d-face with the smallest possible number of vertices, namely $d+1$. The term simplex is related to the dimension of the space it is defined in: a point (for $d=0$), an edge ($d=1$), a triangle ($d=2$) and a tetrahedron ($d=3$) are the simplices (or: *simplexes*) in E^0, E^1, E^2 and E^3, resp. A triangulation is a space-partitioning entirely built up of d-simplices. Non-simplex d-faces with more than $d+1$ points are for instance found in Voronoi diagrams. Voronoi cells are examples

of *polyhedral faces*: faces that are compounds (or: complexes) of k-faces. Faces in this thesis are flat, excluding curved or "skew" edges and edges connecting a vertex with itself, curved triangles, etc.

	General	Arrangement	Polytope	Simplicial Complex
Absolute, depending on d	impr. $(d+1)$-face	arrangement		
	d-face	cell	cell, simplex	simplex
	$(d-1)$-face	hyperplane	(sub)facet	facet
	...	...	...	...
	$(k+1)$-face	superface	superface	superface
relative	k-face	face	face	face
	$(k-1)$-face	subface	subface	subface
	...	...	...	...
absolute, independent of d	3-face	flat	tetrahedron	tetrahedron
	2-face	plane, flat	triangle	triangle
	1-face	line, line segment	edge	edge
	0-face	vertex	vertex	vertex
	impr. -1-face	$\emptyset$	$\emptyset$	$\emptyset$

Table B–1: *polyhedral terminology and parlance.*

B.3 Open and closed faces

A face is called a closed (an open) face if it contains (does not contain) the points of its boundary. Open faces are composed solely of their interiors, or *covered by an open set*. An open edge, for example, does not contain the extremal vertices, spanning it.

B.4 Topological relations among faces

Two topological associations of faces are particularly important in this thesis: the notion of *incidence* and the notion of *neighbourship*.

B.4.1 Incidence relations

Two faces are said to be *direct* (or: *proper*) *incident upon one another*, if one is a proper subface of the other. For combinatorial convenience, an improper -1-face is usually defined, too. In this

thesis, it is the -1-dimensional simplex $\sigma^{(-1)} = \emptyset$, incident upon all vertices and hence contained in each k-simplex.

B.4.2 Incidence graph

An *incidence graph* is a graph in which the k-faces $\sigma^{(k)}$ are represented as nodes and incidence relationships as edges. As such, an incidence graph is capable of representing the incidence relationships of a regular triangulation $\mathcal{T}(\mathbb{S})$, an α-complex or a simplicial complex in general. More formally, an incidence graph $\mathcal{IG} = \{\Sigma, I\}$ is a graph in which the collection $\Sigma = \{\sigma^{(k)}\}$ of k-simplices, $-1 \leq k \leq d+1$, is represented as nodes and incidence relations $I = \{deg(\sigma^{(k)})\}$ as edges. The incidence graph is augmented by two *improper* faces: a $(d+1)$-face upon which all (at most $\Theta(N^{\lfloor \frac{d+1}{2} \rfloor})$) d-faces are upward incident and the empty set $\emptyset$, the only (-1)-face upon which all the N vertices are downward incident. See [Ede87], Seidel in [Sei91] and [Mue93] for further details.

Let $deg(\sigma^{(k)}) \uparrow$ denote the *upward incidence*, i.e., the incidence with respect to a superfaces, and similarly, let $deg(\sigma^{(k)}) \downarrow$ be the *downward incidence* of k-simplex $\sigma^{(k)}$ in a triangulation $\mathcal{T}(\mathbb{S})$, with $\text{card}\,\mathbb{S} = N$. Then an incidence graph of a triangulation shows the following nodal degrees:

$$
\begin{array}{lcll}
k = d+1 & \Rightarrow & deg(\sigma^{(d+1)}) \uparrow & = \quad 0 \\
k = d+1 & \Rightarrow & deg(\sigma^{(d+1)}) \downarrow & \leq \quad \Theta(n^{\lfloor \frac{d+1}{2} \rfloor}) \\
k = d & \Rightarrow & deg(\sigma^{(d)}) \uparrow & = \quad 1 \\
k = d & \Rightarrow & deg(\sigma^{(d)}) \downarrow & = \quad d+1 \\
k = d-1 & \Rightarrow & deg(\sigma^{(d-1)}) \uparrow & = \quad [1,2] \\
k = d-1 & \Rightarrow & deg(\sigma^{(d-1)}) \downarrow & = \quad k+1 \\
\cdots & \cdots & \cdots & \\
k = 2 & \Rightarrow & deg(\sigma^{(2)}) \uparrow & \in \quad [1,2] \\
k = 2 & \Rightarrow & deg(\sigma^{(2)}) \downarrow & = \quad 3 \\
k = 1 & \Rightarrow & deg(\sigma^{(1)}) \uparrow & \in \quad [1,2] \\
k = 1 & \Rightarrow & deg(\sigma^{(1)}) \downarrow & = \quad 2 \\
k = 0 & \Rightarrow & deg(\sigma^{(0)}) \uparrow & \in \quad [2, N-1] \\
k = 0 & \Rightarrow & deg(\sigma^{(0)}) \downarrow & = \quad 1 \\
k = -1 & \Rightarrow & deg(\sigma^{(-1)}) \uparrow & = \quad n \\
k = -1 & \Rightarrow & deg(\sigma^{(-1)}) \downarrow & = \quad 0
\end{array}
$$

B.4.3 Neighbourship

Two faces are said to be *direct* (or: *proper*) *neighbours* if they share a proper subface or superface. Each vertex in a k-simplex is thus a proper neighbour of any of the other vertices in the simplex.

A *nearest neighbour* is a neighbour that is nearest-by. Nearest neighbourship is mostly considered in the context of points in a point process. Analogously, the *k-th nearest neighbour* is the k-th nearest-by neighbour. The *local-furthest neighbour* is the furthest-apart neighbour *within the topological star*, i.e., connected by an edge in the triangulation. With the *nearest-neighbour graph* being a sub-graph of the triangulation, it is obvious that up to local-furthest neighbour, each k-th neighbour, since connected by an edge in the triangulation, is also a direct neighbour within the context of the underlying triangulation.

B.4.4 Examples

The following examples illustrate the above terminology.

Example B.1 (two triangles connected by only a single vertex)
Two 2-faces (triangles, say) that share a common 0-face (vertex) are neither proper incident nor proper neighbours •

Example B.2 (the edges of a triangle)
Two 1-faces (edges) that belong to the same 2-face f (triangle) are direct neighbours, because they share a common 0-face (vertex). In this case, they also share a common superface, the 2-face f they are incident upon •

Example B.3 (vertices sharing the improper simplex $\sigma^{(-1)}$)
All vertices are incident upon the only improper simplex $\sigma^{(-1)}$, but since this is not a proper subface, all vertices are not each others proper neighbours •

B.5 Singular, regular and interior faces

The faces of an α-complex can be classified as *singular*, *regular* or *internal*. With α growing from $\alpha_{\min}$ to its maximum value $\alpha_{\max}$, more and more faces of the triangulation become contained in the α-complex. A k-face is called a:

- **Singular face:**

  If it becomes α-exposed but the $(k+1)$-face it is bound to be incident upon not yet. Singular faces are always contained in the boundary and are never interior.

- **Regular face:**

  If it is α-exposed and so is a $(k+1)$-superface it is incident upon. The k-face can be contained in the boundary of a $(k+1)$-dimensional complex.

- **Interior face:**

If it is contained in the interior of some $(k+1)$-dimensional complex. If the superface is α-exposed, then the k-face is so, too.

Annex C

The Laguerre weighted distance

C.1 Introduction

A topological space endowed with a Euclidean distance based metric is a metric space known as a Euclidean space, denoted E^d. What are the consequences if Euclidean distance is replaced by the Laguerre distance? This annex deals with this question.

C.2 The Laguerre weighted distance

A *metric space* is defined as follows (e.g., [Mun75]):

DEFINITION C.1 (METRIC (METRIZABLE) TOPOLOGICAL SPACE)
A topological space X is said to be metric (metrizable), with a metric $\mu(\mathbf{x}_1, \mathbf{x}_2)$ iff for all $\mathbf{x} \in \mathbb{X}$:

$$\begin{cases} \mu(\mathbf{x}_1, \mathbf{x}_2) \geq 0 \ \wedge \ \mu(\mathbf{x}_1, \mathbf{x}_2) = 0 \Leftrightarrow \mathbf{x}_1 = \mathbf{x}_2 & \textit{positive definiteness} \\ \mu(\mathbf{x}_1, \mathbf{x}_2) = \mu(\mathbf{x}_2, \mathbf{x}_1) & \textit{symmetry} \\ \mu(\mathbf{x}_1, \mathbf{x}_3) \leq \mu(\mathbf{x}_1, \mathbf{x}_2) + \mu(\mathbf{x}_2, \mathbf{x}_3) & \textit{triangle inequality} \end{cases}$$

It is easily verified that the Euclidean metric $\|\mathbf{x}_1 - \mathbf{x}_2\| = \langle \mathbf{x}_1 - \mathbf{x}_2, \mathbf{x}_1 - \mathbf{x}_2 \rangle^{\frac{1}{2}}$, where $\langle \cdot, \cdot \rangle$ defines the standard inproduct, satisfies the axioms of a metric. Apparently, a μ that satisfies the above axioms must be a symmetric positive definite bilinear form. The question is now: is it possible to define a metric using the Laguerre distance rather than the Euclidean distance? Recall that the Laguerre distance is defined as:

$$L(\mathbf{x}_1, \mathbf{x}_2) = \langle \mathbf{x}_1 - \mathbf{x}_2, \mathbf{x}_1 - \mathbf{x}_2 \rangle - (w_1 + w_2) = [\mathbf{x}_1 - \mathbf{x}_2]^T [\mathbf{x}_1 - \mathbf{x}_2] = \|\mathbf{x}_1 - \mathbf{x}_2\|^2 - (w_1 + w_2)$$

To answer this question, all the above axioms have to be checked, for all $\mathbf{x} \in \mathbb{X}$.

C.2.1 Positive definiteness

Let space X be covered by the set $\mathbb{X}$ of 2-tuples $\tilde{\mathbf{x}} = (\mathbf{x}, w)$. Verify that for all $\mathbf{x}_1, \mathbf{x}_2 \in \mathbb{X}$:

$$L(\mathbf{x}_1, \mathbf{x}_2) \geq 0 \ \wedge \ L(\mathbf{x}_1, \mathbf{x}_2) = 0 \Leftrightarrow \mathbf{x}_1 = \mathbf{x}_2$$

By definition:

$$L(\mathbf{x}_1, \mathbf{x}_2) = \|\mathbf{x}_1 - \mathbf{x}_2\|^2 - (w_1 + w_2)$$

which becomes non-positive as soon as:

$$\|\mathbf{x}_1 - \mathbf{x}_2\|^2 \leq w_1 + w_2$$

so in general the positive definiteness axiom does not hold and as a consequence, the Laguerre distance does not permit for a metric space. Moreover:

$$L(\mathbf{x}, \mathbf{x}) = -2w$$

Although this already answers the question raised in this annex, for completeness the verification of the symmetry and the triangle inequality is continued below.

C.2.2 Symmetry

Verify that for all $\mathbf{x}_1, \mathbf{x}_2 \in \mathbb{X}$:

$$\mu(\mathbf{x}_1, \mathbf{x}_2) = \mu(\mathbf{x}_2, \mathbf{x}_1)$$

One has that:

$$\begin{aligned} L(\mathbf{x}_1, \mathbf{x}_2) = \langle \mathbf{x}_1 - \mathbf{x}_2, \mathbf{x}_1 - \mathbf{x}_2 \rangle - (w_1 + w_2) = \\ \langle \mathbf{x}_1, \mathbf{x}_1 \rangle + \langle \mathbf{x}_2, \mathbf{x}_2 \rangle - 2\langle \mathbf{x}_1, \mathbf{x}_2 \rangle - (w_1 + w_2) = \\ \langle \mathbf{x}_2 - \mathbf{x}_1, \mathbf{x}_2 - \mathbf{x}_1 \rangle - (w_2 + w_1) = L(\mathbf{x}_2, \mathbf{x}_1) \end{aligned}$$

so this holds.

C.2.3 triangle inequality

Verify that for all triplets of different $\mathbf{x}_1, \mathbf{x}_2, \mathbf{x}_3 \in \mathbb{X}$:

$$L(\mathbf{x}_1, \mathbf{x}_3) \stackrel{?}{\geq} L(\mathbf{x}_1, \mathbf{x}_2) + L(\mathbf{x}_2, \mathbf{x}_3)$$

In other words:

$$\begin{aligned} L(\mathbf{x}_1, \mathbf{x}_3) \stackrel{?}{\geq} L(\mathbf{x}_1, \mathbf{x}_2) + L(\mathbf{x}_2, \mathbf{x}_3) \Rightarrow \\ \langle \mathbf{x}_1 - \mathbf{x}_3, \mathbf{x}_1 - \mathbf{x}_3 \rangle \stackrel{?}{\geq} \langle \mathbf{x}_1 - \mathbf{x}_2, \mathbf{x}_1 - \mathbf{x}_2 \rangle + \langle \mathbf{x}_2 - \mathbf{x}_3, \mathbf{x}_2 - \mathbf{x}_3 \rangle - 2w_2 \Rightarrow \\ -2\langle \mathbf{x}_1, \mathbf{x}_3 \rangle \stackrel{?}{\geq} -2\langle \mathbf{x}_1, \mathbf{x}_2 \rangle + 2\langle \mathbf{x}_2, \mathbf{x}_2 \rangle - 2\langle \mathbf{x}_2, \mathbf{x}_3 \rangle - 2w_2 \Rightarrow \\ \langle \mathbf{x}_1, \mathbf{x}_3 \rangle \stackrel{?}{\leq} \langle \mathbf{x}_1, \mathbf{x}_2 \rangle - \langle \mathbf{x}_2, \mathbf{x}_2 \rangle + \langle \mathbf{x}_2, \mathbf{x}_3 \rangle + w_2 \end{aligned}$$

which can be rewritten as:

$$\langle \mathbf{x}_1, \mathbf{x}_3 \rangle \stackrel{?}{\leq} \langle \mathbf{x}_1, \mathbf{x}_2 \rangle + \langle \mathbf{x}_2, \mathbf{x}_3 \rangle - \underbrace{(\langle \mathbf{x}_2, \mathbf{x}_2 \rangle - w_2)}_{R}$$

The first part (without rest term R) is equal to an "ordinary" (Euclidean) triangle inequality a proof of which can be found in almost any math textbook. Regarding the rest term R, in which $\langle \mathbf{x}_2, \mathbf{x}_2 \rangle = \|\mathbf{x}_2\|^2 \geq 0$, things split up in three cases:

$$\begin{aligned} w_2 &< \|\mathbf{x}_2\|^2 \Rightarrow \text{inequality does not hold} \\ w_2 &= \|\mathbf{x}_2\|^2 \Rightarrow \text{inequality holds} \\ w_2 &> \|\mathbf{x}_2\|^2 \Rightarrow \text{inequality holds} \end{aligned}$$

so as a general conclusion, the triangle inequality axiom does not generally hold for the Laguerre weighted distance. Observe that weight w_1 and w_3 have dropped from the expressions and apparently play no role in the inequality.

C.3 Laguerre distance and the Lebesgue measure

Let $\mathbb{Y}_i, \mathbb{Y}_j \subseteq \mathbb{X}$ be different subsets of $\mathbb{X}$ so that $i \neq j \Leftrightarrow \mathbb{Y}_i \bigcap \mathbb{Y}_j = \emptyset$. The *Lebesguemeasure* $\nu(\mathbb{X})$ is set function for which:

$$\begin{cases} \nu(\emptyset) \;=\; 0 \\ \nu(\mathbb{Y}_j) \;\geq\; 0, \quad \forall \mathbb{Y}_j \subseteq \mathbb{X} \\ \nu\left(\bigcup_j \mathbb{Y}_j\right) = \sum_j \nu(\mathbb{Y}_j) \end{cases}$$

F rom this definition, it is immediate that non-negative function values are excluded. A Laguerre distance can produce negative such values. Therefore, it violates the definition of a measure.

C.4 Bibliographic notes

F or further details on metric spaces, refer to [Mun75] and [Mun84], [Sha77], [Nag83], and [Edg90]. Regarding the (geometry of the) Laguerre distance, refer to [Coo16], [Sch79], [Aur87b] and [Ede92]. The Lebesgue measure is discussed in [Mun84], [SS94], [SKM95], [Edg90].

Annex D

Set and point process analysis

D.1 Introduction

Set analysis greatly aids in the understanding of the resulting α-complex. Set analysis usually results in the determination of a number of set parameters that together characterise the set. Apart from the customary set parameters, a number of specific geometric set parameters can be defined for the geometric sets used in this thesis. Moreover, in this thesis, point processes are assumed to be Poisson point processes, shortly denoted as *ppp*'s. See for instance the chapters 2, 3 and 6. It is, however, good statistical practice to verify whether this *a-priori hypothesis* or *null-hypothesis* holds, in a statistical verification. And if so, a test has to be performed as to whether the ppp is a *homogeneous* ppp or not. Appropriate discussions of how to perform such verifications can be found in various statistical texts, e.g. in [Dig83] and [SKM95]. There is no such thing as an ultimate test for ppps. Many tests have been proposed in literature, some more mature, some testing only a single aspect. This annex provides an outline of the methods used in this thesis, touching only basic aspects and without any claim or intention to be complete. The ppp itself is not described; see chapter 2 for an introduction.

D.2 Point set analysis

Set parameters

Firstly, the cardinality of the set is of interest. The cardinality of cases to be discussed in this thesis typically range from $O(10^2) - O(10^6)$. If set members are valued, which is always the case in this work, characteristic values such as mean, mode and median, standard deviation, variance, skewness, etc. In the case studies presented in chapter 6, so called *one pass* statistics were used, using Spicer's *provisional mean* algorithms for weighted values. See [Spi72]. Let $0 < k \leq N$. Spicer's algorithm incrementally computes the power sum:

$$\sum_{j=1}^{k}(p_i-\bar{p}_k)^r=\sum_{j=1}^{k-1}(d_i-\delta p)^r+(k-1)^r(\delta p)^r \tag{D–1}$$

where $\bar{p}_k$ means the incremental mean value after including k observations, $d_i=(p_i-\bar{p}_{k-1})$ and $\delta p=(p_k-\bar{p}_{k-1})/k$. These power sums are used to compute the first four central moments about the mean for *weighted* variables. The approach was inspired by [Nor79, Ch. 14]. For further background, see for instance [Hal52, Nor79, PR96, Cra99].

Geometric parameters

For a closed convex set, the diameter always coincides with the distance between two of its members. If not convex, the set can be replaced by its convex hull. Then by definition, the *diameter of a close dconvex set* is given by:

$$\mathrm{diam}(\mathbb{S})=\max\{\|\mathbf{s}_i-\mathbf{s}_j\|,s_i,s_j\in\mathbb{S}\} \tag{D–2}$$

For empty sets, the diameter is undefined, for single member sets the diameter is 0 and for sets with $\mathrm{card}\,\mathbb{S}=2$, the diameter is equal to the nearest and the furthest neighbour distances. The *orthogonal breadth* denoted by $breadth^{\perp}\,\mathbb{S}$, of a closed convex set $\mathbb{S}$ is the minimum distance between two support planes of $\mathbb{S}$ parallel to the line carrying the two extremal points generating the diameter. The (orthogonal) *aspect ratio* ϕ is the ratio between the (orthogonal) breadth and the diameter of the set.

The *convexity ratio* γ is the ratio of the space occupied by $\mathbb{S}$ and the space occupied by the corresponding hull of $\mathbb{S}$. The underlying space of the convex hull is uniquely and unambiguously defined. The problem lies in the definition of the space occupied by $\mathbb{S}$. Various approaches exist for the determination of this space. For open sets, a maximum curvature or some other criterion can be taken to determine the boundary. See for example [Vel94]. The convexity ratio γ is zero for strongly concave shapes and grows to unity for convex shapes.

It is not immediately clear how to quantify strongly clustered points and scattered shapes. For example, an eroding object. For now, the best approach seems to hook up to cluster analysis like approaches and define intra-cluster diameters in a hierarchy, in relation to the inter-cluster distances. The convexity ratio of the α-hull and the convex hull is closely related to convexity ratio γ. For small α-values, up to some α function $\gamma_\alpha(\alpha)$ is likely[1] to be a minorant, i.e., $\gamma_\alpha(\alpha)<\gamma$. The reasoning is that the α-complex is generally not hole-free and the α-complex will be smaller than $|S|$ by the amount of underlying space of the holes. For greater α, when holes have vanished $\gamma_\alpha(\alpha)>\gamma$ because it starts filling in concavities when approaching the convex hull. This underlying space will generally not belong to $|S|$. Finally, for $\alpha=\alpha_{max}$ one has that $\gamma_\alpha=1$. This is the function's global and only maximum, since it is a non-strictly monotonically increasing function. The maximum value of 1 is common to γ and γ_α, but γ becomes 1 for convex shapes only

[1] without an exact definition of the underlying space of $|S|$ for γ only qualitative reasoning is possible

D.3 Poisson point process statistics

In this section, statistics will mainly apply to *empirical* distributions, i.e., to *observed data*. Point processes, generated by a point set $\mathbb{S} \subset \mathbb{E}^d$ are denoted by $\Phi_{\mathbb{S}}(\mathbf{x})$, are assumed *simple*, which means that no points $\mathbf{s}$ coalesce. Finally, the ppp is assumed *fully mapped*, which means that the locations of all of its points are known and the global mean intensity $\bar{\lambda}$ of the point process as a whole is known.

D.3.1 Poisson distribution of point-counts

One of the first things to estimate is the *empirical density* (or: *empirical intensity*) $\hat{\lambda}(\mathbf{x})$ and its dispersion across the ppp, relative to its *expected value* or *first-order moment* $\lambda\nu_{\mathcal{L}}^{(d)} = \mathsf{E}[\Phi(\mathbf{x})]$. This is commonly done by some *point counting* procedure on a *grid cell* (or *quadrat* or *window*), either exhaustively, or by sampling. For fully mapped ppps, point counting procedures are generally preferred over distance-based methods, to be discussed later. The entire space of the ppp is therefor partitioned in equal-sized grid cells and for each cell, the number of points (or: *events*) falling into that cell are recorded. The number of points counted in each cell is expected to follow a Poisson distribution with mean value $\Lambda(\nu_{\mathcal{L}}(\mathsf{D}))$, where D denotes a cell on the ppp and $\nu_{\mathcal{L}}(\mathsf{D})$ its Lebesgue measure. The size and hence the number of cells is depending on the test statistic to be applied further down the hypothesis verification.

Rather than analysing the count distribution, one usually measures its dispersion from a uniform distribution. A frequently used test is the χ^2-goodness-of-fit test for independent and uniform distribution of the points. For the χ^2 test, rules can easily be found. Generally, the size of the grid cell must be taken such that the least-densely populated cell still counts $\Omega(10^1)$ points. To test uniform distribution, there is no need for the grid cells to be equal-shaped: as long as their size is equal, the Lebesgue measure is equal. Unfortunately, the number of grid cells chosen also determines the *degrees-of-freedom*, equal to the number of grid cells minus one, making the result somewhat scale-dependent.

Basically, the χ^2 test sets off the total of the counted number of points $\operatorname{card}\mathsf{D}_\mathsf{j}$ in each of the m cells D_j against expected number of points in those cells:

$$\chi^2 = \sum_{j=1}^{m} \frac{(\operatorname{card}\mathsf{D}_j - \mathsf{E}[\mathrm{D_j}])^2}{\mathsf{E}[\mathrm{D_j}]}$$

where the expected number of points $\mathsf{E}[\mathrm{D_j}] = (\operatorname{card}\Phi_{\mathbb{S}})/m$. The value of each cell is expected to follow a χ^2 distribution with $m-1$ degrees-of-freedom.

When exceeding some critical level, taking into account the degree-of-freedom and a chosen significance level α, the hypothesis of a homogeneous ppp must be rejected, either indicating too high a variability (not stationary enough), in the case that $\chi^2 > \chi^2_{D-1:1-\alpha}$, or too high a regularity (not enough Poisson; regular but not random), if $\chi^2 < \chi^2_{D-1:\alpha}$, both at a significance of $100\alpha\%$. Critical levels are usually looked up in a table. Homogeneity is not only determined by *stationarity* but also by *isotropy* so that the intensity has to be verified for directional patterns as well. If not trivial, this can be done by defining grid cells emanating radially from a *centroid*

The *index-of-dispersion test* (e.g., [SKM95, Ch. 2]) is essentially a variant of the χ^2-test, and an extension in the sense of taking into account the counts of neighbouring cells is known as the *Greig-Smith method*. Another alternative which can be applied if the ppp has been fully mapped is the *reduced second-order moment* verification. See [SKM95, Ch. 2] for further details.

D.3.2 Distance measurements

Distance measurements are performed in this thesis, not directly for the aim of accepting of rejecting the homogeneous ppp hypothesis, but to provide an additional distance analysis as input for the weighting. Nonetheless, the nearest neighbour distances distribution is related to the question as to whether the ppp is homogenous or not. For strongly clustered point patterns, the *empirical* nearest neighbour distance *distribution* will considerably diverge from the *theoretical* ppp nearest neighbour distance distribution function, given by:

$$\mathsf{D}(\mathbf{x}) = 1 - \exp(-\lambda \nu_{\mathcal{L}}^{(d)})$$

and the same holds for the corresponding empirical and theoretical *densities*. Strongly clustered patterns will exhibit a stronger *positive skew* density than ppps.

To illustrate this, consider a point process $\Phi_{\mathbb{S}}(\mathbf{x})$, with $\mathbb{S} \subset E^2$. The model nearest neighbour distance distribution function is given by:

$$\mathsf{D}(y) = 1 - \exp(-\lambda \pi y^2), \qquad y \geq 0$$

and for the corresponding density function, one finds by spatial derivation:

$$\mathsf{d}(y) = 2\lambda \pi y \exp(-\lambda \pi y^2)$$

with mean equal to:

$$\mu_{\mathsf{D}} = \frac{1}{2\sqrt{\lambda}}$$

and variance:

$$\sigma^2_{\mathsf{D}} = \frac{1}{\pi\lambda} - \frac{1}{4\lambda}$$

For clustered processes, $\mu_{\hat{\mathsf{D}}} < \mu_{\mathsf{D}}$, yielding a more positive skew density function. Notice that D is not symmetric and hence its skewness is non-zero. Similar reasoning holds for the k-th nearest neighbourfunction, with $k > 1$.

Abstract

Using Weighted Alpha Complexes in Subsurface Modelling

Reconstructing the shape of observed natural objects

Bart H.M. Gerritsen

Over the passed couple of decades, the study of *natural objects* has advanced dramatically. The advent of boosting computing-power has shown to be a critical precursor. But as of today, modelling natural objects remains complicated. This not only holds for the attainment of photo-realism, but also regarding an adequate description of its shape. Natural objects, with their abundant complexity and level of detail, can be so complicated, that only an observed sampling data point set can accurately capture their shape. Analytic descriptions are either overly complicated or simply infeasible. Properties measured in these sampling points are commonly required to reveal whether a point belongs to the object or to its *natural background*. Generally, sampling data point sets will represent not only the object, but (some of its) background along. With objects being represented this way, the problems is then to reconstruct the solid object from these sample points.

The problem in this thesis is largely compatible with the above problem: after all, *subsurface objects* belong to the class of natural objects. The key issue in this thesis is the finding of an *icon* out of a sampling data point set. An icon can be understood to be the representative of a family of objects that belong to one class. For instance, an icon of a meandering river, a dune, a lens or a point bar. An icon can be stored in a database and a single icon can *instantiate* (reproduce) an entire family of objects again, assigning them dimensions, a location and an orientation. Generally speaking, by applying an instantiation transformation to the icon. Additional constraining sample data may be drawn from an observed target to which the instantiated object must comply. This thesis proposes an *inversion-cycle* and *forward modelling loop* based modelling framework, that anticipates the advent of such constraining data.

With regard to the *basic problem*, the abridging of the gap between the sample point topology and the solid object model contemplated, new math concepts have been proposed in recent literature, appearing well-applicable to the problem at hand. Among others, the notion of an α-complex. In the approach followed in here, α-complexes will be used both for the derivation and storage of the icons and for the instantiated objects. Primary objective is to verify as to whether α-complexes can meet the requirements as stated and fit the approach taken. The use of α-complexes has a couple of characteristics in common with triangulation and convex hull, but also offer a number of distinct advantages, at only little extra computational cost. To some extent, an α-complex can be regarded as a parameterised triangulation, with an upper bound on the edge length. It can describe the geometry and topology of a one-part object, separated object parts, objects with holes, etc., as a single mathematical entity. In this thesis, emphasis is on *weighted* α-complexes, in which parameterisation is by distance, biased by weight.

Manipulation of the spatial distribution of the observed sampling data point set and the attachment of weights allow for "special modelling effects". In order to fruitfully exploit these

capabilities, the effects of transformations of the sample points must be thoroughly apprehended and a weighting strategy has to be designed, adapted to the modelling of sampled natural objects. In this work, various such strategies will be explored and the most promising and appealing will be further worked out. Owing to their general dimension, α-complexes allow for a hyper-spatial approach, which, in turn, aptly applies to the notion of property-ruled geometry and topology of natural objects.

Cluster and/or factor analysis of the observed properties can be used to identify the ruling properties (*factors*) telling object apart from its natural background. In a hyper-spatial approach, a cluster analysis tends to yield the geometry of the property clusters and cluster membership, projections and intersections may be used to find the object's "ordinary" geometry. In a typical application, property subspace will be swapped with resulting weight. Either the hyper-spatial points or the weights can be stored with the icon, mainly depending on the details of the object instantiation process. The weight so obtained can be matched with the typical distances to be abridged, using a transformation. For instance, the globally smallest *nearest-neighbour distance* may be taken to determine the weight scale factor. In this case, the relative distribution goes unchanged and the resulting object is solely determined by the observed properties. Alternately, weights may be *locally* up-scaled to their *local maximum values*, i.e., to the maximum values without enforcing an edge in the α-complex by weight alone. Such local maximum values seek to guarantee a hole-free (part of the) object. The genuine relation with the ruling property values will generally get lost, in this case. Any sampling data point set has an *attractor* associated with it, that denotes these local maximum values.

An α-complex-based definition offers the opportunity to examine various appearances of the same sampling data point set. In this case, this capacity is exploited to find and describe the icon. The family of object appearances to draw from is obtained by varying the value of α. With an increasing α, icons tend to grow more "fat", whereas icons get "leaner" when α comes down. Obviously, the α-value can be manipulated directly, eventually however, crisp criteria and cost functions should be developed underpinning the "right" value of α. For example, stratigraphic constraints or geomechanical process simulation. Optionally, the icon may be improved by *editing*. Editing in this context, comes down to manipulating or augmenting the sampling data point set, for instance by inserting additional points reflecting a modellers *a-priori knowledge* on the object. The customary process of object reconstruction suffers from an inherent lack of data and sufficiently commensurable data. This largely induces the desire to bring in the available a-priori knowledge. E.g., to remove or seed holes in the object. Any kind of knowledge that can be expressed in terms of a configuration of points can trivially be inserted.

The process of analysis, interpretation and editing may be supported by the fit of a theoretical model, in similar vein with fitting a Gaussian curve to a histogram. Once a theoretical model has been matched, many more mature and concise propositions can be made with respect to the underlying sampling data point set.

The notion of an α-complex is well-formalised. It is, nevertheless, of great practical importance for an α-complex to be easily related to, paired with and transcribed into existing (legacy) object model descriptions and representations. Existing model descriptions tend to be rarely based on cellular structures featuring holes and separations. This implies that α-complexes need to be verified and validated as a model description and as a representation scheme. The most widely used representations, the Constructive Solid Geometry (CSG) and the boundary representation (B-rep), will be taken as a reference.

Furthermore, α-complexes shall support numerical modelling, probably after some endowment, and possess the longer-term perspective of serving as a vehicle for *dynamic process modelling*. This thesis presents a novel approach to conduct numerical computations on an α-complex. Exploiting the fact that the α-complex and the corresponding triangulation share faces, a *topological embedding* can be found that allows for instance a finite element approach. Even in the presence of holes and separations. This approach is also the key to process simulations of objects subject to depositional and erosional processes, a frequently occurring and therefore important class of processes in nature.

Application cases are carried out to verify the approach developed in this work. Most applications are drawn from the realm of earth sciences. The selected applications firstly aim at the verification of details of the geometric modelling approach. The analysis and preprocessing of sample points, the assignment of weights and the interpretation of the result α-complexes are discussed. Every "case" yields a model that may act as an icon. Secondly, applications seek to verify the numerical modelling approach with α-complexes and finally, α-complex based process models. As far as the latter is concerned, a deposition/erosion process model has been selected, inducing a change of topology, with the idea that this type of process best demonstrates the power of the developed approach.

Further to these cases, there is a case showing how a previously derived icon can be used to instantiate a complete family of descendent objects. Another case demonstrates the editing. A larger point set case uncovers the largest size that can be implemented on today's computing platforms.

Conclusions

The research of this dissertations sets forth the following conclusions and principle findings.

The concept of α-complexes conveniently abridges the gap between sampling data point sets of observed physical objects, and the targeted solid object models needed for instance for process modelling. Using an α-complex, an icon can be drawn from the sampling data point set and stored in a database. Using transformations, entire families of objects can be generated by the icon. This way, initial objects can be rapidly created, to be further constrained by additional data. Furthermore, it appears feasible to store additional process information enabling the object to act as a process model. The object's dynamic behaviour may be sufficiently formalised, despite deposition and erosion, using morphological operators. This results in an evolutionary map, governed by the morpho-dynamic process. Many natural objects are in fact multi-phase systems. With holes defined as *complementary space* relative to the convex hull, an α-complex preciously defines a two-phase system, like a percolation system or a gas-fluid system.

Weighting can successfully be turned into a modelling instrument. Weighting is of great practical importance, particularly in those cases where neighbouring distances between sample points are equal. Weighting based on a restricted number of factors intuitively and practically conforms to the modelling of sampled natural objects. Intuitively because of the property-ruled nature of geometry and topology and practically because this way of weighting is easily implemented through *hyper-spatialmodelling*. For objects that contrast only faintly with the embedding background, cluster-membership (α) and/or weight should be taken such that the vague boundary between

object and background is sufficiently stored along with the sample data in the icon. If so, the boundary can be reproduced in all its vagueness during instantiation. Sufficient *discriminant power* of the ruling properties is decisive to discriminate the object from its natural background. A lack of strong factors results in a poor weighting and poor modelling. Weighting based on observed properties is best approached as a two-stage process. The first step implements the finding of the normalised weights and the second step transforms weights to match the nearest-neighbour distances. The Stienen model is a suitable attractor guaranteeing maximum local weight without enforcement of any connection by weight alone.

The sampling data point set can be considered as a homogenous or in-homogenous empirical *Poisson point process*. Clustering effects, as expected, turn out to be reflected by the stochastic characteristics of the process fairly well. Using a marked Poisson point process, the problem of weighting may be redefined in terms of a *coverage problem*, which helps to further make the problem transparent.

So far, only the benefits of the approach taken have been highlighted. As ever, the approach comes with a number of flaws and omissions, too. Implicit topology, for instance, blocks a *full* control over the topology. Occasionally, for certain configurations, the sample points generate an incorrect or undesirable topology. The framework anticipates repair of undesired topologies with a couple of "instruments": transformations may be applied to manipulate (i.e., improve) the spatial distribution of the sample points. Line-patterns, for instance. Furthermore, normalisation, a special type of transformation, can be used to homogenise scales and spaces of property values, and the like. Repair of undesired topologies is not always possible this way. In case all this fails, the insertion of *pseudo*-sample points can be tried as a remedy. Further enhancements are also expected from anisotropic forms of weight: weight which is direction dependent. Moreover, alternate solutions have been proposed in literature recently, based on local metric and redefinition of α-complexes. This will also further recently improve topological control. Nonetheless, cases that cannot be sufficiently controlled are not believed to cease occurring in the near future.

Another disadvantage of the approach presented in here is that it takes detailed knowledge on the underlying sampling data point set, in order to fully comprehend the joint effect of transformation and weighting. Also, the consequences for the Lebesgue measure, the hyper-volume, say, continuously have to be kept in mind. A theoretical model may assist in gaining insight, though, but not sufficiently under all circumstances.

As an object model description, an α-complex generally violates the continuity criterion, as well as the criteria for solidity, closure and homogeneous dimensionality. Set regularisation and the "embedding approach" can eliminate these flaws. The introduction of a *nil*-object aids greatly in the search for homeomorphic maps. As a representation scheme, the α-complex is unambiguous but not unique. Validation of the representation scheme is generally expensive.

Contrary to many other object model descriptions, no transcription is needed before running numerical computations on an α-complex. Solutions have to be found, though, for three inherent problems: singular elements, separations and "slivers". Slivers are needle-like elements with a very bad aspect ratio. Singular elements are easily filtered off. Separations can be coped with using the "embedding"-approach. Slivers appear to be primarily generated in the vicinity of the α-complex' border, for higher values of α. Rather than taking the triangulation as the embedding background, an α-complex that approaches the triangulation can be taken, with a slightly smaller α-value. Doing so generally removes the slivers. This strategy, along with

the implicit topology, brings about unattended iterative process modelling with no intervention required by the modeller. Topological changes are implicitly adapted for, much in the fashion of an automatic regridding. This approach turns out to facilitate process modelling of deposition-erosion objects fairly well, covering an extremely important class of natural objects.

Regarding model size and performance, the following conclusions can be drawn. Generally, detailed models require vast amounts of data and large computers to process them. For simple models ($O(10^2)$ to $O(10^3)$ points), results show that implementations can generally be made fast enough for interactive use. For more complex and bigger problems ($O(10^4)$ to (10^6) points), storage becomes increasingly critical. The largest model had approximately $3 \cdot 10^5$ sample points and took more than 1 Gb internal memory and 5 to 6 hours of dedicated processing time on a powerful 4-processor ONYX 2 SILICON GRAPHICS[2]. This case uncovers the current limits which are somewhat too restrictive, still. With the advent of faster computers with more memory this barrier is believed to be trespassed soon. Additionally, domain decomposition, not discussed in this thesis, can help to break down the problem in smaller sub-problems and have a network of moderate computers calculate the solution in parallel. Storage requirements can be reduced by exploiting the fact that α-complexes can be stored as unevaluated descriptions, i.e., the complex itself can uniquely be reproduced from the stored set of sample points plus an α-value.

The use of α-complex-based icons offers good possibilities for a hook-up with *knowledge-based modelling* and *variational geometry*. In a somewhat broader context, the idea of creating a lively collection of communicating co-existing natural objects (shapes) is steadily growing towards reality. In the century lying ahead, technical developments are foreseen to become mature enough to facilitate the technical environment. Modelling technique developments are felt to become the critical factor for appreciable progress. Nevertheless, the approach presented in this thesis is believed to contribute to significant cost savings for the E&P-industry, in the very near future. Mainly due to the accelerated modelling process, and enhanced and more reliable models.

[2] kindly made available by Silicon Graphics Benelux, at De Meern

Samenvatting

Het Gebruik van Gewogen Alpha Complexen bij het Modelleren van de Ondergrond

Het reconstrueren van bemonsterde natuurlijke objecten

Bart H.M. Gerritsen

De studie naar het modelleren van *natuurlijke objecten* heeft een enorme progressie geboekt, de laatste jaren. Vooral de komst van krachtige computers is daarbij van belang geweest. Het modelleren van natuurlijke objecten blijft evenwel een moeilijk probleem, ook met de huidige modelleer-technieken. Dat geldt voor het verkrijgen van foto-realisme, maar zeker ook voor het nauwkeurig beschrijven van de vorm. Natuurlijke objecten, met hun overvloedige complexiteit en mate van detail zijn vaak zo gecompliceerd dat alleen met behulp van een verzameling bemonsteringspunten de vorm ervan op een adequate manier kan worden beschreven. Analytische beschrijvingen zijn ofwel veel te gecompliceerd ofwel simpelweg onmogelijk. Eigenschappen gemeten in de bemonsteringspunten moeten meestal uitsluitsel geven of en zo ja in welke mate dat waarnemingspunt tot het object moet worden gerekend en wat als *natuurlijke achtergrond* moet worden gerekend. In veelgevallen komt er iets van deze natuurlijke achtergrond mee met de verzameling bemonsteringspunten. Het probleem met op deze manier bemonsterde objecten is vervolgens om een solid object te creeëren uit deze puntenverzameling.

Het probleem van deze dissertatie sluit aan bij bovenstaand probleem: *objecten in de ondergrond* zijn immers ook natuurlijke objecten. In deze dissertatie gaat het met name om het vinden van een *icon* uit een verzameling bemonsteringspunten. Een icon is een kenmerkende representant van een familie van soortgelijke objecten. Bijvoorbeeld een icon van een meanderende rivier, een duin, een lens, een point bar, etc. Een icon kan worden opgeslagen in een database en met één enkele icon als "template" kan ook weer een hele familie worden *geinstantieerd* (gereproduceerd), door toekenning van afmetingen, een locatie en een orientatie. Samengevat, door een transformatie toe te passen op de icon. Met aanvullende bemonstering, die als "constraining data" worden gebruikt kan het gecreeerde object zo goed mogelijk in overeenstemming worden gebracht met de observaties van de werkelijkheid. Daartoe wordt in deze dissertatie een modelleeromgeving voorgesteld die uitgaat van een *inversie-cyclus* en een *forward modelling loop* en die voorziet in op invoer van dergelijke constraining data.

Voor het *kernprobleem*, het overbruggen van de kloof tussen punt-topologieën van de bemonsteringspunten en de beoogde solid models zijn in de recente literatuur nieuwe mathematische constructies voorgesteld, die hier met vrucht kunnen worden toegepast. Een daarvan is het α-complex. In de hier beschreven aanpak wordt bij het bepalen van icons en bij het weer instantieren van "afstammelingen" daarvan gebruik gemaakt van α-complexen. In deze dissertatie gaat het er met name om om te bezien of α-complexen daarvoor geschikt zijn en passen in de aanpak als beschreven. Het gebruik van α-complexen op zich heeft een aantal kenmerken gemeen met het gebruik van triangulaties en convex omhullenden, maar biedt ook een aantal specifieke voordelen, tegen slechts geringe extra rekenkosten van de computer. Tot op zekere hoogte kan een α-complex worden opgevat als een geparametriseerde triangulatie, met een bovenlimiet voor

de lengte van een edge. Een α-complex kan de geometrie en topologie beschrijven van een object uit een stuk, maar ook van een een object met gaten en separaties, in één enkele wiskundige entiteit. Dit in tegenstelling tot een triangulatie of een convex omhullende. In deze dissertatie ligt de nadruk op *gewogen* α-complexen, gebaseerd op gewogen punten, waarbij de paramterisatie dan niet alleen is gebaseerd op onderlinge afstand, maar tevens op een "bias" als gevolg van het gewicht.

Manipulatie van de ruimtelijke verdeling van de bemonsteringspunten en het gebruik van gewicht maken "speciale modelleer-effecten" mogelijk. Om deze modelleer-effecten te kunnen benutten moeten de effecten van transformaties van de punten worden geanalyseerd en moet er een weegstrategie worden ontwikkeld die aansluit bij het modelleren van bemonsterde natuurlijke objecten. In dit onderzoek worden verschillende strategieën voorgeteld en degene met de in dit verband beste perspectieven wordt verder uitgewerkt. Het feit dat α-complexen van arbitraire dimensie kunnen zijn, maakt hyper-spatieel modelleren (veel-dimensionaal modelleren) mogelijk, hetgeen weer goed beantwoord aan de door eigenschappen bepaalde geometrie en topologie van natuurlijke objecten.

Een cluster en/of factor analyse wordt gebruikt om te bepalen welke eigenschappen in welke mate bijdragen tot het onderscheiden van een object van zijn natuurlijke achtergrond. In een hyperspatiele aanpak geeft een cluster analyse als het ware de geometrie in de eigenschap-deelruimte ("property space") en cluster membership, projecties en intersecties kunnen dan vervolgens worden gebruikt om de "gewone" geometrie en topologie te bepalen. Voor de meeste toepassingen zal daarbij uiteindelijk de eigenschap-deelruimte worden vervangen door gewicht. Voorwat betreft de icon kunnen ofwel de hyper-spatial bemonsteringspunten worden opgeslagen, ofwel de gewogen bemonsteringspunten, afhankelijk van het instantieringsproces. Hetop deze manier in elk bemonsteringspunt bepaalde gewicht kan door middel van transformaties in relatie worden gebracht met de te overbruggen afstand tussen bemonsteringspunten. Bijvoorbeeld door de kleinste *nearest-neighbour* afstand te bepalen en alle gewichten in gelijk emate op te schalen met een factor die gebaseerd is op die afstand. De onderlinge verdeling van de gewichten blijft dan (in relatieve zin) gelijk en zal dus leiden tot een object dat volledig bepaald is door de bemonsterde eigenschappen. Het gewicht kan *locaal* verder worden opgeschaald tot de *locaal maximale* waarde, d.w.z. de maximale waardezonder dat op dat punt een verbinding in het α-complex wordt afgedwongen door het gewicht alleen. Locaal maximale waarden van de gewichten kunnen bijvoorbeeld worden gebruikt om een gaten-vrij (deel van een) object te krijgen. De duidelijke relatie met de bepalende eigenschappen gaat dan over het algemeen verloren. Bij elke verzameling bemonsteringpunten hoort een *attractor* waaruitdeze locaal maximale waarden kunnen worden afgeleid.

Definitie op basis van een α-complex biedt de mogelijkheid om verscheidene vormen van een en dezelfde puntenverzameling te evalueren. In dit geval wordt deze mogelijkheid dus ingezet om de icon te vinden en eenduidig te beschrijven. De verschillende versies van het object worden uit de bemonsteringspunten verkregen door de waarde van de parameter α te varieren. Neemt α toe, dan wordt de icon "vetter", bij een afnemende α wordt de icon "magerder". De waarde van α kan direct worden gemanipuleerd, maar het uiteindelijke doel is om dit te baseren op "harde" criteria, bijvoorbeeld strategraphische constraints of processimulaties. Eventueel kan de icon nog worden aangepast door middel van *editing*. Editing houdt in dit verband in dat de verzameling punten wordt gemanipuleerd, bijvoorbeeld door het toevoegen van punten om bepaalde a-priori kennis in te brengen. Het reconstructie-proces van het bemonsterde object gaatin het algemeen gebukt onder een gebrek aan voldoende en voldoende gelijksoortige data. Mede daarom is er de

wensom *a-priori kennis* in te brengen. Bijvoorbeeld om gaten weg te werken of aan te brengen. Elke soort kennis die vertaald kan worden in aanvullende punten kan daarbij gemakkelijk worden ingebracht.

Het process van analyse, interpretatie en editing kan worden ondersteund met behulp van een theoretisch model, net zoals een Gausische model curve bij een histogram. Als eenmaal een theoretisch model is "gematched", dan kunnen aanmerkelijk meer en betere uitspraken worden gedaan ten aanzien van de onderliggende verzameling bemonsteringspunten.

De geometrische en topologische beschrijving op basis van een α-complex zijn mathematisch volledig geformaliseerd. Het is van groot praktisch belang dat α-complexen kunnen worden gecombineerd met bestaande object model beschrijvingen en representaties die maar zelden zijn gebaseerd op cellulaire structuren met gaten en separaties. Dit betekent dat α-complexen ook beoordeeld moeten worden als model beschrijving als representatie. De twee meest toegepaste representaties, de Constructive Solid Geometry (CSG) en de boundary representation (B-rep), worden daarbij als referentie aangehouden.

Ook moeten α-complexen geschikt zijn of kunnen worden gemaakt als numeriek model en uiteindelijk kunnen dienen als basis voor een *dynamisch process model*. Er wordt een nieuwe aanpak voorgesteld voor numerieke berekeningen op basis van α-complexen. Door gebruik te maken van het feit dat de elementen waaruit een α-complex is opgebouwd ook voorkomen in de triangulatie van dezelfde punten verzameling kan een *topologische inbedding* (*embedding*) worden gevonden die een berekening met bijvoorbeeld eindige elementen op basis van een α-complex mogelijk maakt. Zelfs als er gaten zijn of het object gesepareerd is. Deze aanpak werktook voor processimulaties van deposities en eroderende objecten, een belangrijke klasse van processen die veelvuldig voorkomen in de natuur.

De ontwikkelde aanpak wordt getoetst met behulp van toepassingen, vooral betrekking hebbend op de aardwetenschappen. De gekozen toepassingen zijn in de eerste plaats bedoeld en geselecteerd om de aspecten van het geometrisch modelleren te belichten. De voorbewerking van bemonsteringspunten, de toekenning van gewichten en het interpreteren van α-complexen komen daarbij aan de orde. Iedere "case" eindigt in een model dat als icon kan worden opgeslagen. Verder het numerieke modelleren op basis van α-complexen en ten slotte het maken van een proces model met behulp van een α-complex. Wat dit laatste betreft is gekozen voor een erosieprocess, dat tot wijzigingen leidt in de topologie, omdat hierin het best de kracht van de gekozen aanpak tot uitdrukking komt.

Een van de toepassing laat zien hoe een eerder afgeleide icon kan worden ingezet om hele familie van objecten te creeren. Ook is er een toepassing die laat zien hoe de verzameling vanbemonsteringspunten waaruitde icon wordt afgeleid kan worden aangepast met behulp van editing. In de perifierie is het verder van belang de grenzen van de techniek te verkennnen: een van de toepassing beoogt daarom de maximale grootte van de verzameling van bemonsteringspunten af te tasten, die op de huidige computerplatforms kan worden verwerkt.

Conclusies

Uit het onderzoek beschreven in deze dissertatie kunnen de volgende conclusies worden getrokken.

Het concept van α-complexen leent zich bij uitstek om het gat te dichten tussen enerzijds de bemonsteringstechnieken die hun resultaten als verzameling punten afleveren en solid models die onder meer nodig zijn voor een proces-simulatie van het object. Met behulp van α-complex kan uit een verzameling van bemonsteringpunten van gelijksoortige objecten een icon worden afgeleid en opgeslagen in een database. Met behulp van transformaties kunnen hiermee complete families van objecten worden gegenereerd. Op deze wijze kan snel en eenvoudig een initieel object worden gecreeerd, dat verder met een waargenomen werkelijkheid in overeenstemming kan worden gebracht. Verder is het zo dat in een op een α-complex gebaseerde icon procesinformatie kan worden opgeslagen, zodat een object kan dienen als een procesmodel. Het blijkt mogelijk om het dynamisch gedrag van dergelijke objecten, ondanks depositie en erosie, voldoende te formaliseren met behulp van morfologische set operatoren. Het resultaat is dan een evolutionary map, bepaald door het morfologische proces. Veel natuurlijke objecten zijn in feite op te vatten als meerfase systemen. Doordat gaten zijn gedefinieerd als *complementaire ruimte* ten opzichte van de convex omhullende, leent een α-complex zich bij uitstek om een twee-fasesysteem te beschrijven, bijvoorbeeld percolatie modellen en gas-vloeistof problemen.

Weging kan met succes worden ingezet als een modelleer-instrument. Weging is van grote praktische betekenis vooral in die situaties waarin de onderlinge afstanden tussen de bemonsteringspunten identiek zijn. Weging op basis van een beperkt aantal bepalende eigenschappen (*factoren*) sluit intuitief en qua opzet het best aan bij het modelleren van bemonsterde natuurlijke objecten. Intuitief omdat de geometrie en topologie immers vooral bepaald worden door de waarden van de eigenschappen in de bemonsteringspunten en qua opzet omdat deze weegstrategiegemakkelijk kan worden geimplementeerd met behulp van *hyper-spatieel modeller en*. Voor objecten die moeilijk te onderscheiden zijn van hun achtergrond is het aan te bevelen om cluster-membership (α) en/of gewichten zodanig te kiezen dat een de vage grens in voldoende mate met de icon wordt opgeslagen. Bij het instantieren is deze grens dan weervoldoende reproduceerbaar. Voldoende *discriminerend vermogen* van de bepalende eigensdhappen is belangrijk om het gezochtte object als hetware te contrasteren met de natuurlijke achtergrond. Als geegeschikte combinatie van zulke factoren kan worden gevonden, dan is als gevolg daarvan het gewicht als modelleer-effect ook zwak. Weging op basis van waarden van bepalende eigenschappen kan het best als een tweestappen strategie worden gezien. In de eerste stap wordt het genormaliseerde gewicht bepaald, in de tweede stap vindt een transformatie plaats om het gewicht qua grootte in overeenstemming te brengen met de spatiëring van de bemonsteringspunten. Het Stienen model is een geschikte attractor die garandeert dat geen enkel punt verbonden wordt met een buurman op basis van het gewicht alleen en elk punt toch zijn locaal maximale waarde heeft.

De verzameling bemonsteringspunten kan worden opgevat als een empirisch homogeen of inhomogeen *Poisson punt proces* Clustering effecten blijken, zoals mag worden verwacht, duidelijk terug te vinden in de stochastische karakteristieken van het process. Met behulp van een marked Poisson point process kan het bepalen van gewicht worden geherformuleerd als een *dekkingsprobleem* (*coverage problem*), hetgeen het bepalen ervan meer intuitief maakt.

Tot nu toe zijn een aantal onderdelen van de voorgestelde aanpak genoemd die met succes kunnen worden ingezet voor de beoogde doelen. Daar staan een aantal (nog) niet opgeloste problemen en nadelen tegenover. Een impliciet afgeleide topologie is een handige eigenschap van een α-complex, tegelijkertijd blokkeert het een *volle dige* controle over de topologie. In een aantal gevallen, voor zekere configuraties van bemonsteringspunten, ontwikkelt zich een onjuiste topologie. Corrigeren lukt niet in alle gevallen volledig. In de voorgestelde aanpak zijn een aantal "instrumenten" aanwezig om de topologie onder controle te krijgen. Met behulp van transfor-

maties kan de ruimtelijke verdeling van de bemonsteringspunten worden beinvloed. Bijvoorbeeld bij sterk lijn-georienteerde bemonsteringspunten. Een speciaal geval van een transformatie, de normalisatie, kan worden gebruikt om ruimtelijke schalen en de schaling van de waarden van eigenschappen op gelijk niveau te brengen. Als dit alles niet afdoende is kunnen aanvullende *pseudo*-bemonsteringspunten worden toegevoegd. Veel wordt ook verwacht van anisotrope vormen van weging, d.w.z., het gewicht wordt richtingsafhankelijk gemaakt. Ook zijn er in de literatuur voorstellen gedaan om te werken met een locale metriek en een voorstel om de definitie van α-complexen aan te passen. Ook hiervan mag een verdere verbetering worden verwacht. Toch blijven er gevallen over die niet de gewenste topologie opleveren.

Een ander nadeel is dat om het samengestelde effect van transformatie en weging volledig te begrijpen, er gedetailleerde kennis nodig is van de onderliggende verzameling bemonsteringspunten. Ook moet continue worden afgevraagd, wat transformaties betekenen voor bijvoorbeeld de Lebesgue measure, eenvoudig voor te stellen als een maat voor hyper-volume. Welliswaar biedt een theoretisch model aanvullend inzicht, maar dit is niet in alle gevallen toereikend.

Een α-complex als object model beschrijving zal in het algemeen continuiteitscriteria schenden, evenals criteria voor solidity, closure and homogeneous dimensionality. Set regularisatie en de "inbedding aanpak" kunnen dit bezwaar wegnemen. De introductie van een nul-object help om homeomorfe afbeeldingen en conversies te verkrijgen. Als representatie schema is het α-complex eenduidig maar niet uniek. Het valideren van het representaieschema is over het algemeen kostbaar.

In tegenstelling to een aantal andere model beschrijvingen is geen vertaling nodig van een α-complex voordat er numerieke berekeningen op uitgevoerd kunnen worden. Wel zijn er oplossingen nodig voor de volgende drie problemen: singuliere elementen, separaties en "slivers". Slivers zijn naald-vormige elementen met een uitermate slechte aspect ratio. Singuliere elementen kunnen eenvoudig verwijderd worden, bijvoorbeeld door filtratie. Separaties kunnen worden opgeheven door gebruikmaking van de ontwikkelde "embedding"-techniek. Slivers blijken voornamelijk gevormd te worden voor hoge waarden van α, nabij de buitengrens van het α-complex. In plaats van de triangulatie als achtergrond voor inbedding kan men daarom beter een α-complex nemen dat de triangulatie benaderd maar waarvan de α-waarde ietwat lager ligt. Deze aanpak zorgt er over het algemeen voor dat de slivers verdwijnen. Deze strategie, gecombineerd met het feit dat de topologie impliciet is gedefineerd, maakt het mogelijk om een procesmodel te "draaien", op basis van een iteratief proces zonder verdere interventie van de modelleerder. Topologie-veranderingen kunnen door het impliciete karakter worden opgevangen, waardoor een soort automatische regridding optreedt. Deze aanpak blijkt ook zeer geschikt voor processimulaties van deposities en eroderende objecten, die veelvuldig voorkomen in de natuur.

Voor wat betreft de model-grootte kan het volgende worden geconcludeerd. Gedetailleerde modellen vragen enorme hoeveelheden bemonsteringspunten. Simpele modellern, in de orde-groote van $O(10^2)$ to $O(10^3)$ bemonseringspunten, resulteren in toepassingen die zich over het algemeen op een gemiddeld recent model werkstation lenen voor interactief gebruik. In geval van grotere en meer complexe modellen ($O(10^4)$ to (10^6) punten), wordt het problematisch. Het grootste model dat kon worden gecreeerd heeft ongeveer $3 \cdot 10^5$ bemonsteringspunten en vergt meer dan 1 Gb internal memory and 5 to 6 CPU-uren berekeningstijd op een 4-processor ONYX 2 SILICON GRAPHICS[3]. Deze case legt duidelijk de huidige grenzen bloot. Met de komst van krachtiger computers kunnen deze grenzen uiteraard worden doorbroken. Daar komt bij dat

[3]ter beschikking gesteld door Silicon Graphics Benelux in de Meern

(hier niet ter sprake gebrachte) technieken als domein decompositie en "parallellisatie" kunnen worden aangewend om het eigenlijke probleem op te delen in kleine soortgelijke deelproblemen en op die manier in stapjes op te lossen, eventueel met een netwerk van samenwerkende kleine computers. Wat de huidige grenzen van de opslag van de icon betreft: eventueel kan worden overgegaan naar een *unevaluated* opslag van het α-complex van de icon. Dat wil zeggen dat het α-complex zelf niet wordt opgeslagen, maar alleen de gewogen puntenverzameling en de α-waarde. Het α-complex kan hieruit opnieuw worden bepaald.

Het gebruikt van icons op basis van α-complexen biedt goede mogelijkheden voor *knowledge-based modelling* en *variational geometry*. In een wat breder verband komt het creëeren van een collectie levende, onderling communicerende objecten die samen een levend model van de aarde vormen, steeds dichterbij. In deze nieuwe eeuw zal de technische vooruitgang van computers snel genoeg gaan om geen belemmering meer te vormen. De voortgang van de ontwikkeling van de modelleertechnieken wordt naar verwachting de beperkende factor. Desalniettemin wordt er vanuit gegaan dat met deze nieuwe technieken belangrijke kostenbesparingen kunnen worden bereikt in de E&P-industrie, op korte termijn. Voornamelijk als gevolg van het sneller beschikbaar komen van betere modellen, met een kleinere onzekerheid.

Curriculum vitae

Bart Gerritsen werd op 19 april 1957 geboren te Renkum. Na de lagere school ging hij naar het Thomas a Kempis College te Arnhem. Hij werkte na de middelbare school enige tijd in de automobielbranche en begon vervolgens aan een opleiding aan de HTS Autotechniek in Apeldoorn. Na afloop van zijn HTS-opleiding besloot hij om zowel te gaan werken als verder te studeren. In 1981 trad hij in dienst van het toenmalige Ministerie van Volksgezondheiden Milieubeheer. Hij hield zich vooral bezig met technische en informatica-vraagstukken betreffende voertuigen en verkeer in relatie tot milieubeleid en -beheer. Daarnaast schreef hij zich in als dagstudent aan de Faculteit der Werktuigbouwkunde van de TU Delft met als doel om zich verder te verdiepen in de voertuigtechniek. In 1987 behaalde hij zijn Kandidaatsexamen, maar besloot zich te verdiepen in Computer-aided design in plaats van voertuigtechniek. Onderwijl was hij in dienst getreden bij het huidige CAP Gemini als technisch IT-specialist. Eind jaren tachtig kwam hij in aanraking met de aardwetenschappen en specialiseerde zich ook tijdens de eindfase van zijn studie steeds meer in het modeleren van de ondergrond. In 1991 studeerde hij af op een onderwerp over het bereiken van datareductie door middel van triangulaties op ondergronddata. Inmiddels was hij in dienst getreden bij de toenmalige Dienst Grondwater Verkenning van TNO, een instituut dat nu is opgegaan in het huidige NITG-TNO. Het voorliggende proefschrift is tot stand gekomen naast zijn werkzaamheden voor dit instituut.

Bart Gerritsen was born on April 19, 1957 at Renkum, the Netherlands. After his primary education, he visited grammar school. Having held various positions in the automotive branch, he decided to attend the Polytechnic School for Automotive Engineering. On leave from the Polytechnic School, he decided to apply for a professional career and, simultaneously, commence a study Mechanical Engineering at the Delft University of Technology, firstly with the objective to further strengthen his skills in automotive engineering. In 1981, he joined the Dutch Ministry of Public Health and Environmental Protection, as a technical expert. His principle concern being technical matters in the area of traffic and transportation and their environmental impact. Also being a student, he received a Bachelor degree in Mechanical Engineering from the Delft University of Technology in 1987, but decided, however, to devote his further study to Computer-aided Design, rather than Automotive Engineering. Meanwhile, his professional career had brought him with CAP Gemini, a globally operating IT-company. It was in the late eighties that he became involved in earth sciences. Computer-aided design gradually became subsurface modelling. In 1991, he received a master degree, treating the subject of data reduction using triangulations of subsurface data. Having joined the TNO Institute of Applied Geoscience, nowadays part of the Netherlands Institute of Applied Geoscience – Dutch Geological Survey, he compiled this thesis.

Nomenclature

Sets and domains

$\emptyset$	=	empty set
$\mathbb{K}$	=	the set of cardinal numbers
$\mathbb{I}$	=	the set of ordinal numbers
$\mathbb{N}$	=	the set of natural numbers
$\mathbb{Z}$	=	the set of integer numbers
$\mathbb{R}$	=	the set of real numbers
$\mathbb{Q}$	=	the set of rational numbers
$\mathbb{C}$	=	the set of complex numbers
(r_1, r_2)	=	open interval $r_1 < r < r_2$
$[r_1, r_2)$	=	half-open interval $r_1 \leq r < r_2$
$[r_1, r_2]$	=	closed interval $r_1 \leq r \leq r_2$
$[e_1..e_2)$	=	half-open (sub)sequence e starting with e_1 up to but not including e_2. Furthermore, similar to intervals

Sets and spaces

X	=	topological space
E^d	=	d-dimensional euclidian space, with $d \geq 0$
$\mathbb{E}^d$	=	set covering d-space E^d; $\mathbb{E}^d = \prod_{k=0}^{d-1} \mathbb{R}_k = \mathbb{R}_0 \times \mathbb{R}_1, \ldots, \times \mathbb{R}_{d-1}$
$\mathbf{x}$	=	point in E^d, with $\mathbf{x} = (x_0, x_1, \cdots, x_{d-1})$
$\mathbb{S}$	=	finite sampling data point set, or: *landmark* set, $\mathbb{S} \subset \mathbb{E}^d$
s	=	sample point, $s \in \mathbb{S}$
$N = \operatorname{card} \mathbb{S}$	=	finite set cardinality of S; $N \in \mathbb{N}$
$\mathbb{S}_1 \times \mathbb{S}_2$	=	Cartesian product of set $\mathbb{S}_1$ and $\mathbb{S}_2$
$\mathbb{S}_1 \otimes \mathbb{S}_2$	=	ordered Cartesian product of set $\mathbb{S}_1$ and $\mathbb{S}_2$, $\operatorname{card} \mathbb{S}_1 = \operatorname{card} \mathbb{S}_2$
$\mathbb{S}_1 \bigcup \mathbb{S}_2$	=	set union of $\mathbb{S}_1$ and $\mathbb{S}_2$; $\mathbb{S}_1 \bigcup \mathbb{S}_2 = \{s \vert s \in \mathbb{S}_1 \text{ or } s \in \mathbb{S}_2\}$
$\mathbb{S}_1 \bigcap \mathbb{S}_2$	=	set intersection of $\mathbb{S}_1$ and $\mathbb{S}_2$; $\mathbb{S}_1 \bigcap \mathbb{S}_2 = \{s \vert s \in \mathbb{S}_1 \text{ and } s \in \mathbb{S}_2\}$
$\mathbb{S} \setminus \mathbb{Y}$	=	set difference of $\mathbb{S}$ and $\mathbb{Y} \subset \mathbb{S}$; $\mathbb{S} \setminus \mathbb{Y} = \{s \in \mathbb{S} \vert s \notin \mathbb{Y}\}$

$\mathbb{S}_1 \oplus \mathbb{S}_2$	=	Minkowski set addition; $\mathbb{S}_1 \oplus \mathbb{S}_2 = \{s_1 + s_2 \vert s_1 \in \mathbb{S}_1, s_2 \in \mathbb{S}_2\}$
$\mathbb{S}_1 \ominus \mathbb{S}_2$	=	Minkowski set subtraction; $\mathbb{S}_1 \ominus \mathbb{S}_2 = \{s_1 - s_2 \vert s_1 \in \mathbb{S}_1, s_2 \in \mathbb{S}_2\}$
$-\mathbb{S}$	=	reflection of $\mathbb{S}$; $-\mathbb{S} = \check{\mathbb{S}} = \{-s \mid s \in \mathbb{S}\}$
$\check{\mathbb{S}}$	=	reflection of $\mathbb{S}$; $\check{\mathbb{S}} = -\mathbb{S}$
$\mathrm{Conv}\,\mathbb{S}$	=	convexset spanned by $\mathbb{S}$
$\mathrm{Compl}\,\mathbb{S}$	=	complement of $\mathbb{S}$
$\mathbb{S}_\hbar$	=	Helmertized, interpolated finite landmark set

Weighted points

$\mathbb{W}$	=	set of real weights to be attached to $\mathbb{S}$; $\mathbb{W} \subset \mathbb{R}$
$\tilde{\mathbb{S}}$	=	weighted sampling data point set; $\tilde{\mathbb{S}} = \mathbb{S} \otimes \mathbb{W}$
$2^{\tilde{\mathbb{S}}}$	=	power set of $\tilde{\mathbb{S}}$; $2^{\tilde{\mathbb{S}}} = \{\mathbb{Y} \vert \mathbb{Y} \subset \tilde{\mathbb{S}}\}$
$\tilde{s}$	=	sample point with attached weight, $\tilde{s} \in \tilde{\mathbb{S}}$; $\tilde{s}$ an ordered 2-tuple $(s, w) \in \mathbb{S} \otimes \mathbb{W}$
$\tilde{\mathbf{x}}$	=	weighted point in $E^d \times R$, with $\tilde{\mathbf{x}} = (x_0, x_1, \cdots, x_{d-1}, w) \cong (\mathbf{x}, w)$
w	=	real weight, $w \in (-\infty..\infty)$

Geometry

$\mathcal{A}$	=	arrangement; a spatial configuration
$St\ \mathbf{s}$	=	(open) star of vertex $\mathbf{s}$; union of interiors of all faces incident upon $\mathbf{s}$
$\bar{St}\ \mathbf{s}$	=	closed star of vertex $\mathbf{s}$; union of all closed faces incident upon $\mathbf{s}$
$Lk\ \mathbf{s}$	=	link of vertex $\mathbf{s}$; $Lk\ \mathbf{s} = \bar{St}\ \mathbf{s} - St\ \mathbf{s}$
$\tilde{\mathbb{S}}^{\tilde{\emptyset}}$	=	finite set of radical centres, generated by $\tilde{\mathbb{S}}$, in which the empty weighted α-balls are located; $\mathrm{card}\,\tilde{\mathbb{S}}^{\tilde{\emptyset}} \neq \mathrm{card}\,\tilde{\mathbb{S}}$; $\tilde{\mathbb{S}}^{\tilde{\emptyset}}$ coincides with the set of Voronoi vertices
$\mathcal{P}$	=	k-polytope; a k-dimensional bounded polyhedron
$\vert\mathcal{P}\vert$	=	the underlying space of $\mathcal{P}$, the part of E^d occupied by $\mathcal{P}$

$\mathrm{Int}\,\mathcal{P}$ = interior of $\mathcal{P}$; $\mathrm{Int}\,\mathcal{P} \cong \mathrm{Cl}\,\mathcal{P} - \mathrm{Bd}\,\mathcal{P}$

$\overset{\circ}{\mathcal{P}}$ = interior of $\mathcal{P}$; $\overset{\circ}{\mathcal{P}} \cong \mathrm{Int}\,\mathcal{P}$

$\mathrm{Bd}\,\mathcal{P}$ = border of $\mathcal{P}$; $\mathrm{Bd}\,\mathcal{P} \cong \mathrm{Cl}\,\mathcal{P} - \mathrm{Int}\,\mathcal{P}$

$\partial\mathcal{P}$ = border of $\mathcal{P}$; $\partial\mathcal{P} \cong \mathrm{Bd}\,\mathcal{P}$

$\mathrm{Ext}\,\mathcal{P}$ = exterior of $\mathcal{P}$.

$\mathrm{Cl}\,\mathcal{P}$ = closure of $\mathcal{P}$; $\mathrm{Cl}\,\mathcal{P} = \bigcap_i Cl\ \mathcal{Q}_i,\ \mathrm{Cl}\,\mathcal{Q}_i \subset \mathcal{P}$

$\bar{\mathcal{P}}$ = closure of $\mathcal{P}$; $\bar{\mathcal{P}} \cong \mathrm{Cl}\,\mathcal{P}$

$\mathcal{H}(\tilde{\mathbb{S}})$ = convex hull of weighted point set $\tilde{\mathbb{S}}$; $\mathcal{H}(\tilde{\mathbb{S}}) \cong \mathcal{W}_{\alpha_{max}}(\tilde{\mathbb{S}})$

$\mathcal{V}(\tilde{\mathbb{S}})$ = weighted Voronoi diagram of weighted point set $\tilde{\mathbb{S}}$

$\Pi(\tilde{\mathbb{S}})$ = power diagram of weighted point set $\tilde{\mathbb{S}}$; $\Pi(\tilde{\mathbb{S}}) \cong \mathcal{V}(\tilde{\mathbb{S}})$

$\mathcal{T}(\tilde{\mathbb{S}})$ = regular triangulation of weighted point set $\tilde{\mathbb{S}}$; $\mathcal{T}(\tilde{\mathbb{S}}) = \mathcal{C}_{\alpha_{max}}(\tilde{\mathbb{S}})$

$\mathcal{F}(\tilde{\mathbb{S}})$ = space filling diagram; $\mathcal{F}(\tilde{\mathbb{S}}) = \bigcup \left(B_\alpha(\tilde{\mathbb{S}}) \right)$

$\mathcal{C}(\tilde{\mathbb{S}})$ = simplicial complex based on $\tilde{\mathbb{S}}$; $\mathcal{C}(\tilde{\mathbb{S}}) = \bigcup \sigma^{(k)}$, with: $\sigma_j^{(0)} \in \mathbb{S}$

$\mathcal{C}_\alpha(\tilde{\mathbb{S}})$ = weighted α-complex; $\mathcal{C}_\alpha(\tilde{\mathbb{S}}) \in \mathcal{A}$ and $\mathcal{C}_\alpha(\tilde{\mathbb{S}}) \subseteq \mathcal{T}(\tilde{\mathbb{S}})$

$\mathcal{K}^{(k)}(\mathcal{C})$ = k-skeleton of simplicial complex $\mathcal{C}$; collection of all k-faces plus subfaces; $\mathcal{K}^{(k)} \subseteq \mathcal{C}$

$\mathcal{N}_{rv}Y$ = nerve of cover Y; $\mathcal{N}_{rv}Y = \{\ X \subseteq Y \parallel X \neq \emptyset\ \}$

$\mathcal{H}_\alpha(\tilde{\mathbb{S}})$ = weighted α-hull; $\mathcal{H}_\alpha(\tilde{\mathbb{S}}) = \mathrm{Compl} \bigcup (B_\alpha(\tilde{\mathbb{S}}^{\emptyset})) \cap \tilde{\mathbb{S}} = \emptyset)$

$\mathcal{W}_\alpha(\tilde{\mathbb{S}})$ = weighted α-shape, underlying space of the α-complex; $\mathcal{W}_\alpha(\tilde{\mathbb{S}}) \cong |\mathcal{C}_\alpha(\tilde{\mathbb{S}})|$

$\mathcal{U}_\alpha(\tilde{\mathbb{S}})$ = weighted α-diagram; $\mathcal{U}_\alpha(\tilde{\mathbb{S}}) = \bigcup B_\alpha(\tilde{\mathbb{S}});\ \mathcal{U}_{\alpha=0}(\tilde{\mathbb{S}}) \cong \mathcal{F}(\tilde{\mathbb{S}})$

$\mathcal{W}(\mathbb{S})$ = shape of landmark set $\mathbb{S}$

$\wp(\mathbb{S})$ = primitive or: *icon* shape, templatized by Helmertized, interpolated landmark set $\mathbb{S}_\hbar$

$\mathcal{D}(\tilde{\mathbb{S}})$ = cell decomposition of the convex polytope spanned by $\tilde{\mathbb{S}}$; inhere: $\mathcal{D}(\tilde{\mathbb{S}}) \cong \mathcal{T}(\tilde{\mathbb{S}})$

$V(\tilde{\mathbb{S}})$ = solid covering the underlying space spanned by $\tilde{\mathbb{S}}$; $V(\tilde{\mathbb{S}}) \cong \mathcal{H}(\tilde{\mathbb{S}})$

α-Complexes

$\mathbb{A}$	=	α-family; finite set of α-complexes generated by a single point set
α	=	real alpha value, with $\alpha \in [0..\infty)$
$\alpha_{\min}$	=	smallest α for which $\mathcal{C}_\alpha > \mathbb{S}$
$\alpha_{\max}$	=	smallest α for which $\mathcal{C}_\alpha \cong \mathcal{T}$
$\Gamma(\mathcal{C}_\alpha, \alpha)$	=	real-v alued signature$\Gamma : \mathbb{E}^d \times [0, \infty) \mapsto \mathbb{R}$ of an α-complex
ρ	=	index into the ordered α-family $\mathbb{A} = \{\mathcal{C}_\alpha^\rho(\tilde{\mathbb{S}})\}$ of all α-complexes for a given set $\tilde{\mathbb{S}}$

Flats and F aces

$\mathtt{H}$	=	h yperplane; a $(d-1)$-flat defined b y: $\Psi(\mathbf{x}) = c$, c a constant
$\mathtt{H}^+$	=	open half-space $\Psi(\mathbf{x}) > c$, beyond hyperplane $\mathtt{H}$
$\mathtt{H}^-$	=	open half-space $\Psi(\mathbf{x}) < c$, beneath hyperplane $\mathtt{H}$
$\mathtt{H}_{ij}^{\emptyset}$	=	radical (hyper)plane of tw o points $\mathbf{s}_i$ and $\mathbf{s}_j$; $\mathtt{H}_{ij}^{\emptyset}$ defined b y: $\pi_{\mathbf{S}_i}(\mathbf{x}) - \pi_{\mathbf{S}_j}(\mathbf{x}) = 0$
$\pi_{\tilde{\mathbf{S}}}(\mathbf{x})$	=	power of $\mathbf{x}$ relative to weighted point $\mathbf{s}$; $\pi_{\tilde{\mathbf{S}}}(\mathbf{x}) = \|\mathbf{x} - \mathbf{s}\|^2 - w_s$
$\mathtt{H}^{\emptyset+}$	=	open half-space for which $\pi_{\mathbf{S}^+}(\mathbf{x}) < \pi_{\mathbf{S}^-}(\mathbf{x})$, beyond radical plane $\mathtt{H}^{\emptyset}$
$\mathtt{H}^{\emptyset-}$	=	open half-space for which $\pi_{\mathbf{S}^-}(\mathbf{x}) < \pi_{\mathbf{S}^+}(\mathbf{x})$, beneath radical plane $\mathtt{H}^{\emptyset}$
$C^{\emptyset}$	=	radical centre; $C^{\emptyset} = \bigcap_j \mathtt{H}^{\emptyset}$
k-face $\mathtt{f}^{(k)}$	=	face of dimension k, $-1 \le k \le d$; typically a simplex inhere.
$\sigma^{(k)}$	=	k-simplex, a simplicial k-face (point, edge, triangle, tetrahe- dron, ...)
Int $\mathtt{f}$	=	in terior of face $\mathtt{f}$; cov ered b y open set $\overset{\circ}{f}$
Bd $\mathtt{f}$	=	boundary of face $\mathtt{f}$; coincides with ∂f
Cl $\mathtt{f}$	=	closure of face $\mathtt{f}$; covered by closed set $\bar{f}$
Ext $\mathtt{f}$	=	exterior of face $\mathtt{f}$; covered by set complement Compl f
$\mathbb{F}^{(k)}$	=	set of k-faces; $\mathbb{F}^{(k)} \subseteq \mathbb{F}$, the set of all faces

Distance, metric

$d(\mathbf{x}_1, \mathbf{x}_2)$	=	Euclidean distance betw een$\mathbf{x}_1$ and $\mathbf{x}_2$; $d(\mathbf{x}_1, \mathbf{x}_2) = \|\mathbf{x}_1 - \mathbf{x}_2\|_2 = \langle \mathbf{x}_1 - \mathbf{x}_2, \mathbf{x}_1 - \mathbf{x}_2 \rangle^{\frac{1}{2}}$
$\langle . \ , \ . \rangle$	=	standard dot product or inproduct; $\langle \mathbf{x}_1, \mathbf{x}_2 \rangle = (\mathbf{x}_1^T \mathbf{x}_2)^{\frac{1}{2}}$
$\tilde{d}(\tilde{\mathbf{x}}_1, \tilde{\mathbf{x}}_2)$	=	Laguerre (or: pow er)distance between $\mathbf{x}_1$ and $\mathbf{x}_2$; $\tilde{d}(\tilde{\mathbf{x}}_1, \tilde{\mathbf{x}}_2) = \|\mathbf{x}_1 - \mathbf{x}_2\|^2 - (w_1 + w_2) = \langle \mathbf{x}_1 - \mathbf{x}_2, \mathbf{x}_1 - \mathbf{x}_2 \rangle - (w_1 + w_2)$
$L(\tilde{\mathbf{x}}_1, \tilde{\mathbf{x}}_2)$	=	Laguerre distance $\tilde{d}(\tilde{\mathbf{x}}_1, \tilde{\mathbf{x}}_2)$
$\nu(E^d)$	=	measure on E^d; a set function: $\mathsf{G} : \mathbb{E}^d \mapsto \mathbb{R}^+$
$\mu(\mathbf{x}_1, \mathbf{x}_2)$	=	metric on E^d; a function: $\mathsf{G} : (\mathbf{x}_1, \mathbf{x}_2) \mapsto \mathbb{R}^+$
Δ, δ	=	arbitrary small Euclidean distance
$\tilde{\Delta}, l$	=	arbitrary small Laguerre distance
L_{12}	=	shorthand notation for $L(\mathbf{s}_1, \mathbf{s}_2)$

Balls and spheres

$\mathtt{B}(\mathbf{s})$	=	d-ball centred at $\mathbf{s}$
$\mathtt{A}_\alpha$	=	α-ball centred at a radical centre, radius $\sqrt{\alpha}$
$\mathtt{S}(\mathbf{s})$	=	$(d-1)$-sphere centred at $\mathbf{s}$; $\mathtt{S}(\mathbf{s}) = \partial \mathtt{B}(\mathbf{s})$
$\mathtt{B}_R^{(d)}(\mathbf{s})$	=	general d-ball centred at $\mathbf{s}$, radius $r = \sqrt{R}$
ρ	=	ball or sphere radius
Δ_1	=	determinant of sphere $\mathtt{S}_1$
Δ_{12}	=	determinant of pencil $\mathcal{P} = \lambda_1(\mathtt{S}_1 + \mathtt{S}_2)$

Weighting

$\mathbb{W}$	=	set of weights; $\mathbb{W} \subseteq \mathbb{R}$
$\mathbf{w}$	=	N-vector of weights; $w_j \in \mathbb{W}$
$\bar{\mathbf{w}}$	=	normalised weight vector
w_0	=	fixed weight offset in weight translation
$\mathcal{N}(\mathbf{s}_j)$	=	neighbourhood of $\mathbf{s}_j$ used for weighting

κ	=	ball coverage; $0 \leq \kappa \leq 1$
$\kappa(\mathbf{s}_j)$	=	local ball coverage around $\mathbf{s}_j$
ϱ	=	weight scaling factor
ω_{T}	=	weight overshoot factor on weight transformation T

Graphs

$\mathcal{G}$	=	graph $\mathcal{G}$; $\mathcal{G} = \{\mathbb{V}, \mathbb{E}\}$
$deg(\mathbf{s})$	=	degree of vertex $\mathbf{s}$; the number of edges emina from $\mathbf{s}$
$\mathcal{NNG}(\mathbb{S})$	=	nearest-neighbour graph on set $\mathbb{S}$
$\mathcal{LFNG}(\mathbb{S})$	=	local furthest-neighbour graph on set $\mathbb{S}$
$\mathcal{IG}(\mathcal{C})$	=	incidence graph of complex $\mathcal{C}$; $\mathcal{IG} = \{\Sigma, \mathbb{I}\}$, $\Sigma = \{\sigma^{(k)}\}$, $-1 \leq k \leq d+1$, $\mathbb{I} = \{deg(\sigma^{(k)})\}$

Shape Analysis

$\mathsf{G}(\mathbb{S})$	=	real shape parameter set function $\mathsf{G} : \mathbb{E}^d \mapsto \mathbb{R}$
g	=	real shape parameter
$\mathbf{X}^{(\mathbb{S})}$	=	configuration matrix spanned by landmarks in $\mathbb{S}$; row vector $\mathbf{x}_j^{(\mathbb{S})} = \mathbf{s}_j$

Stochastics

λ	=	intensity of Poisson point process (ppp)
$\Phi(\mathbb{S})$	=	point process generated by point set $\mathbb{S}$
$Var\ X$	=	variance of random variable X
s_X^2	=	empirical variance of random variable X
σ_X^2	=	theoretical variance of random variable X
$\mathsf{E}[\mathrm{X}]$	=	expected value of random variable X
$\mathsf{Pr}[\mathrm{e}]$	=	probability of event e occurring
D	=	(theoretical) nearest-neighbour distances distribution
$\hat{\mathsf{D}}$	=	empirical nearest-neighbour distances distribution
χ_X^2	=	chi-square of random variable X

Linear algebra

$\mathbf{1}^k$	=	k-dimensional identity vector
$\mathbf{I}^k$	=	$k \times k$-identity matrix
$\det \mathbf{M}$	=	determinant $\lvert\mathbf{M}\rvert$ of matrix $\mathbf{M}$

Permutations

$m!$	=	faculty of m
$\binom{n}{m}$	=	permutation m unique out of n; $\binom{n}{m} = \frac{n!}{m!(n-m)!}$

Complex numbers

z	=	complex number; $z \in \mathbb{C}$
$\bar{z}$	=	complex conjugate of z; $\bar{z} \in \mathbb{C}$
$\operatorname{Re} z$	=	real fraction of z; $\operatorname{Re} z \in \mathbb{R}$
$\operatorname{Im} z$	=	imaginary fraction of z; $\operatorname{Im} z \in \mathbb{R}$

Scale and size

λ	=	real scale or size factor; generally, $\lambda \neq 0$ and in dilations $\lambda > 0$
λ	=	real scale or size d-vector; elements λ_i as above
Λ	=	real scale or size $d \times d$-diagonal matrix; elements λ_{ij}, μ_{ij} as above
$\nu_{\mathcal{L}}^{(d)}$	=	d-dimensional Lebesgue-measure; d-(hyper)volume
$O(10^m)$	=	order of magnitude 10^m
$x_1 \ll x_2$	=	x_1 much smaller than x_2
$x_1 \gg x_2$	=	x_1 much greater than x_2

T ransformations

$\mathsf{T} : S \mapsto U$	=	transformation from domain S (on)to co-domain or range U
S_0	=	kernel space of transformation T
U_0	=	image space of transformation T
$\ker \mathsf{T}$	=	kernel (null-space) of transformation T; the subset $\mathbb{S}_0 \subseteq \mathbb{S}$ sent into $\mathbf{0}$
$\mathrm{im}\, \mathsf{T}$	=	image space of transformation T; the subset $U_0 \subseteq U$ of the range that can be reached by T

Stress, strain

τ_{XY}	=	stress in the XY-plane

Complexity

$\mathcal{O}(\phi(n))$	=	asympthotic upper bound complexity for some $n \geq n_{min}$
$\Omega(\phi(n))$	=	asympthotic lower bound complexity for some $n \geq n_{min}$
$\Theta(\phi(n))$	=	asympthotic exact complexity for some $n \geq n_{min}$

Remarks:

1. When obvious from the context, tilde notations are dropped. F or instance, writing$L(\mathbf{s}_1, \mathbf{s}_2)$ when it obvious that $L(\tilde{\mathbf{s}}_1, \tilde{\mathbf{s}}_2)$ is meant
2. Also, refer to figure 2–1.
3. When essential or further narrowing or clarifying, the above notations may be headed by a "k-" prefix, like in 3-polytope.

Bibliography

[AAL+99] Oswin Aichholzer, Franz Aurenhammer, D.T. Lee, Danny Z. Chen, and Evanthia Papadopoulou. Skew voronoi diagrams. *International Journal of Computational Geometry & Applications*, 1999.

[ABB+97] R. Alms, O. Balovnev, M. Breunig, A. B. Cremers, T. Jentzsch, and A. Siehl. Space-time modelling of the lower rhine basin supported by an object-oriented database. *Physics and Chemistry of the Earth*, 1997.

[ABBM94] I. Aavatsmark, T. Barkve, Ø Bøe, and T. Mannseth. Discretization on non-orthogonal, curvilinear grids for multi-phase flow. In *Proceedings of the 4th European Conference on the Mathematics of Oil Recovery, Røros*, 1994.

[ABBM95] I. Aavatsmark, T. Barkve, Ø Bøe, and T. Mannseth. Discretization on non-orthogonal, quadrilateral grids for inhomogeneous, anisotropic media. *J. Comput. Phys.*, 1995.

[AI87] F. Aurenhammer and H. Imai. Geometric relations among Voronoi diagrams. In *Proc. 4th Sympos. Theoret. Aspects Comput. Sci.*, volume 247 of *Lecture Notes Comput. Sci.*, pages 53–65. Springer-Verlag, 1987.

[AK95] Colin Archibald and Paul Kwok, editors. *Research in Computer and Robot Vision*. World Scientific Publishing Co. Pte. Ltd., Singapore, 1995.

[Aki90] J. Ed Akin. *Computer-Assisted Mechanical Design*. Prentice-Hall, Endlewood Cliffs, N.J., 1990.

[All85] John R. Allen. *Principles of Physical Sedimentology*. Allen and Urwin (Publisher), Ltd., 1985.

[Aur87a] F. Aurenhammer. A criterion for the affine equality of cell complexes in R^d and convex polyhedra in R^{d+1}. *Discrete Comput. Geom.*, 2:49–64, 1987.

[Aur87b] F. Aurenhammer. Power diagrams: properties, algorithms and applications. *SIAM J. Comput.*, 16(1):78–96, February 1987.

[Aur87c] F. Aurenhammer. Recognising polytopical cell complexes and constructing projection polyhedra. *J. Symbolic Comput.*, pages 249–255, 1987.

[Bad85] Michael E. Badley. *Practical Seismic Interpretation*. International Human Resources Development Corporation, Boston, 1985.

[Bak89] Timothy J. Baker. Element quality in tetrahedral meshes. In *Proc. of the 7th International Conference on Finite Element Methods in Flow Problems*, pages 1018–1024, April 1989.

[Ban90] Thomas F. Banchoff. *Beyond the third dimension; geometry, computer graphics and higher dimensions*. Number 33 in Scientific American Library. Freeman, New York, 1990.

[Bar27] J.A. Barrau. *Noordhoff's Verzameling van Wiskundige Werken*. P. Noordhoff, Groningen, The Netherlands, 1927. (in dutch).

[BB91] J. Bear and J-M. Bucklin, editors. *Modelling and Applications of Transport Phenomena in Porous Media*. Kluwer Academic Publishers, Dordrecht, 1991.

[BCER95] Marshall Wayne Bern, L. Paul Chew, David Eppstein, and Jim Ruppert. Dihedral bounds for mesh generation in high dimensions. In *Proc. 6th Symp. Discrete Algorithms*, pages 189–196. ACM and SIAM, January 1995.

[BCM+93] M. S. Beck, E. Campogrande, M. Morris, R. A. Williams, and R. C. Waterfall, editors. *Tomographic Techniques for Process Design and Operation*. Computational Mechanics Publications, Southampton, 1993.

[BD74] Raymond Balbes and Philip Dwinger. *Distributive Lattices*. Univ. of Missouri Press, 1974.

[BHTP92] P. Billi, R.D. Hey C.R. Thorne, and Tacconi P, editors. *Dynamics of Gravel-bed Rivers* John Wiley & Sons, Chichester, 1992.

[Bix94] Robert Bix. *Topics in Geometry*. Academic Press, Inc., San Diego, CA, 1994.

[Bix98] Robert Bix. *Conics and Cubics; A Concrete Introduction to Algebraic Curves*. Undergraduate Texts in Mathematics, S. Axler, F.W. Gehring and K.A. Ribet, Series Eds. Springer Verlag, Inc., New York, 1998.

[BNKVL99] O.E. Barndorff-Nielsen, W.S. Kendall, and M.N.M. Van Lieshout, editors. *Stochastic Geometry; Likelihood and Computation*. Number 80 in Monographs on Statistics and Applied Probability (Cox et al., series eds.). Chapman & Hall/CRC, Boca Raton, 1999.

[Boc96] H. H. Bock. Classification and clustering: Problems for the future. In Diday E., Lechevallier Y., Schader M., Bertrand P., and Burtschy B., editors, *New Approaches in Classification and Data Analysis*, Studies in Classification, Data Analysis, and Knowledge Organization. Springer-Verlag, Berlin-Heidelberg, 1996.

[Bos98] A Bossavit. *Computational Electromagnetism; Variational Formulations, Complementarity, Edge Elements*. Academic Press, San Diego, 1998.

[BP94] Wolfgang Boehm and Hartmut Prautzsch. *Geometric Concepts for Geometric Design*. A. K. Peters, Ltd., Wellesley, MA, 1994.

[Bra47] Louis Brand. *Vector and Tensor Analysis*. John Wiley & Sons, Inc., London, ninth printing edition, 1947.

[Bri90] Erik Brisson. *Representation of d-dimensional geometric objects*. PhD thesis, Univeristy of Washington, Washington, 1990.

[Bro96] A. R. Brown. *Interpretation of Three-dimensional Seismic Data*. Number 42 in AAPG Memoir. AAPG, Tulsa, fourth edition, 1996.

[Bru79] Denys Brunsden. *Process in Geomorphology*, chapter 5: Mass Movements. Edward Arnald (Publishers) Ltd., London, 1979.

[BT00] A.D. Brett and C.J. Taylor. A method of automated landmark generation for automated 3d pdm construction. *Image and Vision Computing*, 18:739–748, 2000.

[Buc88] C. E. Buckley. A divide-and-conquer algorithm for computing4-dimensional convex hulls. In H. Noltemeier, editor, *Computational Geometry and its Applications*, volume 333 of *Lecture Notes Computer Science*, pages 113–135. Proceedings CG'88, International Workshop on Computational Geometry, Springer-Verlag, Berlin-Heidelberg, 1988.

[BW85] Orville Roger Berg and Donald G. Woolverton, editors. *Seismic Stratigraphy II: An Integrated Approach to Hydrocarbon Exploration*. Number 39 in AAPG Memoir. The Americal Association of Petroleum Geologists, Tulsa, Oklahoma, 1985.

[CDFC95] E. Clementini, P. Di Felice, and G. Califano. Composite regions in topological queries. *Information Systems*, 20(7):579–594, 1995.

[CDFvO93] Eliseo Clementini, Paolino Di Felice, and Peter van Oosterom. A small set of formal topological relationships suitable for end-user interaction. In D. Abel and B.C. Ooi, editors, *Advances in Spatial Databases*, volume 692 of *Lecture Notes in Computer Science*, pages 277–295, Singapore, 1993. Third International Symposium. SSD '93., Springer-Verlag.

[CG76] D. J. Cant and Walker R. G. Development of a braided fluvial facies model for the devonian battery point sandstone. *Canada Journal of Earth Science*, 13:102–119, 1976.

[Coo16] Julian L. Coolidge. *A treatise on the circle and the sphere.* Oxford at the Clarendon Press, London, 1916.

[Coo24] J.L. Coolidge. *The geometry of the complex domain.* Oxford at the Clarendon Press, London, 1924.

[Cox73] H. S. M. Coxeter. *Regular Polytops.* Dover Publications, Inc., New York, 1973.

[Cra99] Harald Cramér. *Mathematical Methods of Statistics.* Princeton Landmarks in Mathematics and Physics. Princeton University Press, Princeton, nineteenth reprint, first paperback edition, 1999.

[Dav86] J. C. Davis. *Statistical and Data Analysis in Geology.* John Wiley and Sons, New York, second edition, 1986.

[dBvKOS97] M. de Berg, M. van Kreveld, M. Overmars, and O. Schwarzkopf. *Computational Geometry, Algorithms and Appliations.* Springer, 1997.

[DFM90] M.E. Dyer, Z. Füredi, and C. McDiarmid. Random volumes in the n-cube. In William Cook and Paul D. Seymour, editors, *Polyhedral Combinatorics: Proceedings of the DIMACS Workshop on Polyhedral Combinatorics, held at the NSF Science and Technology Center on June 12–16, 1989*, volume 1 of *DIMACS Series in Discrete Mathematics and Theoretical Computer Science*, pages 33–38. American Mathematical Society, Association for Computing Machinery, 1990.

[Dig83] Peter J. Diggle. *Statistical Analysis of Spatial Point Patterns.* Mathematics in Biology (Sibson and Cohen, series eds.). Academic Press, Inc. LTD., London, 1983.

[DL91] Clive L. Dym and Raymond E. Levitt. *Knowledge-Based Systems in Engineering.* McGraw-Hill, Inc., New York, 1991.

[DM98] I.L. Dryden and K.V. Mardia. *Statistical Shape Analysis.* Wiley series in Probability and Statistics. Wiley & Sons, Chichester, 1998.

[DS90] Patrick A. Domenico and Franklin W. Schwartz. *Physical and Chemical Hydrogeology* John Wiley & Sons, Inc., New York, 1990.

[Ede87] Herbert Edelsbrunner. *Algorithms in Combinatorial Geometry.* Springer-Verlag, Berlin-Heidelberg, 1987.

[Ede92] Herbert Edelsbrunner. Weighted alpha shapes. Technical Report UIUCDCS-R-92-1760 (UILU-ENG-92-1740), University of Illinois at Urbana-Champaign, Department of Computer Science, Urbana, Illinois, July 1992.

[Ede93] Herbert Edelsbrunner. The union of balls and its dual shape. In *Proc. 9th Annu. ACM Sympos. Comput. Geom.*, pages 218–231. ACM, 1993.

[Edg90] Gerald A. Edgar. *Measure, Topology, and Fractal Geometry.* Undergraduate Texts in Mathematics. Springer-Verlag, 1990.

[EFL98] Herbert Edelsbrunner, Michael Facello, and Jie Liang. On the definition and the construction of pockets in macromolecules. *Discrete Applied Mathematics*, 88:83–102, 1998.

[EKS83] H. Edelsbrunner, D.G. Kirkpatrick, and R. Seidel. On the shape of a set of points in the plane. *IEEE Trans. Inform. Theory*, IT-29:551–559, 1983.

[EM94] Herbert Edelsbrunner and Ernst P. Mucke. Three-dimensional alpha shapes. *ACM Transactions on Graphics*, 13:43–72, 1994.

[Eng89] Ryszard Engelking. *General Topology*, volume 6 of *Sigma Series in Pure Mathematics*. Heldermann Verlag, Berlin, revised and completed edition, 1989.

[ES96] H. Edelsbrunner and N. R. Shah. Incremental topological flipping works for regular triangulations. *Algorithmica*, 15:223–241, 1996.

[FBMB90] Bjorn N. Freeman-Benson, John Maloney, and Alan Borning. An incremental constraint solver. *Communications of the ACM*, 33(1):54–63, 1990.

[FFE92] Douglas M. Flewelling, Andrew U. Frank, and Max J. Egenhofer. Constructing geological cross sections with a chronology of geological events. In *Proceedings of the 5th International Symposium on Spatial Data Handling*, volume 5, pages 544–553, Charleston, South Carolina, USA, August 3–7 1992. International Geographical Union.

[FH97] Ioannis Fudos and M. Hoffmann. A graph-constructive approach to solving systems of geometric constraints. *ACM Transactions on Graphics*, 16(2):179–216, April 1997.

[FvD82] J. D. Foley and A. van Dam. *Fundamentals of Interactive Computer Graphics*. Addison-Wesley Publishing Co. Inc., 1982.

[Gar88] Martin Gardner. *Time Travel and other mathematical Bewilderments*. W. H. Freeman and Company, New York, 1988.

[Ger98] Bart H. M. Gerritsen. On the use of alpha complexes in subsurface modelling. In *Proc. ENSG Conference on 3D Modeling of Natural Objects, A Challenge for the 2000's*. ENSG, Nancy, France, June 4–5 1998.

[Gib77] P.J. Giblin. *Graphs, Surfaces and Homology; An Introduction to Algebraic Topology*. Chapman and Hall Mathematics Series. Chapman and Hall, London, 1977.

[Goo87] M. T. Goodrich. Finding the convex hull of a sorted point set in parallel. *Inform. Process. Lett*, 26:176–179, 1987.

[GR97] Bart H. M. Gerritsen and Ipo L. Ritsema. Geoscientific constraint solving using hyperspatial modelling and α-shapes. In *EAGE'97 Extended Abstracts of the 59th Conference and Technical Exhibition, paper D024*, Geneva, Switzerland, 26–30 May 1997. EAGE.

[GT87] Jonathan L. Gross and Thomas W. Tucker. *Topological Graph Theory*. John Wiley & Sons, New York, 1987.

[GVdWV00a] B.H.M. Gerritsen, K. Van der Werff, and R.C. Veltkamp. Geometric modelling with α-complexes. In *Proc. of the 3rd Symp. on Tools and Methods for Competative Engineering*, pages 117–130, held at The Delft Univ. of Technology, Delft, The Netherlands, April 18–21 2000. Delft University Press. ISBN 90-407-1983-7.

[GVdWV00b] B.H.M. Gerritsen, K. Van der Werff, and R.C. Veltkamp. Geometric modelling with α-complexes. Technical Report UU-CS-2000-03, Utrecht University, 2000. `ftp://ftp.cs.uu.nl/pub/RUU/CS/techreps/CS-2000/2000-03.ps.gz`

[GVdWV01] B.H.M. Gerritsen, K. Van der Werff, and R.C. Veltkamp. Modelling natural objects with α-complexes. *CAD*, 33(Special Issue TMCE 2000), 2001. To appear.

[GZT01] Bart H.M. Gerritsen, Wouter Zijl, and Anna Trykozko. From alphacomplexes to finite element analysis: Exemplified by barchan dune avalanching. *Computing and Visualization in Science*, 2001. To appear.

[Hah94] Liang-shin Hahn. *Complex Numbers & Geometry*. Spectrum. The Mathematical Association of America, Washington DC, 1994.

[Hal52] A. Hald. *Statistical Theory with Engineering Applications*. John Wiley & Sons, Inc., New York, 1952.

[Hal67] Michel T. Halbouty. *Salt Domes; Gulf Region, United States and Mexico*. Gulf Publishing Company, Houston, Texas, 1967.

[Hal88] Peter Hall. *Introduction to the Theory of Coverage Processes*. Wiley Series in Probability and Mathematical Statistics. John Wiley & Sons, Chichester, England, 1988.

[Har96] Andreas Hartwig. *Algebraic 3-D Modeling*. A. K. Peters, Ltd, 1996.

[HB94] H. H. Hardy and Richard A. Beier. *Fractals in Reservoir Engineering*. World Scientific Publishing Co. Pte Ltd, Singapore, 1994.

[Hel94] Klaus Helbig, editor. *Modeling the Earth for Oil Exploration. Final Report of the CEC's Geoscience I Program 1990–1993*, chapter 9, pages 687–728. Pergamon Imprint. Elsevier Science Ltd., Oxford, UK, 1994.

[HM83] J. M. Hammersley and G. Mazzarino. Markov fields, correlated percolation and the ising model. In B. D. Hughes and B. W. Ninham, editors, *The Mathematics and Physics of Disordered Media, Minneapolis,1983*, pages 201–245. Springer-Verlag, Berlin-Heidelberg, 1983.

[Hua81] Loo-keng Hua. *Starting with the unit circle; background to higher analysis*. Springer-Verlag, New York, 1981.

[Hug87] Thomas J. R. Hughes. *The Finite Element Method. Linear Static and Dynamic Finite Element Analysis*. Prentice-Hall International, Inc., Englewood Cliffs, New Jersey, 1987.

[Kal89] Yehuda E. Kalay. *Modeling Objects and Environments*. Principles of Computer-Aided Design (Series Ed. Yehuda E. Kalay). John Wiley & Sons, New York, 1989.

[KK96] L. Kadison and M.T. Kromann. *Projective Geometry and Modern Algebra* Brikhauser Boston, Cambridge, MA, 1996.

[Kum92] Vipin Kumar. Algorithms for constraint-satisfaction problems: A survey. *AI Magazine*, 13(1):32–44, spring 1992.

[Kyt98] Prem K. Kythe. *Computational Conformal Mapping*. Birkhauser, Boston, 1998.

[Lam94] Johan Maurice Gisèle Lammens. *A Computational Model of Color Perception and Color Naming*. PhD thesis, State University of New York at Buffalo, June 1994.

[Lee91] C. W. Lee. Regular triangulations of convex polytopes. In *Applied Geometry and Discrete Mathematics: The Victor Klee Festschrift*, volume 4 of *DIMACS Series in Discrete Mathematics and Theoretical Computer Science*, pages 443–456. AMS Press, Providence, RI, 1991.

[Lin94] Tony Lindeberg *Scale-Space Theory in Computer Vision*. The Kluwer international series in engineering and computer science. Robotics: Vision, Manipulation and Sensors. Kluwer Academic Publishers, Dordrecht, The Netherlands, 1994.

[LP82] Leon Lapidus and George F. Pinder. *Numerical Solution of Partial Differential Equations in Science and Engineering*. John Wiley and Sons, Inc., New York, 1982.

[Mar96] Allard W. Martinius. *The Sedimentological Characterisation of Labyrinthine Fluvial Reservoir Analogues* PhD thesis, Delft University of Technology, Delft, The Netherlands, February 1996.

[Max52] E.A. Maxwell. *Elementary Coordinate Geometry*. Oxford at the Clarendon Press, 1952.

[MD00] Mahmoud Melkemi and Mourad Djebali. Computing the shape of a planar point set. *Pattern Recognition*, 33:1423–1436, 2000.

[Meg84] Robert E. Megill. *An Introduction to Risk Analysis*. PennWell Publishing Company, Tulsa, Oklahoma, second edition, 1984.

[Mes89] Pedro Meseguer. Constraint satisfaction problems: An overview. *AICOM*, 2(1):3–17, March 1989.

[Mia78] Andrew D. Miall, editor. *Fluvial Sedimentology*, volume C.S.P.G. memoir, Nr. 5. Canadian Society of Petroleum Geologists, Calgary, ALberta, Canada, 1978.

[MMN+97] Kurt Mehlhorn, Michael Müller, Stefan Näher, Stefan Schirra, Michael Seel, Christian Uhrig, and Joachim Ziegler. A computational basis for higher-dimensional computational geometry and applications. Technicalreport, Max-Planck-Intitute für Informatik, Im Stadtwald, Saarbrücken, Germany, 1997.

[Møl94] Jesper Møller. *Lectures on random Voronoi tessellations*. Number 87 in Lecture notes in statistics ISBN: 0930-0325. Springer, New York, 1994.

[Mos97] Brian P. Moss. The partitioning of petrophysical data: a review. In M. A. Lovell and P. K. Harvey, editors, *Developments in Petrophysics*, Geological Society Special Publication No. 122, pages 181–252. The Geological Society, London, 1997.

[MS82] S. Mardešić and J. Segal. *Shape Theory; The Inverse System Approach*. North-Holland Publishing Company, Amsterdam, 1982.

[MSZ99] Ernst P. Mücke, Isaac Saias, and Binhai Zhu. Fast randomized point location without preprocessing in two- and three-dimensional delaunay triangulations. *Computational Geometry*, 12:63–83, 1999.

[Mue93] Ernst Peter Muecke. *Shapes and Implementations in Three-dimensional Geometry*. PhD thesis, University of Illinois at Urbana-Champaign, 1993.

[Mun75] James R. Munkres. *Topology, a first Course*. Prentice-Hall, Inc., Englewood Cliffs, New Jersey, third edition, 1975.

[Mun84] James R. Munkres. *Elements of Algebraic Topology* Addison-Wesley, Redwood, CA, 1984.

[Nag83] J. Nagata. *Modern Dimension Theory*. Sigma Series in Pure Mathematics. Heldermann Verlag, Berlin, revised and extended edition, 1983.

[ND88] Ben Noble and James W. Daniel. *Applied Linear Algebra*. Prentice-Hall International,Inc., third edition, 1988.

[Nee97] Tristan Needham. *Visual Complex Analaysis*. Clarendon Press, Oxford, 1997.

[New75] Paul D. Newendorp. *Decision Analysis for Petroleum Exploration; An introduction to the application of statistical decision theory concepts to the analysis of risk and uncertainty in petroleum exploration investment decisions*. PennWell Publishing Company, Tulsa, Oklahoma, 1975.

[NM88] Anthony W. Nutbourne and Ralph R. Martin. *Differential Geometry Applied to Curve and Surface Design*, volume 1: Foundations. Ellis Horwood Limited, Chichester, 1988.

[Nor79] M.J. Norušis. *SPSS Statistical Agorithms*. SPSS Inc., 1979. Release 8.0.

[OBSC00] Atsuyuki Okabe, Barry Boots, Kokichi Sugihara, and Sung Nok Chiu. *Spatial Tesselations; Concepts and Applications of Voronoi Diagrams*. Wiley series in probability and statistics. John Wiley & Sons, Ltd., Chichester, England, second edition, 2000.

[Oda88] Tadoa Oda. *Convex Bodies and Algebraic Geometry; An Introduction to the Theory of Toric Varieties*, volume 15 of *Ergebnisse der Mathematik und ihrer Grenzgebiete; A Series of Modern Surveys in Mathematics, E. Bombieri et al. Series Eds.* Springer-Verlag, Berlin-Heidelberg, 1988.

[Ogn94] R.L. Ogniewicz. Skeleton-space: a multiscale shape description combining region and boundary information. In *Proc. CVPR'94, Seattle, WA*, pages 746–751, Seattle, June 1994.

[O'R94] J. O'Rourke. *Computational Geometry in C.* Cambridge University Press, New York, 1994.

[OSNK93] R. Ogniewicz, G. Székely, M. Näf, and O. Kübler. Medial manifold and hierarc hical description of 2d and 3d objects with applications to mri data of the human brain. In *Pr oc. 8th Sc andinavian Conf. on Image A nalysis SCIA '93*, pages 875–883, Tromsø, May 1993.

[PBCF93] A. Paoluzzi, F. Bernardini, C. Cattani, and V. Ferrucci. Dimension-independent modelling with simplicial complexes. *A CM Transactions on Graphics*, 12(1):56–102, January 1993.

[Pin93] Michael J. Pink. Exploration and appraisal technology – maximising rewards by integration. Selected Papers 103761/15m/1.93, Shell SIPM, The Hague, Netherlands, 1993.

[PR96] Jagdish K. Patel and Campbell B. Read. *Handbook of the Normal Distribution*, volume 150 of *STA TISTICS: textbooks and monographs*. Marcel Dekker, Inc., New Y ork, second edition, 1996.

[PS85] F. P. Preparata and M. I. Shamos. *Computational Geometry, an Introduction*. Springer-V erlag, New Y ork, 1985.

[Ram93] Hubert K. Rampersad. *Integraal en Simultaan Ontwerpen; Ontwerpmodellen en -gereedschappen voor het succesvol concipiëren van R ob ot-assemblage Systemen*. Lemma BV, Utrecht, The Netherlands, 1993. (in dutch).

[Ran87] Giogio Ranalli. *Rheolo gy of the Earth, Deformation and Flow Pr ocesses in Geophysics and Geodynamics*. Allen & Unwin, Boston, 1987.

[Rei58] Hans Reichen bac h. *The Philosophy of Space & Time*. Dov er Publications, Inc., New York, do v er (english) edition edition, 1958.

[Req80] A.A.G. Requicha. Representation of rigid solid objects. In Jose Encarnaçao, editor, *Computer Aided Design; Modelling, systems engineering, CAD systems. CREST A dvanced Co arse, Darmstadt, September 1980*, Lecture Notes in Computer Science (series eds. G. Goos and J. Hartmanis). Springer-Verlag, Berlin-Heidelberg, 1980.

[Req83] Aristides A. G. Requicha. T ow ard a theory of geometric tolerancing. *Int. J. Robot. Res.*, 2(4):45–60, Winter 1983.

[RF94] I.L. Ritsema and F.T.J. Floris. Dynamic geometry and topology. T echnical report, TNO Institute of Applied Geoscience, Delft, The Netherlands, 1994.

[RG96] Ipo L. Ritsema and Bart H.M. Gerritsen. Hyperspatial shapes for the description of geoscien tific features. In *EAGE'96 Extended Abstracts of the 58th Conferenc e and Technical Exhibition*, volume 2, L042, Amsterdam, The Netherlands, 3–7 June 1996. EAGE.

[Ric87] Keith Richards. *R iver Channels, Environment and Process*. Basil Blackwell Ltd., Oxford, 1987.

[RNS93] U. Rembold, B.O. Nnaji, and A. Storr. *Computer Integrated Manufacturing and Engineering*. A ddison-Wesley Publishing Company, Wokingham, England, 1993.

[RS80] Hans-Erich Reineck and Indra Bir Singh. *Depositional Sedimentary Environments*. Springer-Verlag, Berlin-Heidelberg, second, revised and updated edition, 1980.

[Ruc82] Rudy Rucker. *Infinity and the Mind*. The Harvester Press, Limited, Brighton, Sussex, 1982.

[RW96] Gerhard X. Ritter and Joseph N. Wilson. *Handbook of Computer Vision Algorithms in Image Algebra*. CRC Press, Boca Raton, Florida, 1996.

[Sam90a] H. Samet. *Applications of Spatial Data Structures, Computer Graphics, Image Processing and GIS*. A ddison Wesly Publishing Corp, Reading MA, 1990.

[Sam90b] H. Samet. *The Design and Analysis of Spatial Data Structures*. Addison Wesly Publishing Corp, Reading MA, 1990.

[Sch79] Hans Schwerdtfeger. *Geometry of complex numbers; Circle geometry, Moebius transformation, non-Euclidean geometry* Dover Publications, Inc., New York, Dover edition, 1979.

[SdGN+90] G. Smets, M. de Groof, J. Nuyts, D. van der Meulen, P. Suetens, G. Marchal, and A. Oosterlinck. Interpretation of 3*d* medical scenes. In Herbert Freeman, editor, *Machine Vision for Three-Dimensional Scenes*, pages 163–193. Academic Press, Inc., Boston, 1990.

[Sei91] Raimund Seidel. Exact upper bounds for the number of faces in d-dimensional voronoi diagrams. In *Applied Geometry and Discrete Mathematics: The Victor Klee Festschrift* volume 4 of *DIMACS Series in Discrete Mathematics and Theoretical Computer Science*, pages 517–529. AMS Press, 1991.

[Sew88] Granville Sewell. *The numerical solution of ordinary and partial differential equations*. Academic Press, Inc., San Diego, CA, 1988.

[SH96] A.M. Stuart and A.R. Humphries. *Dynamical Systems and Numerical Analysis* Number 2 in Cambridge Monographs on Applied and Computational Mathematics (P.G. Gialet, A. Iserles, R.V. Kohn and M.H. Wright, series Eds.). Cambridge University Press, Cambridge, 1996.

[Sha77] Igor R. Shafarevich. *Basic Algebraic Geometry*. Springer-Verlag, Berlin Heidelberg, 1977.

[Sho85] Ken Shoemake. Animating rotation with quaternion curves. In *Proceedings of the ACM SIGGRAPH'85*, volume 19, pages 245–254, San Francisco, July 22–26 1985. ACM.

[Sig95] Karl Sigman. *Stationary Marked Point Processes; An Intuitive Approach*. Stochastic Modelling. Chapman & Hall, New York, 1995.

[Sim92] Reid G. Simmons. The roles of associational and causal reasoning in problem solving. *Artificial Intelligence*, 53:159–207, 1992.

[SK79] J. G. Semple and G. T. Kneebone. *Algebraic Projective Geometry*. Oxford University Press, Oxford, 1979 edition, 1979.

[SKM95] Dietrich Stoyan, Wilfried S. Kendall, and Joseph Mecke. *Stochastic Geometry and its Applications*. Wiley Series in Probability and Statistics. Hohn Wiley & Sons, Chichester, England, second edition, 1995.

[SM86] M. A. Sabin and R. R. Martin. Introduction to the basic mathematical tools. In J. A. Gregory, editor, *The Mathematics of Surfaces*, number New Series Number 6 in The Institute of Mathematics & its Applications Conference Series, pages 1 – 17, Univeristy of Manchester, 17-19 September 1984 1986. Institute of Mathematics and its Applications, Oxford University Press.

[SM94] Chanan S. Syan and Unny Menon, editors. *Concurrent Engineering; Concepts, Implementation and Practice*. Chapman & Hall, London, 1994.

[SNFJ97] Jon Sporring, Mads Nielsen, Luc Florack, and Peter Johansen, editors. *Gaussian Scale-Space Theory: Computational Imaging and Vision*. Kluwer Academic Publishers, Dordrecht, The Netherlands, 1997.

[Spi72] C.C. Spicer. Algorithm as 52: Calculation of power sums of deviations about the mean. *Applied Statistics*, 21:226–227, 1972.

[SS87] Rod Salmon and Mel Slater. *Computer Graphics; Systems & Concepts*. Addison-Wesley Publishing Company, Inc., Wokingham, England, 1987.

[SS94] Dietrich Stoyan and Helga Stoyan. *Fractals, Random Shapes and Point Fields; Methods of Geometrical Statistics*. Wiley Series in Probability and Mathematical Statistics. John Wiley & Sons, Chichester, England, 1994.

[Sta94] J.M.T. Stam. *Process-based Modelling of Aeolian Bedforms*. PhD thesis, Delft University of Technology, Delft, The Netherlands, November 1994.

[Ste97] Philippe Steeghs. *Local Power Spectra and Seismic Interpretation*. PhD thesis, Delft University of Technology, Delft, September 1997.

[Sto91] Jorge Stolfi. *Oriented Projective Geometry*. Academic Press, Inc., San Diego, 1991.

[Str86] Gilbert Strang. *Introduction to Applied Mathematics*. Wellesley-Cambridge Press, Wellesley, MA, 1986.

[Tak98] Yoshi-taka Takeda. Flow in rocks modelled as multiphase continua: application to polymineralic rocks. *Journal of Structural Geology*, 20(11):1569–1578, November 1998.

[Tay92] Dean L. Taylor. *Computer-Aided Design*. Addison-Wesley series in Mechanical Engineering. Addison-Wesley Publishing Company, Inc., Reading, Massachusetts, 1992.

[Tij94] Henk C. Tijms. *Stochastic Models; An Algorithmic Approach*. Wiley Series in Probability and Mathematical Statistics. John Wiley & Sons, Chichester, West Sussex, England, 1994.

[TS92a] K. Thulasiraman and M.N.S. Swamy. *GRAPHS: Theory and Algorithms*. John Wiley & Sons, Inc., New York, 1992.

[TS92b] Christopher Tong and Duvvuru Sriram, editors. *Artificial Intelligence in Engineering Design, Volume I: Design Representation and Models of Routine Design*. Academic Press, Inc., Boston, 1992.

[Tsa93] Edward Tsang. *Foundations of constraint satisfaction*. Computation in cognitive science series. Academic Press Limited, London, 1993.

[vdW73] B. L. van der Waerden. *Einführung in die algebraische Geometrie*. Springer-Verlag, Berlin-Heidelberg, zweite auflage edition, 1973. (in German).

[Vel94] Remco C. Veltkamp. *Closed Object Boundaries from Scattered Points*. Number 885 in Lecture Notes in Computer Science. Springer-Verlag, Berlin-Heidelberg, 1994.

[VH01] Remco C. Veltkamp and Michel Hagedoorn. *Principles of Visual Information Retrieval*, chapter State-of-the-art in shape matching, pages 87–119. Springer, Berlin-Heidelberg, 2001.

[Wal80] Roger G. Walker, editor. *Facies Models*. Reprint Series 1. Geological Association of Canada, Waterloo, Ontario, 1980.

[Wan83] Paul P. Wang. *Advances in Fuzzy Sets, Possibility Theory and Applications*. Plenum Press, New York, 1983.

[Wei86] Kevin J. Weiler. *Topological Structures for Geometric Modelling*. PhD thesis, University of Minnesota, Minnesota, United States, 1986.

[Woo90] Robert F. Woodbury. Variations in solids: A declarative treatment. *Comput. & Graphics*, 14(2):173–188, 1990.

[Wor92] Michael F. Worboys. A generic model for planar geographical objects. *International Journal of Geographical Information Systems*, 6(5):353–372, 1992.

[WR69] P.F. Williams and B. R. Rust. The sedimentology of a braided river. *Journal of Sedimentology and Petroleum*, 39:649–679, 1969.

[XJG+99] L. Xu, M. Jackowski, A. Goshtasby, D. Roseman, S. Bines, C. Yu, A. Dhawan, and A. Huntley. Segmentation of skin cancer images. *Image and Vision Computing*, 17(1):65–74, January 1999.

[Zei91] Ibrahim Zeid. *CAD/CAM Theory and Practice*. McGraw-Hill Series in Mechanical Engineering (series eds. Jack P. Holman and John R. Lloyd). McGraw-Hill, Inc., New York, 1991.

[Zie83] O. C. Zienkiewicz. *The Finite Element Method.* McGraw-Hill Book Company (UK) Limited, London, third expanded and revised edition, 1983.

[ZN93] Wouter Zijl and Marek Nawalany. *Natural Gr oundwaterFlow.* Lewis Publishers, Boca Raton, Florida, 1993.

Index

A

B

C

D

F

G

H

I–J

M

N

O

P

Q

R

S

U

V

W